BIOINFORMATIC AND FUNCTIONAL ANALYSES OF REST DYSREGULATION IN HUMAN iPSC-DERIVED NEURAL PROGENITORS, ASTROCYTES, AND ORGANOIDS IN DOWN SYNDROME

By

HUANG TAN

© COPYRIGHT UPM

Thesis Submitted to the School of Graduate Studies, Universiti Putra Malaysia, in Fulfilment of the Requirements for the Degree of Doctor of Philosophy

January 2025

FPSK(p) 2025 1

All material contained within the thesis, including without limitation text, logos, icons, photographs, and all other artwork, is copyright material of Universiti Putra Malaysia unless otherwise stated. Use may be made of any material contained within the thesis for non-commercial purposes from the copyright holder. Commercial use of material may only be made with the express, prior, written permission of Universiti Putra Malaysia.

Copyright © Universiti Putra Malaysia

© COPYRIGHT UPM

Abstract of thesis presented to the Senate of Universiti Putra Malaysia in fulfilment of the requirement for the degree of Doctor of Philosophy

BIOINFORMATIC AND FUNCTIONAL ANALYSES OF REST DYSREGULATION IN HUMAN iPSC-DERIVED NEURAL PROGENITORS, ASTROCYTES, AND ORGANOIDS IN DOWN SYNDROME

By

HUANG TAN

January 2025

Chairman : Professor Ling King Hwa, PhD
Faculty : Medicine and Health Sciences

This study aimed to confirm RE1-silencing transcription factor (REST)-mediated molecular dysregulation in Down syndrome (DS) brains and neural cells. To explore the role of REST in fate determination in trisomic neural progenitor cells and the reactivity of trisomic astrocytes. This study first analysed transcriptomic data from DS-derived brain tissues, cerebral organoids, neural progenitor cells (NPCs), neurons, and astrocytes to identify differentially expressed genes (DEGs) and determine REST-targeted DEGs using R software and the Galaxy web platform. REST-targeted DEGs were enriched across multiple brain regions, ages, and neural cell types in various signalling pathways, including JAK-STAT, neural cell differentiation, inflammation, neural cell function, and metabolic homeostasis. Further analysis of DS human induced pluripotent stem cell (hiPSC)-derived NPC transcriptomic data revealed that REST-targeted DEGs were associated with neural cell differentiation and JAK-STAT pathway dysregulation. RT-qPCR validation showed the upregulation of all five REST-targeted hub genes (*CD44*, *TGFB1*, *FN1*, *ITGB1*, and *COL1A1*), *JAK2*, and

© COPYRIGHT UPM

STAT3, along with the *NFIA* (a glioblast marker) upregulation and *DCX* (a neuroblast marker) downregulation. Western blot and Immunocytochemistry (ICC) identified the DCX (a neuroblast marker) downregulation and NFIA (a glioblast marker) upregulation. Thus, REST downregulation may be critical to the neurogenic-to-gliogenic shift observed in trisomic NPCs. I further analysed transcriptomic data from DS hiPSC-derived cerebral organoids at different development stages (30-day to 160-day organoids). REST-targeted DEGs in 90-day cerebral organoids were significantly enriched in the JAK-STAT signalling pathway and gliogenesis, distinct from other time points. RT-qPCR validation confirmed the upregulation of six REST-targeted hub genes (*CSTB*, *MCM3AP*, *PFKL*, *POFUT2*, *PRMT2* and *RWDD2B*) and *STAT3* in 90-day cerebral organoids, along with the downregulation of *DCX* and upregulation of *NFIA*. These findings identified that the loss of REST is a critical factor in the neurogenic-to-gliogenic shift during DS brain development. To further investigate the function of increased astrocytes in DS, R software was used to analyse transcriptomic data of DS hiPSC-derived astrocytes. REST-targeted DEGs were related to cell differentiation, neuroinflammation, and lipid metabolism. RT-qPCR and ICC identified the REST loss in trisomic astrocytes compared with controls. RT-qPCR further validated that the loss of REST led to the upregulation of inflammatory cytokines (*IL-10*, *IL-1B*, *TNF-α*, and *TGF -β*) and reactive astrocyte markers (*EAAT2*, *GFAP*, *S100A10*, and *S100B*). These gene expression patterns in disomic hiPSC-derived astrocytes treated with X5050 (100μM, REST-degraded) were like those in trisomic astrocytes. However, trisomic hiPSC-derived astrocytes with lithium carbonate treatment (5mM, REST-restored) repressed inflammatory cytokine and reactive astrocyte markers expression. Thus, REST loss is vital to trisomic astrocyte reactivity. Reactive astrocytes may have dual functions (neurotoxic and

© COPYRIGHT UPM

neuroprotective) in DS, which warrants further investigation. This study lays the foundation for a better understanding of the role of REST in contributing to DS neuropathology by using the trisomic hiPSC-derived cerebral organoids, NPCs, and astrocytes. REST should be an ideal candidate as one of the therapeutic targets for DS.

Keywords: Astrocyte, Cerebral organoid, Down syndrome, NPC; REST

SDG: GOAL 3: Good Health and Well-Being

© COPYRIGHT UPM

Abstrak tesis yang dikemukakan kepada Senat Universiti Putra Malaysia sebagai memenuhi keperluan untuk ijazah Doktor Falsafah

ANALISIS BIOINFORMATIK DAN FUNGSIONAL DISREGULASI REST DALAM PROGENITOR, ASTROSIT DAN ORGANOID SINDROM DOWN JANAAN DARIPADA SEL STEM PLURIPOTEN TERARUH MANUSIA

Oleh

HUANG TAN

Januari 2025

Pengerusi : Profesor Ling King Hwa, PhD
Fakulti : Perubatan dan Sains Kesihatan

Kajian ini bertujuan untuk mengesahkan disregulasi molekul pengantara RE1-silencing transcription factor (REST) dalam otak sindrom Down (DS) dan sel saraf. Untuk meneroka peranan REST dalam penentuan nasib sel progenitor saraf trisomik dan kereaktifan astrosit trisomik, kajian ini menganalisis data transkrip dari tisu otak yang berasal dari DS, organoid serebrum, sel progenitor saraf (NPC), neuron dan astrosit untuk mengenal pasti ekspresi gen yang ketara (DEG) dan menentukan DEG yang disasarkan oleh REST (*REST-targeted DEG*). *REST-targeted DEG* terdapat di pelbagai bahagian otak, peringkat umur, dan jenis sel saraf yang melibatkan pelbagai laluan isyarat, termasuk JAK-STAT, pembezaan sel saraf, keradangan, fungsi sel saraf, dan homeostasis metabolik. Analisis lanjut mengenai data transkrip NPC yang diperolehi oleh sel stem pluripotent teraruh (hiPSC) DS mendedahkan bahawa *REST-targeted DEG* dikaitkan dengan pembezaan sel saraf dan disregulasi laluan JAK-STAT. Analisis RT-qPCR mengesahkan ekspresi jangkaan kesemua gen hab yang

© COPYRIGHT UPM

disasarkan REST (*CD44*, *TGFB1*, *FN1*, *ITGB1*, dan *COL1A1*), *JAK2* dan *STAT3*, bersama-sama *NFIA* (penanda glioblast) dan *DCX* (penanda neuroblast). Analisis *Western blot* dan imunositokimia (ICC) mengenal pasti peraturan menurun DCX dan peraturan menaik NFIA. Oleh itu, peraturan menurun REST mungkin penting kepada anjakan neurogenik-ke-gliogenik yang diperhatikan dalam NPC trisomik. Seterusnya, analisis data transkriptik daripada organoid serebrum janaan sel stem pluripoten teraruh Sindrom Down (DS hiPSC) pada peringkat pembangunan yang berbeza (organoid 30 hari hingga 160 hari *in vitro,* DIV). *REST-targeted DEG* dalam organoid serebrum 90 DIV didapati terlibat dalam laluan isyarat gliogenesis JAK-STAT yang berbeza daripada masa perkembangan yang lain. Analisis RT-qPCR mengesahkan kesemua enam gen hab sasaran REST (*CSTB*, *MCM3AP*, *PFKL*, *POFUT2*, *PRMT2* dan *RWDD2B*) dan *STAT3* dalam organoid serebrum 90 DIV, bersama-sama dengan peraturan menurun *DCX* dan peraturan menaik *NFIA*. Penemuan ini mengenal pasti bahawa kehilangan REST adalah faktor kritikal dalam peralihan neurogenik-ke-gliogenik semasa perkembangan otak DS. Penyiasatan lanjut mengenai bilangan astrosit yang meningkat dalam otak DS dengan menggunakan data transkrip astrosit DS hiPSC menunjukkan bahawa *REST-targeted DEG* berkaitan dengan pembezaan sel, keradangan neuro dan metabolisme lipid. Analisis RT-qPCR dan ICC mengenal pasti kehilangan REST dalam astrosit trisomik berbanding dengan kumpulan kawalan. Pengesahan RT-qPCR juga menunjukkan kehilangan REST membawa kepada penyelarasan sitokin radang (*IL-10*, *IL-1B*, *TNF-α*, dan *TGF-β*) dan penanda astrosit reaktif (*EAAT2*, *GFAP*, *S100A10*, dan *S100B*). Corak ekspresi gen astrosit disomik yang dirawat dengan X5050 (100μM, REST-degraded) adalah seperti yang terdapat dalam astrosit trisomik. Walau bagaimanapun, astrosit trisomik dengan rawatan litium karbonat (5mM, peraturan menaik REST) menindas sitokin radang dan ekspresi

© COPYRIGHT UPM

penanda astrosit reaktif. Oleh itu, kehilangan REST adalah penting untuk kereaktifan astrosit trisomik. Astrosit reaktif mempunyai dua fungsi iaitu bersifat neurotoksik atau neuroprotektif dalam DS di mana penyiasatan lanjut adalah diperlukan. Kajian ini mengukuhkan asas pemahaman yang lebih baik tentang peranan REST dalam menyumbang kepada neuropatologi DS dengan menggunakan organoid serebral, NPC, dan astrocytes janaan daripada hiPSC. REST harus menjadi calon yang ideal sebagai salah satu sasaran terapeutik untuk DS.

Kata Kunci: Astrosit, NPC, Organoid serebrum, REST, Sindrom Down

SDG: MATLAMAT 3: Kesihatan yang Baik dan Sejahtera

© COPYRIGHT UPM

ACKNOWLEDGEMENTS

Throughout this long and fulfilling journey as a Ph.D. student, I have been fortunate to receive support and help from many individuals, enabling me to complete this challenging research. I extend my heartfelt gratitude to all of them.

First and foremost, I would like to express my sincere thanks to my primary supervisor, Professor Ling King Hwa. Over the past three years, Professor Ling King Hwa has provided me with meticulous guidance in academic research and invaluable assistance in my personal growth and studies. Your academic prowess, scholarly attitude, and scientific research dedication have inspired me to pursue excellence. Without your careful guidance and encouragement, I would not have achieved what I have today.

I would also like to extend special thanks to my co-supervisor, Professor Sharida Fakurazi. Professor Sharida has consistently offered patient guidance and valuable advice throughout my research and studies. Your professional knowledge and careful supervision have greatly benefited my academic journey.

Furthermore, I am grateful to Associate Professor Cheah Pike See for your guidance, assistance, understanding, and tolerance. Professor Cheah Pike See has provided important suggestions and support in multiple aspects of my research. Your support has enabled me to progress through every critical stage of my research smoothly, and your academic wisdom and research methods have profoundly impacted me.

I would also like to extend my deepest gratitude to my family, especially my wife, Xie Yu Xi. Your care, companionship, and understanding have been my greatest

© COPYRIGHT UPM

motivation to persevere. Your support and encouragement have allowed me to carry on in times of difficulty and challenge. Your selfless dedication and silent contribution will always be remembered in my heart.

Similarly, I want to thank my friends, the NBGG group, and all the faculty and staff. Thank you for providing essential guidance, laboratory facilities, and resources for my research. Your support has helped me understand the significance of teamwork. I will always be grateful for the opportunity to work with such a talented group. I would also like to thank Universiti Putra Malaysia for the financial support provided by the Geran Putra Inisiatif Putra Siswazah (GP-IPS/2022/9736200).

Finally, once again, I extend my sincerest thanks to everyone who has supported and helped me. Because of your presence, I have completed this research work and begun a new chapter in my life.

© COPYRIGHT UPM

This thesis was submitted to the Senate of the Universiti Putra Malaysia and has been accepted as fulfilment of the requirement for the degree of Doctor of Philosophy. The members of the Supervisory Committee were as follows:

Ling King Hwa, PhD
Professor
Faculty of Medicine and Health Sciences
Universiti Putra Malaysia
(Chairman)

Sharida binti Fakurazi, PhD
Professor
Faculty of Medicine and Health Sciences
Universiti Putra Malaysia
(Member)

ZALILAH MOHD SHARIFF, PhD
Professor and Dean
School of Graduate Studies
Universiti Putra Malaysia

Date: 17 April 2025

© COPYRIGHT UPM

TABLE OF CONTENTS

		Page
ABSTRACT		i
ABSTRAK		iv
ACKNOWLEDGEMENTS		vii
APPROVAL		ix
DECLARATION		xi
LIST OF TABLES		xviii
LIST OF FIGURES		xix
LIST OF ABBREVIATIONS		xxiii
CHAPTER		
1	**INTRODUCTION**	1
1.1	Background	1
1.2	Problem Statement	4
1.3	Hypothesis	5
1.4	Objectives	5
1.4.1	General Objective	5
1.4.2	Specific Objectives	5
1.5	Significance of Study	6
2	**LITERATURE REVIEW**	8
2.1	Down Syndrome (DS)	8
2.1.1	Prevalence and Genetics of DS	8
2.1.2	Molecular Perturbation in DS	10
2.1.3	Neurodevelopment Defects in DS	14
2.2	Repressor Element-1 Silencing Transcription (REST)	17
2.2.1	REST and Its Target Genes	17
2.2.2	Role of REST in Brain Development	19
2.2.3	REST Dysregulation in Neurodegenerative Disorders and DS	20
2.3	Neural Progenitor Cell (NPC) in Down Syndrome	23
2.3.1	Fate Determination of NPC	23
2.3.2	Dysregulation of NPC in DS	26
2.4	Astrocyte Homeostasis and Reactivity	27
2.4.1	Homeostasis of Astrocyte	27
2.4.2	Reactive Astrocytes	30
2.4.3	Astrocyte Reactivity in Neurodegenerative Disorders and DS	32
2.5	Lithium	34
2.5.1	Neuroprotective Effects of Lithium	34
2.5.2	Role of Lithium in Astrocytes	36
2.5.3	Lithium and REST Expression	37
2.5.4	Side Effects of Lithium Treatment	39
2.6	Human-Induced Pluripotent Stem Cells (hiPSCs)	40
2.6.1	Advantages of hiPSC-derived Models for Study	40

© COPYRIGHT UPM

2.6.2 DS iPSC-Derived 2D Cell Model 42
2.6.3 DS iPSC-Derived 3D Cerebral Organoid Model 43

3 REST-MEDIATED MOLECULAR DYSREGULATION IN DOWN SYNDROME HUMAN BRAIN TISSUE AND NEURAL CELLS BY BIOINFORMATIC ANALYSIS 45
3.1 Introduction 45
3.2 Experiment Design 46
3.3 Materials and Methods 47
3.3.1 Acquisition of DS Transcriptomic Datasets 47
3.3.2 Identification of Differentially Expressed Genes (DEGs) between DS Samples and Controls 48
3.3.3 Identification of REST-Targeted DEGs 49
3.3.4 Functional Enrichment Analysis and Visualisation 49
3.3.5 Protein-Protein Interaction (PPI) Network Analysis 50
3.4 Results 50
3.4.1 DEGs of DS Human Brain Tissues and Neural Cells 50
3.4.2 REST-Targeted DEGs in DS Human Brain Tissues and Neural Cells 57
3.4.3 GO and KEGG Enrichment Analyses of REST-Target DEGs 62
3.4.3.1 The Critical Role of REST-Targeted DEGs in DS Different Brain Regions 63
3.4.3.2 The Critical Role of REST-Targeted DEGs in DS Different Age Brain 66
3.4.3.3 The Critical Role of REST-Targeted DEGs in DS-Derived Cerebral Organoids and Neural Cells 69
3.4.4 Construction of DEGs PPI Network and Identification of MCODEs 72
3.5 Discussion 76
3.6 Conclusions 81

4 DYSREGULATION OF REST AND ITS TARGET GENES IMPACTS THE FATE OF TRISOMIC NEURAL PROGENITOR CELLS 82
4.1 Introduction 82
4.2 Experiment Design 84
4.3 Materials and Methods 85
4.3.1 Acquisition and Process of DS hiPSC-Derived NPCs Datasets 85
4.3.2 Processing of the Dataset and Identification of Differentially Expressed Genes (DEGs) 86
4.3.3 Gene Set Enrichment Analysis 86
4.3.4 REST-Targeted DEGs in DS hiPSC-Derived NPCs 87

© COPYRIGHT UPM

4.3.5 Gene Ontology and Pathway Enrichment Analysis 87
4.3.6 WGCNA Network Construction and Module Identification 88
4.3.7 PPI Network Construction for Screening Hub Genes 88
4.3.8 Validation of Hub Genes 89
4.3.9 Cell Culture 89
4.3.10 Immunocytochemistry 91
4.3.10.1 Cell Culture and Fixation on the Coverslip 91
4.3.10.2 Immunocytochemistry Procedure 91
4.3.10.3 Image Analysis 92
4.3.11 Quantitative Real-Time Polymerase-Chain Reaction (RT-qPCR) 94
4.3.11.1 RNA Extraction and Reverse Transcription on RNA Samples 94
4.3.11.2 Primer Design 94
4.3.11.3 RT-qPCR Protocol 97
4.3.11.4 RT-qPCR Analysis 97
4.3.12 Western Blot 98
4.3.12.1 Total Protein Extraction 98
4.3.12.2 Protein Quantification with BCA Assay 98
4.3.12.3 Gel Electrophoresis 98
4.3.12.4 Protein Transfer from Gel to Membrane 99
4.3.12.5 Immunodetection and Visualisation by Transillumination 100
4.3.12.6 Image Analysis 101
4.3.13 Statistical Analysis 101
4.4 Results 102
4.4.1 Differentially Expressed Genes and Their Ontologies 102
4.4.2 GSEA Analysis Revealed Abnormalities in Neural Cell Differentiation 103
4.4.3 REST-Targeted DEGs and Their Ontologies and Pathways 104
4.4.4 REST-Targeted Hub DEGS and NPC Fate Determination 107
4.4.4.1 WGCNA Analysis and Critical Module Identification 107
4.4.4.2 PPI Network Construction and Identification of REST-Targeted Hub DEGs 110
4.4.5 In Silico and Laboratory Validation of REST-Targeted Hub DEGs 114
4.4.6 Nuclear REST Loss in DS hiPSC-Derived NPCs 117
4.4.7 The Neurogenic-to-Gliogenic Shift in DS hiPSC-Derived NPCs 119

© COPYRIGHT UPM

4.5 Discussion 121
4.6 Conclusions 128

5 REST-MEDIATED DYSREGULATION OF DOWN SYNDROME IPSC-DERIVED CEREBRAL ORGANOIDS AT DIFFERENT DEVELOPMENT STAGE 129
5.1 Introduction 129
5.2 Experiment Design 131
5.3 Materials and Methods 132
5.3.1 Acquisition of DS Cerebral Organoids Datasets 132
5.3.2 Processing of the Dataset and Identification of Differentially Expressed Genes (DEGs) 133
5.3.3 Identification of REST-Targeted DEGs in DS Cerebral Organoids 133
5.3.4 WGCNA Network Construction and Module Identification 133
5.3.5 Machine Learning for Screening Critical Genes 134
5.3.6 Gene Ontology and Pathway Enrichment Analysis 134
5.3.7 Gene Set Enrichment Analysis 134
5.3.8 Production of hiPSC-Derived Cerebral Organoids 134
5.3.9 Immunohistochemistry Staining of Cerebral Organoids 136
5.3.9.1 Cryopreservation Procedure 136
5.3.9.2 Cryo-sectioning Procedure 137
5.3.9.3 Immunohistochemistry Procedure 137
5.3.10 Quantitative Real-Time PCR 138
5.3.11 Statistical Analysis 140
5.4 Results 140
5.4.1 Differentially Expressed Genes and Their Ontologies and Pathways in Different Developmental Stages of DS Cerebral Organoids 140
5.4.2 REST-Targeted DEGs in Different Developmental Stages of DS Cerebral Organoids 145
5.4.3 REST as the Pivotal Regulator during DS iPSC-Derived Cerebral Organoid Development 146
5.4.4 GSEA Revealed Abnormal Neurodevelopment in DS-Derived 90-Day Cerebral Organoids 148
5.4.5 WGCNA Identified Critical Module in DS-Derived 90-Day Cerebral Organoids 149
5.4.6 Machine Learning for Identifying Critical Genes 153
5.4.7 In Silico and Laboratory Validation of REST-Targeted Hub DEGs 154
5.4.8 In Laboratory Validation of REST-Targeted Hub DEGs 155
5.4.9 The Neurogenic-to-Gliogenic Shift in 90-Day DS hiPSC-Derived Organoid 158
5.5 Discussion 159
5.6 Conclusions 168

© COPYRIGHT UPM

6 REST RESTORATION INHIBITS DOWN SYNDROME IPSC-DERIVED ASTROCYTIC REACTIVITY 170
6.1 Introduction 170
6.2 Experiment Design 172
6.3 Materials and Methods 173
6.3.1 Acquisition of DS-Derived Astrocytes Datasets 173
6.3.2 Processing of the Dataset and Identification of Differentially Expressed Genes (DEGs) 174
6.3.3 REST-Targeted DEGs in DS-Derived Astrocytes 174
6.3.4 Gene Ontology and Pathway Enrichment Analysis 174
6.3.5 Production of hiPSC-Derived Astrocytes 174
6.3.5.1 Production of Neural Progenitor Cells (NPCs) from hiPSCs 174
6.3.5.2 Production of Astrocytes from NPCs 175
6.3.6 MTT Assay 176
6.3.7 Quantitative Real-Time PCR 176
6.3.8 Immunocytochemistry 178
6.3.9 Statistical Analysis 178
6.4 Results 179
6.4.1 DEGs of DS Astrocytes Derived from Different Cell Sources 179
6.4.2 REST-targeted DEGs in DS-Derived Astrocyte 180
6.4.3 REST Involved in Various Functions and Activities of Astrocytes 181
6.4.4 REST Lost in DS-Derived Astrocytes Restored by Lithium Treatment 184
6.4.5 Restoration of REST Downregulated the REST-Targeted Inflammatory Genes 188
6.4.6 Restoration of REST Suppresses the Expression of Reactive Astrocyte Cell Makers 191
6.5 Discussion 196
6.6 Conclusions 200

7 GENERAL DISCUSSION AND CONCLUSION 201
7.1 General Discussion 201
7.2 Study Limitations and Recommendations for Future Research 208
7.3 General Conclusion 210

REFERENCES 212
APPENDICES 259
BIODATA OF STUDENT 295
LIST OF PUBLICATIONS 296

© COPYRIGHT UPM

LIST OF TABLES

Table		Page
4.1	Details of the Disomic Control and Trisomic DS iPSC Lines	90
4.2	List of Primer Sequences for RT-qPCR	96
4.3	The Top 20 Genes Were Screened through 10 Topological Algorithms of "cytoHubba"	113
5.1	Details of the Disomic Control and Trisomic DS iPSC Lines	136
5.2	List of Primer Sequences for RT-qPCR	139
6.1	Details of the Disomic Control and Trisomic DS iPSC Lines	175
6.2	List of Primer Sequences for RT-qPCR	177

© COPYRIGHT UPM

LIST OF FIGURES

Figure		Page
1.1	The Overall Workflow for This Study	7
2.1	Overexpression of Specific Genes Located on Chromosome 21 Has Been Associated with Down Syndrome Pathological Features	12
2.2	Timeline of Differentiation and Development of Neural Cells	15
2.3	REST Regulates Gene Silencing through Histone Modification	18
2.4	Mechanisms of REST Dysregulation in Different Neurodegenerative Diseases	22
2.5	Regulation of Neural Progenitor Cell Fate by Critical Signalling Pathways.	24
2.6	The Various Functional Roles Played by Astrocytes in the Brain	28
2.7	Characterisation of A1 and A2 Reactive Astrocytes	31
2.8	Lithium Exerts Neuroprotective Effects against Neurological Disorders through a Variety of Mechanisms	35
2.9	Effect of Lithium Treatment on the Expression of REST, Inflammatory Factors and Cellular Markers in Astrocytes	39
3.1	Simplified Diagram of the Experimental Methods, Data Processing, and Analysis Workflow Used for this Study	47
3.2	Heat Map Analysis of Identified DEGs between DS and Controls in Eight Brain Regions	51
3.3	The Volcano Plot for DEGs in DS Eight Brain Regions	52
3.4	Heat Maps of Identified DEGs between DS and Controls, Respectively, in Fetal (16 to 22 Gestational Weeks), Infant Child (2 to 16 years), Child (2 to 16 years) and Adult (18 to 42 years)	53
3.5	Volcano Plots of Identified DEGs between DS and Controls, Respectively, in Fetal (16 to 22 Gestational Weeks), Infant Child (2 to 16 years), Child (2 to 16 years) and Adult (18 to 42 years)	54
3.6	Heat maps of Identified DEGs between DS and Controls in Cerebral Organoid, NPC, Neuron and Astrocyte	55
3.7	Volcano Plots of Identified DEGs between DS and Controls in Cerebral Organoid, NPC, Neuron and Astrocyte	56

© COPYRIGHT UPM

3.8 Depiction of the Overlap between REST Target Genes and DEGs across DS Diverse Brain Regions 58

3.9 The Heatmap and Enrichment Analysis for Common Genes in the DS Different Brain Regions 59

3.10 Depiction of the Overlap between REST Target Genes and DEGs across Diverse Age Groups of DS Brain Tissues 60

3.11 The Heatmap and Enrichment Analysis for the Common Genes in DS Different Age Groups 61

3.12 Depiction of the Overlap between REST Target Genes and DEGs from DS-Derived Cerebral Organoids (A), NPCs (B), Neurons (C) and Astrocytes (D) 62

3.13 Biological Process Enrichment Analysis Associated with REST-Targeted DEGs across DS Various Brain Regions 64

3.14 KEGG Enrichment Analysis Associated with REST-Targeted DEGs across DS Various Brain Regions 65

3.15 Summary of Signalling Pathways and Biological Functions Enriched in DS Different Brain Regions 66

3.16 Analysis of Biological Processes and KEGG Pathways Associated with REST Target DEGs in Fetal (16 to 22 Gestational Weeks), Infant Child (2 to 16 years), Child (2 to 16 years) and Adult (18 to 42 years) 68

3.17 Summary of Signalling Pathways and Biological Functions Enriched in REST-Targeted DEGs Consistently Identified across Ages in DS 69

3.18 Analysis of Biological Processes and KEGG Pathways Associated with REST Target DEGs in DS-Derived Cerebral Organoids, NPCs, Neurons and Astrocytes, Respectively 71

3.19 Summary of Signalling Pathways and Biological Processes Involved in REST Target DEGs in DS-Derived Cerebralorganoids, NPCs, Neurons and Astrocytes, Respectively 72

3.20 Protein-Protein Interaction Networks and Enrichment Analysis of DEGs in DS-Deirved NPCs 73

3.21 Protein-Protein Interaction Networks and Enrichment Analysis of DEGs in DS-Deirved Neurons 74

3.22 Protein-Protein Interaction Networks and Enrichment Analysis of DEGs in DS-Deirved Astrocytes. 75

4.1 Simplified Diagram of the Experimental Methods, Data Processing, and Analysis Workflow Used for This Study 85

© COPYRIGHT UPM

4.2 The Heat Map and Volcano Plot for the DEG Analysis of DS-Derived NPCs 102

4.3 Biological Process Clustering Enrichment Analysis for the DEGs in DS hiPSC-Derived NPCs 103

4.4 GSEA Analysis for DS hiPSC-Derived NPCs 104

4.5 Enrichment Analysis for REST-Targeted DEGs in NPCs 106

4.6 WGCNA for Sample Clustering and Scale-Free Nextwork Construction. 108

4.7 WGCNA Unveiled Gene Co-Expression Networks and Module-Trait Relationships 109

4.8 The PPI Network Was Constructed Using the Overlapping Genes from REST-Targeted DEGs and WGCNA MEbrown Module Genes 111

4.9 UpSet Analysis of 10 Topological Algorithms of "cytoHubba" 112

4.10 Prediction of REST-Targeted Hub DEGs at the Level of Gene Expression 115

4.11 DS hiPSC-Derived NPC Cell Line Establishment and Detection of Hub Genes mRNA (n=3) 117

4.12 Detection of REST mRNA and Protein in DS hiPSC-Derived NPCs. 118

4.13 Detection of DCX and mRNA and Protein in DS hiPSC-Derived NPCs 120

5.1 Simplified Diagram of the Experimental Methods, Data Processing, and Analysis Workflow Used for This Study 132

5.2 : Heat Maps Analysis of Identified DEGs between DS and Controls in Cerebral Organoids at Different Time Points 141

5.3 The Volcano Plot is for DEGs in DS hiPSC-Derived in Cerebral Organoids at Different Time Points 142

5.4 Enrichment Analysis of DEGs in DS-Derived Cerebral Organoids at Different Time Points 144

5.5 (A-D) Depiction of the Overlap between REST Target Genes and DEGs across the Different Time Points DS iPSC-Derived Organoids 145

5.6 Analysis of REST Target DEGs in DS-Derived Cerebral Organoids at Different Time Points 147

5.7 Summary of Signalling Pathways and Biological Processes Involved in REST-Targeted DEGs in DS-Derived Cerebral Organoids at Different Time Points 148

© COPYRIGHT UPM

5.8 GSEA Analysis for 90-Day DS Cerebral Organoids 149

5.9 WGCNA for Sample Clustering and Scale-Free Network Construction. 151

5.10 WGCNA Unveiled Gene Co-Expression Networks and Module-Trait Relationships 152

5.11 Screening Hub Genes from REST Target DEGs in 90-Day DS iPSC-Derived Cerebral Organoids 154

5.12 The Silico Analysis for REST-Targeted Hub DEGs in DS hiPSC-Deirved 90-Day Cerebral Organoids 155

5.13 Culture of Cerebral Organoids and Validation of REST-Targeted Hub Gene in 90-Day Cerebral Organoids 157

5.14 Detection of REST and Neural Differentiation-Related Genes in 90-Day DS iPSC-Derived Cerebral Organoids 159

5.15 Potential Mechanisms by Which REST-Targeted Hub DEGs Affect Neurodevelopment in DS 165

6.1 Simplified Diagram of the Experimental Methods, Data Processing, and Analysis Workflow Used for This Study 173

6.2 Heat Maps and Volcano Map Visualization of Identified DEGs in DS-Derived Astrocytes 180

6.3 Depiction of the Overlap between REST Target Genes and DEGs 181

6.4 Analysis of REST-Targeted DEGs in DS iPSC-Derived Astrocytes (PRJNA600245), DS Fetal Cerebellum-Derived Astrocytes (GSE1397) and DS Fetal Cortical-Derived Astrocytes (GSE42772) 183

6.5 Astrocyte Differentiation and Identification of Cellular Characteristics 184

6.6 The Detection of REST mRNA and Protein in Treated and Untreated DS hiPSC-Derived Astrocytes and Controls 187

6.7 The Detection of Inflammation Factors in Treated and Untreated DS hiPSC-Derived Astrocytes and Controls 190

6.8 The mRNA Expression of Reactive Astrocyte Cell Markers in Treated and Untreated DS hiPSC-Derived Astrocytes and Controls 192

6.9 Immunocytochemical Detection of DS hiPSC-Derived Reactive Astrocyte Markers 195

© COPYRIGHT UPM

LIST OF ABBREVIATIONS

2D	Two dimensional
3D	Three dimensional
AD	Alzheimer's disease
ADARB1	Adenosine deaminase RNA specific B1
ALB	Albumin
APC	Astrocyte precursor cell
APP	Amyloid-beta precursor protein
Aβ42	Amyloid-beta 42
Aβ	Amyloid-beta
BBB	Blood-brain barrier
BDNF	Brain-derived neurotrophic factors (BDNF)
BMP	Bone morphogenetic protein
BMP4	Bone morphogenetic protein 4
BrdU	5-bromo-2-deoxyuridine
BRG1	Brahma-related gene 1
BSA	Bovine serum albumin
CBC	Cerebellar cortex
CBP	CREB-binding protein
cDNA	Complementary deoxyribonucleic acid
cMYC	Transcriptional regulator Myc-like
CNTF	Ciliary neurotrophic factor
CO_2	Carbon dioxide
COL1A1	Collagen type I alpha 1 chain
Con	Control
COX2	Cytochrome c oxidase subunit II

© COPYRIGHT UPM

Cq	Cycle of quantification
CTDSP1	C-terminal domain small phosphatase 1
DAPI	4′,6-diamidino-2-phenylindole
DAVID	Database for Annotation, Visualisation and Integrated Discovery
DCX	Doublecortin
DEG	Differentially expressed gene
DFC	Dorsolateral prefrontal cortex
DIV	Days in vitro
DMSO	Dimethyl sulfoxide
DNA	Deoxyribonucleic
DPBS	Dulbecco's phosphate buffered saline
DS	Down syndrome
DSCR	Down Syndrome Critical or Chromosomal Region
DYRK1A	Dual specificity tyrosine phosphorylation regulated kinase 1A
EAAT1	Excitatory amino acid transporter 1
EAAT2	Excitatory amino acid transporter 2
ECM	Extracellular matrix
EPC	Percolated Component
ESC	Embryonic stem cell
FN1	Fibronectin 1
FITC	Fluorescein isothiocyanate
GAPDH	Glyceraldehyde-3-phosphate dehydrogenase
GEO	Gene Expression Omnibus
GD	Gestational day
GO	Gene Ontology
GW	Gestational week

© COPYRIGHT UPM

GFAP	Glial fibrillary acidic protein
GS	Gene significance
GSEA	Gene set enrichment analysis
GSK-3	Glycogen synthase kinase 3
GSK-3β	Glycogen synthase kinase-3β
GTRD	Gene Transcription Regulation Database
Hes1	Hes family bHLH transcription factor 1
Hes2	Hes family bHLH transcription factor 2
HD	Huntington's disease
HDAC	Histone deacetylase
HGP	Human Genome Project
HIP	Hippocampus
hiPSC	Human induced pluripotent stem cells
HMBS	Hydroxymethylbilane synthase
HSA21	Human chromosome 21
HTT	Huntington protein
ICC	Immunocytochemistry
ID	Intellectual disability
IFN	Interferon
IFNAR1	Interferon (alpha and beta) receptor subunit 1
IL-1	Interleukin 1
IL-10	Interleukin 10
IL-1B	Interleukin 1 beta
IL-6	Interleukin 6
INF-γ	Interferon gamma
iNOS	Inducible nitric oxide synthase

© COPYRIGHT UPM

iPSC	Induced pluripotent stem cell
ITC	Inferior temporal cortex
ITGB1	Integrin subunit beta 1
JAK	Janus kinase
JAK1	Janus kinase 1
JAK2	Janus kinase 2
JAK-STAT	Janus kinase-signal transducer and activator of transcription
KEGG	Kyoto encyclopedia of genes and genomes
KLF4	KLF transcription factor 4
LASSO	Least absolute shrinkage and selection operator
Li_2CO_3	Lithium carbonate
LPS	Lipopolysaccharide
LSD1	Lysine-specific histone demethylase
MCC	Maximum cluster centrality
MCM3AP	Minichromosome maintenance complex component 3 associated protein
MNC	Maximum neighbourhood component
MM	Module membership
mGluR5	Metabotropic glutamate receptors 5
mRNA	Messenger ribonucleic acid
MTT	3-(4,5-dimethylthiazol-2-yl)-2,5-diphenyl-2H-tetrazolium bromide
N6AMT1	N-6 adenine-specific DNA methyltransferase 1
NEUROD1	Neuronal differentiation 1
NFIA	Nuclear factor IA
NF-κB	Nuclear factor kappa-light-chain-enhancer of activated B cells
NGN2	Neurogenin 2

© COPYRIGHT UPM

NGS	Next-generation sequencing
NMDA	N-methyl-D-aspartate
Notch	Neurogenic locus notch homolog protein
NOS	Nitric oxide synthase
NPC	Neural progenitor cells
NRF2	Nuclear factor erythroid 2–related factor 2
NRSF	Neuron-restrictive silencing factor
ns	Not significant
NSC	Neural stem cell
OCT4	POU class 5 homeobox 1
OFC	Prefrontal cortex
Olig2	Oligodendrocyte transcription factor 2
OPC	Oligodendrocyte precursor cell
P	Passage
PBS	Phosphate buffered saline
PCR	Polymerase chain reaction
PD	Parkinson's disease
PFA	Paraformaldehyde
PFC	Prefrontal cortex
PFKL	Phosphofructokinase-liver type
POFUT2	Protein O-fucosyltransferase 2
PPI	Protein-protein interaction
PRMT2	Protein arginine methyltransferase 2
PSMB2	Proteasome subunit beta type-2
PTX3	Pentraxin-3
PVDF	Polyvinylidene fluoride

© COPYRIGHT UPM

REST	Repressor element-1 silencing transcription factor
RE1	Repressor element 1
RF	Representation factor
RGC	Radial glial cell
RIPA	Radioimmunoprecipitation assay
RNA	Ribosomal nucleic acid
ROCKi	Rho-associated protein kinase inhibitor Y-27632
ROI	Region of interest
ROS	Reactive oxygen species
RT-qPCR	Real time quantitative polymerase chain reaction
RUNX1	RUNX family transcription factor 1
RWDD2B	RWD domain containing 2B
S100A10	S100 calcium-binding protein A10
S100B	S100 calcium binding protein B
S1C	Primary somatosensory cortex
SD	Standard deviation
SDS	Sodium dodecyl sulphate
SDS-PAGE	Sodium docecyl sulphate-polyacrylamide gel electrophoresis
SMAD	Downstream mediator of activated BMP receptors
SOD1	Superoxide dismutase 1
SOX2	SRY-box transcription factor 2
SOX5	SRY-box transcription factor 5
SOX9	SRY-box transcription factor 9
STAT	Signal transducer and activator of transcription
STAT1	Signal transducer and activator of transcription 1
STAT3	Signal transducer and activator of transcription 3

© COPYRIGHT UPM

STAT6	Signal transducer and activator of transcription 6
STRING	Search tool for the retrieval of interacting genes
SVZ	Subventricular zone
T21	Triploidy of chromosome 21
TBHP	Tert-butyl hydroperoxide
TBI	Traumatic brain injury
TBST	Tris-buffered saline with 0.1% tween 20 detergent
TGF	Transforming growth factor beta
TGFB1	TGFB1, Transforming growth factor beta 1
TLR	Toll-like receptor
TNF-**α**	Tumor necrosis factor-alpha
TRPV1	Transient receptor potential vanilloid 1
U2AF1	U2 small nuclear RNA auxiliary factor 1
Usp16	Ubiquitin specific peptidase 16
V1C	Primary visual cortex
VEGF	Vascular endothelial growth factor
VFC	Ventrolateral prefrontal cortex
WGCNA	Weighted Gene Co-expression Network Analysis

© COPYRIGHT UPM

© COPYRIGHT UPM

CHAPTER 1

INTRODUCTION

1.1 Background

Down syndrome (DS) is primarily characterised by an extra copy of chromosome 21, a condition known as trisomy 21. It is the most common genetic form of intellectual disability and the leading cause of specific birth defects and medical conditions (Sherman et al., 2007). Transcriptomic analyses of DS individuals affirm an average 50% increase in the expression levels of genes triplicated on HSA21 compared with the controls (Liu et al., 2017). The expression level of some genes located on other chromosomes is also perturbed, indicating that trisomy 21 exerts broader effects on downstream transcriptional and signalling pathways in DS individuals. During the development of the brain, neurogenesis arises first, followed by astrogenesis, and finally oligodendrocytogenesis, with a partial overlap of the three developmental stages (Eck and Waltman, 2009; Synnestvedt et al., 2005; Wu et al., 2022). In DS, the brain exhibits weight, volume, and linear size reductions, with decreased neurons and increased astrocytes (Stagni et al., 2018a, 2018b). In the developmental trajectory of the DS brain, the regular spatiotemporal line of neurogenesis is disrupted, resulting in diminished proliferation of neural progenitor cells (NPCs) and impaired functionality in neurogenesis (Stagni et al., 2018a). The proliferation, differentiation, and normal morphology of these NPCs are impaired. Human trisomic induced pluripotent stem cells (hiPSCs)-derived NPCs demonstrated an altered fate determination in DS, characterised by an enhanced propensity toward glial cell differentiation and a concomitant reduction in neuronal differentiation (Meharena et al., 2022; Qiu et al., 2023).

© COPYRIGHT UPM

The expansion of glial lineages is not uniformly observed in the DS brain, particularly astrocytes, which are predominantly affected (Mizuno et al., 2018; Ponroy Bally and Murai, 2021). Although astrocyte differentiation increases during DS neurodevelopment, their development and maturation are impaired (Ponroy Bally and Murai, 2021). Astrocytes derived from DS brain exhibit altered transcriptomic profiles, adhesion properties, cell dynamics, abnormal morphology, and functional deficiencies, which may disrupt CNS homeostasis (Araujo et al., 2018; Kawatani et al., 2021; Mizuno et al., 2018; Ponroy Bally et al., 2020; Ponroy Bally and Murai, 2021). DS-derived astrocytes produce negative effects in regulating synaptic development and maturation, neuronal excitability and neuronal survival (Ponroy Bally et al., 2020). RNA sequencing reveals that DS-derived astrocytes undergo genome-wide transcriptional disruption, leaving DS neurodevelopment, cell adhesion, mitochondrial function, and extracellular matrix-related molecules severely dysregulated (Kawatani et al., 2021; Ponroy Bally et al., 2020). The upregulation of *S100B* on chromosome 21 in DS-derived astrocytes resulted in cellular accumulation of S100B and GFAP. This abnormality leads to oxidative stress-induced neural death but does not affect DS-derived astrocyte viability. This leads to a sustained neurotoxic effect of astrocytes in DS brains.

The RE1 silencing transcription factor (REST), also referred to as neuron-restrictive silencer factor (NRSF), plays a pivotal role in regulating gene expression in various cell types, particularly in neural cells (Su et al., 2022; Thiel et al., 2015). REST has been shown to regulate the alternative splicing of its transcripts, thereby affecting the REST-targeted gene expression (Burkholder et al., 2018). The dynamic occupancy of REST at RE1 sites is contingent upon cellular REST levels (Ballas et al., 2005).

© COPYRIGHT UPM

Alterations in the RE1 sequence can modulate the DNA-binding affinity of REST, leading to differential occupancy of REST at RE1 sites (Inui et al., 2017). Beyond its association with neuronal genes, the occupancy of REST at RE1/NRSE sites extends to specific non-neuronal genes in the human genome, showcasing the broader regulatory influence of REST in gene expression (Marullo et al., 2010). The Gene Transcription Regulation Database (GTRD) (Kolmykov et al., 2021) offers the most extensive and uniformly processed ChIP-seq datasets available for exploring transcription factor binding sites in humans. This resource has identified 15,450 REST-targeted genes within the human genome. Abrajano et al. employed ChIP-chip to scrutinise RE1 binding sites in all mouse-derived glial cells, identifying 3,178 REST-targeted genes and 4,060 CoREST-targeted genes (Abrajano et al., 2009). Compelling evidence underscores the central role of REST in the intricate processes of brain development, playing a crucial part in regulating neural progenitor/stem cells, neurogenesis, gliogenesis, neural cell genes expression, and neural cell phenotypes preservation (Baldelli and Meldolesi, 2015; Johnson et al., 2008; Thiel et al., 2015).

Abundant research indicates REST dysregulation in various neurodegenerative diseases like Alzheimer's disease (AD), Parkinson's disease (PD), and Huntington's disease (HD) (Garcia et al., 2019; Hwang and Zukin, 2018; Wei et al., 2022). The REST level in the human fetal brain-derived trisomic samples (three copies of chromosome 21) showed a notable reduction compared to disomic samples (two copies of chromosome 21) (Bahn et al., 2002). Considerable evidence indicates that the impediment of REST nuclear translocation leads to the upregulation of target genes as a pathological mechanism in AD and PD. The disruption of REST and its epigenetic reshaping has been identified as a pivotal mechanism in progressive

© COPYRIGHT UPM

neurodegeneration in these diseases (Hwang and Zukin, 2018). A subsequent study has shown that REST levels are reduced by 30% to 60% in DS mouse brains and that this reduction is consistently observed at all stages of brain development, from the embryonic stem cell (ESC) to the adult brain (Canzonetta et al., 2008). Nevertheless, the understanding of the role of REST in the neurodevelopment of individuals with DS and its impact on neural cell function remains limited. Therefore, comprehensive studies are needed to investigate REST-mediated molecular dysregulation in DS-derived (trisomic) NPCs, astrocytes, and cerebral organoids (Figure 1.1).

1.2 Problem Statement

Down syndrome is the leading genetic cause of intellectual disability, characterised by widespread transcriptional dysregulation across the genome. Prominent characteristics of the condition include diminished neurogenesis and enhanced gliogenesis, referred to as the neurogenic-to-gliogenic shift. Previous studies have primarily focused on the mechanisms underlying neurogenesis defects and neuronal abnormalities in DS. However, the mechanisms governing the fate determination of trisomic NPCs and the reactivity of trisomic astrocytes have not been thoroughly evaluated. REST, a critical repressive transcription factor, is known for its role in regulating neuronal gene expression and maintaining the neuronal phenotype. In Alzheimer's disease, the loss of nuclear REST leads to upregulating its target genes, such as *p35*, *BCL2* and *MAPK12*. Although REST downregulation was observed in the fetal brain tissues of individuals with DS, its expression levels in DS-derived neural cells and tissues have not been adequately assessed. Thus, the function of REST and its target genes in DS brain tissues and neural cells remains unclear. The

© COPYRIGHT UPM

relationship between REST and its target genes with the fate determination of trisomic NPCs and reactive astrocytes is yet to be elucidated.

1.3 Hypothesis

This study hypothesises that:

1. REST reduced and mediated molecular dysregulation in trisomic neural progenitor cells, astrocytes and cerebral organoids.
2. An optimal dose of lithium can restore nuclear REST expression in trisomic hiPSC-derived astrocytes and rescue astrocyte responsiveness.

1.4 Objectives

1.4.1 General Objective

This study aimed to investigate REST-mediated neurogenic-to-gliogenic shift in neurodevelopment and lithium-mediated REST restoration in rescuing trisomic hiPSC-derived astrocyte reactivity.

1.4.2 Specific Objectives

1. To predict the REST-mediated molecular dysregulation in Down syndrome human brain tissue and neural cells by bioinformatic analysis.
2. To establish and characterise the cell markers of disomic and trisomic hiPSC-derived neural progenitor cells, astrocytes and cerebral organoids.
3. To determine REST-mediated dysregulation of neural cell differentiation fate in trisomic hiPSC-derived neural progenitor cells and cerebral organoids.
4. To evidence the optimal dose of lithium can restore nuclear REST expression in trisomic hiPSC-derived astrocytes.

© COPYRIGHT UPM

5. To validate the astrocyte reactive in trisomic hiPSC-derived astrocytes with and without lithium and/or X5050 treatment.

1.5 Significance of Study

This study aimed to gain insight into the expression of REST-targeted differential genes and REST-mediated molecular dysregulation in trisomic iPSC-derived neural progenitor cells, astrocytes and cerebral organoids. This could be crucial for future researchers aiming to enhance the existing knowledge of the neuropathogenesis associated with DS. The current study improves the understanding of the mechanisms underlying the neurogenic-to-gliogenic shift in DS, particularly the effect of REST targeting the JAK-STAT signalling pathway on the propensity of differentiation of NPCs. In addition, this study enhances the understanding of reactive astrocytes in DS for future researchers. Restoring nuclear REST levels in trisomic astrocytes by lithium could rescue astrocyte reactivity. These contribute to a potential therapeutic strategy targeting REST for individuals with DS.

© COPYRIGHT UPM

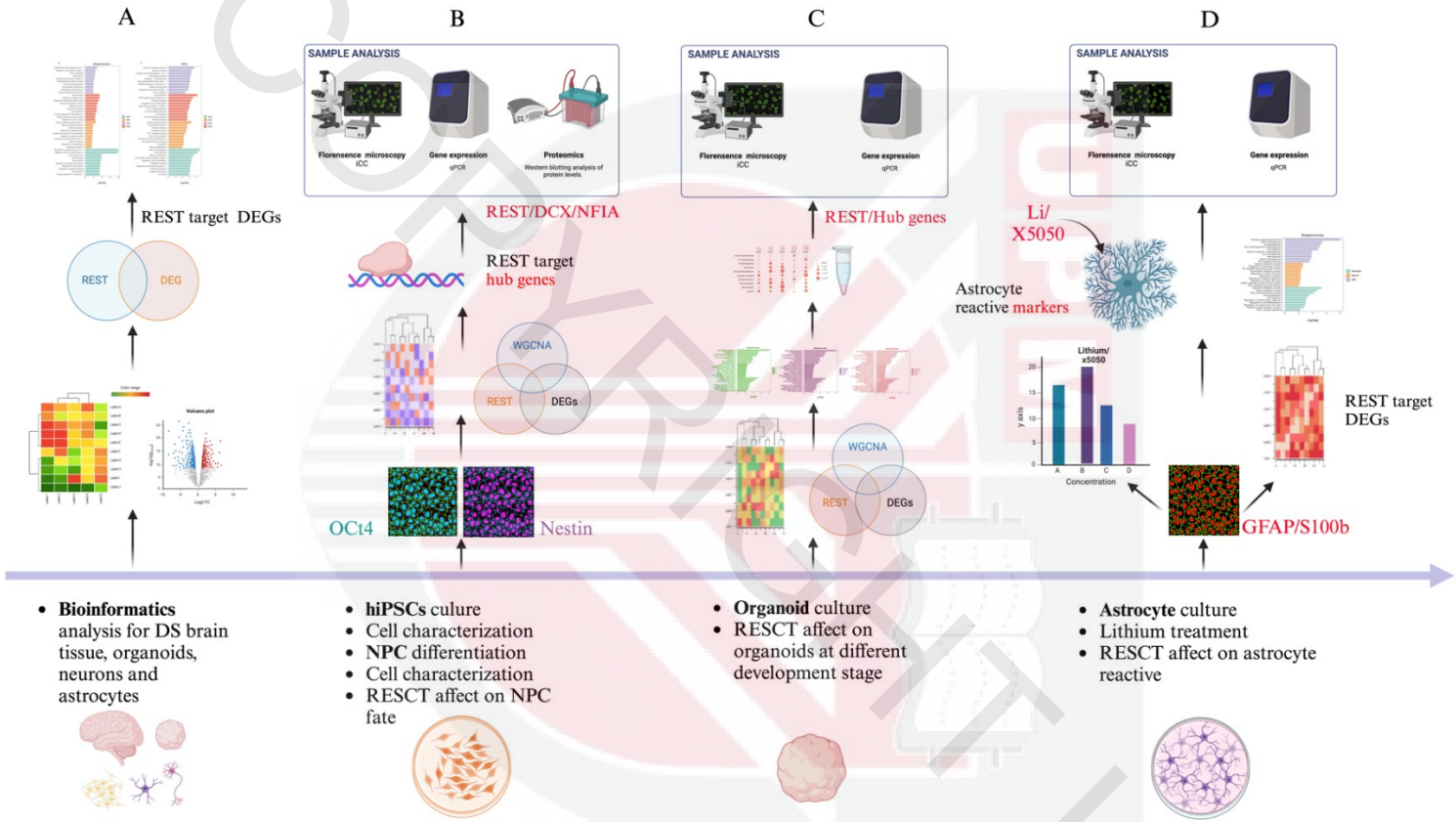


Figure 1.1 : The Overall Workflow for This Study. (A) Bioinformatics analysis was used to explore the role of REST in DS brain tissue, NPCs, neurons and astrocytes (Objective 1). (B) The effect of REST on the differentiation fate of trisomic NPCs was further verified (Objective 2). (C) The role of REST in trisomic cerebral organoids was further verified (Objective 3). (D) The effect of REST expression on the reactivity of trisomic astrocytes was explored (Objective 4-5). The figure was created in BioRender (License number: IY27UO7LLO)

© COPYRIGHT UPM

CHAPTER 2

LITERATURE REVIEW

2.1 Down Syndrome (DS)

2.1.1 Prevalence and Genetics of DS

DS is the predominant genetic factor leading to intellectual disability and the primary contributor to certain congenital anomalies and associated medical conditions (Sherman et al., 2007). The prevalence of Down syndrome has been widely studied. The estimated prevalence of DS varies between 1 in 600 and 1 in 800 live births globally (Bull, 2020; Joseph et al., 2022). Studies have shown that the prevalence of DS varies by geographic region and ethnic population. For instance, in Egypt, the prevalence rate is estimated at 1 in 600-1000 live births (Gufran et al., 2019), while in Europe, the rate of DS is 10.1 per 10,000 live births (Graaf et al., 2021). About 6.7 out of every 10,000 newborns in the United States are born with DS (Graaf et al., 2017). In Korea, the prevalence of DS is estimated at 14 cases per 10,000 births (Kwak et al., 2022). The estimated DS prevalence in China is 4.5 in 10,000 live births (Kang and Wu, 2021). In Malaysia, DS is estimated to be 1:860 to 1:981 live births (Hoe et al., 1989). Thus, the prevalence of DS is a global problem. The incidence of live births with DS is affected by factors including family size, birth spacing, the number of births, and the cultural environment (Bruckner et al., 2019; Neuhäuser and Krackow, 2007). In summary, the occurrence of DS varies among different people. It is affected by several factors, such as the age of the mother, racial and ethnic disparities, access to medical care, and demographic trends.

© COPYRIGHT UPM

Additionally, due to improved medical and social care, the life span of DS individuals has increased significantly, with an average survival of over 50 years (Glasson et al., 2002). The life expectancy of individuals with DS has improved over the past 20 years, with one-third now reaching the age of 60 or older (Motegi et al., 2021). A retrospective cohort study conducted in Sweden from 2002 to 2015 reported an average lifespan of 63.5 years for individuals with Down syndrome (Ng et al., 2017). Similarly, a cohort study of adults with Down syndrome in the United States from 2011 to 2019 found that those diagnosed with Alzheimer's disease had an average lifespan of 59.2 years (Rubenstein et al., 2024). This rise in life expectancy for DS individuals has resulted in neurologists encountering epilepsy and cognitive decline more frequently in this population (Obara et al., 2020). Furthermore, the increased longevity of individuals with Down syndrome means a greater likelihood of adverse health development and diseases associated with ageing, including dementia (Allen et al., 2023). This poses a considerable challenge in terms of healthcare and social support.

DS is primarily characterised by an extra copy of human chromosome 21 (HSA21), a disorder known as trisomy 21. In approximately 95% of cases, this arises due to maternal meiotic nondisjunction, with the risk increasing as the maternal age advances (Gardner et al., 2012; Petersen and Mikkelsen, 2000; Yoon et al., 1996). Approximately 3-4% of cases are attributed to chromosomal translocations, which commonly involve chromosome 21 with chromosome 14, 21, or 22 (Gardner et al., 2012). Translocations involving chromosomes 14/21 are present in about one-third of cases, often with the mother as the carrier (90%). This situation carries a recurrence risk of 10-15% for mothers who are carriers and 2-5% for fathers who are carriers. A

© COPYRIGHT UPM

smaller proportion (1 in 14 cases) involves a 21/21 translocation, with fathers representing 50% of the individuals carrying the translocation. A minority of cases (1-2%) present with mosaic trisomy 21, characterised by varying numbers of affected cells, a range of clinical features, and reduced complications, leading to a milder form of intellectual disability (Papavassiliou et al., 2015). Partial trisomy 21 with segmental duplications represents another uncommon variant, accounting for under 1% of all cases (Pelleri et al., 2016). The extra copy results in the upregulation of genes located on HSA21 believed to be the causative factor for the DS phenotype. However, research on the diverse manifestations associated with the DS phenotype in DS individuals remains a significant challenge.

2.1.2 Molecular Perturbation in DS

Researchers have proposed the gene dosage effect hypothesis to comprehend the intricate biological disturbances underpinning the diverse manifestations of DS. Transcriptomic analyses of DS individuals affirm an average 50% elevation in triple copy gene expression levels on HSA21 compared to the controls (Liu et al., 2017). The most direct consequence of HSA21 involvement lies in the cumulative impact of altered gene dosage on the DS phenotype (Figure 2.1). For instance, the overexpression of amyloid precursor protein (APP) leads to the accumulation of β-amyloid protein (Aβ) in the brain, heightening the susceptibility of DS individuals to early-onset AD (Sawa et al., 2022). Further exploration reveals that APP participates in various pathways, such as the Wnt signalling pathway, Notch signalling pathway, and JAK-STAT signalling pathway, coordinating the modulation of neurogenesis and gliogenesis (Coronel et al., 2023). However, in a trisomic HSA21 mouse model, reverting *APP* to a disomy state fails to fully mitigate the dosage effect (Salehi et al.,

© COPYRIGHT UPM

2006). Only 62% of the HSA21 gene in fibroblasts showed differential expression between DS and normal samples, compared to 39% in lymphoblastoid (Prandini et al., 2007). This suggests that not all trisomic genes on HSA21 undergo increased expression. The mechanisms behind this inconsistent expression level may encompass negative feedback, dosage compensation, and epigenetic alterations. Additionally, the expression of some non-HSA21 genes is perturbed in DS individuals, indicating that trisomy 21 destabilises the mechanisms of transcription and signalling pathways (Antonarakis et al., 2020). The increased transcriptional activity of genes on HSA21 might enhance or suppresse other genes activity on other chromosomes within the genome.

© COPYRIGHT UPM

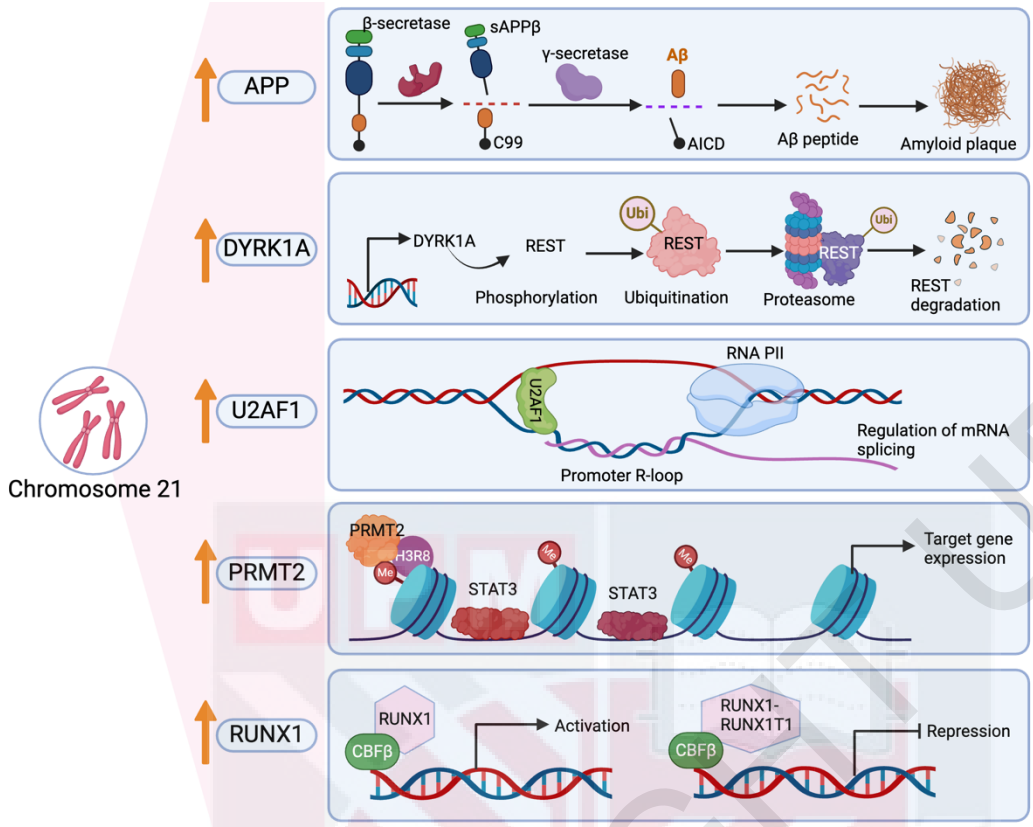


Figure 2.1 : Overexpression of Specific Genes Located on Chromosome 21 Has Been Associated with Down Syndrome Pathological Features. Overexpression of the *APP* gene, encoding an amyloid precursor protein, leads to the aggregation of Aβ42 in the brain to form amyloid plaques. An imbalance of *DYRK1A* leads to the degradation of the REST protein, a neurogenic gene-silencing transcription factor. U2AF1 protein binds to the R-loop of the promoter in cells, leading to a greater distribution of RNA polymerase II (RNAPII) on gene bodies, which regulates pre-transcriptional mRNA clipping and leads to greater distribution of RNA polymerase II (RNAPII) to promoters on the gene body, thereby regulating cotranscriptional pre-mRNA splicing. The methylation of histones by PRMT2 enhances STAT3 accessibility, resulting in the upregulation of STAT3 target genes. The heterodimerisation of *RUNX1* with *CBFβ* is essential for increased DNA binding, stability, and interaction with other transcriptional regulators, which facilitates the induction or repression of target genes. The figure was created by using Biorender.com (License number: ZJ27UPH0L8)

An alternative perspective on the biological disruptions in DS revolves around the disturbance of overall gene transcription balance. The increased expression of genes on HSA21 can disrupt the transcriptome and proteome, leading to an imbalance in protein composition and adversely affecting cellular function (Shapiro et al., 1983). Genes located on HSA21 are implicated in chromatin remodeling and transcription

control—such as *ADARB1*, which plays a critical role in adenosine-to-inosine RNA editing, the constitutive splicing factor *U2AF1* (Figure 2.1), and *DYRK1A* (a dual-specificity kinase regulating the phosphorylation of splicing factor 60)—are upregulated (Gonzales et al., 2018). This upregulation potentially alters the overall patterns of gene expression throughout the genome. The disruption of gene dosage balance in DS, particularly in the well-studied core gene *DYRK1A*, is shown to impact REST expression (Figure 2.1), thereby influencing chromosomal restructuring (Canzonetta et al., 2008). Particular genes on HSA21, including *RUNX1*, *PRMT2*, *N6AMT1*, and *MIS18A*, have a significant impact on global DNA methylation patterns (Iwasaki et al., 2010; Kim et al., 2012; Mendioroz et al., 2015; Scott et al., 1998; Xiao et al., 2018). For example, methylation of histones by PRMT2 enhances STAT3 accessibility, resulting in the upregulation of STAT3 target genes (Iwasaki et al., 2010; Sauter et al., 2024) (Figure 2.1). These HSA21 genes have a critical role in epigenetic disruptions, and their overexpression may contribute to various mechanisms of transcriptional epigenetic changes in DS. A thorough proteomic analysis of fibroblasts derived from monozygotic twins with DS uncovered significant changes in protein levels associated with both HSA21 and non-HSA21 genes (Liu et al., 2017). In-depth scrutiny of cells extracted from DS patients showed impaired autophagic function, suggesting compromised clearance of excess proteins, thus disrupting the delicate equilibrium of protein homeostasis (Krivega et al., 2021; Krivega and Storchova, 2023). The combined impact of gene dosage, the overall genome disruption, and proteome balance contribute to the biological perturbations observed in DS.

© COPYRIGHT UPM

2.1.3 Neurodevelopment Defects in DS

During the development of the brain, neurogenesis arises first, followed by astrogliogenesis, and finally oligogliogenesis, with a partial overlap of the three developmental stages (Figure 2.2) (Eck and Waltman, 2009; Synnestvedt et al., 2005; Wu et al., 2022). Neural progenitor cells (NPCs) appear on gestational day (GD) 14 during embryonic development (Stagni and Bartesaghi, 2022). Expansion of the size of neural progenitor cells (NPCs) pool by symmetric cell division of NPCs is the initial step in neurogenesis. Commencing at GD 28, NPCs undergo differentiation into radial glial cells (RGCs), engaging in asymmetric division to generate a proliferative RGC and a neuron (Bystron et al., 2008). Initiating at gestational week (GW) 16, RGCs gradually undergo differentiation into astrocytes and oligodendrocytes, marking a transition from a neurogenic to a gliogenic cell fate, commonly referred to as the "gliogenesis switch" (Stagni and Bartesaghi, 2022). However, in the developmental trajectory of the brain in individuals with DS, the normal spatiotemporal line of neurogenesis is disrupted (Figure 2.2 C), resulting in diminished proliferation of NPCs and impaired functionality in neurogenesis (Stagni et al., 2018a). In DS, the brain exhibits weight, volume, and linear size reductions, with decreased neurons and increased astrocytes (Stagni et al., 2018a, 2018b). This neuropathologic feature of DS is known as the neurogenic-to-gliogenic shift.

© COPYRIGHT UPM

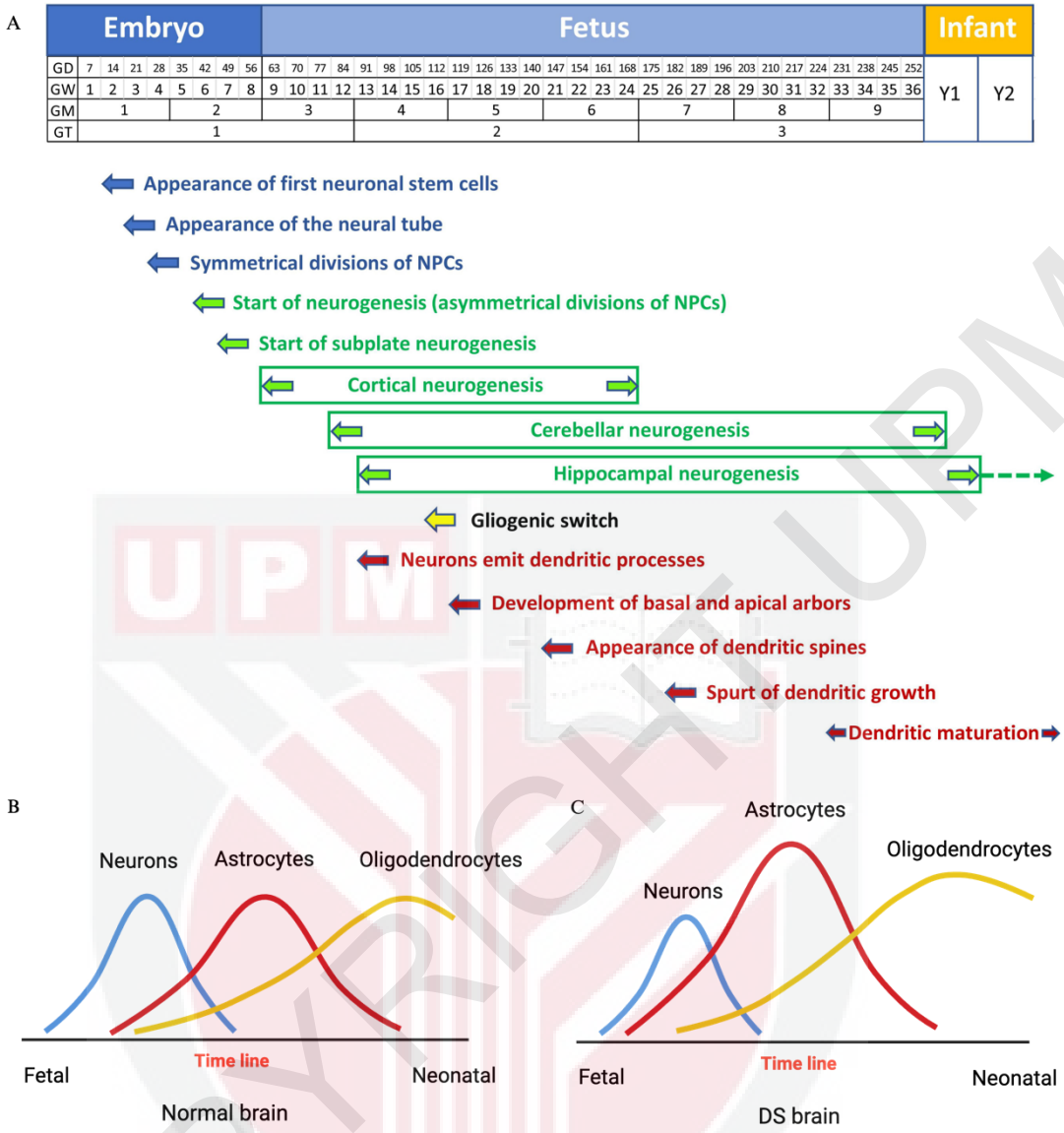


Figure 2.2 : Timeline of Differentiation and Development of Neural Cells. (A) Timeline depicting the generation of NPCs, neurogenesis, gliogenesis, and neuron maturation in the normal human brain. (B) The relative timing and quantity of neurons, astrocytes, and oligodendrocytes produced during typical human development. (C) Relative timelines of disrupted neurogenesis and gliogenesis in the DS brain (Stagni and Bartesaghi, 2022)

In the prenatal period of DS diagnosis (17-21 GW), a consistent decrease in the number of proliferating NPCs is evident in various brain regions, including the dentate gyrus, lateral ventricle germinal matrix, and third ventricle (Contestabile et al., 2007; Stagni et al., 2020). This reduction in proliferation appears to result in a diminished NPC pool, particularly noted in the mid-gestation (18-24 GW) fetal brain development

© COPYRIGHT UPM

of DS-affected fetuses in the outer subventricular zone, where there is a lower count of SOX2+ cells, potentially restricting the production of neural cells (Baburamani et al., 2020). The primary neurodevelopmental anomaly identified in DS grey matter is the diminished generation of neurons. In the same gestational period (17-21 GW), fewer neurons are observed in the hippocampus, cerebellum, and multiple thalamic nuclei (Guidi et al., 2011, 2008; Stagni et al., 2020). Adolescents and adults with DS (15-35 years) consistently demonstrate a persistent reduction in the number of cells in the temporal gyri, resulting in a reduced neuronal population (Giffin et al., 2022). Furthermore, individuals with DS show significant reductions in dendritic length and spine numbers compared to control groups. These pathological features are reported in various age groups, ranging from infants (0-12 months) to children, young individuals (3-23 years), and middle-aged individuals (47-55 years) (Ferrer and Gullotta, 1990; Suetsugu and Mehraein, 1980; Takashima et al., 1981). Therefore, the diminished neurogenesis and abnormal development of neuronal dendrites and spines persist from fetal to adulthood.

Distinctions in glial cells, particularly astrocytes, are observed in the central nervous system (CNS) of individuals with DS. The increase in astrocyte generation aligns with the decrease in neurogenesis. Developing fetuses with DS (17-21 GW) exhibit increased astrocytes in the inferior temporal gyrus, cingulate gyrus, and frontal lobe (Guidi et al., 2018; Zdaniuk et al., 2011). Immunostaining to GFAP is elevated compared to control tissues, and astrocytes display a more active morphology (Chen et al., 2014). In summary, individuals with DS display atypical neurodevelopment, characterised by developmental anomalies across multiple stages and various types of neural cells. These effects persist into adulthood, forming the neurobiological basis

© COPYRIGHT UPM

for the diverse neurological phenotypes observed in DS, including early-onset Alzheimer's disease, neuroinflammation, and intellectual disabilities.

2.2 Repressor Element-1 Silencing Transcription (REST)

2.2.1 REST and Its Target Genes

The RE1 silencing transcription factor (REST), also referred to as neuron-restrictive silencer factor (NRSF), plays a vital role in regulating gene expression across many cell types, with a particular emphasis on neural cells (Su et al., 2022; Thiel et al., 2015). REST exerts its regulatory function by binding to a specific DNA motif, a conserved 23 bp DNA pattern, called the RE1 (repressor element 1) near its target genes (Butler-Ryan and Wood, 2021). Upon binding, REST recruits corepressors such as CoREST, mSin3A, and other repressive mechanisms to the chromatin, thereby preventing the transcription of REST-targeted genes (Figure 2.3). Additionally, REST has been demonstrated to influence the alternative splicing of its transcripts, thereby affecting the expression of REST-targeted genes (Burkholder et al., 2018). Estimations indicate the presence of approximately 1000-2000 RE1 regulatory elements in the human genome, characterised by the known RE1 consensus sequence (Bruce et al., 2004; Johnson et al., 2006). The dynamic occupancy of REST at RE1 sites is contingent upon cellular REST levels (Ballas et al., 2005). Beyond its association with neuronal genes, the occupancy of REST at RE1 sites extends to specific non-neuronal genes in the human genome, showcasing the broader regulatory influence of REST in gene expression (Marullo et al., 2010).

© COPYRIGHT UPM

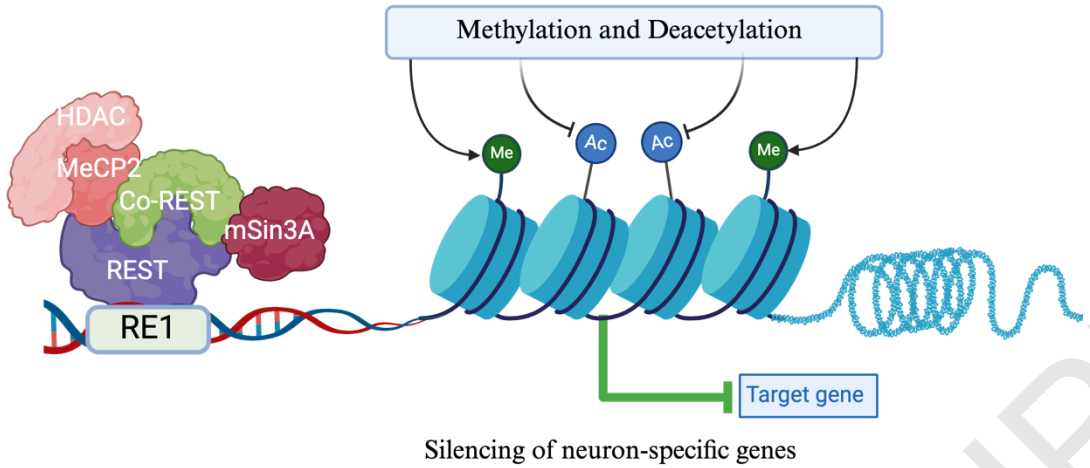


Figure 2.3 : REST Regulates Gene Silencing through Histone Modification. REST is bound to the RE1 motif of target genes and recruits Sin3A, CoREST, and co-regulators to form a regulatory complex to regulate target gene expression. The figure was created by using Biorender.com (License number: JR27UPH0N1)

Comprehensive genomic analyses have pinpointed REST binding sites in 1,892 human and 1,894 mouse genes (Bruce et al., 2009). Utilising ChIP-seq, researchers uncovered 2,172 REST-targeted genes in human embryonic stem cells (ESCs) and 308 REST-targeted genes in neurons differentiated from ESCs (Rockowitz and Zheng, 2015; Satoh et al., 2013). A recent study of the human hippocampus revealed 1,735 REST target genes (McGann et al., 2021). Abrajano et al. employed ChIP-chip to scrutinise RE1 binding sites in all mouse-derived glial cells, identifying 3,178 REST-targeted genes and 4,060 CoREST-targeted genes (Abrajano et al., 2009). The GTRD (Kolmykov et al., 2021) reveals 15,450 REST-targeted genes in the human genome by analysis of Chip-seq datasets. Single-cell transcriptome analysis shed light on relatively modest levels of REST transcripts across the adult hippocampus, with the highest concentration observed in astrocytes (males aged 40-65) (Habib et al., 2017). While REST transcript levels were more pronounced in neural stem cells than other neural glial subtypes, these cells represented a minority of the total cell population

© COPYRIGHT UPM

(Zhang et al., 2016). Thus, these findings strongly propose astrocytes as a potential primary source of REST binding sites throughout our genome.

2.2.2 Role of REST in Brain Development

Compelling evidence underscores the central role of REST in the intricate processes of brain development, playing a crucial part in regulating neural progenitor/stem cells, neurogenesis, gliogenesis, modulation of neuronal gene expression, and the preservation of neural cell phenotypes (Baldelli and Meldolesi, 2015; Johnson et al., 2008; Thiel et al., 2015). The CNS developmental progression depends on the tightly regulated expression of REST within neural cells. During the early stages of CNS development, REST demonstrates heightened expression levels in ESCs and NPCs (Johnson et al., 2008). Its function involves silencing a specific set of neuron-specific genes in NPCs, thereby preserving the undifferentiated state of NPCs/neural stem cells (NSCs) (Aoki et al., 2016). Notably, REST also upholds an inhibitory chromatin state in embryonic hippocampal NSCs, contributing to the epigenetic regulation of neural genes (Greenway et al., 2007). REST has been demonstrated to regulate radial migration and the timing of neuronal specification throughout neocortical development, underscoring its pivotal role in coordinating the spatiotemporal transition of NPCs into neurons (Mandel et al., 2011).

The neural cell types in the CNS—neurons, astrocytes, and oligodendrocytes—originate from a shared NPC. The fate of these distinct neural lineages is intricately governed by the dynamic expression levels of REST in NPCs. REST stability or degradation is regulated by two key mechanisms: (1) REST recruits C-terminal domain small phosphatase 1 (CTDSP1) to neuronal genes, stabilising REST in

© COPYRIGHT UPM

NPCs/NSCs and promoting their self-renewal. Concurrently, (2) ERK-dependent phosphorylation and the activation of peptidyl-prolyl cis/trans isomerase (Pin1) trigger REST degradation in NPCs/NSCs, directing them toward neuronal differentiation (Burkholder et al., 2018; Nesti et al., 2014). The diminished levels of REST alleviate the inhibition of the set of neuron-specific genes, leading to their upregulation and driving NPCs to differentiate into neurons (Soldati et al., 2012). REST maintains a low expression level in mature neurons, contributing to the regulation of axonal function and synapse plasticity (Baldelli and Meldolesi, 2015). REST orchestrates the formation and diversity of the glial lineage, with its expression activated and sustained during NPC differentiation into astrocytes via BMP signalling (Kohyama et al., 2010). This activation promotes the maturation and expression of phenotypic factors in astrocytes. Investigations reveal that REST exhibits distinct target gene profiles in different glial cell subtypes, emphasising their predominantly non-overlapping and developmentally stage-specific regulatory roles in the neuroglial lineage (Abrajano et al., 2009). However, the precise mechanisms governing the regulation of REST in NPC fate transitions, and the formation of diverse glial lineages warrant further exploration.

2.2.3 REST Dysregulation in Neurodegenerative Disorders and DS

Abundant research indicates REST dysregulation in various neurodegeneration disorders, such as AD, PD, and HD (Figure 2.4) (Garcia et al., 2019; Hwang and Zukin, 2018; Wei et al., 2022). The disruption of REST and its epigenetic reshaping has been identified as a pivotal mechanism in progressive neurodegeneration in these diseases (Hwang and Zukin, 2018). In a healthy brain, wild-type Huntington protein (HTT) prevents REST nuclear translocation by sequestering it in the cytoplasm, thereby

© COPYRIGHT UPM

silencing REST activity. However, in HD, mutated Huntington protein disrupts this complex, releasing rab-interacting lysosomal protein (RILP), which binds directly to REST, promoting its nucleus translocation to the nucleus (Nho et al., 2015; Ravache et al., 2010). The aberrant nuclear accumulation of REST in the nucleus leads to the excessive suppression of numerous REST-targeted genes, causing functional impairments in neurons, including disruptions in neural development, ion channels, synaptic plasticity, and neuronal cell death regulation (Conforti et al., 2013; Nho et al., 2015). Interestingly, in the context of AD and PD, the pathogenic mechanism of REST is opposite to that of HD, where REST is lost in the nucleus. In AD, REST is lost from the cell nucleus but co-localizes with misfolded pathological proteins, including amyloid-beta proteins and tau, within autophagosomes (Tecalco et al., 2020; Zhao and Huai, 2023). Studies suggest that activated autophagosomes in AD accelerate REST degradation (Lu et al., 2014; Zhao and Huai, 2023). In PD, the decrease in nuclear REST levels has been noted in dopaminergic neurons affected by PD, while elevated REST expression is found in pathological structures such as Lewy bodies and pale bodies (Kawamura et al., 2019). The primary component of Lewy bodies, α-synuclein, has been discovered to bind to REST and appears in autophagosomes, leading to the sequestration and degradation of REST (Kawamura et al., 2019). Therefore, targeting the regulation of REST nuclear translocation holds therapeutic potential for treating neurodegenerative diseases.

© COPYRIGHT UPM

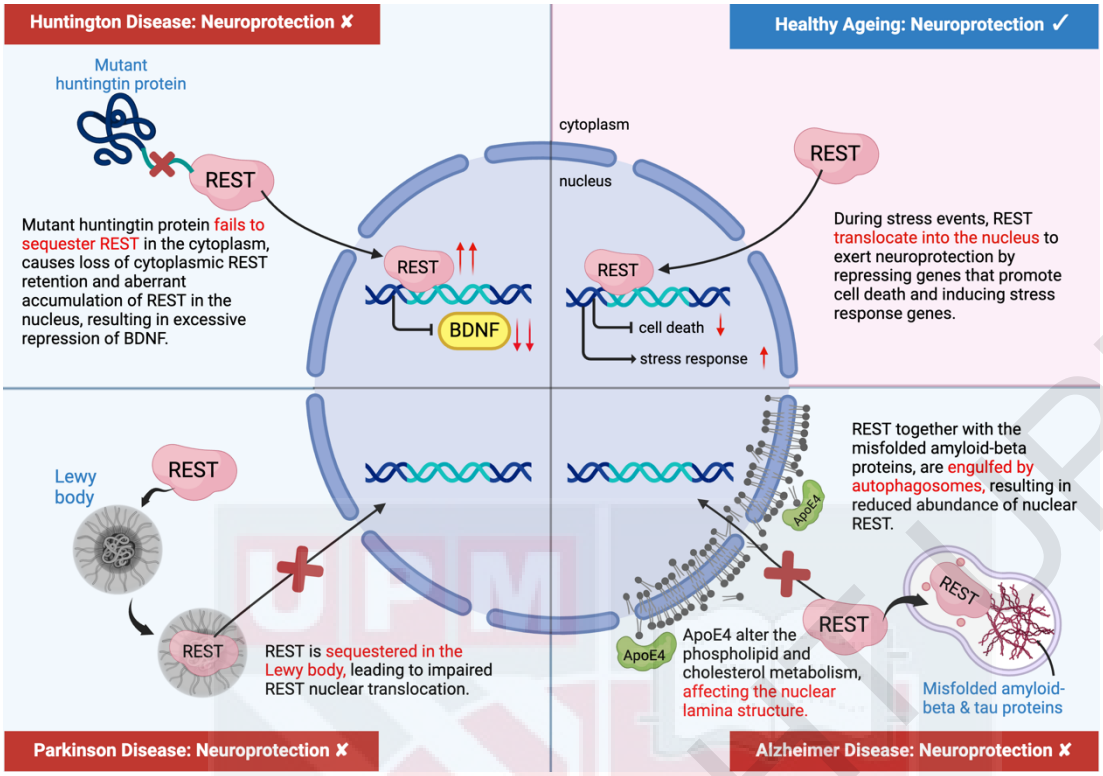


Figure 2.4 : Mechanisms of REST Dysregulation in Different Neurodegenerative Diseases. Nuclear translocation of REST plays a neuroprotective role in the healthy aged brain. Impaired nuclear translocation of REST in PD and AD leads to upregulation of REST target genes, causing corresponding neuropathology. In HD, excessive nuclear translocation of REST leads to over-repression of important gene expression (Lam et al., 2023)

Research into DS has uncovered significant dysregulation of the REST in the brain. An early study revealed a significant reduction in the expression of REST and the splice variants in NPCs derived from fetuses with DS. This downregulation correlated with increased apoptosis in differentiating neuronal cells, resulting in shortened, twisted neurites and abnormal overbranching (Bahn et al., 2002). In the fetal cortex, NPCs of individuals with DS, REST, and its targets show a notable downregulation, indicating a link to observed neurodevelopmental disturbances (Dauphinot et al., 2005). However, studies on REST expression in DS mouse models have shown inconsistent findings. Bahn et al. reported REST downregulation in Ts1Cje mice related to wild-type mice (Bahn et al., 2002). In trisomy 21 mouse brains, the REST

level was reduced by 30% to 60%, persisting from undifferentiated embryonic stem cells to the adult brain (Canzonetta et al., 2008). Conversely, REST expression was elevated in embryos of the 152F7 DS mouse model but reduced in postnatal mice (Aude Marie Lepagnol-Bestel et al., 2009). A recent study examining the spatiotemporal dynamics of REST in the Ts1Cje mouse model revealed a marked downregulation in neurospheres cultured from embryonic DS and in the brains of adult DS mouse. The study also highlighted defective REST nuclear translocation in the Ts1Cje mouse brain (Lim et al., 2024). A potential explanation is that REST dysregulation in DS may be attributed to the dosage imbalance of the *DYRK1A*, a gene located on HSA21. A complex regulatory feedback mechanism exists between *DYRK1A* and *REST*: REST enhances DYRK1A expression by binding to promoter regions of the *DYRK1A* gene, whereas an imbalance in *DYRK1A* dosage leads to REST deactivation through ubiquitination and subsequent proteasomal degradation. However, the downregulation of REST expression, impaired nuclear translocation, and their impact on neurodevelopment in DS neural cells require further investigation (Lu et al., 2011).

2.3 Neural Progenitor Cell (NPC) in Down Syndrome

2.3.1 Fate Determination of NPC

NPCs exhibit remarkable capabilities in differentiating into various cell types in the CNS. Previous research indicates that these cells can generate neurons, oligodendrocytes, and astrocytes (Imayoshi et al., 2013). The fate determination of NPCs is intricately governed by many signalling pathways and molecular mechanisms, with notable involvement from the NOTCH, WNT, and JAK-STAT signalling

© COPYRIGHT UPM

pathways (Figure 2.5). In the early phases of neural progenitor cell development, the Notch signalling pathway is pivotal in promoting self-renewal and suppressing differentiation, thus maintaining these cells in a stem cell-like state of these cells (Ramasamy and Lenka, 2010). Notably, Notch signalling also orchestrates the balance between the symmetric and asymmetric division of NPC, which is crucial for acquiring radial glia cell (RGC) identity (Ohata et al., 2011). Notch-deficient RGCs display an early onset of neurogenesis and a loss of apical-basal polarity, highlighting the crucial role of Notch in both the initiation of RGC development and the preservation of their undifferentiated state (Imayoshi et al., 2010).

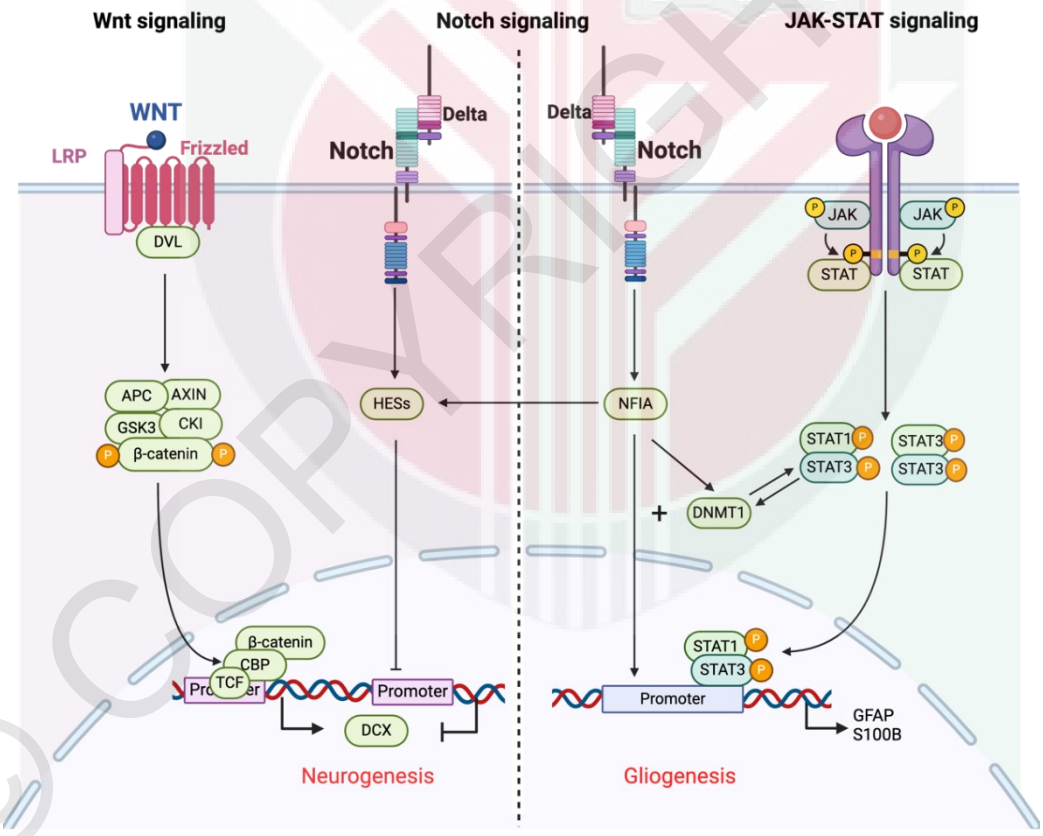


Figure 2.5 : Regulation of Neural Progenitor Cell Fate by Critical Signalling Pathways. Activation of the Wnt signalling pathway enhances neurogenesis and contributes to the differentiation of NPCs towards neurons. Activation of the Notch signalling pathway and the JAK-STAT signalling pathway inhibits neurogenesis and enhances gliogenesis, contributing to the differentiation of NPCs towards glial cells. The figure was created by using Biorender.com (License number: SR27UPHQMG)

© COPYRIGHT UPM

In neurogenesis, the WNT signalling pathway emerges as a critical regulator. Activation of the Wnt pathway has been demonstrated to enhance neurogenesis, whereas its inhibition hinders the NPCs proliferation and differentiation of neural progenitor cells (Knotek et al., 2020). Wnt signalling promotes the maturation of RGCs and guides them towards neuronal fate by regulating key factors such as N-myc and the proneural gene Neurogenin1(Hirabayashi et al., 2004; Kuwahara et al., 2010). Glycogen synthase kinase 3 (GSK-3) exerts a central role in neurodevelopment and adult neurogenesis, operating in opposition to the classical Wnt/β-catenin signalling pathway (Cheng et al., 2020; Yu et al., 2019). Activation of the JAK-STAT signalling pathway causes a shift in the differentiation fate of NPCs from neurogenesis to gliogenesis (Lee et al., 2016). During the neurogenic phase, the activity of the JAK-STAT signal in NPCs remains subdued. This phenomenon is largely attributed to the methylation of genes linked to the STAT pathway, which is mediated by transcriptional co-activators, including CREB-binding protein (CBP), p300, and Smad1 (Fan et al., 2005; He et al., 2005). However, this suppression of methylation and sequestration is relieved by the Notch signalling transduction, and STAT factor positive self-regulatory activity enhanced (He et al., 2005). Notch receptors form transcriptional activation complexes on the GFAP promoter, facilitating the transition between RGC states (Grandbarbe et al., 2003). This prevents the differentiation of RGCs into neurons while promoting their differentiation into astrocytes. Furthermore, Notch signalling can directly activate nuclear factor IA (NFIA) within neural progenitor cells. The collaborative action of NOTCH and NFIA results in the demethylation of astrocytic gene promoters like *GFAP* and *S100B*, accomplished through the displacement of DNA methyltransferases (Namihira et al., 2009). This

© COPYRIGHT UPM

renders these promoters responsive to further activation of JAK-STAT. Thus, integrating Notch and JAK-STAT pathways provides robust signals for gliogenesis.

2.3.2 Dysregulation of NPC in DS

Dysfunctions and anomalies in DS NPCs involve alterations in proliferation, differentiation, gene expression, and signalling pathways critical for neurodevelopment (Klein et al., 2022). Overexpression of cell cycle protein D1 in neural stem cells correlates with shortened G1 phase, delayed neurogenesis, and increased basal progenitor proliferation, highlighting the impact of cell cycle dysregulation on NPC proliferation (Lange et al., 2009). Mitotic dysregulation in NPCs can lead to excessive apoptosis or premature differentiation, resulting in diminished NPC pools (Mo et al., 2023). Research indicates significant impairment in neurogenesis in brain organoids derived from DS patient iPSCs, showing reduced proliferation and decreased expression of specific neuronal markers (Tang et al., 2021). However, further research is essential to elucidate the neurogenic-to-gliogenic shift resulting from the preferential gliogenic fate acquisition of DS NPCs.

The impaired neurogenesis of DS NPCs involves dysregulation of key genes controlling neurogenesis. Dysregulation of NPC biology-related gene expression may be a critical factor contributing to changes in proliferation and reduced interneuron differentiation (Bhattacharyya et al., 2009). One significant factor is the overexpression of *DYRK1A*, a gene associated with DS, identified as a major contributor to impaired neurogenesis of DS hiPSC-derived NPCs and neurons (Hibaoui et al., 2014). *DYRK1A* overexpression leads to premature neuronal differentiation yet impaired neuronal maturation (Soppa et al., 2014). Overexpression

© COPYRIGHT UPM

of *Olig2* in NPCs has been shown to impair proliferation, resulting in neurogenic defects and neuronal cell death, contributing to brain development abnormalities in DS (Lu et al., 2012). The *Usp16* elevated in DS NPCs results in defects in proliferation and self-renewal (Xu et al., 2013). In addition, Multiple signalling pathway transduction dysfunctions occur in DS NPCs. Dysregulation of Notch signalling transduction is associated with alterations in neural progenitor fate determination, leading to abnormal neurogenesis in DS (Aguirre et al., 2010; Yang et al., 2004). Notch signalling is involved in regulating the transition between neurogenesis and gliogenesis, playing a role in determining the fate of NPCs in DS (Sanalkumar et al., 2010). Furthermore, previous work has shown that the JAK-STAT signalling pathway has a crucial role in the neurogenic-to-gliogenic shift in the brain with DS (Lee et al., 2016). The JAK-STAT signalling pathway upregulation triggers the expression of *S100B*, *GFAP*, and *Vimentin*, further promoting astrocyte differentiation (Cau and Blader, 2009).

2.4 Astrocyte Homeostasis and Reactivity

2.4.1 Homeostasis of Astrocyte

Astrocytes, one of the most prevalent and functionally intricate glial cell types in CNS, have a critical role in maintaining CNS homeostasis. Astrocytes manifest distinct subtypes, including protoplasmic astrocytes (GFAP+/S100B+) in grey matter, characterised by complex morphologies and numerous processes, and fibrous astrocytes (GFAP+/S100B–) in white matter, characterised by fewer but longer processes (Bushong et al., 2002; Du et al., 2021; Oberheim et al., 2009). Mature astrocytes are actively engaged in essential processes related to homeostasis in the

© COPYRIGHT UPM

CNS (Figure 2.6), such as the cycling of neurotransmitters, ionic homeostasis, regulation of synapse formation, neuroimmunomodulation, and synaptic transmission, and the maintenance of the blood-brain barrier (BBB) (Abbott et al., 2006; Alvarez et al., 2013; Volterra and Meldolesi, 2005).

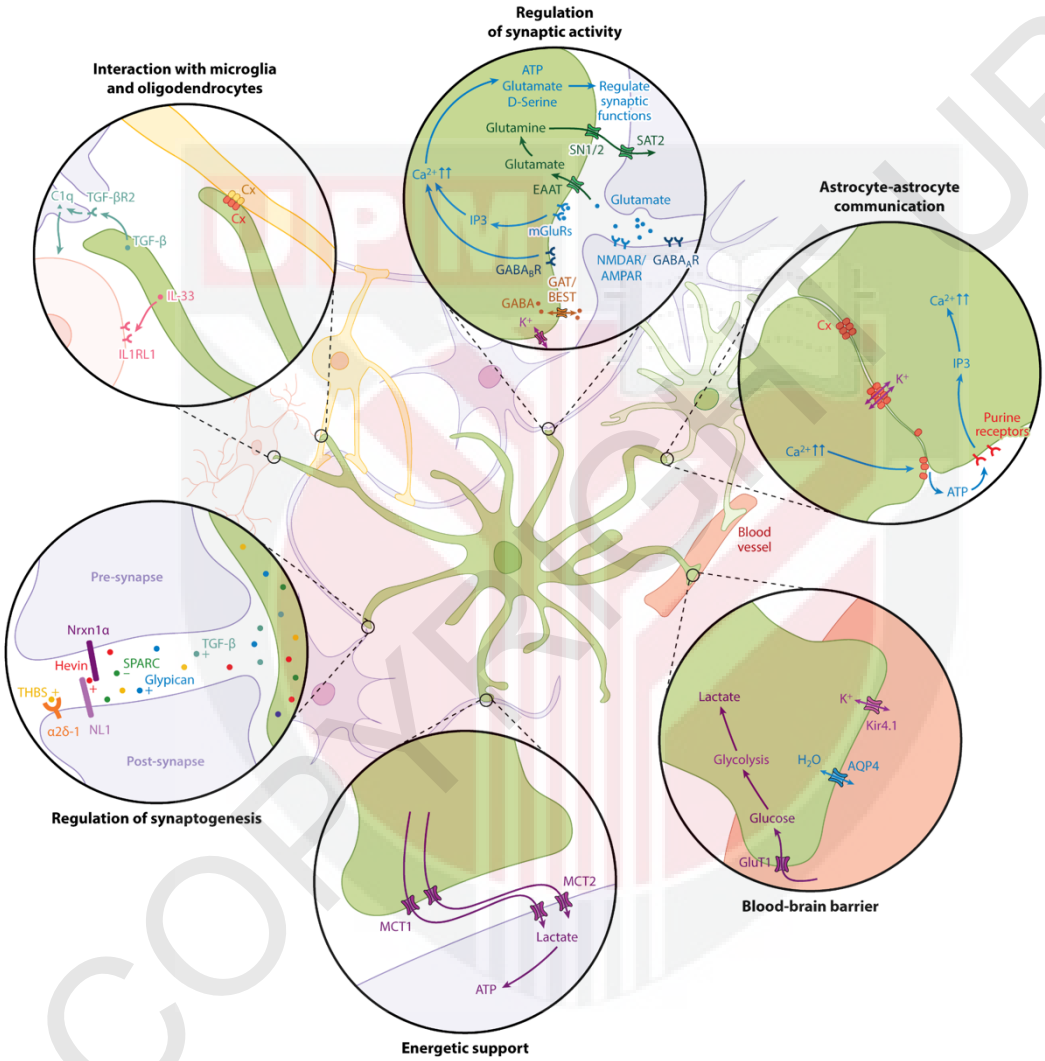


Figure 2.6 : The Various Functional Roles Played by Astrocytes in the Brain. Astrocytes Perform Various Important Functions, Including Involvement in the Blood-Brain Barrier, Synapse Formation, Ion Homeostasis, Neurotransmitter Regulation and Secretion of Neuroactive Factors (Khakh and Deneen, 2019)

Astrocytes play a pivotal role in maintaining glutamatergic homeostasis within the CNS by finely regulating the balance of the uptake and release of glutamate

(Mahmoud et al., 2019). Glutamate, the predominant excitatory neurotransmitter in the CNS, can induce excitotoxicity, leading to neuronal cell death when excessively accumulated in the synaptic cleft (Meldrum, 2000). In response to such conditions, astrocytes employ glutamate transporters, Excitatory Amino Acid Transporter 1 (EAAT1) and EAAT2, to efficiently clear extracellular glutamate from the synapse. This intricate process orchestrated by astrocytes is pivotal for glutamate homeostasis, synapse plasticity, and neuronal cell survival (Anderson and Swanson, 2000; Bylicky et al., 2018). Moreover, astrocytes play a critical role in preserving the ion balance of nerve cells. They modulate potassium and glutamate homeostasis through inward rectifying potassium channels, which are indispensable for maintaining normal neuronal excitability (Kinboshi et al., 2020; Ohno et al., 2021). Astrocyte energy metabolism is a critical component to maintaining brain energy homeostasis. In a cooperative metabolic relationship with neurons, astrocytes respond to neuronal activity by employing mitochondrial β-oxidation to utilise stored fatty acids from lipid droplets within neurons. This intricate lipid metabolism mechanism, interlinked between neurons and astrocytes, serves as a protective barrier, shielding neurons from the toxic effects of fatty acids and oxidative stress damage (Ioannou et al., 2019). The involvement of lipid metabolism in astrocyte structure and function has been established to connect astrocytic β-oxidation with inflammation and mitochondrial energy production in neurons (Lee et al., 2021). Disruption of astrocytic homeostasis is strongly associated with excitotoxicity, dysregulated synaptic activity, neuroinflammation, and oxidative stress.

© COPYRIGHT UPM

2.4.2 Reactive Astrocytes

Astrocytes responding to various injuries to the brain, including trauma, infection, ischemia, and neurodegeneration, astrocytes are activated from their resting state. The activated astrocytes are reactive astrocytes classified as type A1 and type A2 (Figure 2.7) (Escartin et al., 2021). Common features of A1/A2 astrocytes include cell body and protrusion hypertrophy and heightened number and elongation of protrusions. However, A1 astrocytes exhibited lengthy dendrites in living brains and laboratory conditions (Zou et al., 2019), whereas A2 astrocytes showed hypertrophy and fewer dendrites (Althammer et al., 2020). A1 astrocytes upregulate *GFAP*, *S100B*, and complement protein C3 levels, causing pro-inflammatory responses and neurotoxic substance release (Figure 2.7) (Escartin et al., 2021; Zou et al., 2019). A1 astrocytes also gather and release pro-inflammatory cytokines, including *TNF-α*, *interleukin 1 (IL-1)*, and interleukin *6 (IL-6)*, near amyloid plaques (Cai et al., 2017; Shi et al., 2017). These astrocytes have the capability to elevate reactive oxygen species (ROS) production, express inducible nitric oxide synthase (iNOS), and release the neurotoxin D-serine, ultimately resulting in neuronal apoptosis (Fan and Huo, 2021). Nevertheless, A2-reactive astrocytes upregulate *EAAT1*, *EAAT2*, *S100A10*, and *pentraxin-3* (PTX3), which have anti-inflammatory properties and neuroprotective effects (Figure 2.7) (Escartin et al., 2021; King et al., 2020). A2 astrocytes support neuronal survival and remodelling by increasing the expression of advantageous neurotrophic and inflammatory factors, including HIF (hypoxia-inducible factor), *IL-4*, *interleukin 10 (IL-10)*, and platelet-responsive proteins. These factors confer protective effects on neurons directly or indirectly (Ding et al., 2021; Escartin et al., 2021).

© COPYRIGHT UPM

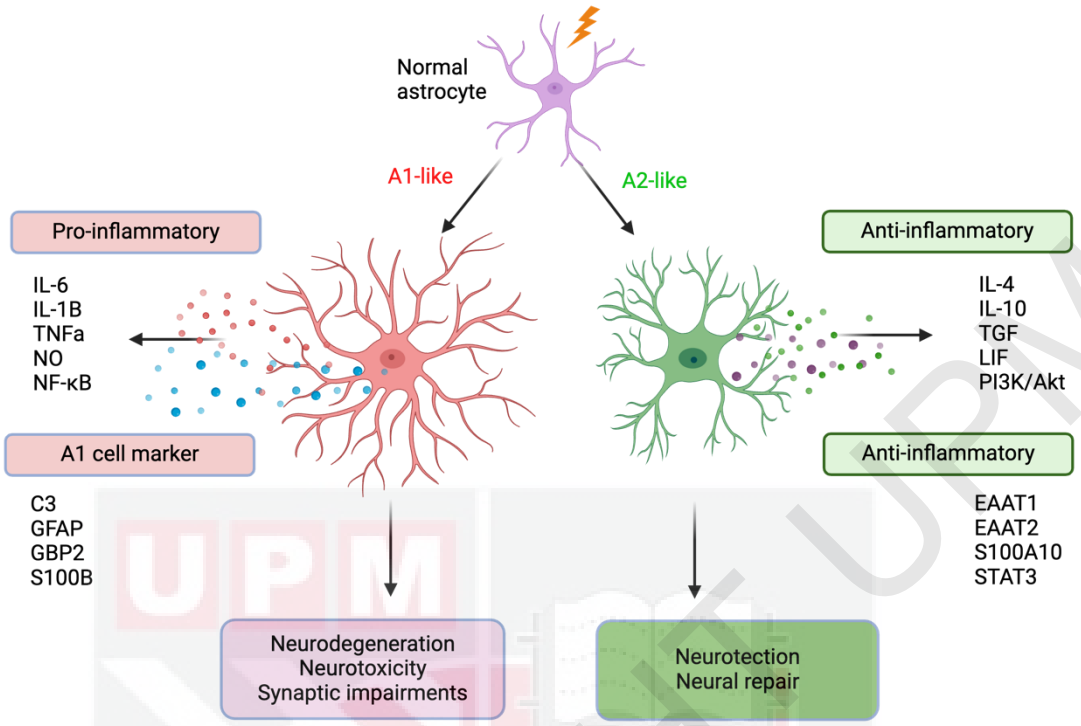


Figure 2.7 : Characterisation of A1 and A2 Reactive Astrocytes. A1-reactive astrocytes enhance the secretion of pro-inflammatory factors with neurotoxic effects. A2-reactive astrocytes enhance the secretion of anti-inflammatory factors with neuroprotective functions. A2-reactive astrocytes enhance the secretion of anti-inflammatory factors with neuroprotective functions. This figure was created in BioRender (License number: WH27UPH0OD)

Various signalling pathways and transcription factors, including NF-κB and STAT3, regulate astrocytic responses in neurodegenerative diseases. Selective inhibition of NF-κB can suppress astrocyte activation, reduce the release of astrocyte-derived chemokines, and mitigate secondary inflammatory damage in CNS diseases (Liu et al., 2019). NF-κB activation is associated with the formation of A1-type reactive astrocytes, while its inhibition is linked to the formation of A2-type reactive astrocytes, indicating the intricate involvement of NF-κB in astrocyte polarisation and function (Guo et al., 2021). Furthermore, STAT3 is recognised as a pivotal transcription factor in reactive astrocytes (Ben Haim et al., 2015; Ceyzériat et al., 2016). The early activation of STAT3 is associated with regulating the proliferation of reactive

astrocytes induced by various forms of neurotoxicity (Ceyzériat et al., 2016). The involvement of the JAK-STAT3 pathway in astrocyte activation is documented in a range of conditions, including spinal cord injury, AD, ischemia, and additional neurodegenerative disorders (Ceyzériat et al., 2018; Herrmann et al., 2008). Previous research indicates that blocking STAT3 activation reduces markers of reactive astrocytes and stress-related transcripts (Qian et al., 2019). Recent research demonstrated that the JAK2-STAT3 pathway promotes the beneficial protein homeostatic response in reactive astrocytes in HD (Abjean et al., 2023). Therefore, the JAK-STAT3 pathway may mediate the activation of reactive astrocytes.

2.4.3 Astrocyte Reactivity in Neurodegenerative Disorders and DS

Increasing research attention is directed towards understanding the role of reactive astrocytes in neurodegenerative disorders, including AD, PD, and HD. Reactive astrocytes can be categorised into two primary subtypes: A1 and A2. A1 reactive astrocytes are associated with neurotoxic effects, while A2 reactive astrocytes are believed to exert neuroprotective functions (Wang and Li, 2023; Zhang et al., 2020). Numerous studies emphasise the dual nature of reactive astrocytes in the context of neurodegeneration.

Recent evidence indicates that different states of reactive astrocytes correlate with specific stages of AD (Preman et al., 2021). Postmortem examination of AD brains reveals the coexistence of A1 and A2 reactive astrocytes, with an increase in A2 reactive astrocytes potentially exerting a protective role (Zhang et al., 2023). Studies suggest that diminishing the presence of A1 reactive astrocytes can ameliorate pathology in AD (Gomez-Arboledas et al., 2018; Price et al., 2021). Inhibiting STAT3

© COPYRIGHT UPM

has shifted the A1 reactive astrocyte phenotype towards the A2 phenotype in AD models, indicating its potential as a therapeutic target for modulating astrocyte reactivity in this condition (Ding et al., 2021). In PD, astrocytes exhibit disease-associated reactive phenotypes, with their activation predicting the latent period and contributing to disease progression (Makarava et al., 2021). Upregulation of oxidative/nitrosative stress in astrocytes promotes PD pathogenesis, and reactive astrocytes secrete lipocalin-2, contributing to neuronal death, further supporting the involvement of A1 reactive astrocytes in PD pathogenesis (Bi et al., 2013; Rizor et al., 2019). In HD individuals brain, A1 reactive astrocytes may contribute to the pathogenesis at various stages of the disease (Cong et al., 2023). Analysis of gene expression for astrocyte markers at various stages of disease progression indicates that pro-inflammatory astrocyte markers are upregulated in the third stage but not in the earlier stages (Diaz et al., 2019). These reactive astrocytes are associated with the loss or dysfunction of striatal neurons in HD (Diaz et al., 2019).

The reactivity of astrocytes is linked to various aspects of DS pathology, including disrupted neuronal development, compromised synaptogenesis and synaptic density, excitotoxicity, and neuroinflammation (Ponroy Bally and Murai, 2021). Studies indicate that astrocytes in DS exhibit altered transcriptomic features, adhesive capabilities, and increased cell dynamics, influencing neuronal development and survival (Ponroy Bally et al., 2020; Ponroy Bally and Murai, 2021). Elevated levels of neuroinflammation, including cytokines such as interleukins, interferons, and other inflammatory factors, have been observed in individuals with DS (Flores et al., 2020). Overexpression of genes on chromosome 21, such as *S100β* and genes associated with neuroinflammation (*IFNAR1*, *IFNAR2* and *PRMT2*), may lead to astrocyte activation

© COPYRIGHT UPM

and the subsequent release of pro-inflammatory mediators (García and Flores, 2022; Meraz et al., 2013). Research confirms that the overexpression of the S100β gene in DS is linked to early and robust activation of astrocytes (Royston et al., 1999). Increased *GFAP* expression in cerebrospinal fluid and plasma is also observed in individuals with DS (Montoliu et al., 2023). Notably, both GFAP and S100β are crucial markers of reactive astrocytes. Furthermore, astrocytes in DS have been found to accumulate intracellular amyloid-beta 42 (Aβ42), a hallmark of AD pathology (Busciglio et al., 2002). Therefore, A1/A2 reactive astrocytes, implicated in the pathogenesis of AD, may be present in DS. However, there is currently limited information regarding reactive astrocytes in DS, and their exact pathogenic mechanisms remain unclear.

2.5 Lithium

2.5.1 Neuroprotective Effects of Lithium

The neuroprotection potential of lithium in neurological disorders has sparked significant interest. Studies have elucidated that the therapeutic effects of lithium are multifaceted, involving mechanisms crucial for neuronal health, such as activation of neurotrophic responses, mitigation of apoptosis, regulation of oxidative stress, modulation of inflammatory pathways, enhancement of mitochondrial function, and modulation of autophagy (Figure 2.8) (Forlenza et al., 2014; Ghanaatfar et al., 2023). Lithium plays a crucial role in enhancing neuronal resilience and plasticity by stimulating the production and release of neurotrophic factors such as brain-derived neurotrophic factor (BDNF) and vascular endothelial growth factor (VEGF) (Figure 2.8) (Velosa et al., 2020). Moreover, lithium is demonstrated to modulate calcium

© COPYRIGHT UPM

levels related to N-methyl-D-aspartate (NMDA) receptors (Figure 2.8), which are integral to synaptic plasticity and neurotrophic signalling (Velosa et al., 2020). Lithium enhances the expression of the anti-apoptotic protein Bcl-2 and reduces the levels of pro-apoptotic proteins such as p53 and Bax, thereby providing protection against neuron death (Camins et al., 2009; Forlenza et al., 2014; Mehrafza et al., 2019). Furthermore, lithium exhibits anti-inflammatory properties by modulating various inflammatory factors and pathways, including *TNF-α*, *IL-1B*, *IL-6*, *IL-10*, *INF-γ*, and *COX-2*, thereby attenuating neuroinflammation (Paula et al., 2016; Nassar and Azab, 2014). Lithium acts as a potent activator of antioxidant enzymes, effectively scavenging free radicals and inhibiting the production of ROS and NOS during neurodegenerative processes (Vasconcellos et al., 2006; Frey et al., 2006).

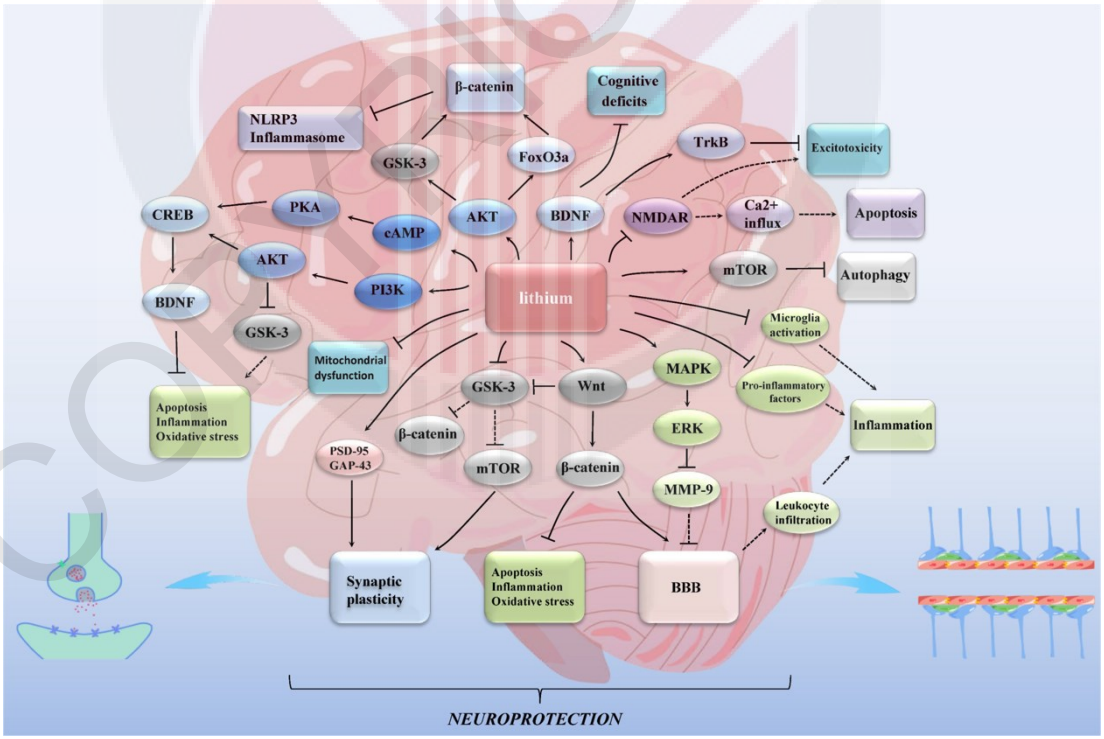


Figure 2.8 : Lithium Exerts Neuroprotective Effects against Neurological Disorders through a Variety of Mechanisms (Wang et al., 2024)

The neuroprotective potential of lithium spans various neurodegenerative conditions. In PD, it mitigates synaptic loss induced by neurotoxins (Margiotta, 2021). The study in PD model with α-synuclein overexpression demonstrate the ability of lithium to prevent oxidative stress-related cell death (Kim et al., 2011). In AD, lithium inhibits GSK-3β, reducing amyloid precursor protein phosphorylation and tau accumulation (Rockenstein et al., 2007). Its potential to mitigate AD risk in elderly bipolar disorder patients by targeting key AD pathogenic processes has been observed (Nunes et al., 2007). Lithium also holds therapeutic potential in HD, possibly by promoting autophagy and clearing mutant huntingtin protein (Rybakowski et al., 2018). Lithium enhances autophagy, aiding in the breakdown of aggregation-prone proteins associated with HD (Vallée et al., 2021). Nevertheless, the role of lithium in DS remains uncertain.

2.5.2 Role of Lithium in Astrocytes

Lithium diminishes lipopolysaccharide (LPS)-induced COX-2 expression and prostaglandin E2 production in primary rat astrocytes, highlighting its anti-inflammatory properties (Nahman et al., 2012; Wang et al., 2013). The impact of lithium extends to microglia and astrocytes, inhibiting 6-hydroxydopamine-induced activation and reducing *TNF-α* levels (Green and Nolan, 2012; Wang et al., 2013; Yuskaitis and Jope, 2009). Pre-treatment with lithium significantly attenuates *TNF-α*, *IL1-β*, and NO levels in primary glial cells following LPS-induced inflammation, highlighting its potential in dampening neuroinflammatory responses (Green and Nolan, 2012; Wang et al., 2013; Yuskaitis and Jope, 2009). By inhibiting GSK3β activity, lithium can suppress astrocyte activation and cytokine overproduction, thereby alleviating neuronal damage (Gao et al., 2013). Lithium has been shown to

© COPYRIGHT UPM

exert multiple effects on astrocytes. Studies indicate that lithium treatment increases the levels of VEGF in astrocytes, modulating astrocyte-neuron interactions and brain function, thereby influencing neuroprotection and angiogenesis (Daniels et al., 2015; Guo et al., 2009; Hertz et al., 2014). Additionally, lithium has been shown to impact astrocyte metabolism, enhancing glycolytic and Krebs cycle activities in both astrocytes and neurons (Almeida Souza et al., 2010). Lithium treatment inhibits glycogen synthesis in brain astrocytes and induces autophagy, protecting against astrocytic damage (Shen et al., 2016).

A previous study has suggested that lithium induces morphological and genomic phenotypic changes in neuron-supportive astrocytes, indicating a distinct morphological transformation favourable for neuron support, different from typical reactive astrocytes (Rivera and Butt, 2019). Astrocytes treated with lithium form a dense scaffold comparable to radial astrocytes in the developing CNS (Rivera and Butt, 2019), crucial for supporting neuronal growth, axonal targeting, dendritic branching, and synaptogenesis (McDermott et al., 2005). GFAP is one of the crucial markers of reactive astrocytes. A study has demonstrated that lithium suppression of interleukin-6 (IL-6) production and STAT3 activation leads to decreased expression of astrocyte-specific genes, including *GFAP*, thereby mitigating astrogliosis (Beurel and Jope, 2009).

2.5.3 Lithium and REST Expression

Lithium has been demonstrated in numerous studies to elevate nuclear REST protein levels (Meyer et al., 2023; Song, et al., 2017), a phenomenon associated with the interplay among lithium, GSK3β, and REST (Figure 2.9). GSK3β plays a pivotal role

© COPYRIGHT UPM

in regulating various cellular functions by phosphorylating and degrading β-catenin, a vital component of the Wnt signalling pathway (Yuan et al., 2012). In the absence of Wnt signalling transduction, GSK3β phosphorylates β-catenin, marking it for degradation (Zhang et al., 2022). Lithium is a well-established inhibitor of GSK3β, known to stabilise β-catenin (Wada, 2009). It has indicated that lithium treatment restores β-catenin expression at both mRNA and protein levels (Cheng et al., 2021). Stable β-catenin can translocate into the nucleus, activating gene expression and influencing gene regulation (Hou et al., 2021). The accumulation of β-catenin in the nucleus has been demonstrated to activate genes associated with cell proliferation, differentiation, and various other cellular processes (Cong et al., 2021). Remarkably, REST expression is modulated by the Wnt pathway. Studies have revealed that genes containing REST binding sites within the Wnt signalling pathway exhibit upregulated expression in response to REST knockout, suggesting a regulatory interplay between REST and the Wnt signalling cascade (Aksoy et al., 2016). A study underscored that the LRP6-Wnt-β-catenin signalling pathway induces REST expression (Song et al., 2017a).

© COPYRIGHT UPM

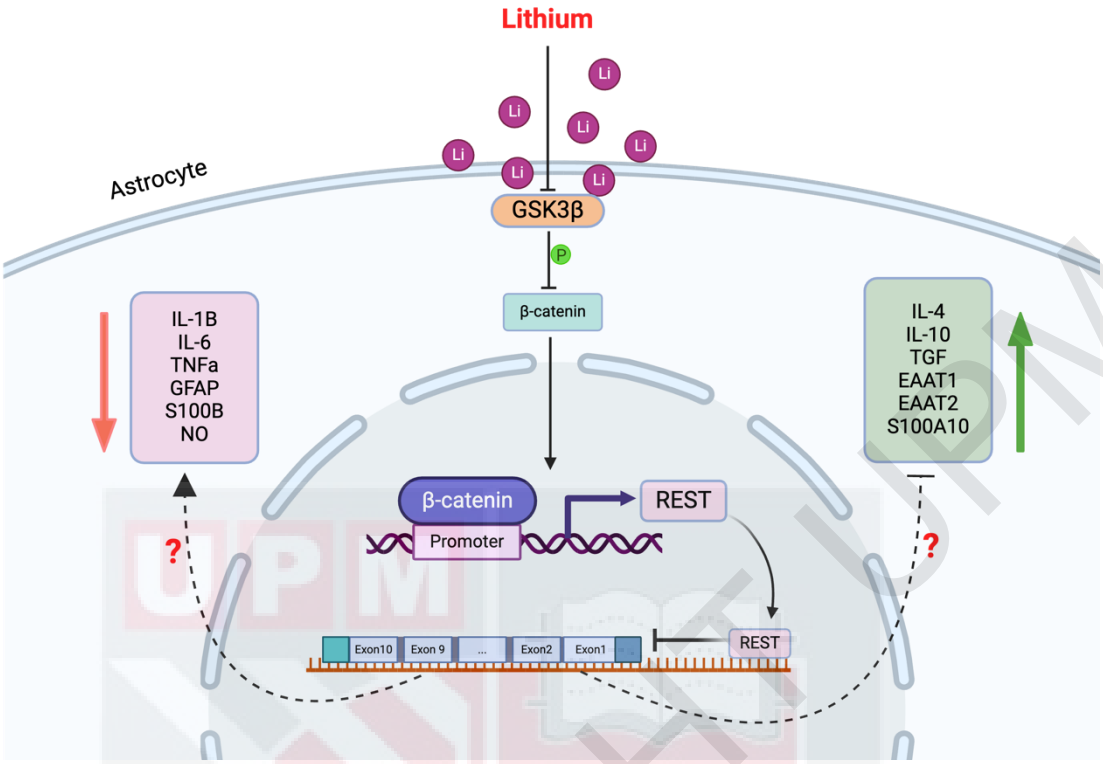


Figure 2.9 : Effect of Lithium Treatment on the Expression of REST, Inflammatory Factors and Cellular Markers in Astrocytes. Lithium enhances the expression of REST by inhibiting the activity of GSK3β, which induces an increase in the nuclear translocation of β-catenin.REST acts as a transcriptional silencing factor and represses the expression of target genes when it binds to the promoters of the target genes. This figure was created in BioRender (License number: CQ27UPH0PV)

2.5.4 Side Effects of Lithium Treatment

Lithium is widely recognised for its efficacy in the treatment of various neurological and psychiatric disorders, particularly bipolar disorder. However, its use is accompanied by a range of side effects, especially when treated with lithium over a long period. The therapeutic range for lithium is very narrow, with effective serum concentrations typically ranging from 0.6 to 1.2 mEq/L; nevertheless, neurotoxicity can occur even in this range (Ryu et al., 2020). Severe lithium toxicity can lead to more serious consequences, including seizures, coma, and even irreversible neurological damage such as dementia (Bhardwaj et al., 2021; Buckley et al., 2020;

Foulser et al., 2017). Previous research has shown that prolonged inhibition of GSK-3 induces neuronal apoptosis and leads to cognitive deficits, especially in neurodegenerative diseases (Gómez-Sintes and Lucas, 2010). Lithium has been shown to interfere with calcium signalling within neurons, particularly affecting Purkinje cells in the cerebellum, leading to neuronal damage and death when calcium influx is excessive (Atagun et al., 2013). Altered intracellular calcium levels impair synaptic transmission and plasticity, impairing metabotropic glutamate receptor signalling (Khayachi et al., 2021). Furthermore, excessive lithium treatment leads to mitochondrial dysfunction characterised by impaired energy production and increased ROS production, causing neuronal death and damage (Gawli et al., 2016). It is, therefore, essential to monitor serum lithium levels to prevent acute and chronic neurotoxic effects.

2.6 Human-Induced Pluripotent Stem Cells (hiPSCs)

2.6.1 Advantages of hiPSC-derived Models for Study

In 2007, the generation of hiPSCs was first reported, achieved through the application of the reprogramming factors OCT4, SOX2, KLF4, and cMYC, which effectively converted differentiated human somatic cells into pluripotent stem cells (Takahashi et al., 2007). They can exhibit characteristics similar to embryonic stem cells. The iPSC technology allows the generation of patient-specific cell lines, providing a valuable tool for disease modelling and personalised medicine (Takahashi et al., 2007). The capacity of these cells to differentiate into a range of cell types renders them a highly adaptable platform for investigating diverse diseases (Liu and Deng, 2016). iPSC applications in disease modelling have revolutionised regenerative medicine and drug

© COPYRIGHT UPM

discovery. Patient-derived iPSC helps to reproduce disease phenotypes in vitro, providing insights into disease mechanisms and potential therapeutic targets (Ito et al., 2012). By generating iPSC from individuals with specific genetic mutations or diseases, researchers can study the pathophysiology of these diseases and screen potential drug candidates (Hedges et al., 2016).

DS-derived iPSC cells are induced pluripotent stem cells reprogrammed from adult somatic cells, including blood cells and epithelial cells of urinary origin obtained from individuals with DS (Takahashi et al., 2007; Teles e Silva et al., 2023). In studies related to DS, several research groups reported the initial isogenic lines (Maclean et al., 2012; Weick et al., 2013). These investigations employed the spontaneous loss of chromosome 21 copies to isolate disomic and trisomic iPSCs derived from a single parental iPSC line. In contrast, isogenic pairs were created by subcloning cells from individuals with chimeric Down syndrome (Murray et al., 2015; Weick et al., 2013). By utilising iPSC technology, researchers can create patient-specific cell lines that highly mimic the genetic background of individuals with DS. These iPSC-derived models allow for the study of molecular, cellular, and developmental changes associated with DS, providing insight into disease progression and potential therapeutic interventions (Chen et al., 2022). The iPSC technology can use iPSC derived from individuals with DS to identify transcriptomic changes caused by trisomy of chromosome 21. This in-depth analysis of gene expression changes provides insights into the molecular alterations associated with Down syndrome (Gonzales et al., 2018). A key application of iPSCs in DS research is the ability to derive patient-specific cells (neural stem cells, neurons, astrocytes) and generate brain-like organoids from the iPSC of individuals with Down syndrome, thus enabling

© COPYRIGHT UPM

a personalised approach to the study of Down syndrome (Rispoli et al., 2024; Zhao and Haddad, 2022). This provides an optimised approach to mimic the neurodevelopmental abnormalities in DS, enabling researchers to explore the earliest cellular and molecular changes during fetal brain development (Zhao and Haddad, 2022).

2.6.2 DS iPSC-Derived 2D Cell Model

By utilising iPSC derived from DS individuals, researchers can create 2D neural cell models that highly mimic the genetic background of the disease, allowing for more accurate disease modelling and drug screening (Barral and Kurian, 2016). DS iPSC can derive various cell types in the brain, including NPCs (Hibaoui et al., 2014), various neuronal cells (Burke et al., 2020), astrocytes (Chen et al., 2014), oligodendrocytes (Klein et al., 2022) and microglia (Dräger et al., 2022). DS-derived iPSC 2D neural cell models have significantly enhanced our comprehension of DS neuropathophysiology, neurodevelopmental abnormalities, and potential therapeutic strategies. These cell models became ideal for studying the mechanisms of T21-induced epigenomic and transcriptional differences specific to different cell types.

NPC differentiated from DS iPSC exhibits reduced proliferation, impaired neurogenesis, biased gliogenesis, dysfunctional mitochondrial metabolism, cellular senescence, and perturbations in genome-wide transcription (Briggs et al., 2013; Klein et al., 2022; Meharena et al., 2022; Prutton et al., 2023). The mechanisms underlying how T21 impacts the fate specification of NPCs remain unresolved. Currently, iPSC-derived neurons represent the most extensively utilised model for studying DS. The passive differentiation of DS-derived iPSCs approaches have shifted towards astrocyte

© COPYRIGHT UPM

differentiation at the expense of neurons (Chen et al., 2014; Hirata et al., 2020). Research into the 2D differentiation of iPSC-derived neurons has elucidated several key characteristics associated with the DS brain, such as aberrant differentiation processes, synaptic abnormalities, and Alzheimer's disease-related pathology (Dashinimaev et al., 2017; Hirata et al., 2020; Huo et al., 2018; Toshikawa et al., 2021).

The numerous methods are limited by prolonged culture periods surpassing 180 days, challenges in increasing scalability, and/or the inability to reproduce the unique morphology of astrocytes seen in the native environment of the brain (Voulgaris et al., 2022). A standard approach for differentiating iPSCs into astrocytes involves initially directing them towards an NPC lineage. Overexpressing glial transcription factors such as SOX9, NFIA, and/or NFIB in iPSCs has enabled the generation of induced astrocytes within weeks, in contrast to the months required by conventional methods (Li et al., 2018; Neyrinck et al., 2021; Tchieu et al., 2019). Although studies have increasingly focused on the mechanisms responsible for the increased number of astrocytes seen in the DS brain, a thorough understanding of the functional consequences of T21 in astrocytes is still lacking.

2.6.3 DS iPSC-Derived 3D Cerebral Organoid Model

In 2013, human induced pluripotent stem cell-derived 3D cerebral organoid models were first characterized (Lancaster et al., 2013). These hiPSC-derived cerebral organoids closely replicate the intricate architecture of brain, encompassing multiple cell types. The majority of cerebral organoid cultures predominantly mimic the dorsal forebrain, developing ventricle-like neural clusters and replicating the inside-out migration pattern of cerebral cortex. Nevertheless, the quantity of oligodendrocytes

© COPYRIGHT UPM

and interneurons in these models is restricted because they primarily originate from the ventral forebrain. Studies have shown that activating SHH signalling can promote the ventralisation of neural progenitor cells and cerebral organoids (Maroof et al., 2013; Nicholas et al., 2013). Furthermore, In addition, incorporating growth factors like PDGF-AA and IGF-1 has demonstrated effectiveness in enhancing the development of the oligodendrocyte lineage (Hubler et al., 2018; Madhavan et al., 2018). The inconsistency in the occurrence of mesodermal progenitor cells and microglial cells among various organoid types remains a considerable challenge. Moreover, the absence of a fully developed cerebrovascular network, particularly the BBB, represents a critical limitation in the current cerebral organoid models.

Distinct regions within DS iPSC-derived brain organoids have significantly contributed to elucidating the regional pathological characteristics of the disease. Importantly, DS organoids are generally smaller in size than those derived from neurotypical iPSCs (Campbell et al., 2023; Li et al., 2022). Electrophysiological evaluations of the T21 hiPSC-derived organoids revealed that while DS organoids can develop characteristics indicative of mature neuronal function following 6-10 months in culture, they exhibited compromised neuronal network connectivity, an altered excitatory-inhibitory balance, and functional deficits (Foliaki et al., 2021). Single-cell RNA sequencing analysis has revealed disrupted proliferation, delayed neurogenesis, and impaired production of excitatory neurons, especially within layer IV neurons (Li et al., 2022; Tang et al., 2021).

© COPYRIGHT UPM

CHAPTER 3

REST-MEDIATED MOLECULAR DYSREGULATION IN DOWN SYNDROME HUMAN BRAIN TISSUE AND NEURAL CELLS BY BIOINFORMATIC ANALYSIS

3.1 Introduction

REST is a critical transcription factor regulating the neurodevelopmental process involving neural cell differentiation and maturation (Abrajano et al., 2009; Johnson et al., 2008; Thiel et al., 2015). However, whether REST plays a role in DS neurodevelopmental defect pathology has not been reported. REST can act as a transcriptional repressor of neuron-specific genes in non-neuronal cells, and its high expression leads to the repression of essential neuronal genes (Zhao et al., 2017). This transcriptional repression of REST was also found to be as effective for non-neuronal genes such as glial-specific genes (Abrajano et al., 2009). Conversely, downregulation of REST levels leads to de-repression and upregulation of expression of its target genes (Kawamura et al., 2019; Meyer et al., 2023). Hence, alterations in REST levels within neural cells may be a pivotal factor contributing to the pathological mechanism of DS, such as neurogenesis impairments, gliogenesis abnormalities, and neural cellular functionality.

In 2002, REST levels were first reported to be reduced in human DS fetal brains compared to healthy controls (Bahn et al., 2002). A subsequent study has shown that REST levels are reduced by 30% to 60% in the brains of the DS mouse model and that this reduction is consistently observed at all stages of brain development, from the ESC to the adult brain (Canzonetta et al., 2008). Unfortunately, these studies did not delve into the effects of decreased REST levels on DS brain development and function.

© COPYRIGHT UPM

A recent study revealed impaired nuclear translocation of REST in the brain of the Ts1Cje DS mouse model (Lim et al., 2024). As a transcriptional regulator, REST may lose precise regulation of its target genes due to nuclear translocation impairment. REST loss or impaired nuclear translocation in DS may contribute to the disrupted expression of REST target genes in neural cells. However, little is known about the mediating functions and molecular mechanisms of REST in DS brain and neural cells.

This study aimed to comprehensively investigate the REST-mediated molecular dysregulation in DS human brain and neural cells. Extensive enrichment of REST-targeted differentially expressed genes was analysed across developmental stages and different brain regions in DS individuals. Additionally, REST-targeted differentially expressed genes were also enrichment analysed in DS-derived human brain organoids, NPCs, neurons, and astrocytes. The results indicate that REST modulates the neurodevelopmental process of DS and significantly affects the JAK-STAT signalling pathway in specific brain regions, at different developmental stages, and in a variety of cell types, thus highlighting its critical role in regulating the development of the central nervous system.

3.2 Experiment Design

The role of REST was explored across multiple brain regions, ages, and different neural cell types in DS. Transcriptomic data from DS brain tissues, DS-derived cerebral organoids, NPCs, neurons, and astrocytes were downloaded for analysis. High-throughput raw data were processed using the Galaxy web-based platform, while microarray data were analysed with R software to identify differentially expressed genes (DEGs). Enrichment analysis and visualisation of REST-targeted DEGs were

© COPYRIGHT UPM

subsequently conducted using R software to identify the biological processes and signalling pathways targeted by REST in DS. A simplified diagram of the data processing and analysis workflow or criteria used in this study is presented in Figure 3.1.

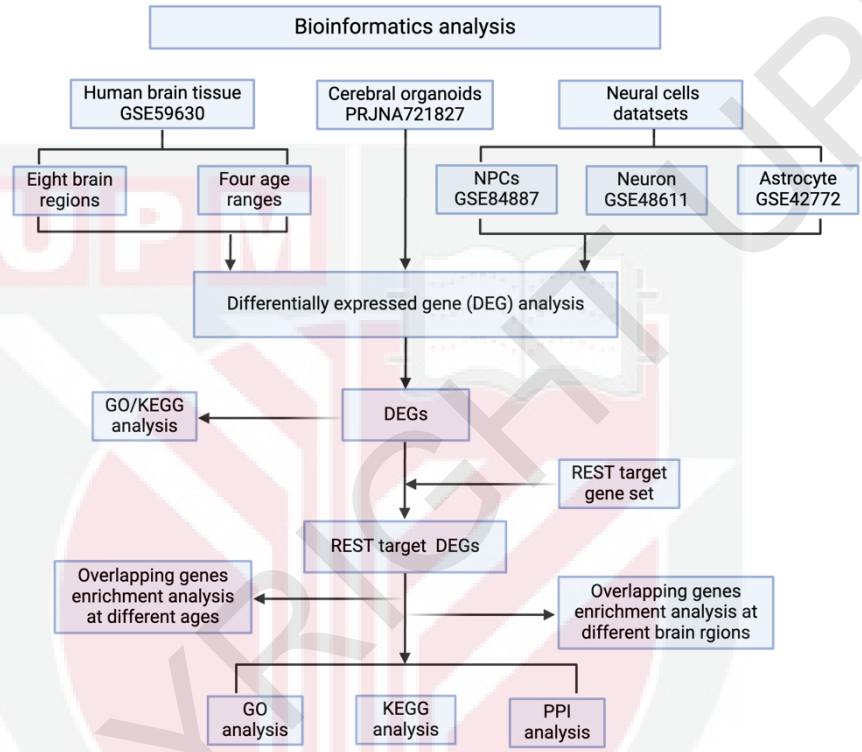


Figure 3.1 : Simplified Diagram of the Experimental Methods, Data Processing, and Analysis Workflow Used for this Study. DS, Down syndrome; GO, Gene Ontology; KEGG, Kyoto Encyclopedia of Genes and Genomes; PPI, Protein-protein interaction. The figure was created in BioRender (License number: XU27U4G0WW)

3.3 Materials and Methods

3.3.1 Acquisition of DS Transcriptomic Datasets

The raw data of expression profiles was sourced from the Gene Expression Omnibus (GEO; http://www.ncbi.nlm.nih.gov/geo) for DS-derived human brain tissues, NPCs, neurons, and astrocytes. The GSE59630 series consisted of 58 DS and 58 control

© COPYRIGHT UPM

samples from human brain tissues. The samples included individuals with DS ranging in age from 16 weeks of conception to 42 years based on the GPL5175 platform (Olmos et al., 2016). These samples were categorised based on various brain regions, including the cerebellar cortex (CBC; 10 DSs and 10 control samples), dorsolateral prefrontal cortex (DFC; 8 DSs and 12 control samples), hippocampus (HIP; 3 DSs and 3 control samples), inferior temporal cortex (ITC; 5 DSs and 5 control samples), prefrontal cortex (OFC; 6 DSs and 6 control samples), the primary somatosensory cortex (S1C; 2 DSs and 2 control samples), primary visual cortex (V1C; 11 DSs and 11 control samples), and ventrolateral prefrontal cortex (VFC; 7 DSs and 7 control samples). The GSE84887 series (NPCs from DS-derived embryonic stem cells) contained 5 DS samples and 3 controls based on the GPL570 platform (Halevy et al., 2016). The GSE48611 series (neurons from DS-derived hiPSCs) contained 6 DS samples and 3 controls based on the GPL570 platform (Weick et al., 2013). The GSE42772 series (astrocytes from DS human cortex cells) contained 5 DS samples and 3 controls based on the GPL6255 platform (Helguera et al., 2013). The DS hiPSC-derived human cerebral organoid dataset (PRJNA721827; days in vitro, DIV 30) were retrieved from the Sequence Read Archive database (SRA, https://www.ncbi.nlm.nih.gov/sra), which included three DS samples and three matched isogenic controls (Tang et al., 2021).

3.3.2 Identification of Differentially Expressed Genes (DEGs) between DS Samples and Controls

The differential expression analysis between DS samples and controls for each microarray dataset was conducted using the R programming language, employing the *limma* package to identify differentially expressed genes (DEGs) (Appendix A1). For

© COPYRIGHT UPM

the next-generation sequencing (NGS) dataset, the analysis was performed utilising the tools on the Galaxy web-based platform (https://usegalaxy.org) (Galaxy Community, 2022). *Trim Galore* software (Galaxy Version 0.6.7+galaxy0) was applied for the trimming and processing of FASTQ files. Subsequently, *HISAT2* software (Galaxy Version 2.2.1+galaxy1) was used to align transcriptome sequences. The human reference genome (HG38) was employed as the annotation file. The *htseq-count* software (Galaxy Version 2.0.5+galaxy0) was used to count aligned reads. Differential expression analysis was subsequently performed using *DESeq2* software (Galaxy Version 2.11.40.8+galaxy0), with DEGs identified based on a p-value < 0.05 and |log2 FC| > 0.5 as DEGs. The analysis results were visualised by creating heatmaps and volcano plots using RStudio software (version: 2022.02.2) (Appendix A2).

3.3.3 Identification of REST-Targeted DEGs

The Gene Transcription Regulation Database (GTRD; http://gtrd.biouml.org) provided the human REST target genes (Kolmykov et al., 2021). A Venn diagram (https://bioinfogp.cnb.csic.es/tools/venny/) was then used to show how REST target genes and DEGs overlapped. The hypergeometric probability model (http://nemates.org) was used to calculate the representative factor and significance in statistics for the overlapping between these two sets of genes, using the human genome as the background. A p-value < 0.05 was considered statistically significant.

3.3.4 Functional Enrichment Analysis and Visualisation

The Bioconductor software package *clusterProfiler* was utilised to induce gene ontology (GO) (Ashburner et al., 2000) and Kyoto Encyclopedia of Genes and

© COPYRIGHT UPM

Genomes (KEGG) (Kanehisa and Goto, 2000) enrichment analysis for REST-targeted DEGs (Wu et al., 2021) (Appendix A3). This investigation was performed to elucidate the biological processes and pathways affected by DEGs targeted by REST. The top 10 GO and KEGG terms were presented. The p-value less than 0.05 was considered statistically significant, indicating that the gene set was significantly enriched in the biological pathway.

3.3.5 Protein-Protein Interaction (PPI) Network Analysis

The Search Tool for the Retrieval of Interacting Genes (STRING; http://string-db.org) was used to explore protein-protein interactions (PPI) networks (Mering et al., 2003), with an interaction score threshold set at ≥ 0.4. Cytoscape software (version 3.9.1) was utilised for visualising the network. Different colours distinguished DEGs and REST-target DEGs. The significance of key modules within the PPI network was further validated using the Molecular Complex Detection plugin (MCODE) (Bandettini et al., 2012).

3.4 Results

3.4.1 DEGs of DS Human Brain Tissues and Neural Cells

In the GSE59630 dataset, covering eight human brain regions, distinct gene expression patterns were observed. Notably, we found 1,497 DEGs in the CBC region, 2,095 DEGs in DFC, 1,092 DEGs in HIP, 2,396 DEGs in ITC, 1,503 DEGs in OFC, 4,743 DEGs in S1C, 2,173 DEGs in V1C, and 1,699 DEGs in VFC. For visual representation, refer to Figure 3.2 and Figure 3.3, which include heat maps and volcano plots.

© COPYRIGHT UPM

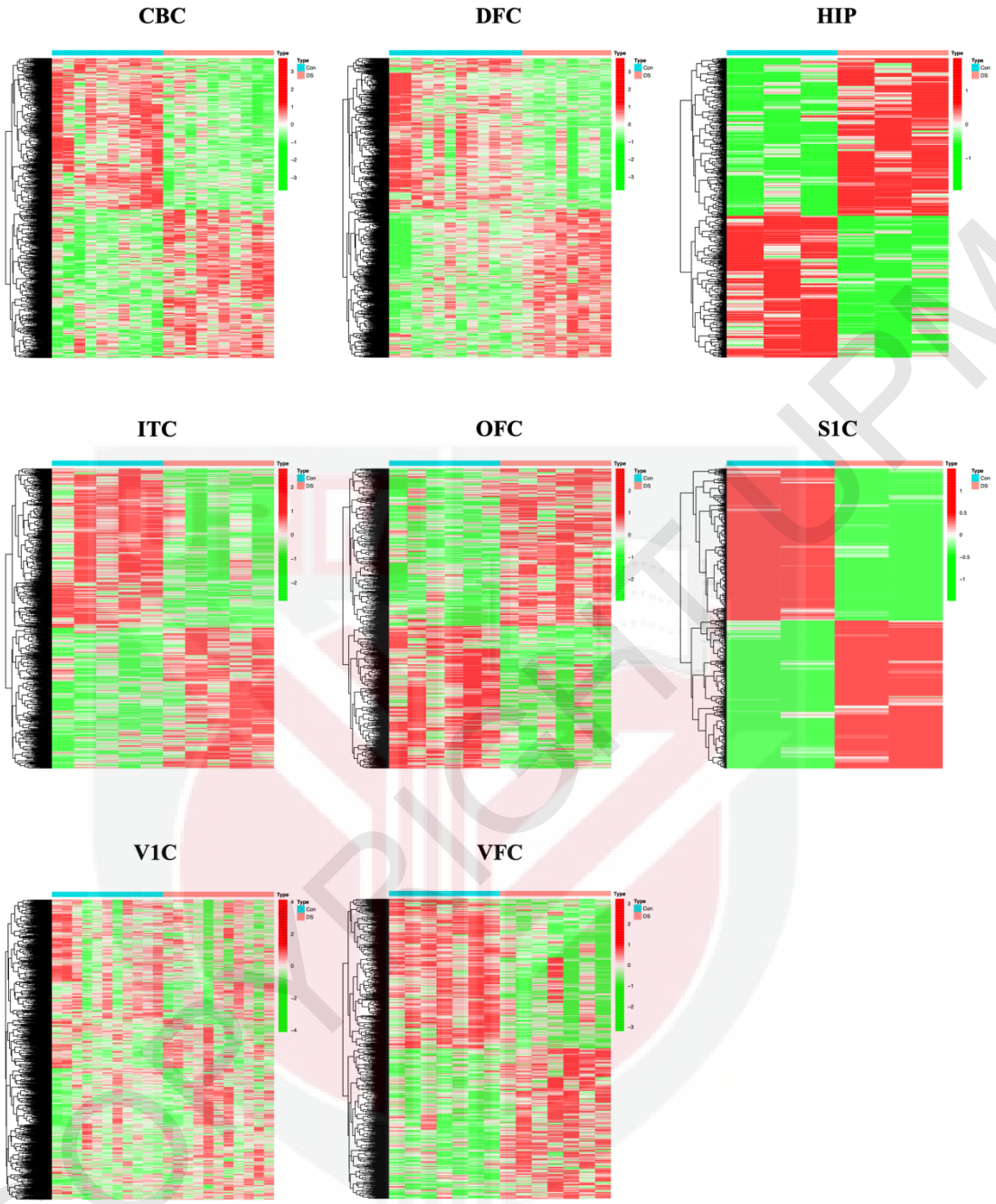


Figure 3.2 : Heat Map Analysis of Identified DEGs between DS and Controls in Eight Brain Regions. Red represents upregulated genes, while green represents downregulated genes. Cerebellar cortex: CBC; Dorsolateral prefrontal cortex: DFC; Hippocampus: HIP; Inferior temporal cortex: ITC; Prefrontal cortex: OFC; Primary somatosensory cortex: S1C; Primary visual cortex: V1C; Ventrolateral prefrontal cortex: VFC

© COPYRIGHT UPM

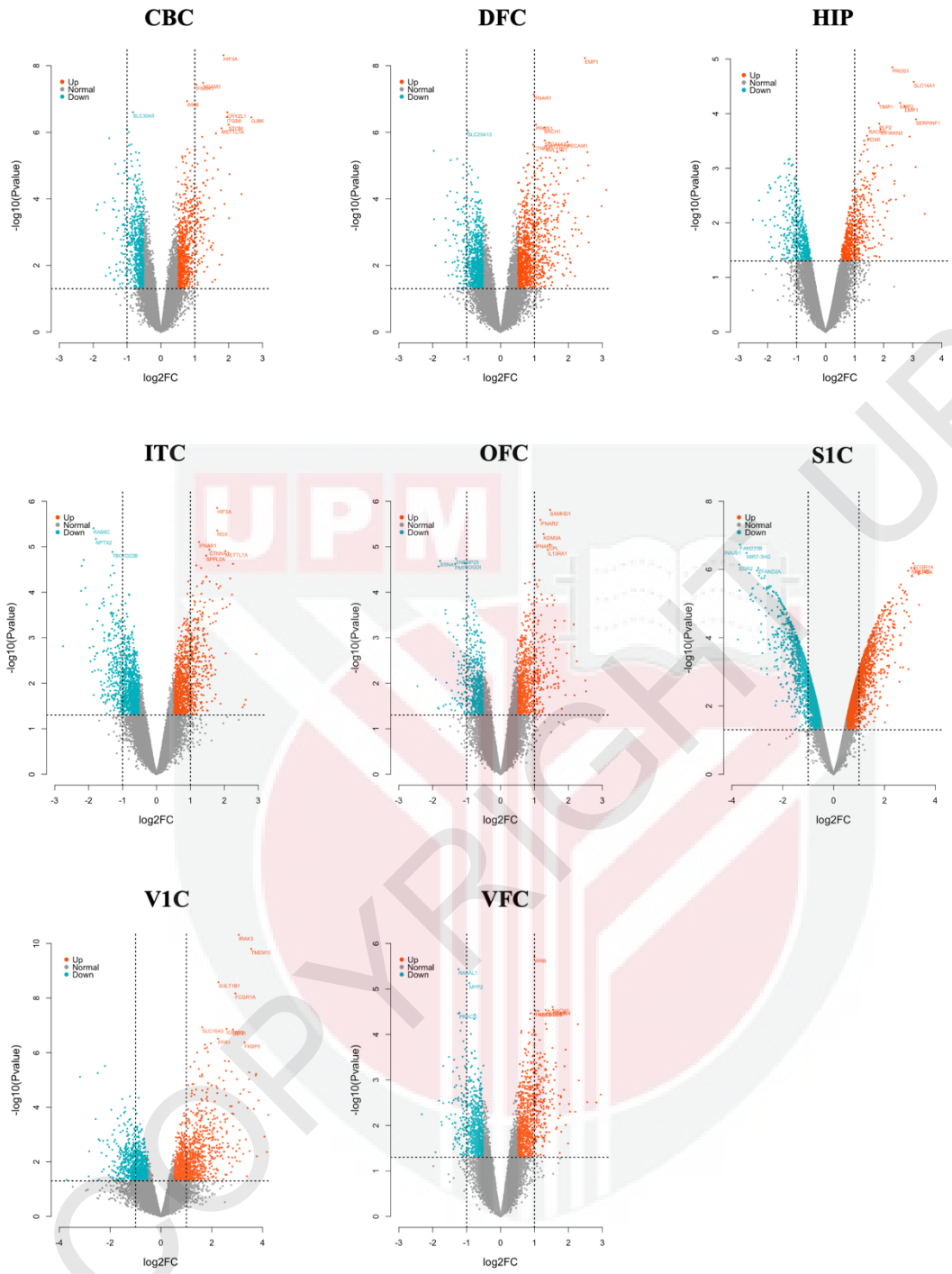


Figure 3.3 : The Volcano Plot for DEGs in DS Eight Brain Regions. The top 10 DEGs with the most significant p-values are shown in Appendix A4. Red represents upregulated differentially expressed genes, blue represents downregulated differentially expressed genes, and grey represents genes with no differential expression. Cerebellar cortex: CBC; Dorsolateral prefrontal cortex: DFC; Hippocampus: HIP; Inferior temporal cortex: ITC; Prefrontal cortex: OFC; Primary somatosensory cortex: S1C; Primary visual cortex: V1C; Ventrolateral prefrontal cortex: VFC

© COPYRIGHT UPM

This study explored different developmental stages of human brain tissues, including fetal (16 to 22 gestational weeks), infant (0 to 12 months), child (2 to 16 years), and adult (18 to 42 years) periods. The distinct gene expression patterns were observed across these stages, identifying 2,167 DEGs in fetal brains, 1,940 DEGs in infants, 948 DEGs in children, and 3912 DEGs in adults. Heatmaps (Figure 3.4) and volcano plots (Figure 3.5) provided visual insights.

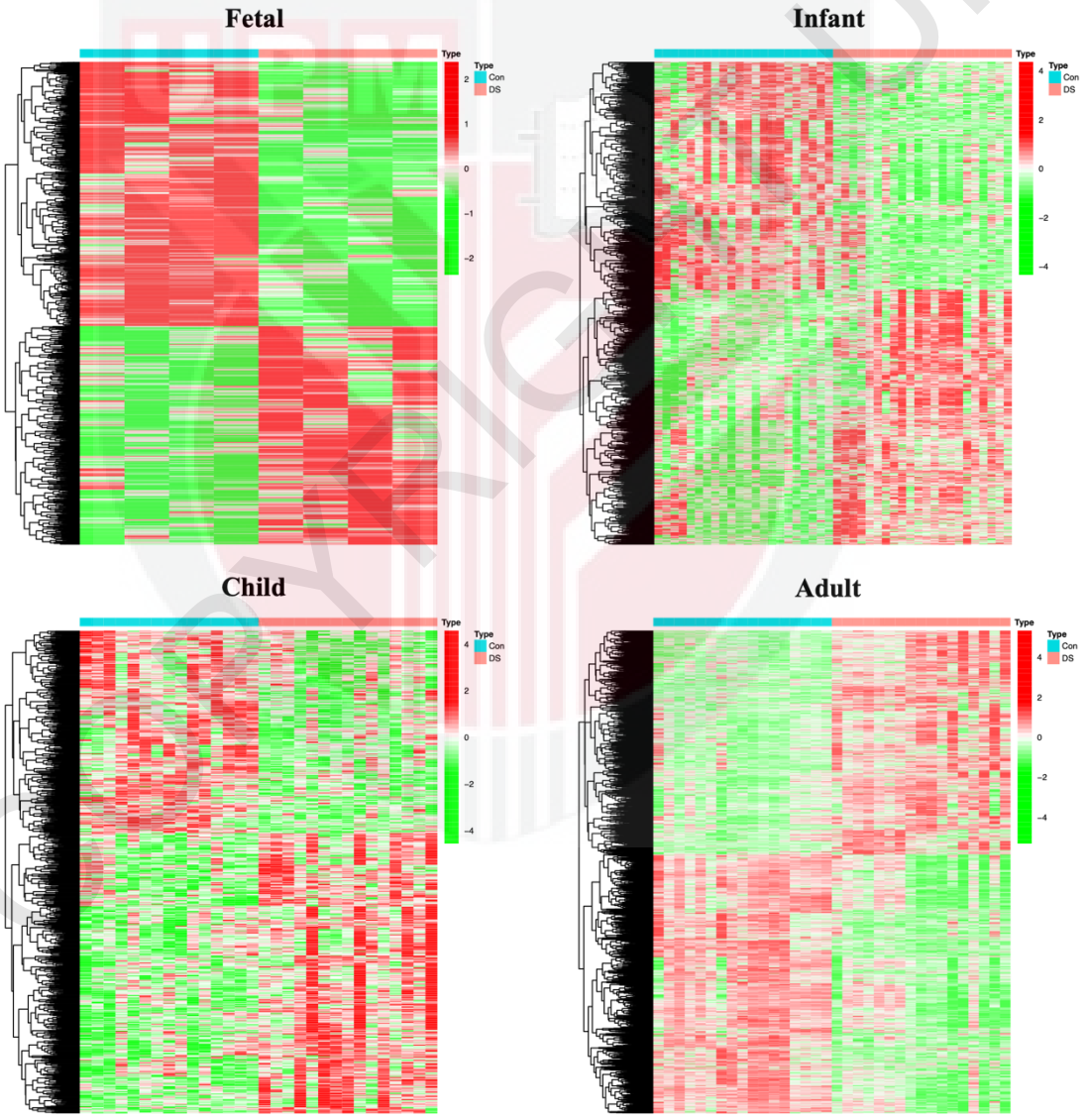


Figure 3.4 : Heat Maps of Identified DEGs between DS and Controls, Respectively, in Fetal (16 to 22 Gestational Weeks), Infant Child (2 to 16 years), Child (2 to 16 years) and Adult (18 to 42 years). Red represents upregulated genes, while green represents downregulated genes

© COPYRIGHT UPM

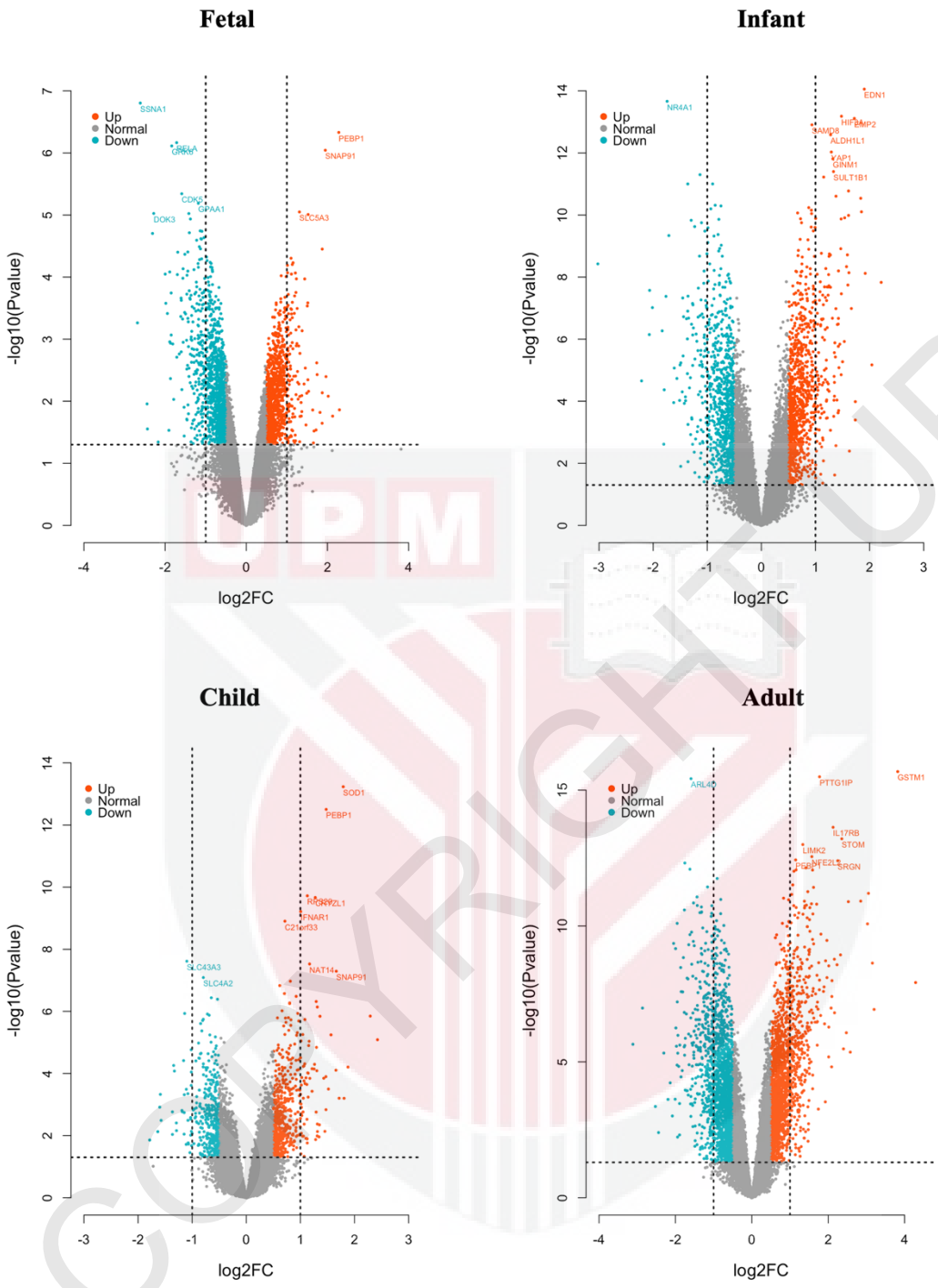


Figure 3.5 : Volcano Plots of Identified DEGs between DS and Controls, Respectively, in Fetal (16 to 22 Gestational Weeks), Infant Child (2 to 16 years), Child (2 to 16 years) and Adult (18 to 42 years). The top 10 DEGs with the most significant p-values are shown in Appendix A5. Red represents upregulated differentially expressed genes, blue represents downregulated differentially expressed genes, and grey represents genes with no differential expression

© COPYRIGHT UPM

In the PRJNA721827 dataset (cerebral organoid), 1,385 DEGs were identified. In GSE84887 (NPC), 707 DEGs were identified. In GSE48611 (neuron), 136 DEGs were identified. In GSE42772 (astrocyte), 110 DEGs were identified. Heatmaps (Figure 3.6) and volcano plots (Figure 3.7) provided visual insights.

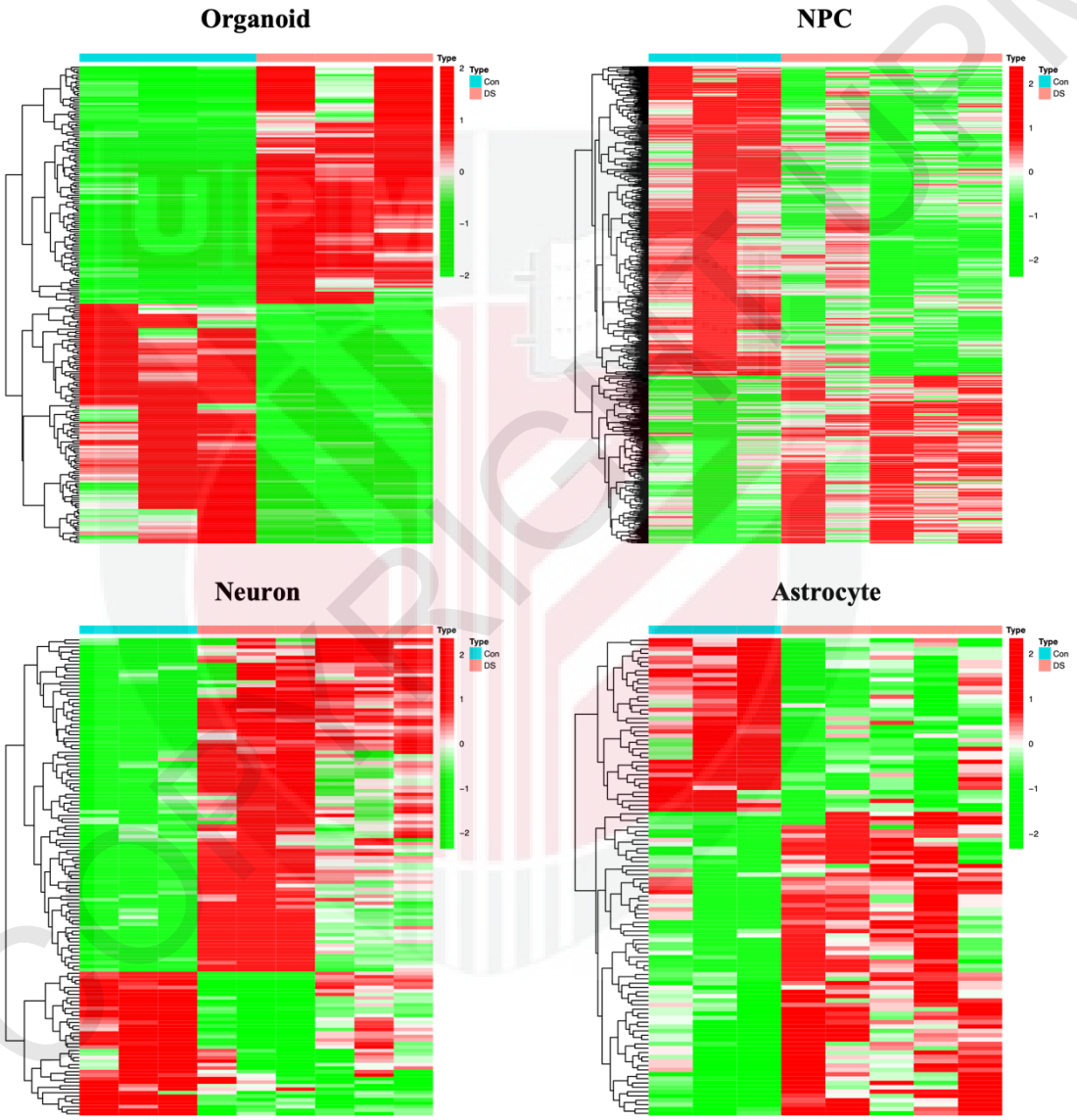


Figure 3.6 : Heat maps of Identified DEGs between DS and Controls in Cerebral Organoid, NPC, Neuron and Astrocyte. Red represents upregulated genes, while green represents downregulated genes. The volcano plots for DEGs in cerebral organoids, NPC, neurons, and astrocytes

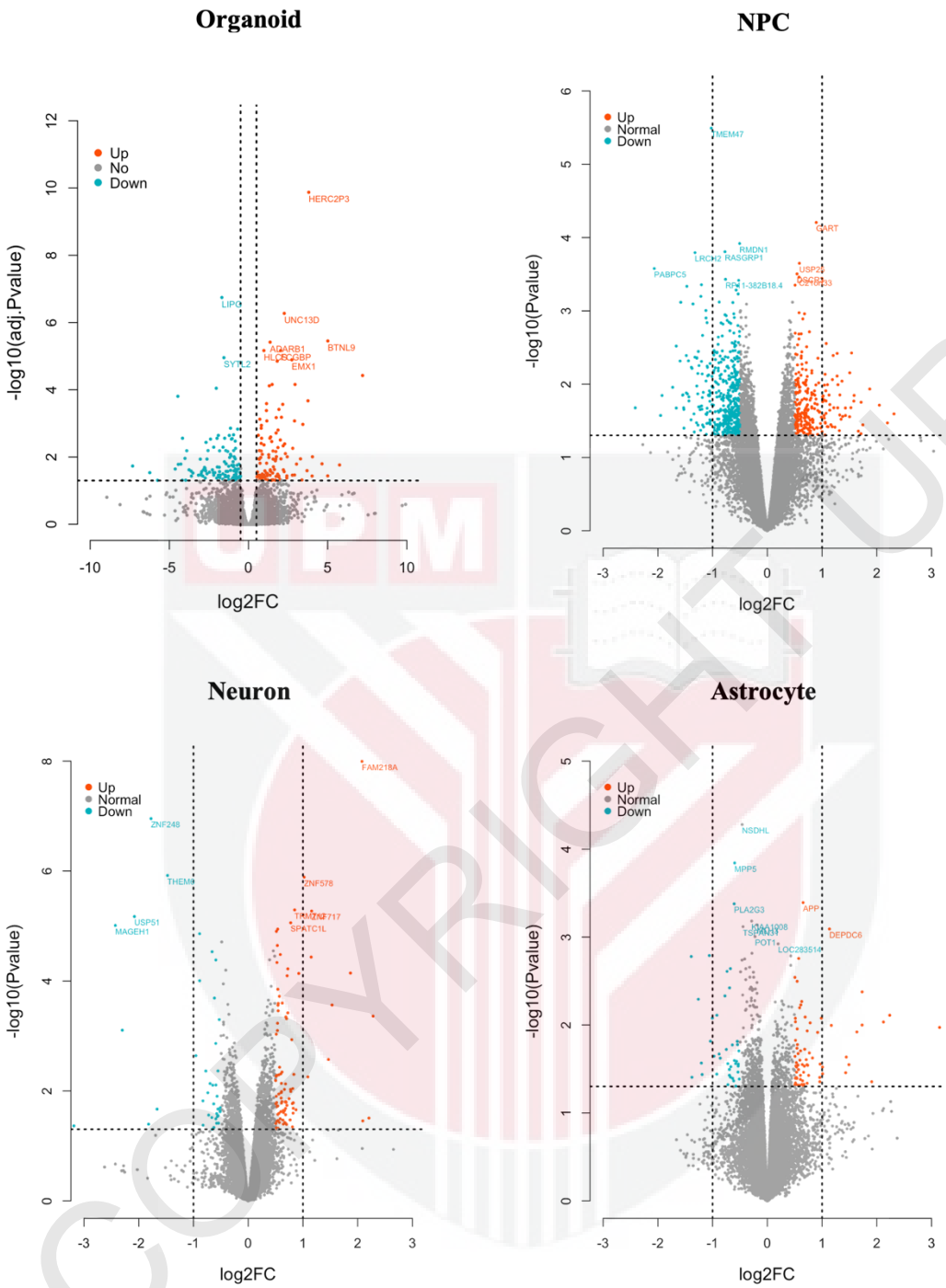


Figure 3.7 : Volcano Plots of Identified DEGs between DS and Controls in Cerebral Organoid, NPC, Neuron and Astrocyte. The top 10 DEGs with the most significant p-values are shown in Appendix A6. Red represents upregulated differentially expressed genes, blue represents downregulated differentially expressed genes, and grey represents genes with no differential expression

© COPYRIGHT UPM

3.4.2 REST-Targeted DEGs in DS Human Brain Tissues and Neural Cells

It was comprehensively analysed that the overlapping genes between REST-targeted genes and DEGs in DS human brain tissues, visually shown in Venn diagrams (Figure 3.8). The verification process revealed a significant overlap, with 1,262 (84.30%) REST-targeted DEGs confirmed in CBC (representation factor, RF = 1.9 and $p < 6.567 \times 10^{-237}$), 1,721 (82.15%) in DFC (RF = 1.9 and $p < 2.034 \times 10^{-298}$), 879 (80.49%) in HIP (RF = 1.8 and $p < 2.178 \times 10^{-138}$), 1,981 (82.67%) in ITC (RF = 1.9 and $p < 0.000 \times 10^{0}$), 1,208 (80.37%) in OFC (RF = 1.8 and $p < 1.461 \times 10^{-190}$), 3,945 (83.17%) in S1C (RF = 1.9 and $p < 0.000 \times 10^{0}$), 1,775 (81.68%) in V1C (RF = 1.9 and $p < 4.537 \times 10^{-302}$), and 1,325 (77.99%) in VFC (RF = 1.9 and $p < 2.025 \times 10^{-187}$). Subsequently, a set of 51 common REST-targeted DEGs consistently dysregulated across all brain regions was identified (Figure 3.8), comprising 41 up-regulated DEGs and 10 down-regulated DEGs in DS (Figure 3.9).

© COPYRIGHT UPM

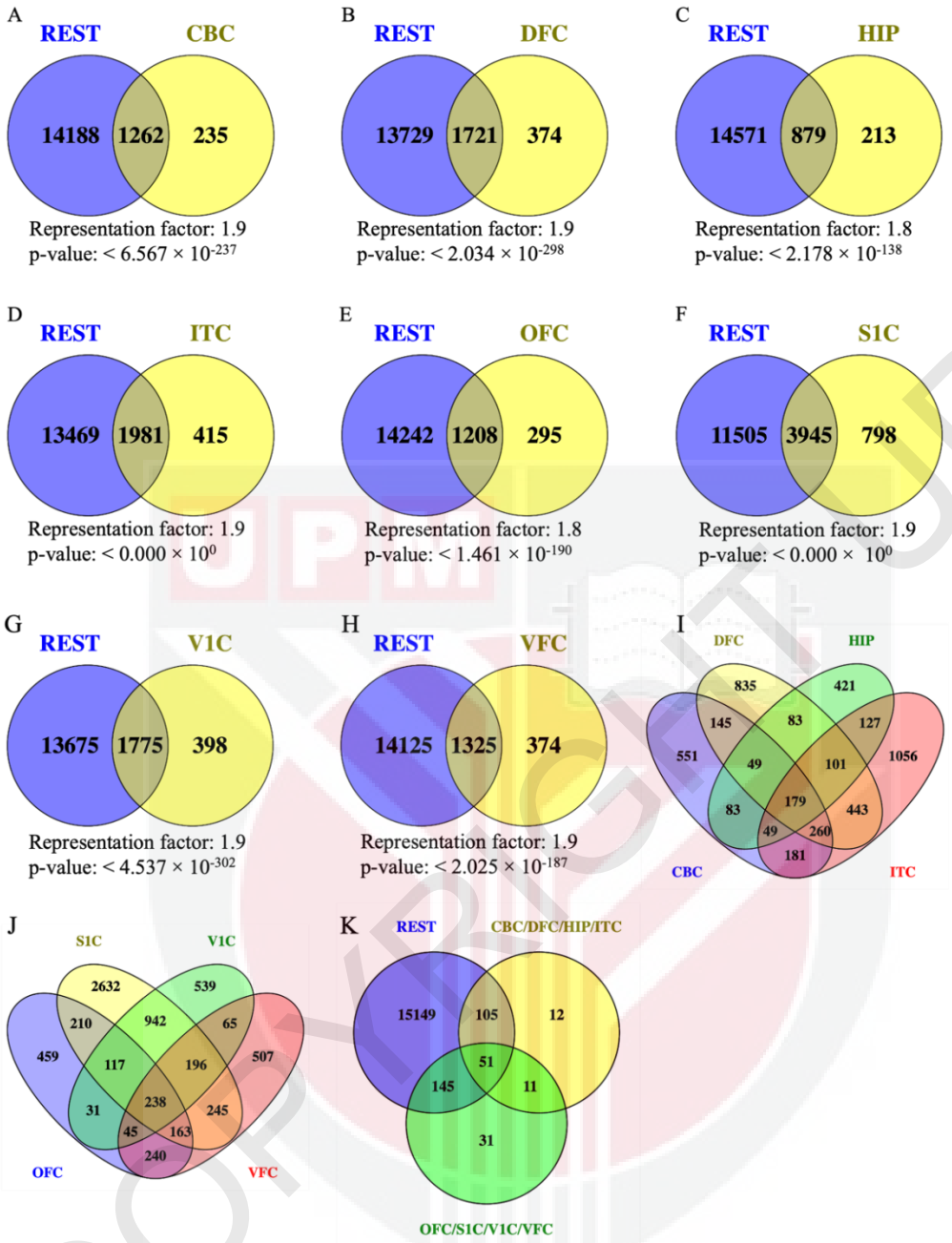


Figure 3.8 : Depiction of the Overlap between REST Target Genes and DEGs across DS Diverse Brain Regions. (A-H) Demonstration of REST-targeted DEGs in different brain regions. (I-K) Step-by-step illustration of REST-targeted DEGs common to all brain regions. A total of 51 common REST-targeted DEGs were identified across brain regions (Appendix A7). Fisher's test determined the statistical significance of this gene overlap, revealing all p-values < 0.01. A representation factor > 1 indicates more overlap than expected of two independent groups, a representation factor < 1 indicates less overlap than expected, and a representation factor of 1 indicates that the two groups by the number of genes expected for independent groups of genes. Cerebellar cortex: CBC; Dorsolateral prefrontal cortex: DFC; Hippocampus: HIP; Inferior temporal cortex: ITC; Prefrontal cortex: OFC; Primary somatosensory cortex: S1C; Primary visual cortex: V1C; Ventrolateral prefrontal cortex: VFC

© COPYRIGHT UPM

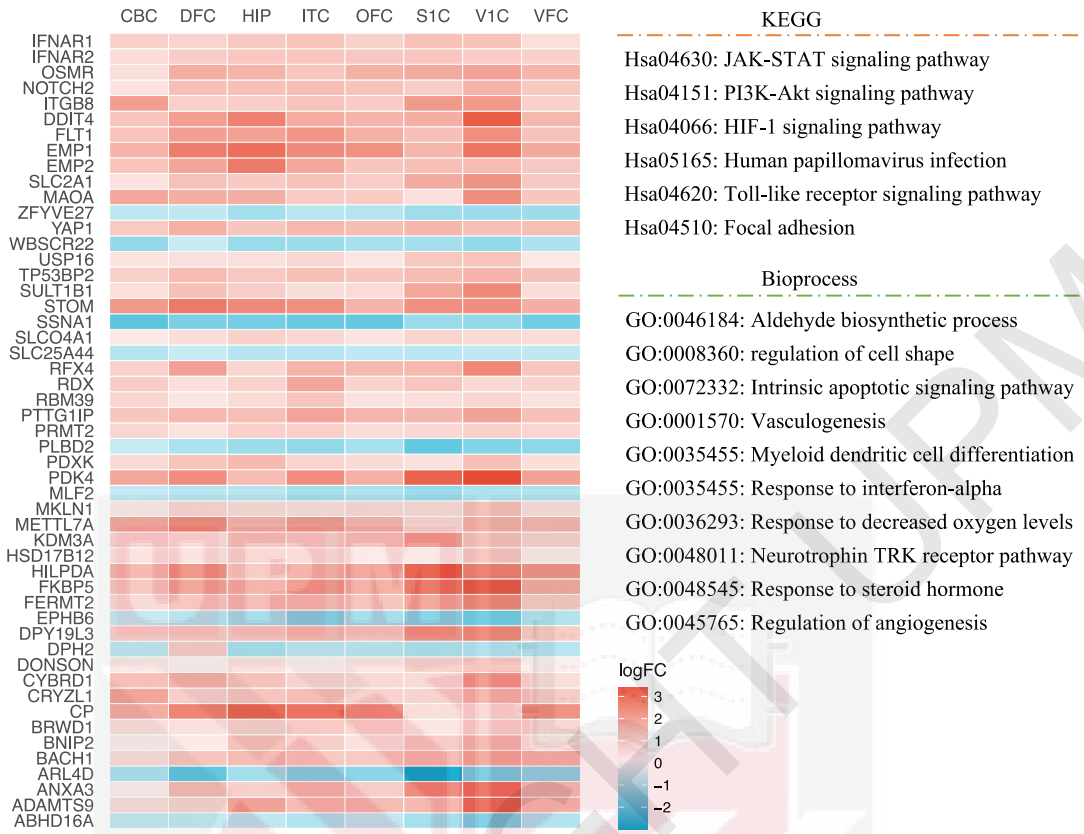


Figure 3.9 : The Heatmap and Enrichment Analysis for Common Genes in the DS Different Brain Regions. The heatmap visually represents the 51 common REST-targeted DEGs found in different brain regions (CBC, DFC, HIP, ITC, OFC, S1C, V1C, and VFC) and an overview of the signalling pathways and biological functions associated with these genes. Red indicates that these genes are up-regulated in DS, and blue indicates that these are down-regulated in DS. The top 10 biological processes and KEGG pathways are shown. Cerebellar cortex: CBC; Dorsolateral prefrontal cortex: DFC; Hippocampus: HIP; Inferior temporal cortex: ITC; Prefrontal cortex: OFC; Primary somatosensory cortex: S1C; Primary visual cortex: V1C; Ventrolateral prefrontal cortex: VFC

Concurrently, the overlap between REST-targeted genes and DEGs across diverse age groups of brain tissue was investigated (Figure 3.10). The analysis revealed 1,839 (70.88%) REST-targeted DEGs in fetal brain tissue (RF = 1.6 and $p < 6.306 \times 10^{-149}$), 1,664 (85.77%) in infant brain tissue (RF = 1.9 and $p < 0.000 \times 10^{0}$), 766 (80.80%) in postnatal brain tissue (RF = 1.8 and $p < 4.495 \times 10^{-122}$), and 3,170 (81.03%) in adult brain tissue (RF = 1.8 and $p < 0.000 \times 10^{0}$). The 56 REST-targeted DEGs were

consistently dysregulated across all age groups (Figure 3.10), comprising 39 up-regulated DEGs and 17 down-regulated DEGs in individuals with DS (Figure 3.11).

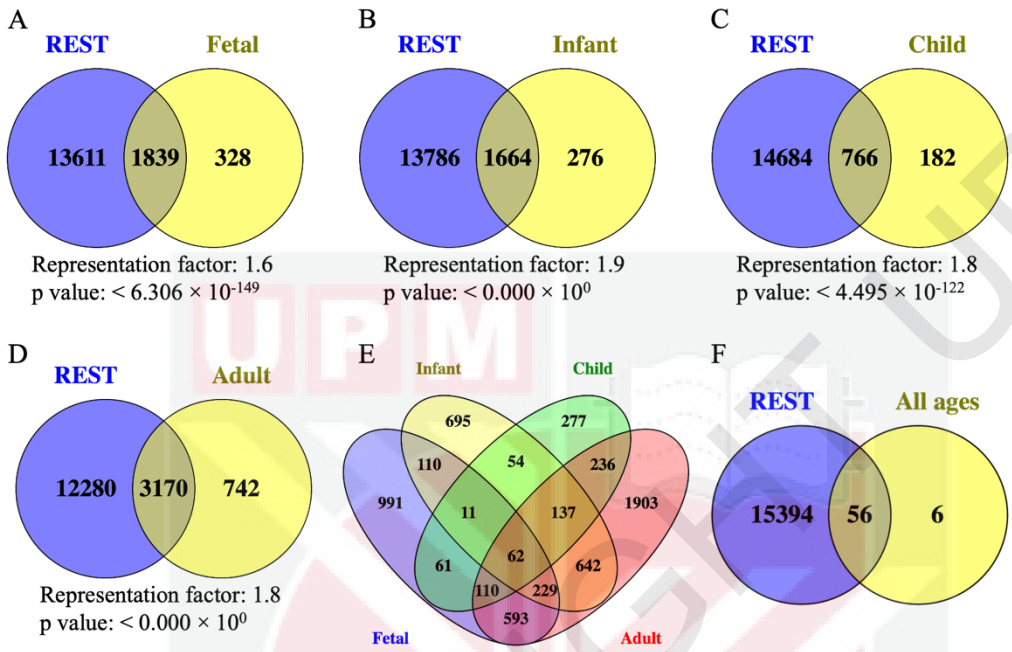


Figure 3.10 : Depiction of the Overlap between REST Target Genes and DEGs across Diverse Age Groups of DS Brain Tissues. (A-D) Demonstration of REST-targeted DEGs in different age brain groups. (E-F) Step-by-step illustration of REST-targeted DEGs common to all age brain groups. Total 56 common REST-targeted DEGs were identified across brain regions (Appendix A8).Fisher's test determined the statistical significance of this gene overlap, revealing all p-values < 0.01. A representation factor > 1 indicates more overlap than expected of two independent groups, a representation factor < 1 indicates less overlap than expected, and a representation factor of 1 indicates that the two groups by the number of genes expected for independent groups of genes. Fetal (16 to 22 gestational weeks), Infant child (2 to 16 years), Child (2 to 16 years) and Adult (18 to 42 years)

© COPYRIGHT UPM

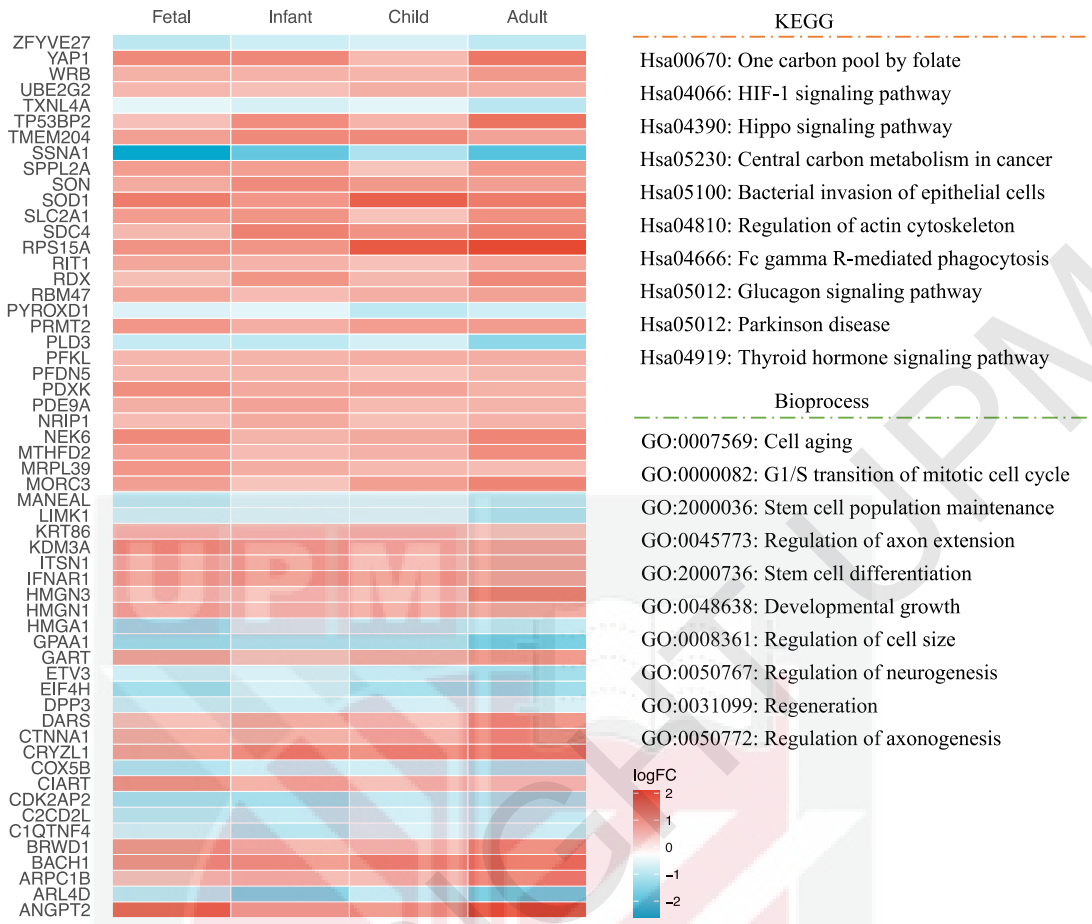


Figure 3.11 : The Heatmap and Enrichment Analysis for the Common Genes in DS Different Age Groups. The heatmap visually represents the 56 common REST-targeted DEGs found in different age groups (Fetal, Infant, Child, Adult) and an overview of the signalling pathways and biological functions associated with these genes. Red indicates that these genes are up-regulated in DS, and blue indicates that these are down-regulated in DS. The top 10 biological processes and KEGG pathways are shown

Additionally, the overlap between REST-target genes and DEGs in DS hiPSC-derived brain organoids was investigated. The findings revealed a total of 913 (65.92%) REST-targeted DEGs (RF = 1.6 and $p < 3.608 \times 10^{-8}$) (Figure 3.12). Specifically focusing on DEGs in neural cells, this analysis uncovered 482 (68.18%) REST-targeted DEGs in DS NPC (RF = 1.5 and $p < 5.477 \times 10^{-39}$), 81 (59.56%) in DS neurons (RF = 1.3 and $p < 2.088 \times 10^{-4}$), and 77 (70.00%) in DS astrocytes (RF = 1.6 and $p < 3.608 \times 10^{-8}$) (Figure 3.12).

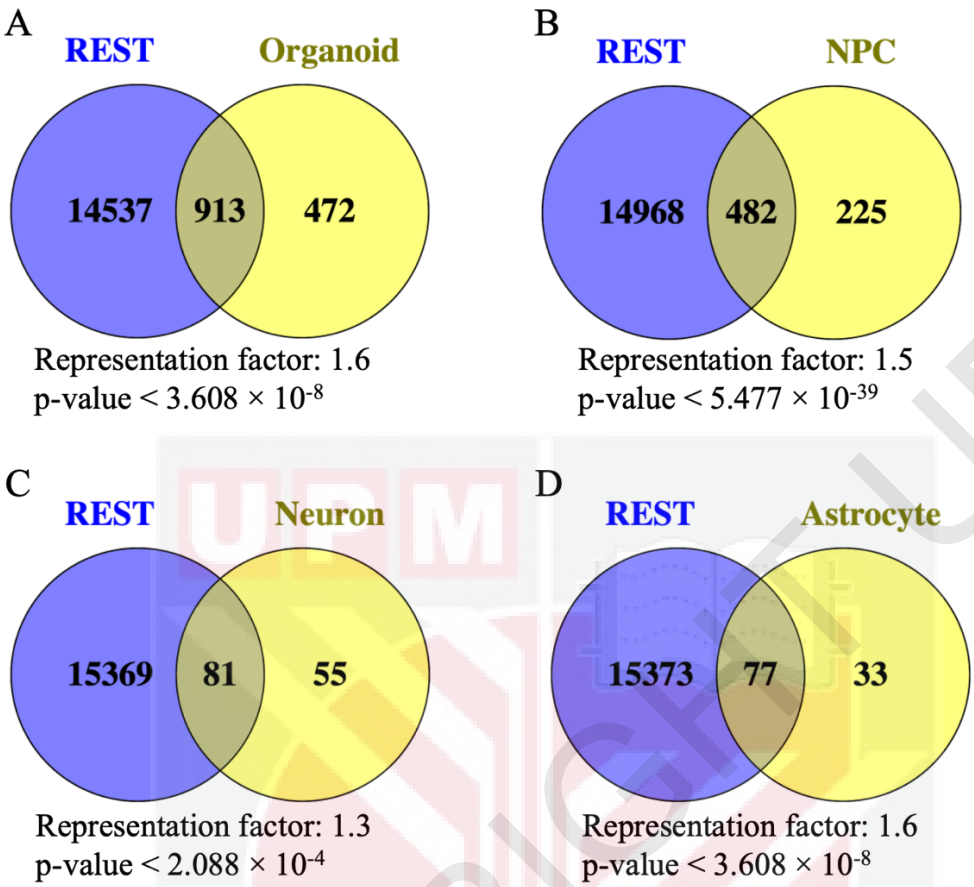


Figure 3.12 : Depiction of the Overlap between REST Target Genes and DEGs from DS-Derived Cerebral Organoids (A), NPCs (B), Neurons (C) and Astrocytes (D). The blue circles represent REST target genes, the yellow circles represent DEGs, and the overlapping parts are REST target DEGs. Fisher's test determined the statistical significance of this gene overlap, revealing all p-values < 0.01. A representation factor > 1 indicates more overlap than expected of two independent groups, a representation factor < 1 indicates less overlap than expected, and a representation factor of 1 indicates that the two groups by the number of genes expected for independent groups of genes

3.4.3 GO and KEGG Enrichment Analyses of REST-Target DEGs

To gain a deeper understanding of the functional and molecular characteristics of REST in DS, the GO and KEGG enrichment analyses were conducted using the RStudio software. This analysis focused on all REST-targeted DEGs in DS brain tissue, including the common REST-targeted DEGs in the different brain regions and ages, as well as in DS-derived cerebral organoids, NPCs and astrocytes.

3.4.3.1 The Critical Role of REST-Targeted DEGs in DS Different Brain Regions

The DEGs targeted by REST were found to be significantly involved in important biological processes in eight specific regions of the human brain. These processes include developing the nervous system, response to oxygen levels, development of neuron projections, regulation of neurogenesis, cell morphogenesis, axon development, and neuron death (Figure 3.13). Furthermore, these genes had significant involvement in many signalling pathways, including the HIF-1 signalling pathway, axon guidance, focal adhesion, MAPK signalling pathway, and fatty acid degradation/metabolism (Figure 3.14). Examining the shared DEGs targeted by the REST protein in all brain areas revealed the predominance of neurogenesis, gliogenesis, neuron projection development, the JAK-STAT signalling pathway and the HIF-1 signalling pathway. This observation indicates a possible decrease in the suppression of REST (Figure 3.15).

© COPYRIGHT UPM

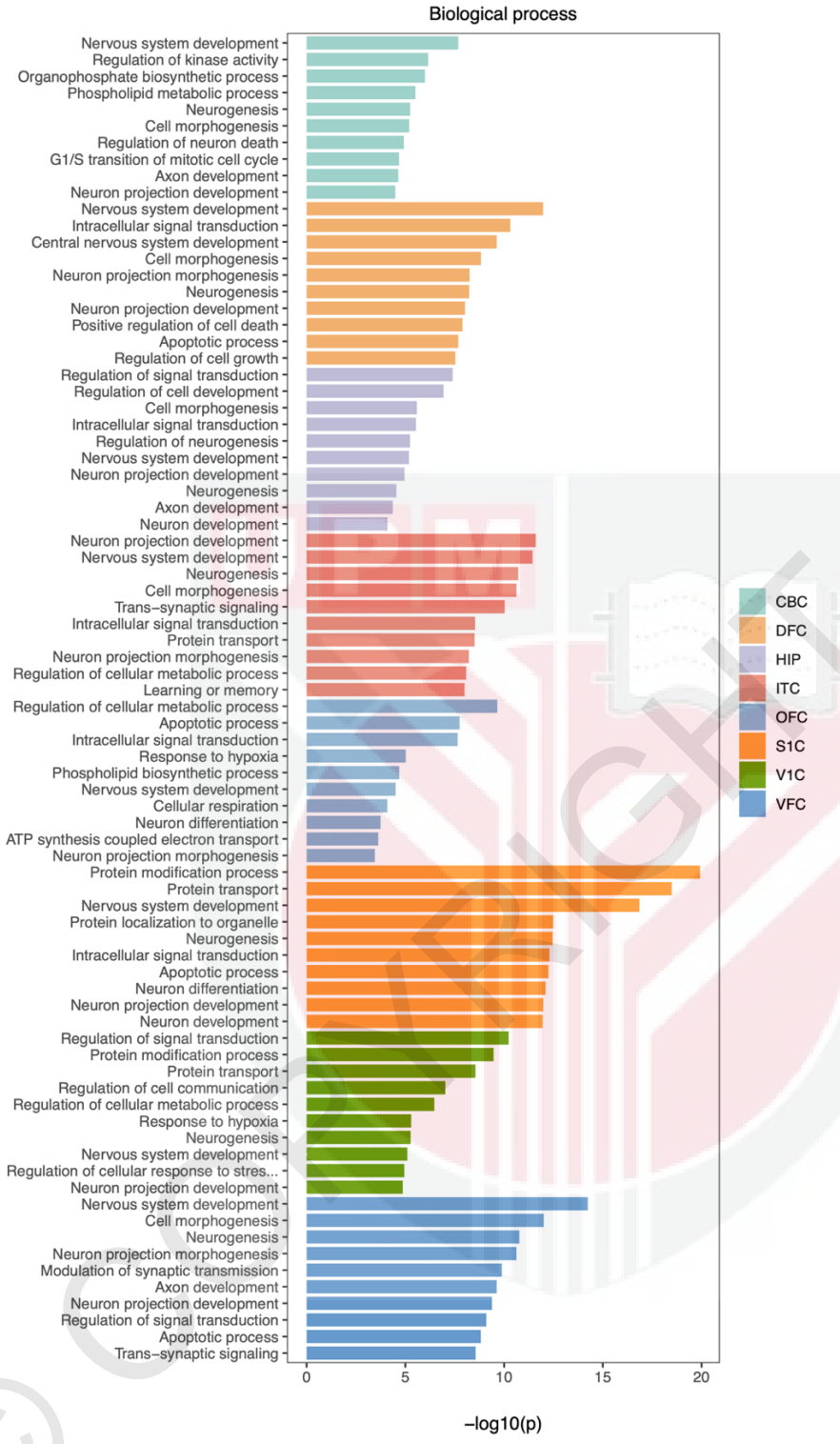


Figure 3.13 : Biological Process Enrichment Analysis Associated with REST-Targeted DEGs across DS Various Brain Regions. Different colours indicate different regions of the DS brain. The top 10 GO terms for each region are shown. Cerebellar cortex: CBC; Dorsolateral prefrontal cortex: DFC; Hippocampus: HIP; Inferior temporal cortex: ITC; Prefrontal cortex: OFC; Primary somatosensory cortex: S1C; Primary visual cortex: V1C; Ventrolateral prefrontal cortex: VFC

© COPYRIGHT UPM

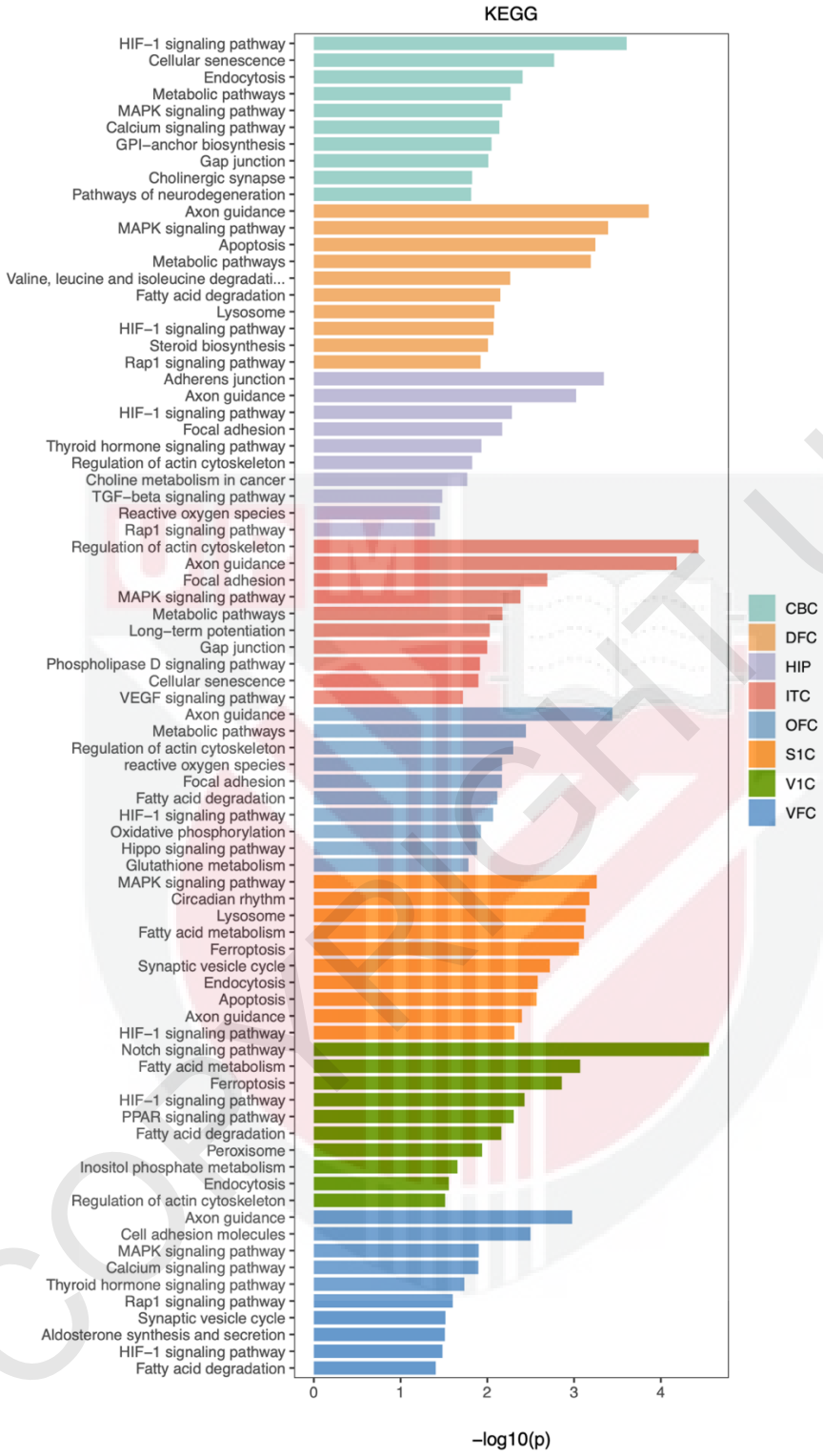


Figure 3.14 : KEGG Enrichment Analysis Associated with REST-Targeted DEGs across DS Various Brain Regions. Different colours indicate different regions of the DS brain. The top 10 KEGG pathways for each region are shown. Cerebellar cortex: CBC; Dorsolateral prefrontal cortex: DFC; Hippocampus: HIP; Inferior temporal cortex: ITC; Prefrontal cortex: OFC; Primary somatosensory cortex: S1C; Primary visual cortex: V1C; Ventrolateral prefrontal cortex: VFC

© COPYRIGHT UPM

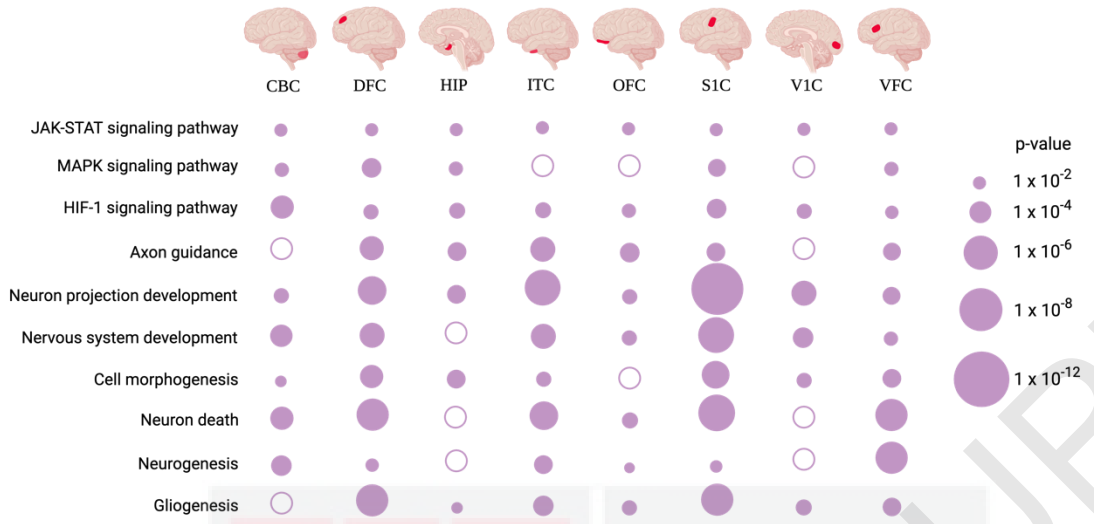


Figure 3.15 : Summary of Signalling Pathways and Biological Functions Enriched in DS Different Brain Regions. Hollow circles indicate that the term was not enriched. The larger the solid circle, the smaller the p-value of the enrichment. Cerebellar cortex: CBC; Dorsolateral prefrontal cortex: DFC; Hippocampus: HIP; Inferior temporal cortex: ITC; Prefrontal cortex: OFC; Primary somatosensory cortex: S1C; Primary visual cortex: V1C; Ventrolateral prefrontal cortex: VFC. The figure was created in BioRender (License number: SS27U4WI9C)

3.4.3.2 The Critical Role of REST-Targeted DEGs in DS Different Age Brain

The DEGs targeted by the REST in the fetal brain were mainly linked to ontologies connected with the formation of neurogenesis, neuron death, neuron projection development, and intracellular protein transport (Figure 3.16, 3.17). The KEGG enrichment results revealed that these genes are implicated in cellular senescence, apoptosis, processes associated with neurodegeneration and HIF-1 signalling pathways (Figure 3.16, 3.17). The postnatal brains showed significant enrichment of GO terms for DEGs targeted by REST. These DEGs are linked to multiple processes, such as gliogenesis, neurogenesis, neuron death, axonal guidance, cellular morphological development and response to hypoxia (Figure 3.16, 3.17). According to the KEGG enrichment analysis, these genes are implicated in JAK-STAT, HIF-1 signalling pathways, and focal adhesion (Figure 3.16, 3.17). In child's brains, these

© COPYRIGHT UPM

DEGs are linked to multiple processes, such as neurogenesis, neuron death, cell morphogenesis and response to hypoxia (Figure 3.16, 3.17). According to the KEGG enrichment analysis, these genes are implicated in fatty acid metabolism, reactive oxygen species and HIF-1 signalling pathways (Figure 3.16, 3.17). The DEGs targeted by REST in adults were enriched in processes associated with the neurogenesis, neuron death, axon development, axonogenesis, and trans-synaptic signalling (Figure 3.16, 3.17). The enrichment analysis performed with KEGG indicated a specific association of these genes with guiding the axon, fatty acid metabolism and HIF-1 signalling pathways (Figure 3.16, 3.17).

© COPYRIGHT UPM

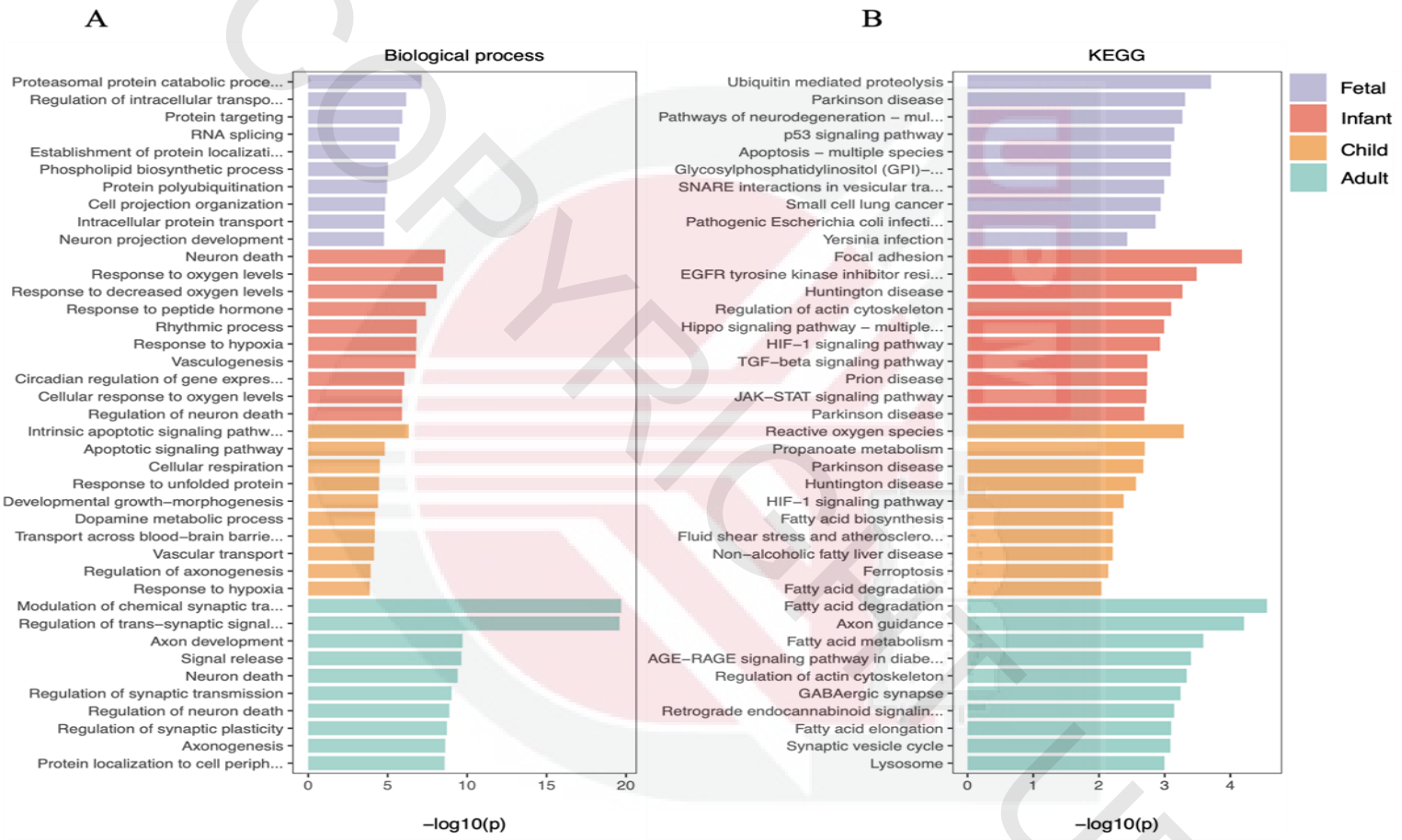


Figure 3.16 : Analysis of Biological Processes and KEGG Pathways Associated with REST Target DEGs in Fetal (16 to 22 Gestational Weeks), Infant Child (2 to 16 years), Child (2 to 16 years) and Adult (18 to 42 years). Different colours indicate different age groups. The top 10 biological processes (A) and KEGG pathways (B) for each age group are shown

© COPYRIGHT UPM

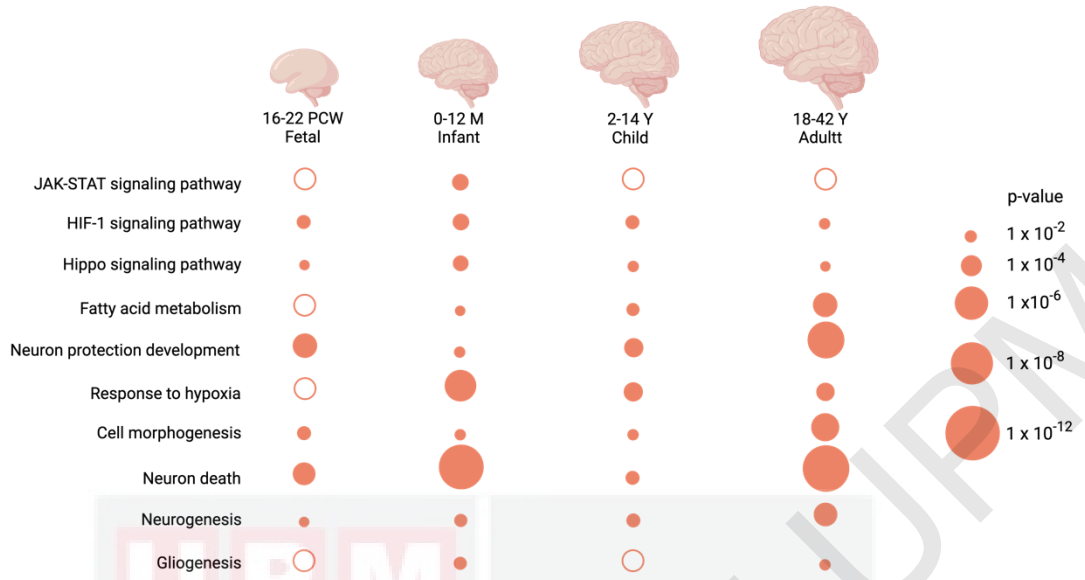


Figure 3.17 : Summary of Signalling Pathways and Biological Functions Enriched in REST-Targeted DEGs Consistently Identified across Ages in DS. Hollow circles indicate that the term was not enriched. The larger the solid circle, the smaller the p-value of the enrichment. PCW = post-conception weeks, M = month, Y = year. The figure was created in BioRender (License number: MZ27U4WIB3)

3.4.3.3 The Critical Role of REST-Targeted DEGs in DS-Derived Cerebral Organoids and Neural Cells

The analysis of the enrichment of GO terms in DEGs targeted by REST in cerebral organoids revealed important information on key processes such as forebrain development, neural precursor cell proliferation, and cell mitosis (Figure 3.18A). The KEGG enrichment data revealed significant enrichment in pathways associated with the cell cycle, neuroactive ligand-receptor interaction, and axon guidance (Figure 3.18B). Notably, DEGs targeted by REST in DS NPCs show enrichment in biological processes related to embryonic development, neural tube formation, axon development, and cell differentiation (Figure 3.18A). These processes match with KEGG pathways associated with JAK-STAT signalling pathway, TNF signalling pathway, and axon guidance (Figure 3.18B). The DEGs targeted by REST in DS neurons exhibit a notable enrichment in processes related to the cell cycle and

© COPYRIGHT UPM

immune-inflammatory responses (Figure 3.18A). This finding was consistent with the JAK-STAT signalling pathway identified in the KEGG study (Figure 3.18B). The DEGs targeted by REST in DS astrocytes primarily contributed to cell development, regulation of inflammatory response, and fatty acid degradation/metabolism (Figure 3.18A). This was determined through KEGG enrichment analysis, which specifically identified the involvement of these genes in the fatty acid metabolism pathway (Figure 3.18B). The integration of KEGG and GO important findings from cerebral organoids, NPCs, neurons, and astrocytes was depicted in Figure 3.19.

© COPYRIGHT UPM

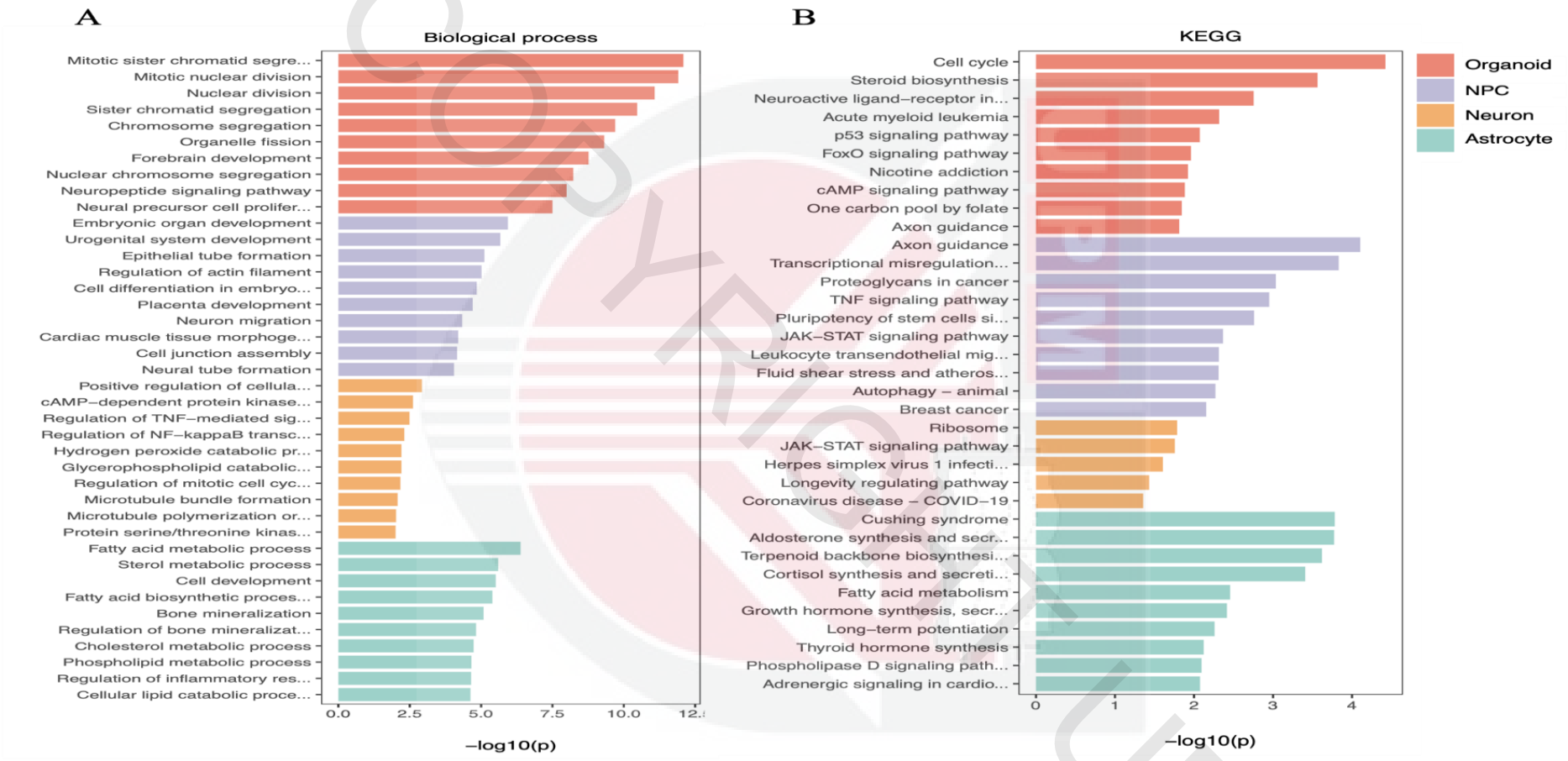


Figure 3.18 : Analysis of Biological Processes and KEGG Pathways Associated with REST Target DEGs in DS-Derived Cerebral Organoids, NPCs, Neurons and Astrocytes, Respectively. Different colours indicate different neural cell types. The top 10 biological processes (A) and KEGG pathways (B) for the neural cells are shown

© COPYRIGHT UPM

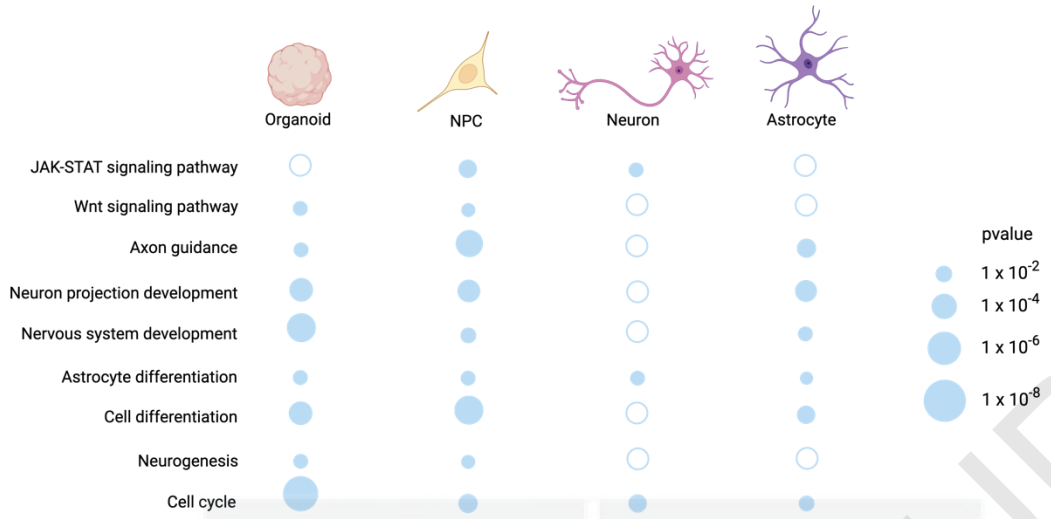


Figure 3.19 : Summary of Signalling Pathways and Biological Processes Involved in REST Target DEGs in DS-Derived Cerebralorganoids, NPCs, Neurons and Astrocytes, Respectively. Hollow circles indicate that the term was not enriched. The larger the solid circle, the smaller the p-value of the enrichment. The figure was created in BioRender (License number: QR27U4WICH)

3.4.4 Construction of DEGs PPI Network and Identification of MCODEs

The Protein-Protein Interaction (PPI) networks of DEGs and the three most significant modules in neural progenitor cells, neurons, and astrocytes were created (Figure 3.20, 3.21, 3.22). The important modules mainly consisted of DEGs specifically targeted by REST. These DEGs were highlighted in red and green, indicating up-regulation and down-regulation inside the modules. The research demonstrated that the genes in the modules of NPCs were essential for determining cell fate, guiding axonal growth, and projecting neurons [Figure 3.20E]. The genes in the modules of neurons were mainly linked to astrocyte activation, glucose catabolic process, and NADH regeneration [Figure 3.21E]. In addition, the genes inside the astrocyte modules showed a notable increase in sterol metabolic process, neuron projection organisation, and neuron projection maintenance [Figure 3.22E].

© COPYRIGHT UPM

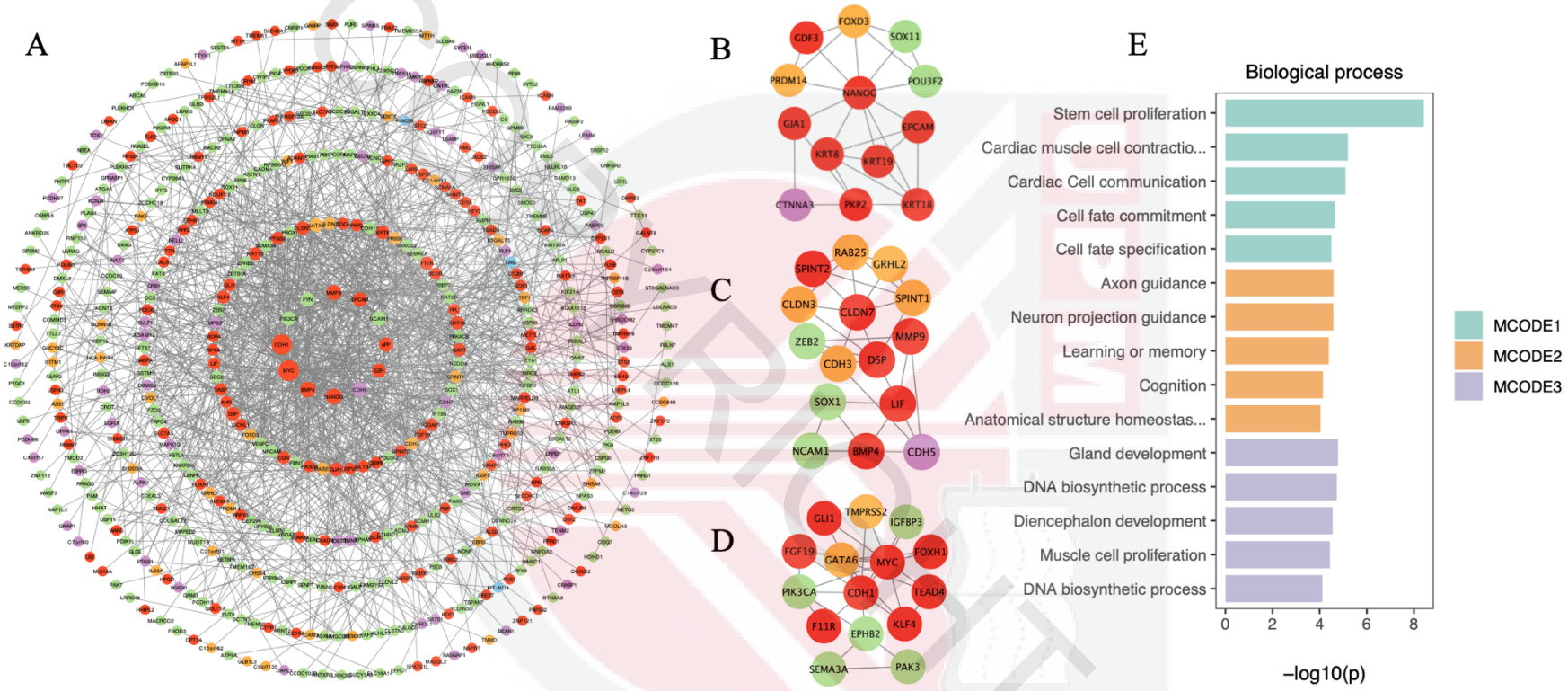


Figure 3.20 : Protein-Protein Interaction Networks and Enrichment Analysis of DEGs in DS-Deirved NPCs. (A) Protein-protein interaction networks for the DEGs in NPCs are constructed using Cytoscape. The red nodes indicate genes that are upregulated and targeted by REST, while the green nodes indicate genes that are downregulated and targeted by REST. The yellow nodes represent upregulated genes not targeted by REST, while the purple nodes reflect downregulated genes not targeted by REST. Greater node sizes correspond to a higher distribution of network node degrees. (B-D) The top three modules discovered by the MCODE plug-in of Cytoscape for DEGs in NPCs. (E) The top three essential modules in NPC DEGs and the four most significant GO enrichment terms for each module

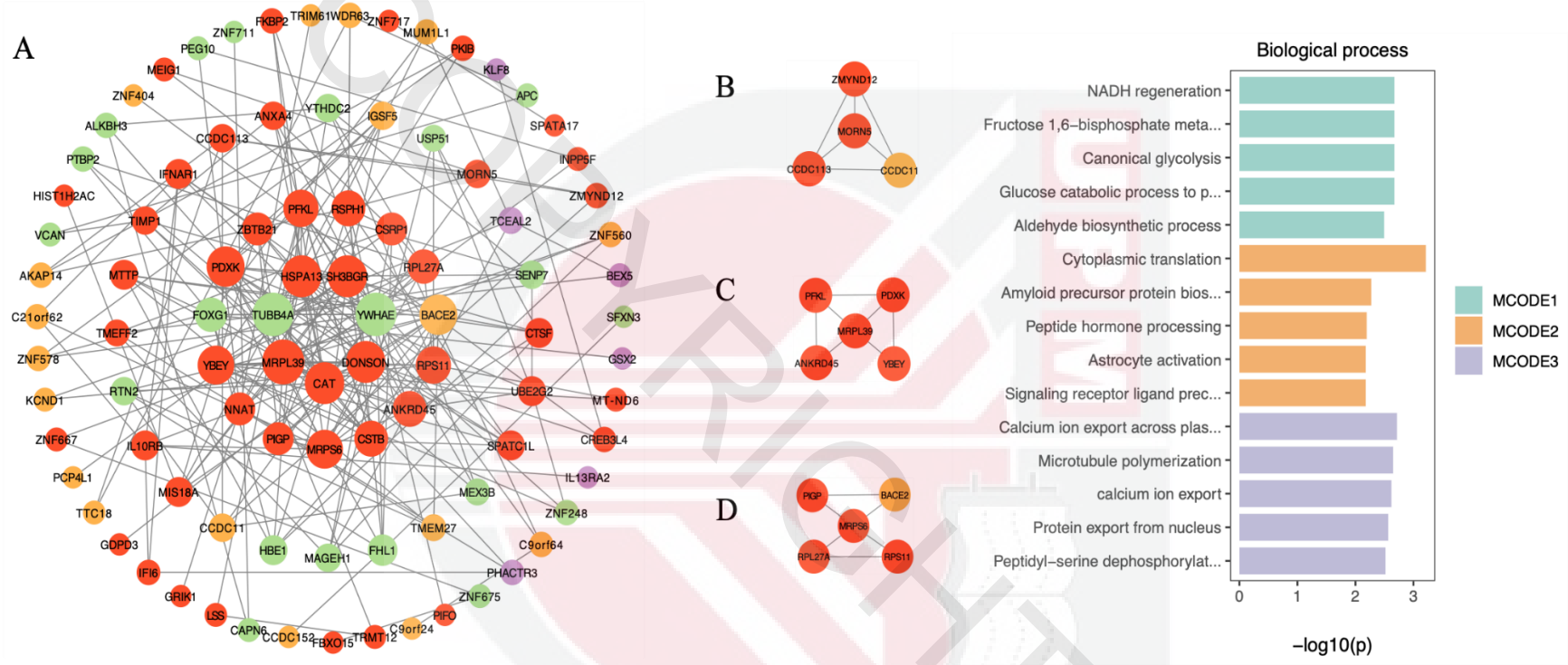


Figure 3.21 : Protein-Protein Interaction Networks and Enrichment Analysis of DEGs in DS-Deirved Neurons. (A) Protein-protein interaction networks for the DEGs in neurons are constructed using Cytoscape. The red nodes indicate genes that are upregulated and targeted by REST, while the green nodes indicate genes that are downregulated and targeted by REST. The yellow nodes represent upregulated genes not targeted by REST, while the purple nodes reflect downregulated genes not targeted by REST. Greater node sizes correspond to a higher distribution of network node degrees. (B-D) The top three modules discovered by the MCODE plug-in of Cytoscape for DEGs in neurons. (E) The top three essential modules in neuron DEGs and the four most significant GO enrichment terms for each module

© COPYRIGHT UPM

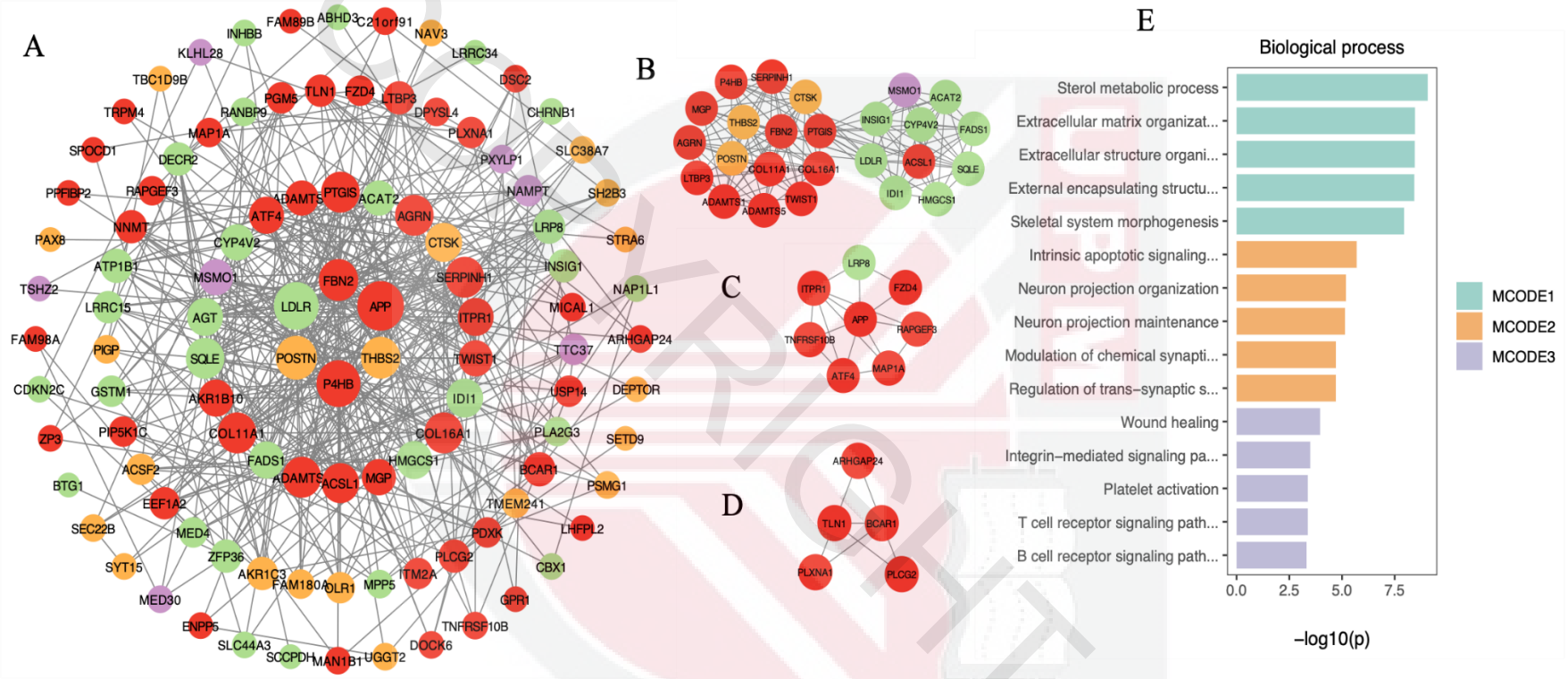


Figure 3.22 : Protein-Protein Interaction Networks and Enrichment Analysis of DEGs in DS-Deirved Astrocytes. (A) Protein-protein interaction networks for the DEGs in astrocytes are constructed using Cytoscape. The red nodes indicate genes that are upregulated and targeted by REST, while the green nodes indicate genes that are downregulated and targeted by REST. The yellow nodes represent upregulated genes not targeted by REST, while the purple nodes reflect downregulated genes not targeted by REST. Greater node sizes correspond to a higher distribution of network node degrees. (B-D) The top three modules discovered by the MCODE plug-in of Cytoscape for DEGs in astrocytes. (E) The top three essential modules in astrocyte DEGs and the four most significant GO enrichment terms for each module.

3.5 Discussion

This investigation revealed fifty-one differentially expressed genes targeted by REST consistently found in all areas of individual brains with DS. Among these, forty-one genes exhibited upregulation. Additionally, fifty-six DEGs targeted by REST were discovered at every developmental stage of the DS brain, with thirty-nine genes showing upregulation. These REST-targeted genes demonstrated enrichment in the Janus kinase and the signal transducers and activators of the transcription (JAK-STAT) pathway, hypoxia-inducible factor 1 (HIF-1) pathway, neural development, inflammation, response to hypoxia, neurogenesis and gliogenesis. Furthermore, this study revealed that the DEGs targeted by REST in organoids and neural cells were also involved in similar biological processes and signalling pathways. Therefore, the disruption of REST regulation may significantly contribute to the complex neurological phenotype of DS.

REST, a pivotal transcription factor, is a critical inhibitory regulator for numerous genes, especially those involved in neuronal functions. It exerts its influence by binding to specific DNA consensus sequences within gene regulatory regions, thereby depressing the transcription of these genes, including those associated with NPC differentiation, neurogenesis, and neuronal maturation (Mozzi et al., 2017; Ovando et al., 2014; Wang et al., 2012). Elevated expression of REST inhibits the activity of genes that are located further downstream in the genetic pathway. It has been indicated that overexpression of REST has been associated with brain tumours, ischaemic injury, epilepsy and Huntington's disease (Bates et al., 2015; Calderone et al., 2003; Kamal et al., 2012; Singh et al., 2011). Conversely, a reduction or loss of REST diminishes its ability to suppress the activation of genes farther down the line, resulting in their

© COPYRIGHT UPM

increased expression. Previous work has reported that the lack of REST in neurons leads to the upregulation of genes associated with oxidative stress and ageing (Rocchi et al., 2021). Therefore, the disruption of REST in the cell nuclear may interfere with the transcription of its target genes in DS.

This study revealed the JAK-STAT signalling pathway is targeted by REST in multiple brain regions and neural cells in DS. Evidence demonstrates that the JAK-STAT pathway has a role in neural stem/progenitor cell proliferation and migration, cell differentiation, cell fate determination, neurogenesis, gliogenesis, and neuroinflammation (Chen et al., 2021; Gutiérrez and Soto, 2020; Todd et al., 2016). This pathway is activated by a wide range of cytokines, interferons, and growth factors, such as *IFNAR1*, *IFNAR2*, *IL6*, and *COX-2*. Notably, the distinctive neurogenic-to-gliogenic shift observed in DS brains, characterized by decreased neurons and increased astrocytes, is a prominent pathological feature (Stagni et al., 2018a). Activation of the JAK-STAT pathway during brain development prompts NPCs to undergo astrogenesis, thereby influencing the fate of glial cells (Nicolas et al., 2013). Phosphorylating JAKs, specifically JAK1 and JAK2, triggers the activation of STAT3, which in turn induces the transcription of astrocyte specificity genes such as *S100B* and *GFAP* (Hong and Song, 2014; Nicolas et al., 2013). Astrocytes have a critical role in maintaining neurons and controlling important processes like synaptogenesis and neurotransmitter stability. However, in DS, the abnormal growth of astrocytes leads to problems such as mitochondrial malfunction, increased levels of reactive oxygen species (ROS), and the death of neurons (Freeman, 2010; Siracusa et al., 2019). Dysfunctional astrocytes in DS, indicated by impaired maturation, underscore the pivotal role of the JAK–STA signalling system in the neurogenic-to-gliogenic shift

© COPYRIGHT UPM

(Lee et al., 2019). This study identified upregulation of key JAK-STAT pathway activators, including *IFNAR1*, *IFNAR2*, and *OSM*, in DS brains, indicating a potential role for REST in modulating the gene dosage and influencing gliogenesis.

Understanding the intricate connection between REST and the JAK-STAT pathway sheds light on the potential therapeutic avenues for mitigating neurogenic-to-gliogenic shifts and neuroinflammation in DS and related neurological disorders (Thompson and Chan, 2018). While previous research demonstrated reduced REST expression in DS fetal brain cells, the direct regulatory link between REST and JAK-STAT remains elusive. Nonetheless, parallels observed in other neurological disorders, such as Parkinson's disease and glioblastoma, emphasise the potential significance of the loss of REST in over-activating the JAK-STAT pathway (Kawamura et al., 2019; Lashgari et al., 2021; Lepagnol et al., 2007; Ou et al., 2021). Notably, the imbalance of gene dosage in *DYRK1A* disrupted REST protein levels in DS, potentially contributing to JAK-STAT pathway activation and abnormal astrogliogenesis (Canzonetta et al., 2008; Kurabayashi et al., 2015). Therefore, the elucidation of the REST target JAK-STAT pathway is expected to advance therapeutic interventions for DS and to understand the mechanisms underlying neurodevelopmental deficits in DS.

This work also revealed a substantial influence of REST on regulating the HIF-1 signalling pathway in DS. Without control of REST, hypoxia excessively activates the HIF-1 signalling pathway. During a state of low oxygen levels (hypoxia), astrocytes and microglia become stimulated to release interleukin-1 (IL-1), a biological mechanism that relies on hypoxia-inducible factor 1 (Inada et al., 2021). In extended periods of low oxygen (hypoxia), REST steped in to negatively control HIF-1,

© COPYRIGHT UPM

hindering its mRNA transcription and promoting protein breakdown (Cavadas et al., 2016). When REST was reduced or eliminated, *HIF-1* mRNA and protein levels notably increased (Cavadas et al., 2015). In individuals with DS, the JAK-STAT pathway activation has been linked to increased activity in microglia and astrocytes. Studies indicated a complex interaction between the JAK-STAT and HIF-1 pathways. HIF-1 promoted JAK2 and STAT3 expression under hypoxic conditions, hence initiating the JAK-STAT pathway. Conversely, JAK-STAT activation, particularly STAT3, enhanced HIF-1 expression and stability (Wang et al., 2021). This crosstalk between STAT3 and HIF-1 was observed in ischemia and glioma (Carlsson et al., 2018; Dvorakova et al., 2024). REST appeared crucial in influencing the interplay between JAK-STAT and HIF-1 pathways, impacting astrocyte reactivity (Cavadas et al., 2015).

Additionally, the abundance of REST protein dictates the outcome of NPCs differentiation, steering them towards neurons or astrocytes (Baldelli and Meldolesi, 2015; Pajarillo et al., 2021). In NPCs, REST serves as a pivotal transcription factor for the regulation of differentiation in the neural cell lineage. It exhibits heightened expression in NPCs, enhancing glial cell development. Simultaneously, its natural decline in late NPCs prompted the expression of neural specificity genes, guiding them toward a neuronal phenotype (Zhao et al., 2017). REST exerted exact regulation over neural epigenomes, cell differentiation, axonal development, vesicle transport, ionic channel transduction, and plasticity of synapses by suppressing target genes (Su et al., 2022). Previous research has shown that the nucleus REST protein serves as a protective mechanism for neurons against oxidative stress, which is linked to a longer lifespan (Lu et al., 2014). Moreover, the primary external apoptotic pathways,

© COPYRIGHT UPM

specifically the tumour necrosis factor (TNF) and apoptotic process linked to TNF pathways, including the ligand TRAIL, have significant importance. TNF and TRAIL attach the death ligands to their corresponding death receptors, which then recruit adaptor proteins like TNFR1-linked death domains and death domain-linked protein molecules. These adaptor proteins serve as a framework for the activation of apoptosis initiation molecules (Jin and Deiry, 2005). REST is indispensable for suppressing adaptor protein expression, curbing receptor complex production, and disrupting downstream apoptotic signalling (Lu et al., 2014).

The analysis also revealed that REST has a crucial role in regulating fatty acid metabolism in the brains of both children and adults, along with astrocytes. The metabolism relationship between neurons and astrocytes is dependent on the clearance of lipids in neurons. Specifically, fatty acids from lipid droplets in neurons are transferred to astrocytes in a manner that is influenced by the ApoE isoform (Qi et al., 2021). Astrocytes utilise mitochondrial β-oxidation to digest fatty acids derived from stored neurons, thereby safeguarding neurons against the harmful effects of fatty acids neurotoxicity and oxidative stress damage (Ioannou et al., 2019). Disruptions in astrocytic metabolism of lipids, oxidative damage, mitochondrial metabolism, and anti-inflammation pathways, as evidenced by the storage and transport of astrocyte lipid droplets, disturb the metabolic balance of the central nervous system. This results in disrupted energy production, inflammation, excessive neuronal stimulation, toxicity, and pathological processes associated with many neurodegenerative conditions (Lee et al., 2021).

© COPYRIGHT UPM

3.6 Conclusions

By analysing the genes that are expressed differently in brain tissues, organoids, and neural cells of individuals with DS, this study discovered that the REST protein has a significant influence on the regulation of gene expression (suach as *IFNAR1*, *IFNAR2*, *PFKL* and *SLC2A1*) in many regions of the brain (CBC, DFC, HIP, ITC, OFC, S1C, V1C, and VFC), at different ages (Fetal, Infant, Child, and Adult), and in different types of cells (NPCs, neurons and astrocytes). Significantly, REST specifically targets many DEGs in DS, showing its crucial role in the overall neuro-pathological process. The GO and KEGG enrichment analyses highlight the potential of REST potential as a therapeutic target. REST exerts regulatory control over pathways such as JAK-STAT and HIF-1, NPCs development, and astrocyte heterogeneity.

© COPYRIGHT UPM

CHAPTER 4

DYSREGULATION OF REST AND ITS TARGET GENES IMPACTS THE FATE OF TRISOMIC NEURAL PROGENITOR CELLS

4.1 Introduction

To explore the molecular mechanisms underlying the widespread neurodevelopmental defects in Down syndrome (DS), many studies have analysed genomic transcripts in DS-derive neural progenitor cells. In DS human embryonic stem cell-derived NPCs, although the relative expression of genes on chromosome 21 was approximately 1.5-fold higher than that on other chromosomes, most of the differentially expressed genes were located on other autosomes other than chromosome 21 compared with disomic NPCs (Halevy et al., 2016). This study found that apoptosis-related genes were up-regulated, and prefrontal developmental genes were down-regulated in DS-derived NPC (including neuron-related *POU3F2* and *ASCL1*) (Halevy et al., 2016). Genome-wide transcriptional analysis of DS hiPSC-derived NPCs showed that trisomy 21 induced genome-wide transcriptional disruption, including "chromosome introgression" and overall chromatin accessibility changes (Meharena et al., 2022). Although this study did not observe *GFAP* expression in DS hiPSC-derived NPCs, suggesting that they do not differentiate prematurely into astrocytes, an exploration of the fate propensity of DS-derived NPCs is absent (Meharena et al., 2022). Single-cell sequencing studies of hiPSC-derived neural stem cells showed that the generalised lineage of disomy hiPSC-derived NPCs consisted of 66.5% neural stem cells, 19.5% neural progenitor cells, and 13.9% radial glial progenitor cells (Qiu et al., 2023). Nevertheless, the proportion of neural stem cells in trisomy hiPSC-derived NPCs was only 46.5%, whereas the proportion of radio-glial progenitors was as high as 38.1%,

© COPYRIGHT UPM

in addition to the presence of 3.9% oligodendrocyte progenitors (Qiu et al., 2023). This suggests an abnormal differentiation fate of DS hiPSC-derived NPCs, with premature differentiation of NPCs toward glial cells and reduced differentiation toward neuronal cells. However, these studies did not provide further insight into the molecular mechanisms that influence the fate decisions of DS-derived NPCs.

In a previous chapter, REST has been shown to mediate neural development in DS. REST proteins are maintained at high expression levels in NPCs to regulate cell pluripotency, differentiation and proliferation (Johnson et al., 2008). As differentiation progresses towards the neuronal lineage, a reduction in REST expression occurs, resulting in the expression of target genes in neurogenesis and neuronal function (Baldelli and Meldolesi, 2015). This process governs axon elongation, synaptic communication, membrane responsiveness, and the establishment of neuronal identity. Additionally, REST is pivotal in overseeing the development of glial cell lineages, gliogenesis, and the interactions between neurons and glial cells (Pajarillo et al., 2021). During NPC differentiation, the appropriate level of REST is crucial for transitioning from neurogenesis to gliogenesis and maintaining the correct neuron-to-glial cell ratio. REST, initially active during fetal brain development, is later reactivated in the nucleus to safeguard neurons from various stressors, preserve cognitive functions, and promote longevity (Lu et al., 2014). In a transchromosomal model of DS, a 30-60% reduction in REST expression was found, an alteration that persists from undifferentiated embryonic stem cells (ESCs) to the adult brain in trisomy 21 (Canzonetta et al., 2008). Despite its known functions, the specific role of REST in DS-derived NPCs remains inadequately understood. Further research is necessary to elucidate how dysregulation of REST affects these cells.

© COPYRIGHT UPM

In this study, the effects of trisomy chromosome 21 on NPCs was explored and the potential effects of REST in molecular and cellular dysregulation was examined. HiPSC-derived NPCs served as a powerful platform for investigating the neurodevelopmental aspects of DS. The publicly available datasets of DS hiPSC-derived NPCs was obtained and a comprehensive transcriptomic analysis associated with REST target genes was conducted. This study demonstrated that REST-targeted DEGs significantly impact cellular functions and pathways in DS hiPSC-derived NPCs, leading to considerable disruptions during development and differentiation. Laboratory validations confirmed the REST-targeted DEGs involved in the neurogenic-to-gliogenic shift in DS hiPSC-derived NPCs.

4.2 Experiment Design

The transcriptome datasets of DS hiPSC-derived NPCs were downloaded and processed using the Galaxy online platform for differentially expressed genes (DEGs) analysis. The GSE185192 dataset was employed for the primary analysis, whereas the GSE208625 dataset was utilised for validation purposes. Enrichment analysis and visualisation of REST-targeted DEGs were conducted using R software to identify the biological processes and signalling pathways targeted by REST in DS. Hub genes were identified through Weighted Gene Co-expression Network Analysis (WGCNA) and PPI analysis. Further experimental validation of these key genes was performed using hiPSC-derived NPC models and additional experimental analyses. Figure 4.1 presents a simplified diagram of the data processing and analysis workflow and the experimental procedures used in this study.

© COPYRIGHT UPM

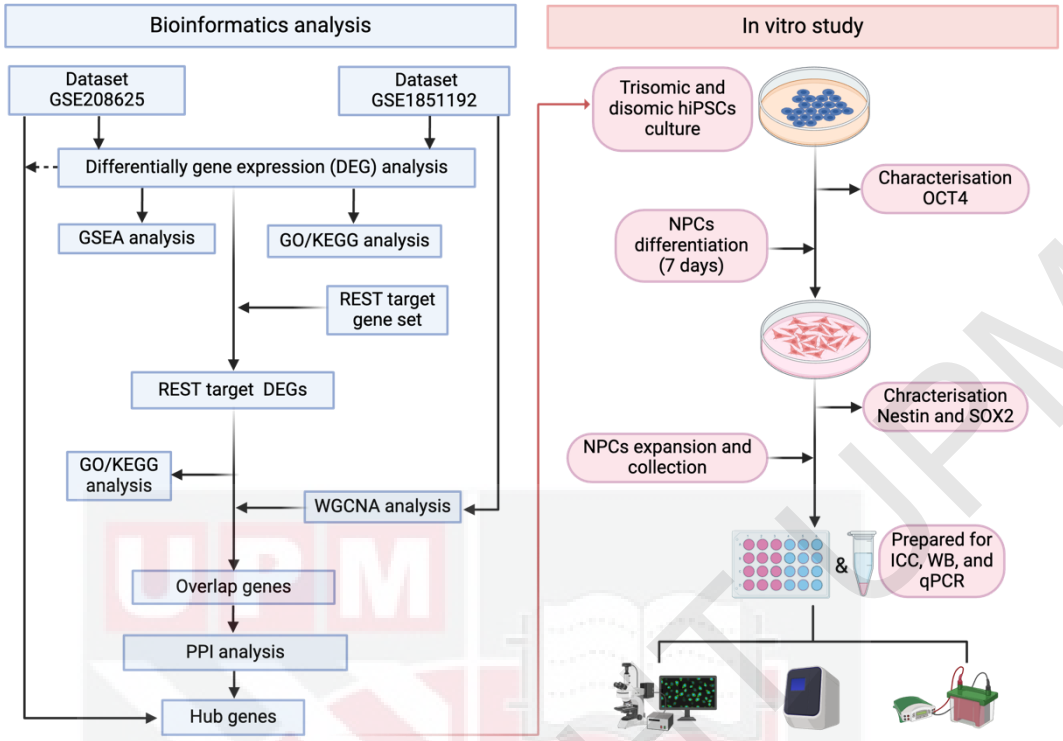


Figure 4.1 : Simplified Diagram of the Experimental Methods, Data Processing, and Analysis Workflow Used for This Study. DS, Down syndrome; GO, Gene Ontology; KEGG, Kyoto encyclopedia of genes and genomes; PPI, Protein-protein interaction; hiPSC, Human induced pluripotent stem cells; NPC, Neural progenitor cells; ICC, Immunocytochemistry. The figure was created by Biorender.com (License number: HG27U4G12I)

4.3 Materials and Methods

4.3.1 Acquisition and Process of DS hiPSC-Derived NPCs Datasets

The sequence data for hiPSC-derived NPCs were acquired from the Gene Expression Omnibus database (GEO, https://www.ncbi.nlm.nih.gov/geo/). The GSE185192 dataset with the Affymetrix GPL18573 platform includes 18 transcriptome samples from one isogenic pair (3 DS samples and 3 controls) and two non-isogenic pairs (6 DS samples and 6 controls) (Meharena et al., 2022). The GSE208625 dataset with the Affymetrix GPL16791 includes six transcriptome samples from one non-isogenic pair

© COPYRIGHT UPM

(3 DS samples and 3 controls) (Qiu et al., 2023). The GSE185192 was utilised for the primary analysis, and the GSE208625 was used for validation purposes.

4.3.2 Processing of the Dataset and Identification of Differentially Expressed Genes (DEGs)

The Galaxy web-based platform (https://www.usegalaxy.org/) was used to analyse the Next-Generation Sequencing (NGS) dataset (Galaxy Community, 2022). The *Trim Galore* software (Galaxy Version 0.6.7+galaxy0) was used to read and trim the FASTQ files. The *FASTQC* software (Galaxy Version 0.74+galaxy1) was used to test the quality of individual samples. Subsequently, the *HISAT2* software (Galaxy Version 2.2.1+galaxy1) was employed to align the transcriptome sequences, using the *hg38* human reference genome for annotation. The *htseq-count* software (Galaxy Version 2.0.5+galaxy0) was used to count aligned reads. Lastly, *DESeq2* software (Galaxy Version 2.11.40.8+galaxy0) was utilised to analyse differentially expressed genes between DS and control groups. Genes were classified as DEGs based on adjusted p-value < 0.05 (Benjamini-Hochberg method) and |log2 FC| > 1. The analysis results were visualised with a heatmap and volcano plot created using RStudio software (Version: 2023.03.0+386) (Appendix A2).

4.3.3 Gene Set Enrichment Analysis

The gene set enrichment analysis (GSEA) (Subramanian et al., 2005) was employed to evaluate the statistical significance of GO and KEGG pathways enrichment (Appendix B1), which was statistically significant in DS hiPSC-derived NPCs and controls from the GSE185192 dataset. The three packages (*org.Hs.eg.db*, *clusterProfiler* and *enrichplot*) in R software were utilised for GSEA analysis and

© COPYRIGHT UPM

visualisation. Findings exhibiting a normalised enrichment score (NES) of |NES| > 1 and an adjusted p-value < 0.05 (Benjamini-Hochberg method) were considered statistically significant.

4.3.4 REST-Targeted DEGs in DS hiPSC-Derived NPCs

Human-specific REST target genes were retrieved from the Gene Transcription Regulation Database (http://gtrd.biouml.org). To visualise the overlap compared these REST-targeted genes with the DEGs from the GSE185192 dataset, Venn diagrams were generated using the web tool https://bioinfogp.cnb.csic.es/tools/venny/. The significance of the gene overlap was then evaluated using the hypergeometric probability model, with the human genome as the reference background (http://nemates.org).

4.3.5 Gene Ontology and Pathway Enrichment Analysis

GO and KEGG enrichment analyses were performed on DEGs and REST-targeted DEGs using on DEGs and REST-targeted DEGs with R package *clusterProfiler* (Wu et al., 2021) (Appendix A3). The significant enrichment results from GO and KEGG with p-values < 0.05 were considered. The *rrvgo* and *simplifyEnrichment* packages perform semantic similarity analysis on the GO analysis results and cluster the results (Appendix B2). The *heatmapPlot* and *complexheatmap* packages were used to visualise the enriched GO and KEGG results (Appendix B3).

© COPYRIGHT UPM

4.3.6 WGCNA Network Construction and Module Identification

Weighted Gene Co-expression Network Analysis (WGCNA) is a comprehensive biological method used to group genes exhibiting similar expression profiles, organising them into modules according to their correlation (Zhang and Horvath, 2005). The network was developed and visualised utilising the *WGCNA* package in R software (Appendix B4). This study performed WGCNA on the GSE185192 dataset, which consists of 9 DS and 9 corresponding control samples. The network development was performed using a soft-threshold parameter (β). The value of β was selected by identifying the lowest power achieved at a scale-free topological overlap matrices fit value of 0.9. Pearson correlation analyses was conducted to investigate the interrelationships among gene modules and determine the module that exhibits the strongest correlation with DS. Gene significance (GS) and module membership (MM) values were calculated, and the genes exhibiting a GS of more than 0.5 and MM exceeding 0.8 were recognised as being highly correlated with the module.

4.3.7 PPI Network Construction for Screening Hub Genes

The protein-protein interaction (PPI) network was induced through the Search Tool for the Retrieval of Interacting Genes database (STRING, https://string-db.org/) (Szklarczyk et al., 2019) with an interaction score of at least 0.4. To pinpoint hub genes within the overlapping genes of REST-targeted DEGs and core modules of WGCNA, we constructed a modular gene network using Cytoscape software (version 3.9.1) (Shannon et al., 2003). The "cytoHubba" plugin was utilised to predict and explore significant nodes or hub genes (Chin et al., 2014). To identify hub genes, a total of ten topological algorithms of "cytoHubba", including Betweenness,

© COPYRIGHT UPM

Bottleneck, Closeness, EcCentricity, Edge Percolated Component (EPC), Maximum Cluster Centrality (MCC), Maximum Neighbourhood Component (MNC), Radality, and Stress were used to obtain the top 20 ranked genes, respectively. The overlap of these 10 gene sets was then identified as the hub genes.

4.3.8 Validation of Hub Genes

To determine whether the expression levels of the REST-targeted hub gene varied significantly between DS hiPSC-derived NPCs and controls, these levels were visualised using scatter plots and box-and-line plots for the GSE185192 dataset. Real-time quantitative RT-PCR will then be conducted to validate the mRNA expression level of these hub genes.

4.3.9 Cell Culture

Three trisomic iPSC lines [DS2 (WC-24-02-DS-M), DS3 (UWWC1-2DS3), and DS4 (HPS4270)) and three disomic iPSC lines [C2 (WC-24-02-DS-A), C4 (ATCC-DYS0100), and C5 (HPS4272)] were utilized in this study. These lines included two pairs of isogenic cell lines (DS2 and C2; DS4 and C5) and one pair of non-isogenic cell lines (DS3 and C4). DS2, C2, and DS3 were obtained from the WiCell Research Institute at the University of Wisconsin (Giffin-Rao et al., 2020; Weick et al., 2013); C5 and DS4 were sourced from the RIKEN BioResource Center in Japan (Wakita et al., 2022); and C4 was acquired from the American Type Culture Collection (Wren et al., 2015). Detailed information on the cell lines is provided in Table 4.1. HiPSCs were cultured in complete mTeSR™ Plus medium (STEMCELL Technologies, Canada, Cat. no. 100-0276) on six-well plates coated with Geltrex (Gibco, USA, Cat. no. A1413302), following the instructions of the manufacturer. Upon reaching

© COPYRIGHT UPM

approximately 80% confluency, the hiPSCs were dissociated with accutase and seeded onto Geltrex-coated six-well plates at a density of 300,000 cells per well in complete mTeSR™ Plus medium supplemented with 5μM Y27632 (STEMCELL Technologies, Canada, Cat. no. 72304). For neural induction, hiPSCs at 20% confluency were exposed to a complete Neural Induction Medium (Gibco, USA, Cat. no. A1647801) for 7 days, with medium changes every two days, following the instructions of the manufacturer. The resulting hiPSC-derived NPCs were expanded in Neural Expansion Medium [comprising Neural Induction Medium and AdvancedTM DMEM/F-12 (Gibco, USA, Cat. no. 12634028)] on a Geltrex-coated 6-well plate, following the instructions of the manufacturer.

Table 4.1 : Details of the Disomic Control and Trisomic DS iPSC Lines

Cell label	Cell line	Donor origin	Reprogramming method	Provider
C2 DS2	WC-24-02-DS-A WC-24-02-DS-M	• Mosaic DS individual • Female • Aged 25 • Skin fibroblast	Non-integrating episomal vector	WiCell Research Institute, University of Wisconsin
C4	ATCC-DYS0100	• Healthy individual • Male • Neonate • Skin fibroblast	Sendai viral transfection system	American Type Culture Collection (ATCC)
DS3	UWWC1-2DS3	• Trisomy 21 individual • Male • Neonate • Skin fibroblast	Non-integrating episomal vector	WiCell Research Institute, University of Wisconsin
C5 DS4	HPS4272 HPS4270	• Trisomy 21 individual • Male • Aged <10 • Skin fibroblast	Non-integrating episomal vector	RIKEN BioResource Center, Japan

© COPYRIGHT UPM

4.3.10 Immunocytochemistry

4.3.10.1 Cell Culture and Fixation on the Coverslip

Cells were seeded onto the coverslips (Marienfeld, Germany, Cat, no. 0111530) coated by Geltrex in 0.5 mL of full media, changed media every two days. Once the cells have reached the desired confluence (~60% confluence), discard the medium and rinse the cells with 1X dulbecco's phosphate-buffered saline (DPBS) [10X DPBS (Thermo Fisher Scientific, USA, Cat. no. 14200075) was diluted to 1X DPBS with double distilled water]. The cells were then fixed on coverslips in the 4% paraformaldehyde (PFA) (VWR, USA, Cat. no. J351) solution for 15 minutes at room temperature. The coverslips were washed with 1X DPBS 3 times for 5 minutes each time. The fixed cells are stored in 1X DPBS at 4ºC until use.

4.3.10.2 Immunocytochemistry Procedure

The immunochemical staining procedure was performed according to previously published paper (Lam et al., 2025). The coverslip was washed in 1X phosphate-buffered saline (PBS) [10X PBS (Thermo Fisher Scientific, USA, Cat. no. 70011044) was diluted to 1X DPBS with double distilled water] 3 times for 10 minutes each time. The coverslip was incubated with 100µL of blocking solution for 30 minutes at room temperature. The blocking solution was prepared by mixing 10% donkey serum (Solarbio, China, Cat. no. SL050) and 0.3% triton X-100 (Thermo Fisher Scientific, USA, Cat. no. 85112) in 1X PBS. Next, the cells were incubated with 100µL of primary antibody, prepared in the blocking solution and incubated overnight at 4ºC. The next day, the cells were washed thrice with 1X PBS at room temperature for 10 minutes each time. The cells were then incubated in 100µL secondary antibody

© COPYRIGHT UPM

(prepared in 1X PBS) for 2 hours at room temperature in the dark. The solution was removed, and the sample was rinsed three times with 1X PBS at room temperature, allowing 10 minutes for each wash. ProLong® Gold Antifade mountant with DAPI (Thermo Fisher Scientific, USA, Cat. no. S36920) was added on a microscopic slide. The coverslip was carefully inverted onto the DAPI mounting media. The slide was kept dark for 24 hours at 4°C before imaging.

The primary antibodies used for immunodetection were as follows: anti-REST (Host: Rabbit; Proteintech, USA, Cat. no. 22242-1-AP; 1:200 dilution), anti-DCX (Host: Rabbit; Cusabio, USA, Cat. no. CSB-PA006576DA0HU; 1:200 dilution), anti-NFIA (Host: Rabbit; Elabscience, USA; Cat. no. E-AB-67569; 1:200 dilution), anti-SOX2 (Host: Goat; Abcam, USA, Cat. no. ab239218; 1:200 dilution) and anti-Nestin (Host: Mouse; Invitrogen, USA, Cat. no. MA1-110; 1:200 dilution). The secondary antibodies used for immunodetection were as follows: donkey anti-rabbit IgG conjugated with Alexa Fluor 488 (Invitrogen, USA, Cat. no. A-21206; 1:1000 dilution) for REST, DCX and NFIA; donkey anti-mouse IgG conjugated with Alexa Fluor 488 (Invitrogen, USA, A-21202; 1:1000 dilution) for Nestin; donkey anti-goat IgG H&L with Alexa Fluor 594 (Abcam, USA, Cat. no. ab150132; 1:2000 dilution) for SOX2.

4.3.10.3 Image Analysis

Fluorescence microscopy was employed to capture images, utilising an Olympus microscope (Olympus, Japan). The acquired fluorescence micrographs were subsequently analysed using Fiji software (https://imagej.net/software/fiji/). Prior to analysis, measurement parameters were defined, including “Area,” “Mean Grey Scale,” and “Integrated Density.” To ensure accurate quantification, a calibration step was

© COPYRIGHT UPM

performed by opening a JPEG image with a known scale from the same microscope, zooming in to visualise the scale clearly, and applying the "Set Scale" function to standardise measurements in micrometers (μm). Quantitative fluorescence intensity analysis required background signal correction, particularly for images stained with Alexa Fluor 488 or Texas Red dye. A technical negative control, consisting of an image of section incubated solely with the secondary antibody (Alexa Fluor 488/Texas Red dye) without a primary antibody, was used for this correction. In Fiji, the negative control image (TIFF format) was opened, and its channels were separated using the "Split Channel" function, retaining only the green channel. The image was then converted to greyscale, and brightness and contrast were adjusted to define an exposure range where no signal was visible. This exposure range was applied to the experimental TIFF images to normalize fluorescence signal intensity.

For nuclear REST fluorescence intensity detection, REST-stained images (TIFF format) were processed in Fiji by separating the channels and converting the target channel to greyscale. The normalised signal intensity was subtracted to minimise background interference. The corresponding DAPI-stained image was then used to identify nuclei overlapping with the REST signal. The "Threshold" and "Analyze Particles" functions were applied to segment and select the nuclei. Once identified, fluorescence intensity measurements were performed simultaneously across all selected nuclei, generating a dataset that was subsequently exported to an Excel spreadsheet for further analysis.

Whole-cell fluorescence intensity measurements followed a similar approach. The image channels were separated, the desired channel was converted to greyscale, and

© COPYRIGHT UPM

the normalised signal intensity was subtracted. The “Threshold” function was then used to select the region of interest, and fluorescence intensity measurements were performed for all selected cells. The resulting quantitative data were saved to an Excel spreadsheet for further statistical analysis.

4.3.11 Quantitative Real-Time Polymerase-Chain Reaction (RT-qPCR)

4.3.11.1 RNA Extraction and Reverse Transcription on RNA Samples

RNA was extracted from hiPSC-derived NPCs using the GeneAll® Ribospin™ II II RNA extraction kit (GeneAll, Korea, Cat. no. 314-150) following the protocol of manufacturer. The concentration and purity of the isolated RNAs will be measured using the NanoDrop™ 1000 spectrophotometer (Thermo Fisher Scientific). Reverse transcription was then carried out with the LunaScript® RT SuperMix kit (New England Biolabs, USA, Cat. no. E3010L). RNA concentrations will be adjusted with nuclease-free water, and the 1ug total RNA will be reverse-transcribed in a 20µL reaction volume following the manufacturer's guidelines.

4.3.11.2 Primer Design

Primers were designed utilising the primers finding tool Primer-BLAST (https://www.ncbi.nlm.nih.gov/tools/primer-blast/). PCR Primer Stats (https://www.bioinformatics.org/sms2/pcr_primer_stats.html) are used to assess the properties of PCR derivatives, including melting temperature, GC content percentage and PCR suitability. A suitable PCR derivative further verified the product of the primers in the UCSC In-Silico PCR database (https://genome.ucsc.edu/cgi-bin/hgPcr) to ensure specificity and optimal performance. All RT-qPCR primers are shown in

© COPYRIGHT UPM

Table 4.2. RT-qPCR was conducted on a LightCycler® 480 system (Roche Diagnostics, Australia).

© COPYRIGHT UPM

Table 4.2 : List of Primer Sequences for RT-qPCR

Gene	Forward primers (5'→3')	GC%	Reverse primers (5'→3')	GC%	Annealing temperature (℃)	Amplicon size (bp)
CD44	TACCCCAGCAACCCTACTGA	55.00	GGTCCTGTCCTGTCCAAATCT	52.38	60	155
COL1A1	AGGGACACAGAGGTTTCAGT	50.00	AGCACCATCATTTCCACGAG	50.00	60	188
DCX	GAAGGGAAACCCATCAGCCA	55.00	GAGGTTCCGTTTGCGTCTTG	55.00	60	138
FN1	CCGCCGAATGTAGGACAAGA	55.00	CCGAACCTTATGCCTCTGCT	55.00	60	231
HMBS	GCCGTGCATACAGCTATGAAG	52.38	TTACGAGCAGTGATGCCTACC	52.38	60	179
ITGB1	GCCAAATGGGACACGCAAGA	55.00	TTGACCACAGTTGTTACGGC	50.00	60	140
JAK2	CCGGGTTTCAGAAGCA	56.25	TCAGAACATTTGCCGTCG	50.00	60	100
NFIA	TGAAGTGGAGCCAGGAATGC	55.00	ATGACAGGTCGGTGATGCTG	55.00	60	129
PSMB2	GAGGGCAGTGGAACTCCTTAG	57.14	GATGTTAGGAGCCCTGTTTGG	52.38	60	149
REST	GAGAACGCCCATATAAATGTG	42.86	CACATAACTGCACTGATCAC	45.00	60	172
STAT3	AGAAGGACATCAGCGGTAAG	50.00	CGTTGGTGTCACACAGATAA	45.00	60	275
TGFB1	TTGAGGGCTTTCGCCTTAGC	55.00	CGGTAGTGAACCCGTTGATG	55.00	60	84

F, Forward Primer; R, Reverse Primer; *CD44*, CD44 molecule; *COL1A1*, Collagen type I alpha 1 chain; *DCX*, Doublecortin; *FN1*, Fibronectin 1; *HMBS*, Hydroxymethylbilane synthase; *ITGB1*, Integrin subunit beta 1; *JAK2*, Janus kinase 2; *NFIA*, Nuclear factor I A; *PSMB2*, Proteasome 20S subunit beta 2; *REST*, RE1 silencing transcription factor; *STAT3*, Signal transducer and activator of transcription 3; *TGFB1*, Transforming growth factor beta 1.

© COPYRIGHT UPM

4.3.11.3 RT-qPCR Protocol

RT-qPCR preparation was performed on the cDNA using 2x Luna® Universal qPCR Master Mix (New England Biolabs, USA, Cat. no. M3003E) following the guidelines of the manufacturer. The RT-qPCR assays with a final volume of 20 µl will be conducted with the LightCycler® 480 Real-Time PCR System (Roche Diagnostics, Australia). Samples will undergo duplicate assays, with *PSMB2* and *HMBS* as internal controls. The primers for the RT-qPCR validation are listed in Table 4.2. The condition for the RT-qPCR induced an initial denaturation step with 1 cycle of 95ºC for 60 seconds, followed by 45 cycles of 95ºC (denaturation) for 15 seconds and 60ºC (extension) for 30 seconds, I cycle of 72ºC (melt curve) for 30 seconds. After completing all the RT-qPCR processes, take out the 96-well plate and store it in a 4-degree refrigerator.

4.3.11.4 RT-qPCR Analysis

The cycle of quantification (Cq) for each signal was calculated according to the second-order derivative maximum method (Luu-The et al., 2005). Multiple sets of mixed, serially diluted cDNA synthesised from 1ug of RNA from human neural cells were used to construct a standard curve of four data points per PCR assay in each run. Successful assays were defined as PCR efficiencies between 90% and 110% with an R-squared value > 0.98. Relative quantification of target gene expression in trisomic and disomic samples was performed using a comparative CT approach. In-sample data were normalised for two endogenous control reference genes: hydroxymethylbilane synthase (*HMBS*) and proteasome subunit β type 2 (*PSMB2*).

© COPYRIGHT UPM

4.3.12 Western Blot

4.3.12.1 Total Protein Extraction

The cell samples were stored at -80ºC till the protein extraction procedure. Total cellular protein extraction was performed as described in previous study (Kirby et al., 2015). For protein extraction from NPCs, cell lysis buffer was prepared by mixing RIPA buffer (Thermo Fisher Scientific, USA, Cat. no. 89901,) and 100X proteinase inhibitor at a 100:1 ratio, then adding phosphatase inhibitor pellet (1 pellet for 10mL solvent). The cell lysis buffer was added to the cells, and gentle pipetting suspended the mixture. The tube containing the mixture was shaken gently for 30 minutes on the ice. Next, the tube was centrifuged with 13,000rpm at 4ºC for 30 minutes. The supernatant was transferred to a new tube, then stored in a -80ºC freezer.

4.3.12.2 Protein Quantification with BCA Assay

Protein concentration was analysed by using the Pierce™ BCA Protein Assay Kit (Thermo Fisher Scientific, USA, Cat. no. 23225) and bovine serum albumin (BSA) protein standard control according to the standard microplate protocol in the manufacturer's instruction manual on a 96-well plate. Biochrom Asys UVM 340 microplate reader with MikroWin software was used to detect colourimetric signal in BCA assay. The standard curve was constructed, and the protein concentration of cell samples was calculated based on the standard curve.

4.3.12.3 Gel Electrophoresis

The Western Blotting process was performed according to the Bio-Rad protocol. The Laemmli loading buffer was prepared by mixing 4X Laemmli buffer with 10% β-

© COPYRIGHT UPM

Mercaptoethanol. A total of 20µl protein samples was prepared by mixing 6.25µL of Laemmli loading buffer and the respective volume of 1 X Laemmli buffer. The protein samples were heated at 100°C for 5 minutes. The denatured protein samples were cooled on ice and kept at -20°C until usage. The 10-well TGX pre-cast gels (Bio-Rad, USA, Cat. No. 4561083) were assembled into the electrophoresis module. The module was then placed into the electrophoresis tank (Bio-Rad, USA). The assembly (middle and outside of the chamber) was filled with 1X running buffer [mixed 10X premixed electrophoresis buffer (Bio-Rad, USA, Cat. no. 1610732) and distilled water in a ratio of 1:9]. 7.5 microliters of pre-stained protein ladder (Kaleidoscope™ Prestained Protein Standards, USA, Cat. no. 1610375) and 20 µl protein sample were loaded into the wells. The lid was placed on the tank, and electrical leads were inserted into a power pack. The electrophoresis was run at 80 volts for 20 minutes, then 120 volts for 1 hour on ice for two gels and bubble formation at the bottom of the assembly indicated the electrophoresis was running. The assembly was carefully removed from the electrophoresis tank, and the running buffer was discarded after the electrophoresis was completed. The two plastic plates of pre-cats gel were removed from the assembly and separated gently. The gel was equilibrated in a 1X transfer buffer [mixed 10X transfer buffer (Thermo Fisher Scientific, USA, Cat. no. 35040,), distilled water, and methanol in a ratio of 1:6:2] for 10 minutes.

4.3.12.4 Protein Transfer from Gel to Membrane

Polyvinylidene fluoride (PVDF) membrane (GE Healthcare, 7.5cm x 8.5cm) was pre-treated by soaking in methanol for 30 seconds, distilled water for 1-2 minutes, and then in 1X transfer buffer for 10 minutes with agitation. Two sponge pads (Bio-Rad, USA， Cat. no. 1703914) were soaked in 1X transfer buffer for at least 15 minutes.

© COPYRIGHT UPM

The blotting cassette of the Trans-Blot® TurboTM Transfer System (Bio-Rad, USA) was removed and opened, exposing the cassette base. A sponge pad was laid on the centre of the cassette base as the anode stack, followed by the PVDF membrane. The pre-cast gel was carefully aligned onto the PVDF membrane, followed by the second sponge pad. Then, the cassette lid was placed on the cassette base and locked. The second sponge pad was gently placed onto the gel as a cathode stack. The cassette was placed back into the Trans-Blot Turbo instrument bay with the transfer protocol "Mixed mode, 2.5 A,10 minutes". Upon completion of the transfer, the sandwich was disassembled, and the membrane was gently removed. The membrane was kept wet by soaking in Tris-buffered saline with 0.1% Tween 20 Detergent (Thermo Fisher Scientific, USA, Cat. no. 85114) (TBST). Each band of the protein ladder was gently re-labelled by using a pencil.

4.3.12.5 Immunodetection and Visualisation by Transillumination

The PVDF membrane was washed in 1X TBST and then closed with 5% nonfat milk (Bio-Rad, USA, Cat. no. 1706404). This 5% nonfat milk was prepared in 1X TBST at room temperature on a laboratory shaker. Next, the PVDF membrane was incubated with 4 ml of primary antibody, which was prepared in 5% nonfat milk and incubated overnight at 4ºC on a laboratory shaker. The next day, the PVDF membrane was washed three times on a laboratory shaker with 1X TBST at room temperature for 20 minutes each time. The PVDF membrane was then incubated in 4 ml of secondary antibody (Goat Anti-Rabbit IgG H&L (HRP); Abcam, USA, Cat. no. ab6721; 1:2000) diluted in 1X TBST. for 1 hour at room temperature on a laboratory shaker in the dark. The secondary antibody solution was discarded, and the membrane was washed three times with 1X TBST for 10 min each under laboratory conditions protected from light.

© COPYRIGHT UPM

The immunoreactivity of the proteins was then visualised using chemiluminescence. Pierce™ ECL Western Blotting Substrate (Thermo Scientific, USA, Cat. no. 32106) was used to visualise GAPDH, REST, DCX, and NFIA. The assay solution was added at a one-to-one ratio, left at room temperature, and protected from light for 2 minutes. Signals were detected using the Syngene G: BOX gel documentation system with GeneSys software (Synoptics Ltd, UK). The following primary antibodies were used for immunodetection: anti-REST (Host: Rabbit; 22242-1-AP; Proteintech, USA; 1:1000 dilution), anti-DCX (Host: Rabbit; CSB-PA006576DA0HU; Cusabio, USA; 1:1000 dilution), anti-NFIA (Host: Rabbit; E-AB-67569; Elabscience, USA; 1:1000 dilution), and anti-GAPDH (Host: Rabbit; E-AB-40337; Elabscience, USA; 1:4000 dilution).

4.3.12.6 Image Analysis

Pixelated analysis of the bands was performed using FIJI software according to the standard protocol published on https://fiji.sc/#. The blot images of each protein were combined and analysed with GAPDH as the housekeeping protein. Histograms were generated by Fiji analysis of the combined blot images. Band intensities are expressed as the area of the peaks in the histogram results.

4.3.13 Statistical Analysis

The data are presented as mean ± standard deviation (SD), with all experiments conducted in triplicate. Statistical analyses were performed using Prism 9.0 (version 9.5.0, GraphPad) or R software (version 2023.03.0+386). An independent samples t-test was used to compare the differences between the two independent experimental groups. A significance threshold of $p\text{-value} < 0.05$ was applied, and statistical

© COPYRIGHT UPM

significance is represented as follows: ns, not significant; * p-value < 0.05; ** p-value < 0.01; *** p-value < 0.001.

4.4 Results

4.4.1 Differentially Expressed Genes and Their Ontologies

This study analysed the DEGs in DS hiPSC-derived NPCs (GSE185192). We identified 3,106 DEGs in DS-derived NPCs, including 1,544 upregulated and 1,562 downregulated DEGs (Figure 4.2 for heat map and volcano plot). The GO enrichment analyses from all DEGs in DS-derived NPCs reveal that these genes are enriched for cell differentiation, nerve development, neuron fate commitment, neuron recognition, Wnt signalling pathway, stem cell development, and neural precursor cell proliferation (Figure 4.3).

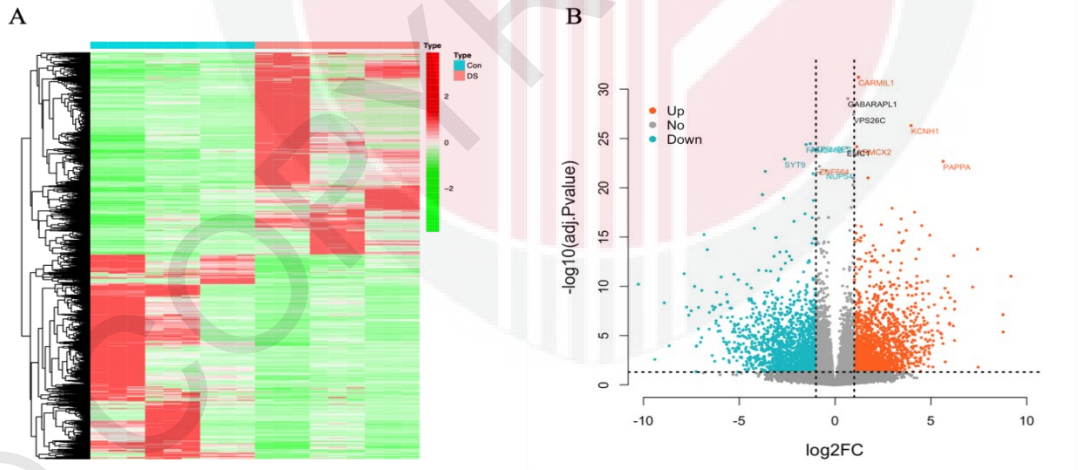


Figure 4.2 : The Heat Map and Volcano Plot for the DEG Analysis of DS-Derived NPCs. (A) Heat map analysis of identified DEGs between DS-derived NPCs and controls. Red represents upregulated genes, while green represents downregulated genes. (B) The volcano plot is for DEGs in DS hiPSC-derived NPCs. The top 10 DEGs with the most significant p-values are shown in Appendix B5. Red represents upregulated differentially expressed genes, blue represents downregulated differentially expressed genes, and grey represents genes with no differential expression

© COPYRIGHT UPM

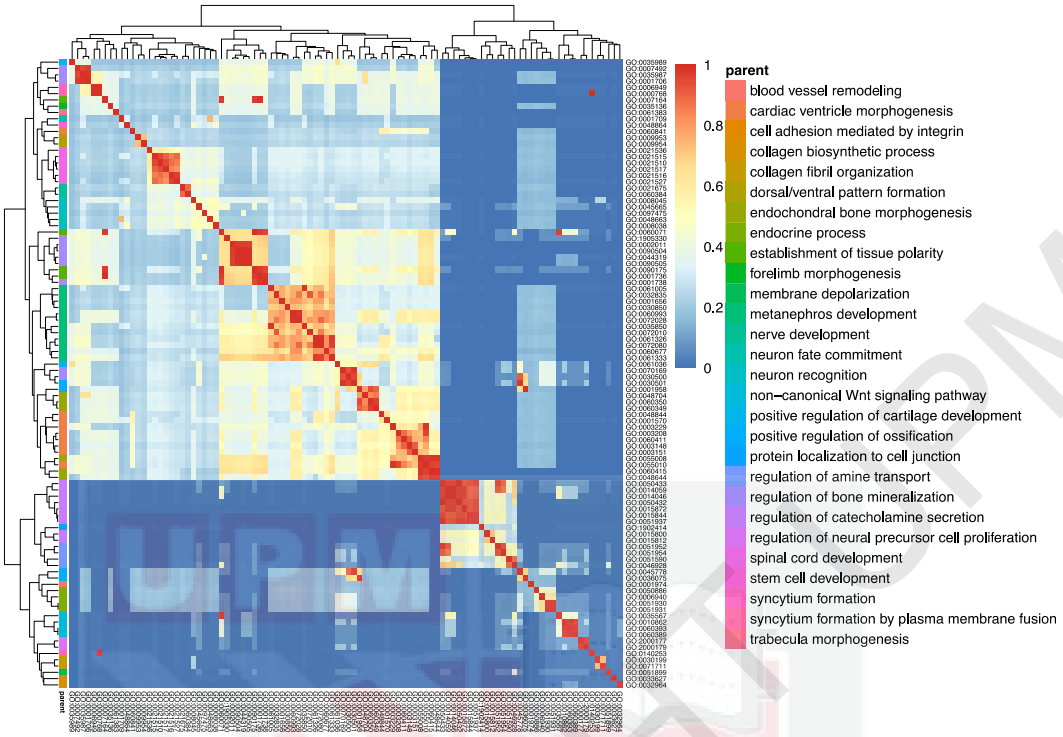


Figure 4.3 : Biological Process Clustering Enrichment Analysis for the DEGs in DS hiPSC-Derived NPCs. The top 100 GO terms were clustered based on semantic similarity. The similarity scale ranges from 0 to 1, with colours ranging from blue to red, as indicated by the colour bar. The redder the colour, the closer the similarity value is to 1, indicating higher similarity. GO terms with high semantic similarity are grouped into clusters, as shown by the *parent bar*

4.4.2 GSEA Analysis Revealed Abnormalities in Neural Cell Differentiation

The results of the GSEA-GO analysis revealed that gene sets associated with biological processes such as cell fate commitment, central nervous system neuron differentiation, negative regulation of gliogenesis, neuron fate commitment, and regulation of neurogenesis were all downregulated in the DS hiPSC-derived NPCs. These GO-related gene sets were significantly enriched with NES < -1, p<1e-10 and adj. p< 2.383e-08 (Figure 4.4A). Then GSEA-KEGG analysis was performed, which showed that the JAK-STAT signalling pathway with NES > 1 was upregulated in DS hiPSC-derived NPCs. At the same time, Wnt signalling pathways with NES < -1 were

© COPYRIGHT UPM

downregulated (Figure 4.4B). The Wnt pathway is crucial for NPC proliferation and neurogenesis.

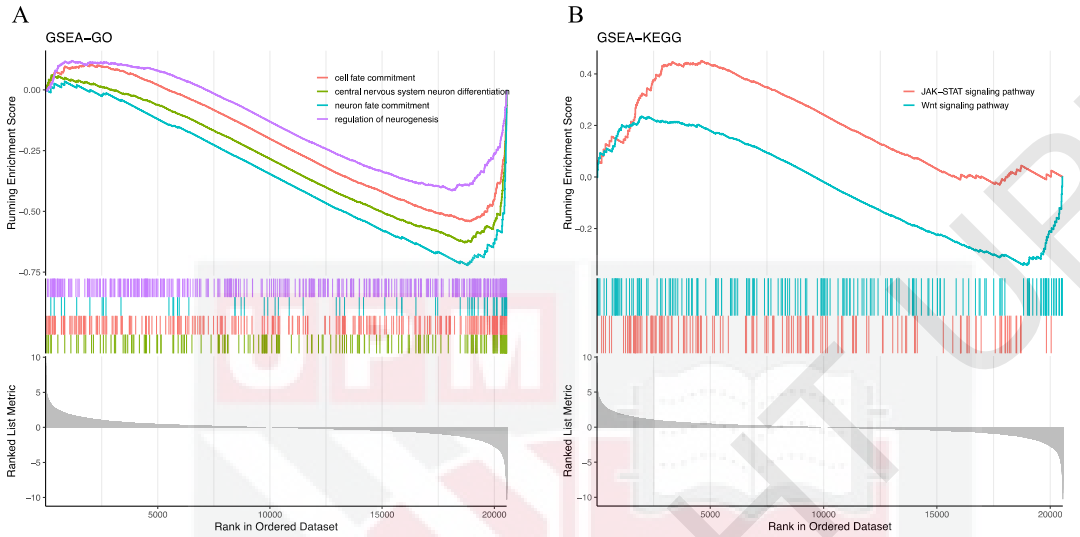


Figure 4.4 : GSEA Analysis for DS hiPSC-Derived NPCs. (A) GSEA-GO and (B) GSEA-KEGG analysis for the DEGs in DS hiPSC-derived NPCs. All results shown are |NES| >1 and adjusted $p < 0.05$. The graphical representation of the GSEA analysis results is divided into three parts. The top section displays the enrichment score (ES) curves, where different coloured curves represent the ES of gene sets associated with various biological processes and signalling pathways within the ranked gene list (expression matrix). A positive ES indicates that the gene set is enriched at the top of the list, signifying upregulated pathways, while a negative ES indicates enrichment at the bottom, signifying downregulated pathways. The middle section contains coloured bars, each line representing a gene from the corresponding gene set of biological processes and signalling pathways, indicating its position in the ranked gene list. The bottom section shows the distribution of gene expression within the ranked gene list, providing a visual representation of the gene expression levels across the dataset

4.4.3 REST-Targeted DEGs and Their Ontologies and Pathways

To identify DEGs targeted by REST in DS hiPSC-derived NPCs, REST-targeted genes were compared with the DEGs, and the results were visualised using a Venn diagram (Figure 4.5A). A total of 1,965 (63.26%) REST-targeted DEGs were identified in hiPSC-derived NPCs (representation factor, RF = 1.2 and $p < 9.346 \times 10^{-45}$). The GO biological process clustering results revealed that REST-targeted DEGs

in hiPSC-derived NPCs are mainly involved in neuron function, cell differentiation, nervous system development, morphogenesis, proliferation, signalling pathway transduction, neurotransmitter secretion and transport, ion concentration, homeostasis, molecular adhesion and metabolism (Figure 4.5C). KEGG pathway enrichment analysis indicated the REST-targeted DEGs are involved in the Wnt signalling pathway, TGF-beta signalling pathway, regulating pluripotency of stem cells, MAPK signalling pathway, PI3K-Akt signalling pathway, human papillomavirus infection, focal adhesion and axon guidance (Figure 4.5B). The GO and KEGG enrichment analysis results for genes targeted by REST imply that REST is a critical player in functional regulation and pathological mechanisms for DS hiPSC-derived NPCs.

© COPYRIGHT UPM

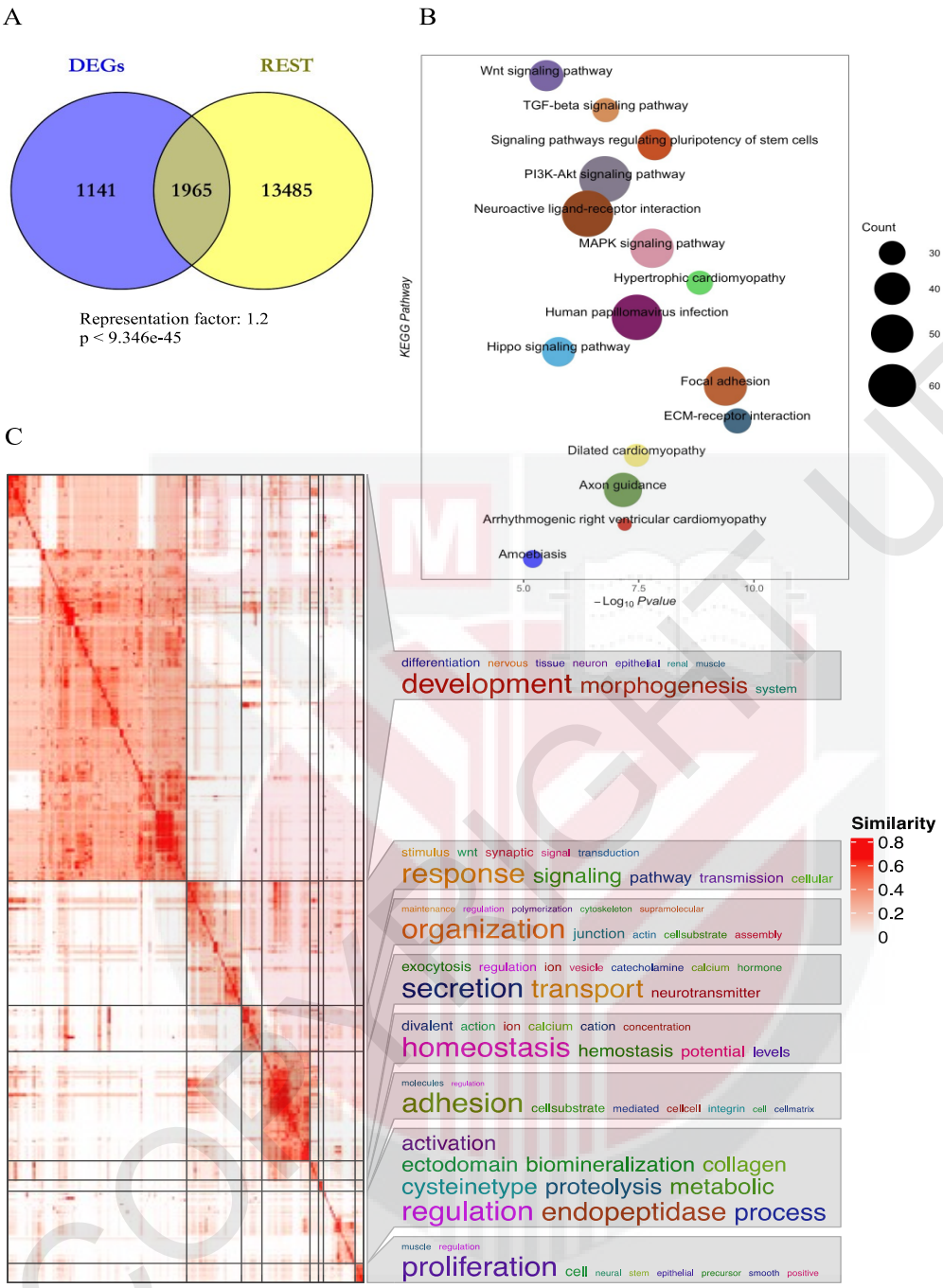


Figure 4.5 : Enrichment Analysis for REST-Targeted DEGs in NPCs. (A) The Venn diagram displayed the overlap between REST target genes and DEGs. The overlapping genes are REST-targeted DEGs. (B) The top 15 results of KEGG analysis for REST-targeted DEGs in DS hiPSC-derived NPCs were shown. The count refers to the gene numbers enriched in these pathways. The larger the number of genes, the bigger the corresponding circle. (C) The biological process clustering enrichment analysis for REST-targeted DEGs in DS hiPSC-derived NPCs. All 1,175 GO terms were semantically clustered into 10 categories. On the left is the visualisation of the similarity matrix, where the similarity bar ranges from 0 to 1, indicating the degree of similarity from low to high. Redder colours represent higher similarity values. On the right is the annotation of the clustered GO items in a word cloud

4.4.4 REST-Targeted Hub DEGS and NPC Fate Determination

4.4.4.1 WGCNA Analysis and Critical Module Identification

To identify the critical module associated with DS hiPSC-derived NPCs, WGCNA analysis was performed on all genes from the GSE185192 dataset. Hierarchical clustering of samples was performed based on the distribution of expression values using average chaining and Pearson's correlation to detect outliers (Figure 4.6A). The soft threshold power value β was determined to be 13 when the scale-free topology index R^2 initially reached 0.9 (Figure 4.6 B). A co-expression network was created using the scale-free topology criteria to detect genes displaying similar expression trends within the same module. Eight co-expression modules were identified in the expression profiles of DS-derived NPCs, each represented by a distinct colour (Figure 4.7A). The analysis of module feature correlation revealed that the strongest association with DS-derived NPCs was found in the MEbrown module, comprising 1,278 genes, with a correlation coefficient of 0.73, as illustrated in Figure 4.7B. Therefore, 1,278 genes in the MEbrown module were considered as DS-related genes. REST-targeted DEGs were compared with MEbrown module genes to further screen essential genes in REST-targeted DEGs, and 507 overlapping genes (RF=6.1 and $p < 3.036 \times 10^{-276}$) were obtained for subsequent analysis (Figure 4.7C).

© COPYRIGHT UPM

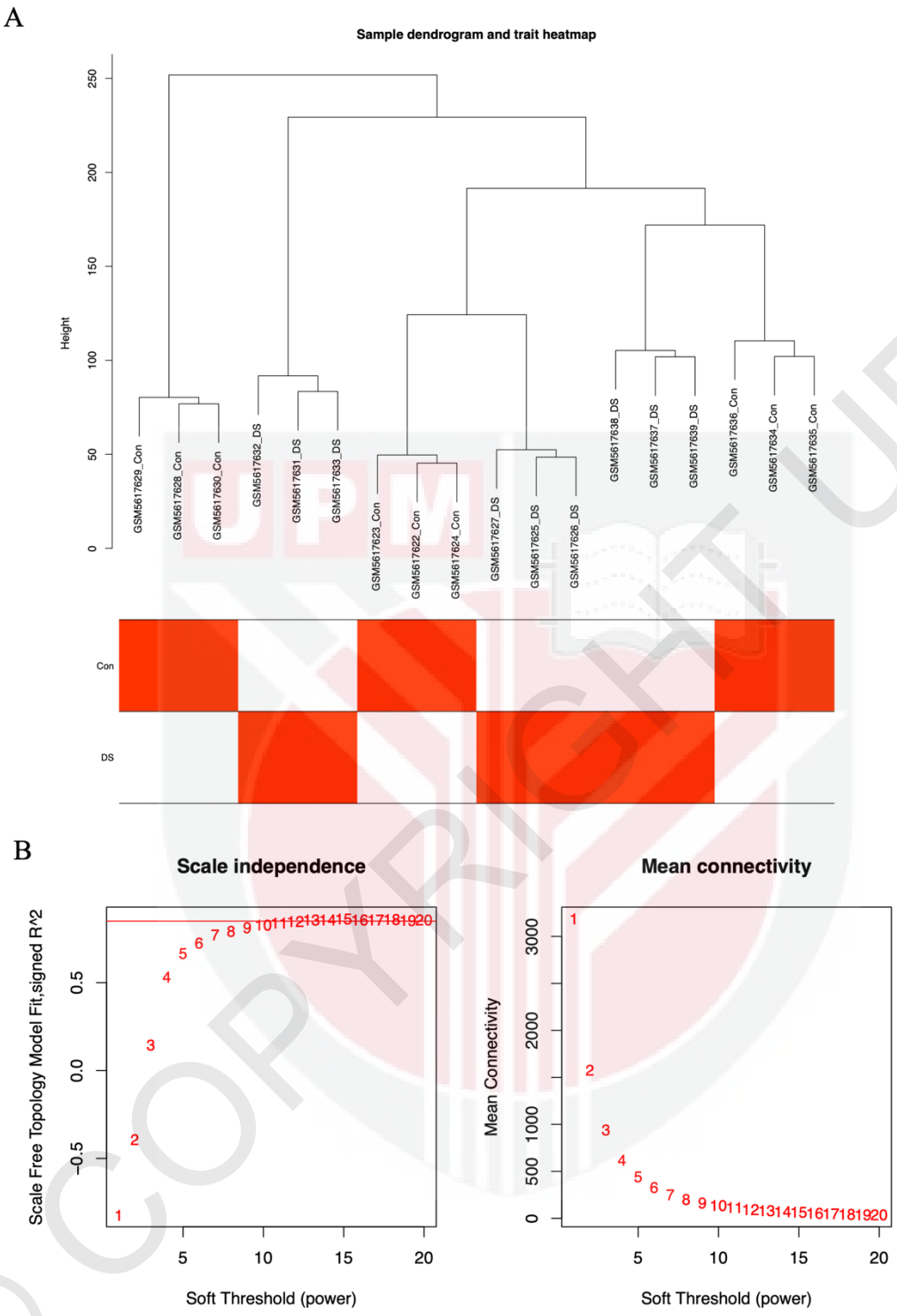


Figure 4.6 : WGCNA for Sample Clustering and Scale-Free Nextwork Construction. (A) Sample clustering was utilised to identify outliers, and a feature heatmap was used to visualise sample characteristics. (B) The network topology was analysed at different soft threshold powers. The graph on the left displays the relationship between the scale-free fit index (y-axis) and the soft threshold powers (x-axis). The graph on the right shows the relationship between mean connectivity (degree, y-axis) and the soft threshold powers (x-axis)

© COPYRIGHT UPM

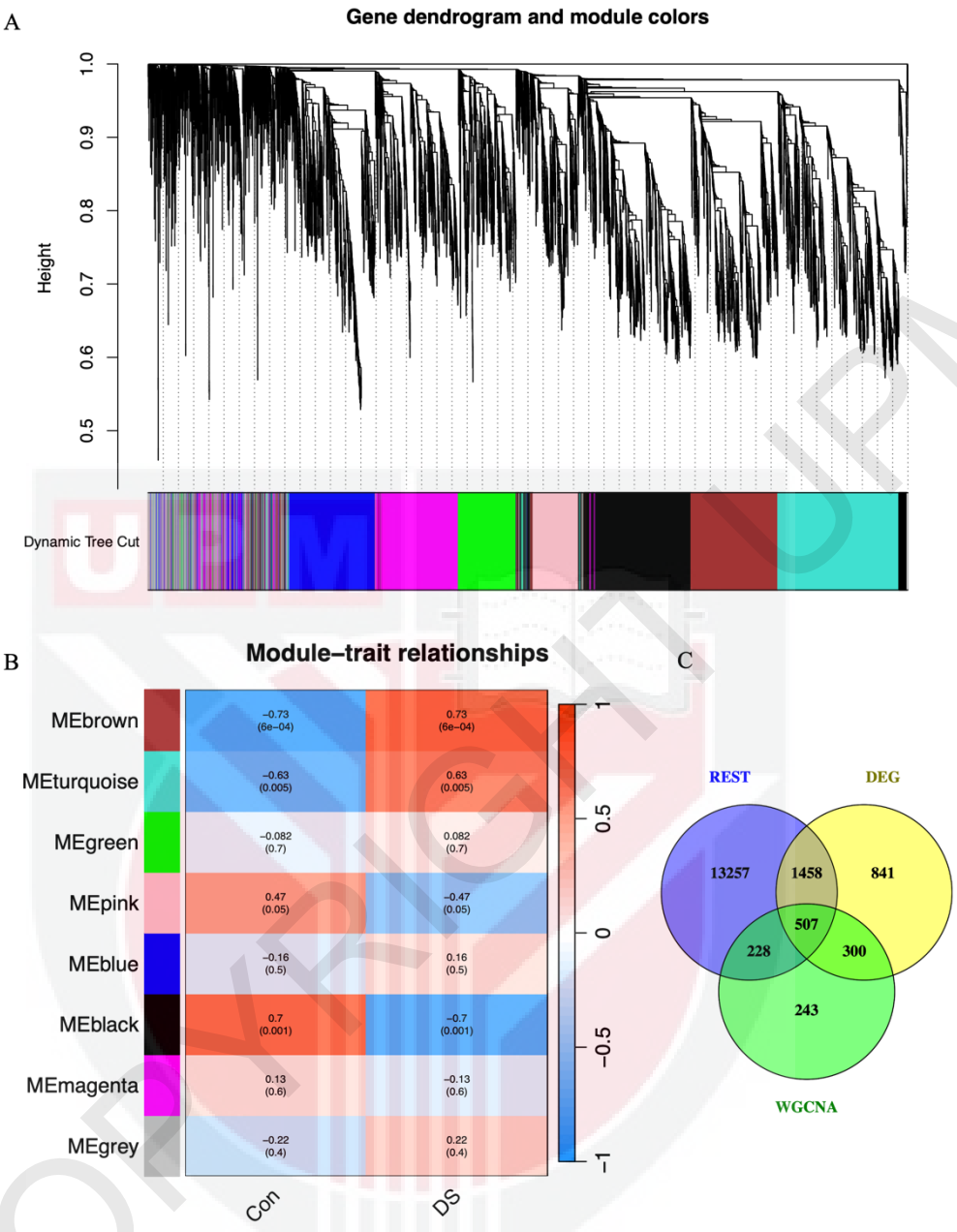


Figure 4.7 : WGCNA Unveiled Gene Co-Expression Networks and Module-Trait Relationships. (A) Clustering dendrograms of all genes based on the topological overlap and assigned module colours was constructed, resulting in 8 distinct co-expression modules represented by different colours. The image displays the relationship between the gene dendrogram at the top and the gene modules at the bottom. (B) The analysis examined the relationships between modules and traits. The table displays correlations and P-values with different traits for each module. The brown module was identified as the most significantly associated with DS. (C) The Venn diagram illustrates the overlap between REST-targeted DEGs and the genes in the MEbrown module

© COPYRIGHT UPM

4.4.4.2 PPI Network Construction and Identification of REST-Targeted Hub DEGs

To further elucidate the hub genes among the overlapping genes from REST-targeted DEGs and WGCNA MEbrown module genes, the PPI network (Figure 4.8) was constructed using the overlap genes, which included 490 nodes and 1,495 edges. To identify the top 20 most essential genes in the PPI network, the10 different approaches of "cytoHubba" were applied. Based on the intersection of the top 20 genes through all 10 topological algorithms (Table 4.3), 6 hub genes were identified, including *CD44*, *TGFB1*, *ALB*, *FN1*, *ITGB1*, and *COL1A1* (Figure 4.9). All genes, except for ALB, were upregulated in DS hiPSC-derived NPCs. Based on GO analysis of terms (GO:0048863, GO:0051960, GO:0045664, GO:0022604), in addition to *ALB*, the set of genes in which *CD44*, *TGFB1*, *FN1*, *ITGB1*, and *COL1A1* reside are involved in the development and differentiation of NPCs.

© COPYRIGHT UPM

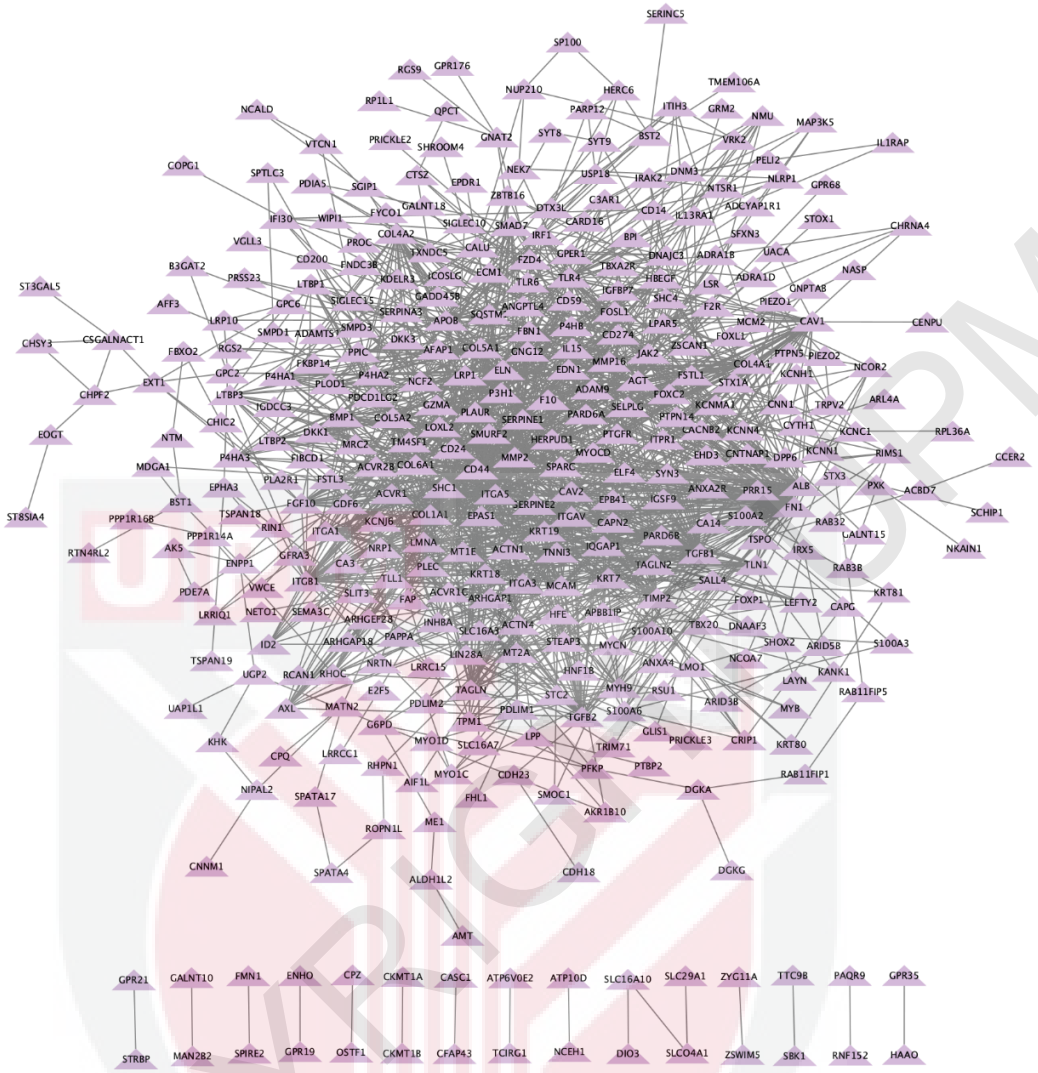


Figure 4.8 : The PPI Network Was Constructed Using the Overlapping Genes from REST-Targeted DEGs and WGCNA MEbrown Module Genes

© COPYRIGHT UPM

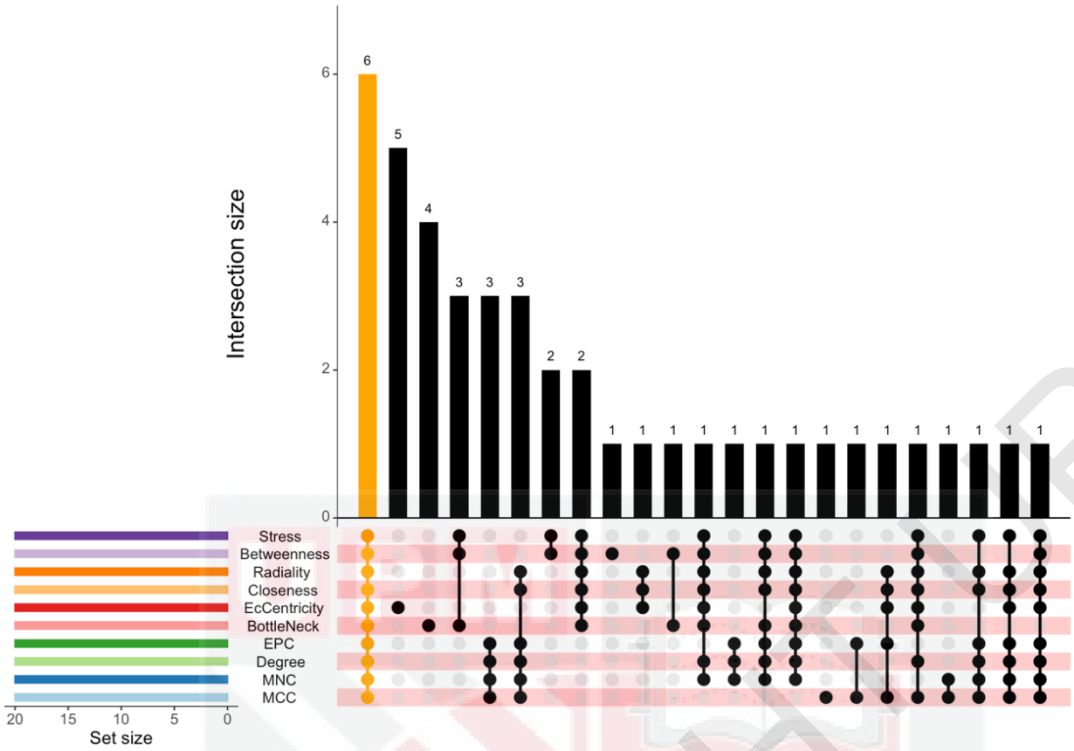


Figure 4.9 : UpSet Analysis of 10 Topological Algorithms of "cytoHubba". The data used for the Upset graph analysis was from Table 4.3. The UpSet graph provides a comprehensive view of the relationships between the 10 sets, with 6 overlapping genes (*CD44*, *TGFB1*, *ALB*, *FN1*, *ITGB1*, and *COL1A1*). Vertical bars represent the number of genes in the corresponding intersection, while dots with lines represent genes shared between sets. EPC, Edge Percolated Component; MCC, Maximal Clique Centrality; MNC, Maximum Neighborhood Component

© COPYRIGHT UPM

Table 4.3 : The Top 20 Genes Were Screened through 10 Topological Algorithms of "cytoHubba"

MCC	MNC	Degree	EPC	BottleNeck	EcCentricity	Closeness	Radiality	Betweenness	Stress
ALB	*ITGAV*	*ITGAV*	*COL5A2*	*APOB*	*SPARC*	*ELN*	*ELN*	*IRF1*	*EXT1*
CD44	***TGFB2***	*TGFB2*	*COL5A1*	*TLN1*	*ELN*	*ITGA5*	*ITGA5*	*TLN1*	*TLN1*
COL1A1	***FN1***	***FN1***	***FN1***	***ALB***	*CD274*	***FN1***	***FN1***	***FN1***	***CD44***
COL4A1	*AGT*	*SERPINE1*	*TGFB2*	*GNG12*	***ALB***	*AGT*	*AGT*	*FGF10*	*FGF10*
COL5A1	***ITGB1***	***ITGB1***	***ITGB1***	***TGFB1***	*MMP2*	*MMP2*	*MMP2*	***TGFB1***	*TLR4*
COL5A2	*ITGA5*	*ITGA5*	*TIMP2*	*SQSTM1*	***ITGB1***	*SPARC*	*EDN1*	*SPARC*	*SPARC*
COL6A1	*COL6A1*	*COL6A1*	*ITGAV*	*KRT19*	***FN1***	*COL6A1*	*TGFB2*	*SQSTM1*	*GNG12*
ELN	*MMP2*	*MMP2*	***ALB***	*AGT*	*AGT*	*CAV1*	*CAV1*	*CAV1*	*AGT*
FBN1	***COL1A1***	***COL1A1***	*MMP2*	***ITGB1***	*EDN1*	***ITGB1***	***ITGB1***	*AGT*	*CAV1*
FN1	***CD44***	***CD44***	***TGFB1***	*TLR4*	*HBEGF*	***CD44***	***CD44***	***ALB***	***FN1***
ITGA5	*FBN1*	*COL4A2*	*AGT*	*G6PD*	*NRP1*	*EDN1*	*COL6A1*	*MATN2*	*SQSTM1*
ITGAV	*COL4A2*	*SPARC*	*COL4A2*	*TSPO*	*LRP1*	*APOB*	*APOB*	*SERPINE1*	*ITGA5*
ITGB1	*COL5A2*	*COL5A2*	*ELN*	*SPARC*	***CD44***	*FGF10*	*SPARC*	*G6PD*	*MMP2*
MMP2	*TGFB1*	***TGFB1***	***COL1A1***	***CD44***	*IL15*	***TGFB1***	***ALB***	***CD44***	***ALB***
SERPINE1	*CAV1*	*CAV1*	*SERPINE1*	*CAV1*	*APOB*	***COL1A1***	*SERPINE1*	***ITGB1***	***ITGB1***
SPARC	*TLR4*	*TLR4*	*COL6A1*	*SLC16A3*	***TGFB1***	*TLR4*	*TLR4*	*APOB*	*APOB*
TAGLN	*COL4A1*	*COL4A1*	*CAV1*	***COL1A1***	*SERPINE1*	*COL4A1*	*FGF10*	*GNG12*	*SERPINE1*
TGFB1	***ALB***	***ALB***	***CD44***	***FN1***	*TLR4*	***ALB***	***TGFB1***	*TLR4*	***TGFB1***
TGFB2	*SERPINE1*	*AGT*	*COL4A1*	*FGF10*	*FGF10*	*SERPINE1*	***COL1A1***	***COL1A1***	***COL1A1***
TIMP2	*COL5A1*	*COL5A1*	*ITGA5*	*PLAUR*	***COL1A1***	*TGFB2*	*COL4A1*	*EXT1*	*IRF1*

© COPYRIGHT UPM

4.4.5 In Silico and Laboratory Validation of REST-Targeted Hub DEGs

To explore the differences in expression levels of the identified hub genes between DS-derived NPCs and controls, the expression levels of these genes were extrcated from the GSE185192 dataset. There was a statistically significant difference (p-value < 0.05) between the DS hiPSC-derived NPCs and the control group for all the gene expression levels (Figure 4.10A). All 6 hub genes except *ALB* were upregulated and involved in the development and differentiation of NPCs. The expression levels of these genes were further validated using a different transcriptomic dataset (GSE208625) derived from the DS hiPSC-derived NPCs. Except for *ALB*, other gene expression levels were significantly upregulated (p-value < 0.05) in the DS hiPSC-derived NPCs group compared to the control group (Figure 4.10B).

© COPYRIGHT UPM

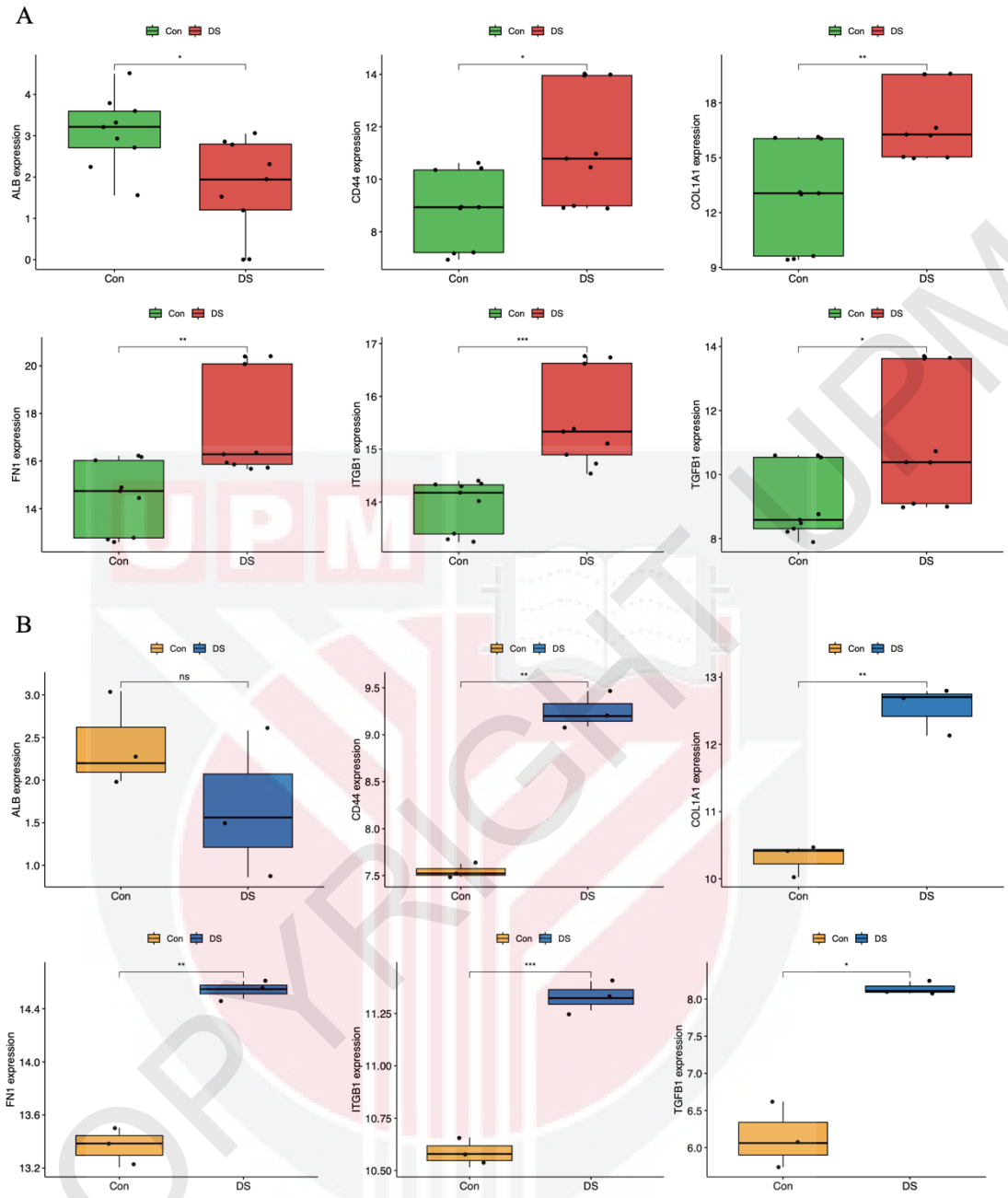


Figure 4.10 : Prediction of REST-Targeted Hub DEGs at the Level of Gene Expression. (A) The expression levels of the 6 REST-targeted hub genes of the GSE185192 dataset. (B) The expression levels of the 6 REST-target hub genes of the GSE208625 validation dataset. The group comparisons were made using the t-test, with a p-value < 0.05 considered statistically significant. *p-value< 0.05, **p-value< 0.01, ***p-value< 0.001. ns, no significance; Con, Control; DS, Down syndrome

© COPYRIGHT UPM

To validate the predicted REST-targeted hub genes, NPCs were derived from 3 controls and DS hiPSCs (Figure 4.11A), whose pluripotency was confirmed via immunocytochemistry analysis for the OCT4 cell marker (Figure 4.11B). After 7 days of neural induction in PSC Neural Induction Medium, the hiPSCs differentiated into NPCs. Following one passage, these NPCs were characterised and expanded. Immunocytochemistry showed that NSCs were positive for Nestin and SOX2 markers (Figure 4.11C). To verify the expression of REST-targeted hub genes, the DS hiPSC-derived NPCs samples were collected for RT-qPCR analysis for *CD44*, *TGFB1*, *FN1*, *ITGB1*, and *COL1A1* mRNA expression levels (*ALB* was excluded because no statistically significant differences in mRNA expression levels between DS-derived NPCs and controls in the validation dataset). This study has shown that the mRNA levels of *CD44*, *TGFB1*, *FN1*, *ITGB1*, and *COL1A1* were significantly upregulated (p-value < 0.05) between 1.5 and 2.3 folds in DS-derived NPC compared to the control group (Figure 4.11D).

© COPYRIGHT UPM

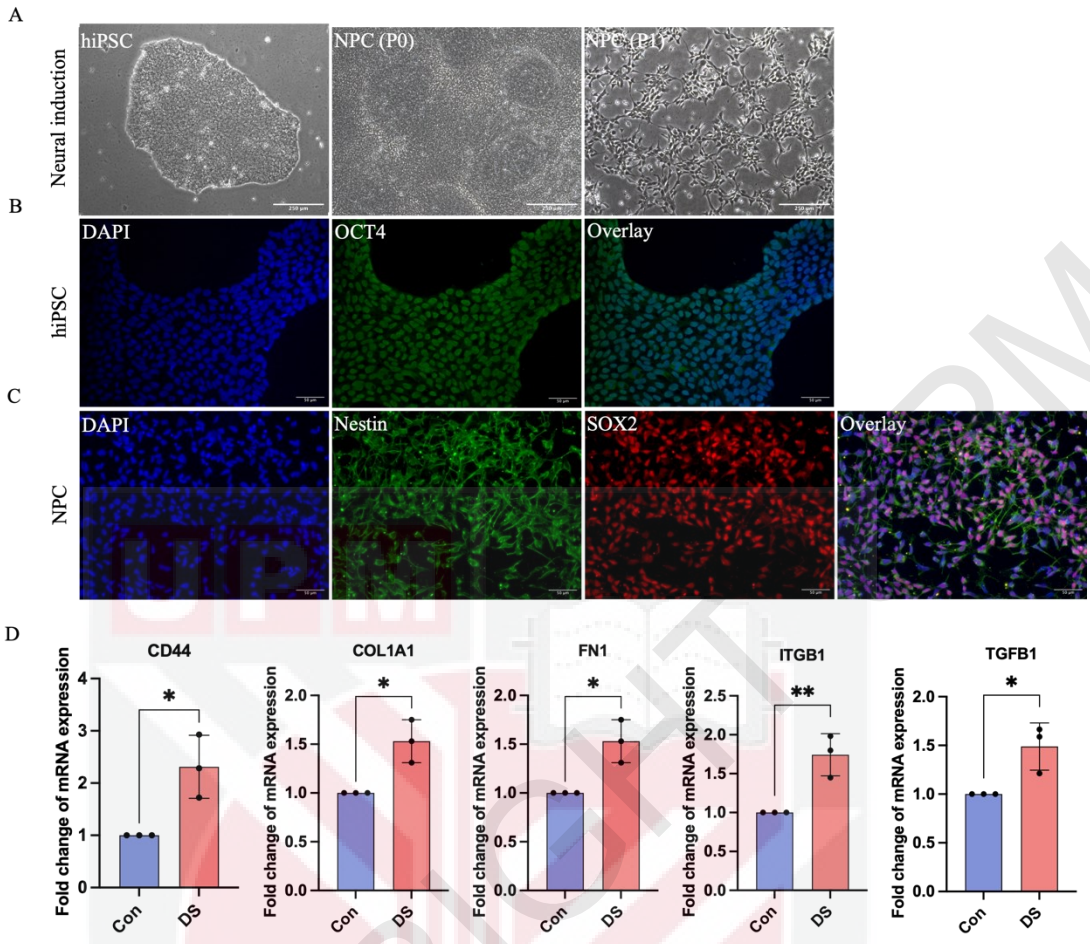


Figure 4.11 : DS hiPSC-Derived NPC Cell Line Establishment and Detection of Hub Genes mRNA (n=3). (A) hiPSC undergoing neural induction for 7 days can differentiate into NPC (P0); The stable NPC cell line (P1) can be formed after one passaging (Scale bar = 250µm) (Appendix B6). (B) Immunocytochemical staining of hiPSC characteristic cell markers (Scale bar = 50µm). (C) Immunocytochemical staining for NPC characteristic cell markers (Scale bar = 50µm). (D) The mRNA levels of *CD44*, *TGFB1*, *FN1*, *ITGB1*, and *COL1A1* were detected by RT-qPCR. The mean ± SD is from experiments of three independent cell lines. * p-value < 0.05, ** p-value < 0.01. Con, Control; DS, Down syndrome

4.4.6 Nuclear REST Loss in DS hiPSC-Derived NPCs

The expression of REST-targeted hub genes (*CD44*, *TGFB1*, *FN1*, *ITGB1* and *COL1A1*) was upregulated in DS-derived NPCs. To further elucidate the role of REST in DS hiPSC-derived NPCs, RT-qPCR, Western blot, and ICC analyses were conducted on REST expression. The *REST* mRNA was significantly downregulated (p-value < 0.01) in DS hiPSC-derived NPCs compared to controls (Figure 4.12A). The

total REST protein in NPCs was then examined, with Western blot results showing a significant reduction (p-value < 0.05) in REST protein in DS NPCs compared to the control group (Figure 4.12B, C). Given that REST is a transcription factor, the analysis also included the changes in nuclear REST protein in NPCs. ICC results indicated a significant reduction (p-value < 0.001) in nuclear REST in NPCs derived from DS. (Figure 4.12D, E). This suggests potential disruptions in the transcriptional regulatory processes targeted by REST.

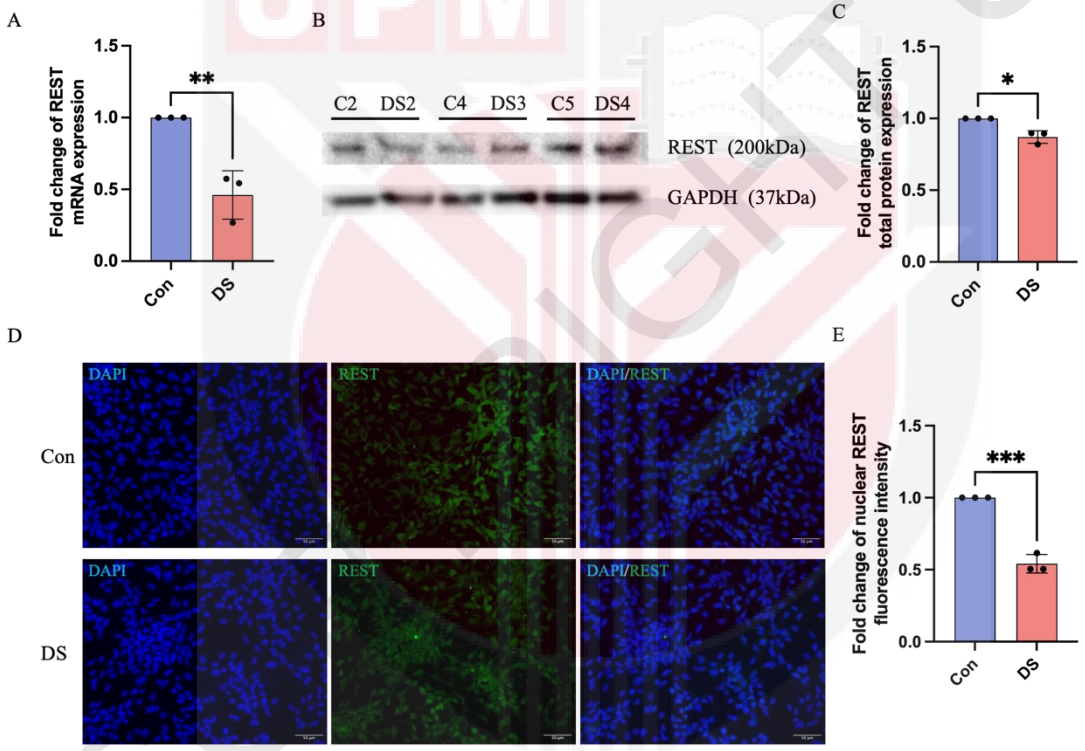


Figure 4.12 : Detection of REST mRNA and Protein in DS hiPSC-Derived NPCs. Three pairs of cell lines (C2 vs DS2, C4 vs DS3, and C5 vs DS4) were used for downstream analyses, including ICC, qPCR, and western blot. All measurements (n=3) were normalised by dividing DS values with their corresponding controls. (A) RT-qPCR for detection of *REST* mRNA expressed in DS-derived NPCs and controls; (B, C) Western blot (Appendix B7) and relative quantitative analysis for the total REST protein expressed in DS-derived NPCs and controls; (D, E) ICC validation and fluorescence intensity analysis of REST expressed in DS-derived NPCs and Controls; Statistical analysis of fluorescence intensity of nucleus REST. * p-value < 0.05, ** p-value < 0.01. Con and C, Control; DS, Down syndrome. Scale bar = 50µm

4.4.7 The Neurogenic-to-Gliogenic Shift in DS hiPSC-Derived NPCs

Although the loss of nuclear REST protein and the upregulation of REST-targeted hub genes in DS NPCs may disrupt their differentiation, the exact fate of DS NPCs remains unclear. The DCX (a neuroblast marker) and NFIA (a glioblast marker) expression levels in NPCs were identified to investigate their effect on the fate of DS-derived NPCs. Interestingly, ICC (Figure 4.13A, C), RT-qPCR (Figure 4.13D), and Western blot (Figures 4.13G, H) results consistently showed that DCX was significantly downregulated (p-value < 0.01) in DS NPCs compared to the control group (Figure 13A). Conversely, ICC (Figures 4.13B, E) and RT-qPCR (Figure 4.13F) showed that *NFIA* was significantly upregulated (p-value < 0.01) in DS NPCs. Although Western blot results did not show a significant difference in NFIA (p-value > 0.05) protein expression between DS NPCs and the control group, an upward trend was observed in DS NPCs (Figure 4.13G, I), possibly due to variations among different cell lines. This suggests that losing nuclear REST may lead NPCs to differentiate into glial cells rather than neurons.

GSEA analysis reveals that the JAK-STAT signalling pathway is significantly upregulated in DS hiPSC-derived NPCs (Figure 4.4B). Given that the JAK2-STAT3 signalling pathway activation is crucial for shifting NPC fate from neurons to glial cells in the central nervous system (Kong et al., 2019), we further examined the mRNA expression levels of *JAK2* and *STAT3* in control and DS hiPSC-derived NPCs. We found that *JAK2* and *STAT3* were upregulated 7.12-fold (p-value < 0.01) and 5.21-fold (p-value < 0.01), respectively, in DS NPCs compared to controls (Figure 4.13J, K). It provides evidence that the loss of nuclear REST may be a critical factor in the neurogenic-to-gliogenic shift in NPCs.

© COPYRIGHT UPM

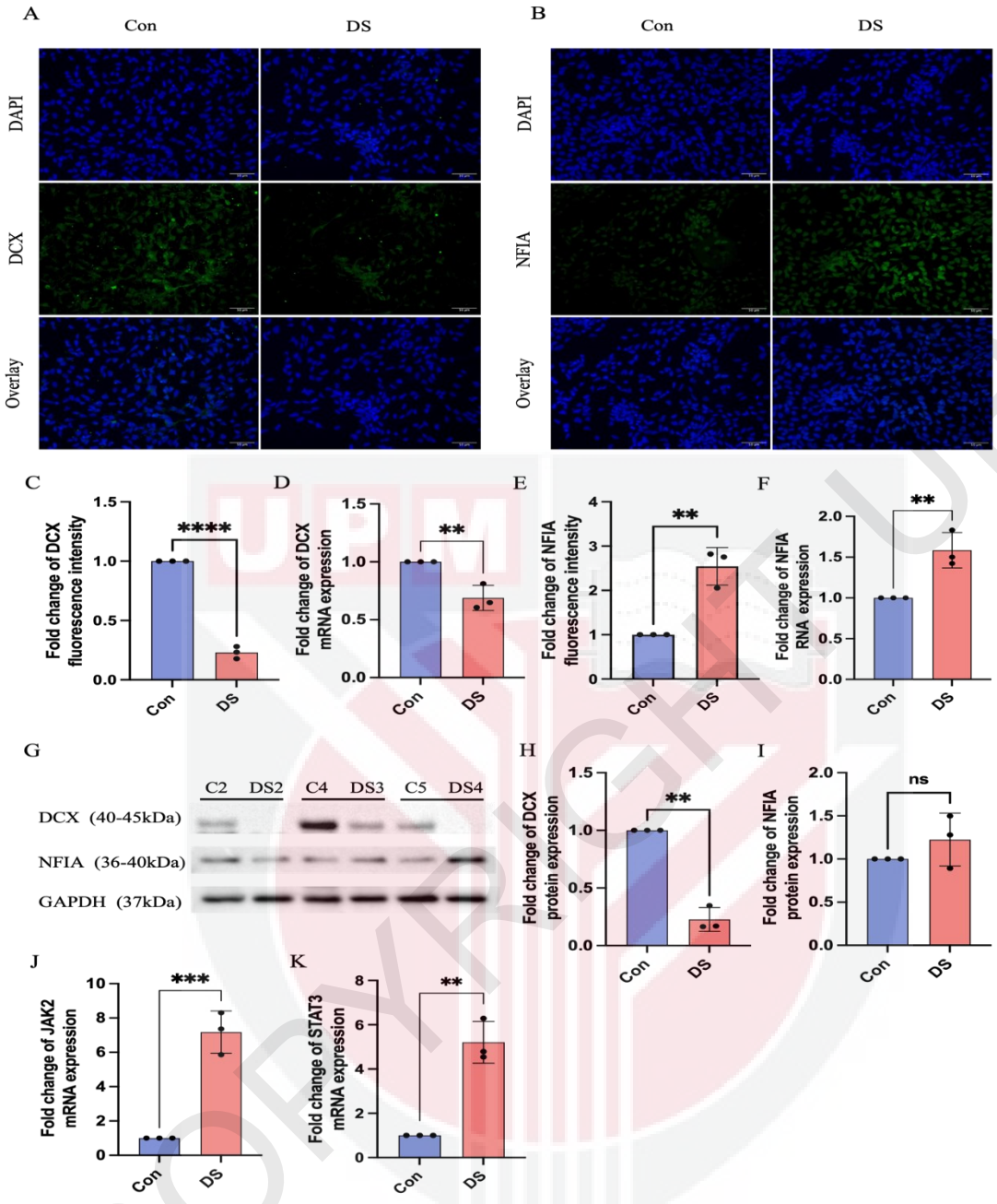


Figure 4.13 : Detection of DCX and mRNA and Protein in DS hiPSC-Derived NPCs. Three pairs of cell lines (C2 vs. DS2, C4 vs. DS3, and C5 vs. DS4) were used to perform ICC, qPCR, and western blot. All measurements (n=3) were normalised by dividing DS values with the corresponding controls. (A, B) ICC validation for DCX and NFIA expressed in DS-derived NPCs and controls, respectively; (C, D) Fluorescence intensity analysis and RT-qPCR detection for DCX protein and mRNA expression in DS-derived NPCs and control, respectively; (E, F) Fluorescence intensity analysis and RT-qPCR detection for NFIA protein and mRNA expression in DS-derived NPCs and control, respectively; (G, H, I) Western blot (Appendix B7) and relative quantitative analysis for DCX and NFIA expression in DS-derived NPCs and controls, respectively; (J, K) RT-qPCR for detection of *JAK2* and *STAT3* mRNA expression in DS-derived NPCs and controls, respectively. *p-value< 0.05, **p-value< 0.01, ***p-value< 0.001. Con and C, Control; DS, Down syndrome

©COPYRIGHT UPM

4.5 Discussion

This study explores the role of REST and its target genes in NPCs derived from DS individuals. DS is characterised by severe developmental and functional deficits in the brain, marked by an increase in the number of glial cells and a decrease in neurons. Studies have consistently shown a neurogenic-to-gliogenic shift in DS brains during development, leading to enhanced astrocyte differentiation and functional abnormalities and impaired neuronal cell maturation (Kawatani et al., 2021; Lee et al., 2016). Genome-wide transcriptional dysregulation in DS-derived NPCs disrupts their ordered differentiation, resulting in abnormal fate determination with increased glial cell differentiation and decreased neuronal differentiation (Stagni et al., 2018c). Previous research underscores the critical role of REST levels in NPCs for maintaining their function. The timely down-regulation or up-regulation of REST serves as a vital switch governing the differentiation of NPCs into neurons and glial cells. Recently, a study reported reduced REST expression in neural progenitor cells and adult cortex and impaired REST nuclear translocation in the prefrontal cortex of the Ts1Cje mouse model of Down syndrome (Lim et al., 2024). In the present study, based on the comprehensive analysis of REST expression in NPCs derived from DS hiPSCs, the nuclear translocation of REST reduction was identified. This dysregulation of REST is expected to trigger a cascade of functional abnormalities manifested from downstream abnormal expression of genes.

WGCNA was employed to pinpoint REST target genes associated with DS. Subsequently, we constructed a PPI network, identifying five hub genes—*CD44*, *TGFB1*, *FN1*, *ITGB1*, and *COL1A1*. The upregulation of these genes was identified and validated in DS iPSC-derived NPC by gene expression datasets. To further

© COPYRIGHT UPM

validate these findings, RT-qPCR was performed to confirm the upregulation of gene mRNA expression in NPCs derived from hiPSCs. Notably, all five REST target hub genes were found to be intricately linked with the regulation of gliogenesis and neurogenesis.

CD44 is the cell surface receptor for hyaluronan, an extracellular matrix (ECM) component. It plays a crucial role in many physiological and pathological processes in the brain, such as NPCs proliferation and differentiation, neurodevelopment, axon guidance, synaptic plasticity, and neurodegeneration (Dzwonek and Wilczynski, 2015; Kochlamazashvili et al., 2010). Previous research has shown that glial cells, especially astrocytes, are the significant sce of CD44 protein in the human brain (Girgrah et al., 1991). *CD44* has been widely expressed in astrocyte precursor cells (APCs), and its expression has also been observed in NPCs and oligodendrocyte precursor cells (OPCs) (Naruse et al., 2013). *CD44* deficiency inhibits neural stem cell (NSC) proliferation, leading to delayed neuronal differentiation (Su et al., 2017). The previous study have also found that *CD44* expression is upregulated in transcriptomic data from the brain tissue in DS individuals (Zamanian et al., 2021). Overexpression of *CD44* triggers NSCs to differentiate into astrocyte lineage, resulting in greater *GFAP* expression and increased astrocytes (Liu et al., 2004). The upregulation of *CD44* in DS-derived NPCs may, therefore, be a critical factor in promoting the differentiation of NPCs into astrocytes.

TGF-β1, a member of the TGF-β family, is involved in various processes such as neurogenesis, neuronal migration, synapse formation, growth regulation, axon targeting, gliogenesis, and angiogenesis (Stipursky et al., 2014; Yi et al., 2010). A

© COPYRIGHT UPM

previous study has shown that TGF-β1 treatment reduces neurogenesis and induces premature gliogenesis in both in vitro and in vivo models of mice (Stipursky et al., 2014); however, another study has shown that in vitro hiPSC-derived neural models, TGF-β1 treatment not only increased gliogenesis but also promoted neurogenesis (Izsak et al., 2020). TGF-β1 is thought to be a potent inducer of the transition of NPCs from neurogenic-to-gliogenic differentiation. During neurodevelopment, NPCs differentiate into the radial glial (RG) cell stage, the starting point for neurons and glial cells. TGF-β1 reduces the pool of Nestin-positive RG cells through activation of the Smad2/3 and MAPK/PPI3K signalling pathways. The expression level of *TGF-β1* also induces an increase in the expression of *GFAP* in the somatic cells, which activates signals for gliogenesis (Stipursky et al., 2014, 2012). Through direct binding of Smad3 to STAT3, TGFβ also cross-talks with JAK-STAT signalling to regulate stem cell self-renewal and differentiation (Wang et al., 2016). Interestingly, the *GFAP* gene promoter activation for astrocytogenesis was observed in cortical neurons by inducing TGF-β1 secretion in a mouse model (Sampaio e Spohr et al., 2002). Thus, the role of *TGF-β1* in NPCs is a critical mechanism in regulating neurogenesis and gliogenesis.

Fibronectin 1 (FN1) is an ECM protein that regulates cell adhesion, migration, proliferation, differentiation and glioblastoma (Pankov and Yamada, 2002; Song et al., 2021). Cell adhesion and migration play an essential role in regulating NSC function. A previous study showed that cell-to-cell contact and cell-ECM adhesion actively promote NSC self-renewal and NSC fate determination by placing stem cells in the vicinity of different signalling signals (Morante-Redolat and Porlan, 2019). A study by Oria et al. showed that *FN1* plays a critical role in the differentiation of NPCs into

© COPYRIGHT UPM

astrocytes and regulates astrocyte migration (Oria et al., 2022). In addition, it has been demonstrated that *FN1* can activate the JAK-STAT signalling pathway through adhesion molecule mediation and phosphorylation of STAT3 (Song et al., 2021), which is a crucial pathway for NPC differentiation and turns on the gliogenic switch (Lee et al., 2016). Nevertheless, the precise function of *FN1* in NPCs and nervous system development is not yet fully understood.

ITGB1 (β1-integrin) is an integrin family member highly expressed in mammalian embryos and NPCs. *ITGB1* is involved in maintaining and differentiating NPCs, cell migration, regulating neurogenesis and gliogenesis, neuronal development, synaptic development and plasticity, and axon formation (Chang et al., 2021). Activated ITGB1 crosstalks with the MAPK/PI3K signalling pathway and Wnt/β-catenin signalling pathway to regulate the cell cycle, maintain stem cell properties, and differentiate NSCs (Campos et al., 2004; Chang et al., 2021). High expression of *ITGB1* in neural progenitor cells is essential for the generation of radial glial cells and astrocyte differentiation (Belvindrah et al., 2007; Radakovits et al., 2009). The previous study has shown that elevated *ITGB1* expression in astrocyte precursor cells promotes astrocyte maturation and migration (Miyajima et al., 2024). Furthermore, *ITGB1* promotes glial cell proliferation through the regulation of the Notch signaling pathway (Min et al., 2020). Transcriptomic and proteomic analyses of the DS hiPSC-derived NPC model revealed increased expression of *ITGB1*, which was not further investigated (Sobol et al., 2019).

COL1A1 is the gene encoding the α1 chain of type I collagen, a significant component of the ECM of many tissues (Hayashi et al., 2014). The ECM has been shown to play

© COPYRIGHT UPM

essential roles in neurodevelopmental processes, including neural progenitor cell proliferation, differentiation, morphology, axon and dendritic elongation and connectivity, neuronal migration, and cortical folding (Franco and Müller, 2011; Long and Huttner, 2022). The ECM and the ECM receptors (integrin family) have long been known to regulate NPCs behaviour. The binding of ECM to integrins regulates many critical downstream signalling pathways involved in various neurodevelopment aspects, including PI3K-AKT, MAPK, TGF-β, Wnt, and Notch signalling pathways (Astudillo, 2020; Hastings et al., 2019). Recently, it has been demonstrated that COL1A1 is a marker for oligodendrocyte precursor cells and that increased expression of *COL1A1* may be associated with the generation of oligodendrocyte lineages from NPCs (Marques et al., 2018). However, the mechanism by which *COL1A1* regulates the differentiation of NPCs into oligodendrocytes remains unclear, and there are few studies of *COL1A1* in DS-derived NPCs.

It has been reported that REST and its target gene are involved in Notch signalling (Shue et al., 2022), WNT signalling (Nishihara et al., 2003), PI3K-AKT signalling (Stipursky et al., 2012), MAPK signalling (Campos et al., 2004), JAK-STAT signalling (Huang et al., 2023), TGF-beta signalling (Izsak et al., 2020; Stipursky et al., 2012), TNF signalling (Pajarillo et al., 2020), and HIF-1 signalling (Huang et al., 2023), which may impact the differentiation of NPCs. GSEA analysis revealed that the JAK-STAT signalling pathway was up-regulated in DS iPSC-derived NPCs. The previous study demonstrated that REST targets the JAK-STAT signalling pathway across human brain tissue and neural cell types in DS (Huang et al., 2023). The JAK-STAT pathway is crucial in promoting the switch from neurogenesis to gliogenesis. In this study, the upregulation of JAK2-STAT3 in DS hiPSC-derived NPCs was

© COPYRIGHT UPM

identified. STAT3 plays a pivotal role in the self-renewal and differentiation of NPCs. It can be phosphorylated by gp130/LIFR-associated JAK1/2 kinases, enabling its translocation to the nucleus and activating the transcription of target genes. STAT3 also promotes gene expression through tyrosine phosphorylation-independent mechanisms (Yang et al., 2007). In NPCs, STAT3 is both necessary and sufficient for astrogenesis. Activated STAT3 forms a complex with SMAD1 and p300, which binds to the glial fibrillary acidic protein (GFAP) promoter containing several STAT3 binding sites, inducing its expression (Nakashima et al., 1999). The Notch, BMP, TGF, and JAK-STAT3 signalling pathways, intersecting at STAT3, synergistically promote astrocyte differentiation from NPCs (Martynoga et al., 2012; Wang et al., 2016). STAT3 activation promotes NPC proliferation and astrogenesis during neurogenesis while negatively regulating neurogenesis (Cao et al., 2010). Therefore, REST may influence the fate shift of DS NPC by regulating JAK-STAT signalling pathways.

To confirm whether the differentiation of DS-derived NPCs would favour neuronal lineage differentiation or glial cell lineage, the expression of neuroblast marker (DCX) and glioblast marker (NFIA) were further validated in DS-derived NPCs. *DCX* expression was downregulated, and *NFIA* expression was upregulated. DCX, a microtubule-associated protein, undergoes transient expression in the early stages of neurogenesis (Couillard et al., 2005). Its presence in neuronal precursor cells and immature neurons correlates with cell migration and differentiation (Couillard et al., 2005; Koizumi et al., 2006). Widely utilised as a marker for neurogenesis and neuronal migration in both developing and adult brains, DCX contributes to various aspects of early human brain development, including neurogenesis, neuronal plasticity, axon growth, and synaptogenesis (Hwang et al., 2008). Maintenance of optimal DCX

© COPYRIGHT UPM

expression in NPCs is a reliable indicator of neurogenic capability (Shu et al., 2006). Disruptions such as knockout and knockdown/reduced *DCX* expression are linked to impaired neurogenesis, developmental disorders, compromised neuronal migration, and neuronal death, highlighting the multifaceted role of *DCX* in neurogenesis (Koizumi et al., 2006).

In contrast, NFIA is pivotal in neural progenitor and genesis of glial cells. Its necessity and sufficiency for embryonic glial cell generation involve regulating genes crucial for astrocyte migration and maturation (Miller and Gauthier, 2007). The NF1A transcription factor binds to the GFAP gene promoter, an astrocyte-specific protein, leading to the demethylation of GFAP (Namihira et al., 2009). Designated as a switch for gliogenesis, NFIA efficiently directs the rapid derivation of functional human astrocytes from pluripotent stem cells (Tchieu et al., 2019). NFIA orchestrates neurogenesis inhibition by inducing the Notch effector Hes5 (Tchieu et al., 2019) while promoting gliogenesis by suppressing the Notch effector Hes1 (Piper et al., 2010). In conclusion, the critical role of NFIA in regulating gliogenesis and neurogenesis within neural progenitor cells is underscored by its interactions with various transcription factors and signalling pathways, which are crucial for the normal development and differentiation of neural cells. This suggests that the dysregulation of REST is the key factor for the DS-derived NPCs favouring glial cell lineage differentiation.

© COPYRIGHT UPM

4.6 Conclusions

REST is a transcriptional repressor that regulates the proliferation and differentiation of neural stem cells. However, a few studies have explored the role of REST and its target genes in DS-derived NPCs. This study revealed that REST and its target genes play crucial roles in proliferation, differentiation, and development of DS-derived NPCs. We propose that the loss of REST is critical in the neurogenic-to-gliogenic shift observed in DS-derived NPCs and that REST and its target genes may collectively regulate the NPC fate. However, further studies are needed to explore the role of REST at different time points during Down syndrome brain development.

© COPYRIGHT UPM

CHAPTER 5

REST-MEDIATED DYSREGULATION OF DOWN SYNDROME IPSC-DERIVED CEREBRAL ORGANOIDS AT DIFFERENT DEVELOPMENT STAGE

5.1 Introduction

The three-dimensional (3D) cerebral organoid recapitulates many of the unique features of the human brain, and its developmental state matching that of the fetal brain in vivo has been reported in several studies. At days 11-16, the cell lineages in cerebral organoids predominantly consist of neuroepithelial cells, with neurogenesis initiating around days 18-20 (Lindenhofer et al., 2024). By days 23-25, early immature neurons can be observed in the cerebral organoids (Lindenhofer et al., 2024; Uzquiano et al., 2022). The transcriptome of cerebral organoids at days 30-60 corresponds to the human fetal cortex at 56-112 days post-conception (PCD) (Luo et al., 2016; Mariani et al., 2015; Trevino et al., 2020). The 60-day forebrain minimally-guided organoids and the unguided 100-day cortical brain organoids were similar to the fetal cortex after 140 PCD (Cheroni et al., 2022). Notably, GFAP positivity can be observed in 3% of the cells in the 30-day cerebral cortex organoids, indicating that astrocytes had been differentiated at that stage (Paşca et al., 2015). In the 90-day dorsal forebrain organoids, astrocytes accounted for approximately 13% of the total cells. From day 90 to day 180, the proportion of astrocytes in the dorsal forebrain increased rapidly, and up to 53.5% of the cells were observed to be positive for GFAP and S100B at day 180 (Velasco et al., 2019). The transcriptome of cerebral organoids at days 80-250 maps to the human fetal cortex at 84-259 PCD (Gordon et al., 2021; Kang et al., 2011; Lewis et al., 2021). And 250- to 300-day-old organoids can map to the fetal cerebral cortex during the

© COPYRIGHT UPM

transition between prenatal and postnatal stages in vivo (Gordon et al., 2021; Kang et al., 2011).

Recent studies have demonstrated that the 3D cerebral organoid models derived from hiPSCs of individuals with DS can be ideal platforms for studying DS brain development (Amin and Paşca, 2018; Briggs et al., 2013; Centeno et al., 2018; Chen et al., 2014). The cerebral organoids derived from hiPSCs mimic essential characteristics of the human brain, including cellular distribution, organisational patterns, physiological structures, electrical activity, and neural networks (Paşca et al., 2015; Qian et al., 2016). These models have greatly enhanced the comprehension of the developmental and neuropathological mechanisms underlying DS. Multiple studies have shown that a third copy of chromosome 21 leads to extensive transcriptomic changes, resulting in genome-wide transcriptional dysregulation (Bianco et al., 2016; Letourneau et al., 2014; Ponroy Bally et al., 2020). High-throughput sequencing technology applied to cerebral organoids has become crucial for studying transcriptomic differences between DS and euploid brains. It has been revealed that reduced NPC proliferation during early neurodevelopment was observed in 30-day trisomy 21 cerebral organoids, impairing neuronal differentiation (Tang et al., 2021). Single-cell sequencing of 70-day trisomy 21 cerebral organoids demonstrated a significant reduction in the composition of mature deep cortical and mature upper cortical neurons compared with that of disomic cerebral organoids (Tang et al., 2021). The research of 90-day 21 trisomy cerebral-like organs showed an overrepresentation of glial progenitor cells and a reduction in the number of neurons compared to the dimorphic control group (Czerminski et al., 2022). Hence, analysing these differences at various developmental time points in organoids can provide

© COPYRIGHT UPM

clearer insights into the molecular mechanisms driving the dynamic changes and abnormalities in the DS brain transcriptome during early neurodevelopment.

Studies in the previous chapter have found that the loss of REST in NPCs may be critical to the neurogenic-to-gliogenic shift in DS. Further exploration of the mechanisms underlying the molecular dysregulation mediated by REST at different neurodevelopmental stages and the critical time points at which the neurogenic-to-gliogenic shift occurs during DS neurodevelopment are necessary. In this study, high-throughput sequencing datasets from brain organoids at various developmental stages were utilized to investigate the role of REST target genes in the neurological development and pathogenesis of DS. These results indicate that REST is a promising target for developing personalized therapies for individuals with DS.

5.2 Experiment Design

To further investigate the role of REST across different stages of brain development in DS, transcriptomic data from DS hiPSC-derived cerebral organoids at various developmental stages were obtained and analysed. Sequencing datasets for 30-day, 35-day, 56-day, 90-day and 120-day organoids are available after a comprehensive search of public databases. Differential expression gene (DEG) analyses were performed using the Galaxy platform. Enrichment analyses for GO and KEGG pathways related to REST-targeted DEGs were conducted with R software. Focused analyses on REST-targeted hub DEGs were carried out using transcriptomic data from 90-day cerebral organoids. To experimentally validate the findings, hiPSC-derived cerebral organoids were cultured, and the expression levels of REST and its targeted hub DEGs were assessed. Figure 5.1 illustrates a streamlined overview of the data

© COPYRIGHT UPM

processing and analytical workflow, along with the experimental procedures employed in this study.

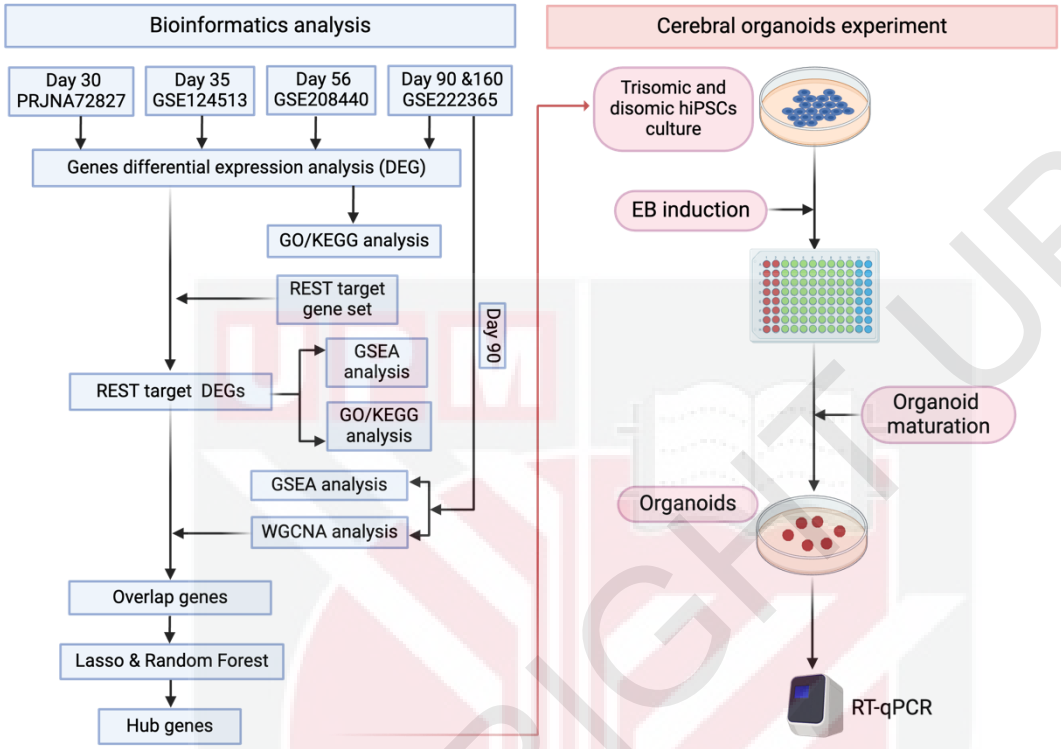


Figure 5.1 : Simplified Diagram of the Experimental Methods, Data Processing, and Analysis Workflow Used for This Study. EB, Embryoid body; GSEA, Gene Set Enrichment Analysis; GO, Gene Ontology; hiPSC, Human induced pluripotent stem cells; KEGG, Kyoto encyclopedia of genes and genomes; WGCNA, Weighted correlation network analysis. The figure was created in BioRender (License number: QD27U4G144)

5.3 Materials and Methods

5.3.1 Acquisition of DS Cerebral Organoids Datasets

The next-generation sequencing datasets for human cerebral organoids derived from human induced pluripotent stem cells (hiPSC) were sourced from the Gene Expression Omnibus database (GEO, https://www.ncbi.nlm.nih.gov/geo/). The PRJNA721827 (bulk) dataset (days in vitro, DIV 30) has six samples, comprising three trisomic

© COPYRIGHT UPM

samples and three isogenic disomic samples (Tang et al., 2021). The GSE124513 dataset (DIV 35) encompasses two pairs of trisomic and trisomic cell lines, featuring a trisomic cell line and the isogenic disomic cell line, as well as a trisomic cell line and a non-isogenic disomic cell line (Xu et al., 2019). The DIV 35 organoids contained 16 samples, with four samples allocated to each cell line. The GSE208440 dataset (DIV 56) included three trisomic samples and their corresponding isogenic disomic samples (Shaker et al., 2024). The GSE222365 dataset records DIV 90 and DIV 160 organoids (Czerminski et al., 2022). The DIV 60 organoids incorporate ten samples derived from trisomic cell lines and their isogenic disomic cell lines, with five samples for each cell line. The DIV 90 organoids comprise 48 samples, originating from three pairs of trisomic cell lines and their corresponding disomic cell lines, with eight samples per cell line.

5.3.2 Processing of the Dataset and Identification of Differentially Expressed Genes (DEGs)

Refer to 4.3.2

5.3.3 Identification of REST-Targeted DEGs in DS Cerebral Organoids

Refer to 3.3.3

5.3.4 WGCNA Network Construction and Module Identification

Refer to 4.3.6

© COPYRIGHT UPM

5.3.5 Machine Learning for Screening Critical Genes

Machine learning emerges as a formidable tool in mining existing gene expression data, enabling the derivation of rules and models for predicting pivotal genes within the genome. This study deploys a sophisticated computational method that synergistically incorporates Random Forest (RF) and Least Absolute Shrinkage and Selection Operator (LASSO) logistic regression algorithms. This integrated approach aims to meticulously sift through genetic data, identifying hub genes specific to the landscape of DS brain organoids. The specialised packages such as 'glmnet' for LASSO analysis, 'randomForest' for Random Forest algorithm analysis, and 'e1071' for SVM_RFE analysis were performed to execute this comprehensive analysis (Appendix C1). By applying these advanced algorithms, we seek to uncover and characterise genetic markers of significance. The convergence of genes identified by the three algorithms is recognised as a set of critical genes, offering insights into the genomic intricacies of DS brain organoids.

5.3.6 Gene Ontology and Pathway Enrichment Analysis

Refer to 4.3.5

5.3.7 Gene Set Enrichment Analysis

Refer to 4.3.3

5.3.8 Production of hiPSC-Derived Cerebral Organoids

This study included three trisomic iPSC lines [DS1 (UWWC1- DS1), DS2 (WC-24-02-DS-M), and DS4 (HPS4270)]and three isogenic disomic iPSC lines [(C1

© COPYRIGHT UPM

(UWWC1- DS2U), C2 (WC-24-02-DS-A), and C5 (HPS4272)]. DS1, C1, DS2, and C2 were obtained from the WiCell Research Institute at the University of Wisconsin (Giffin-Rao et al., 2020; Weick et al., 2013); C5 and DS4 were sourced from the RIKEN BioResource Center in Japan (Wakita et al., 2022). Detailed information on the cell lines is provided in Table 5.1. HiPSCs were cultured in complete mTeSR™ Plus medium (STEMCELL Technologies, Canada, Cat. no. 100-0276) on Geltrex-coated six-well plates, adhering to the manufacturer's guidelines. The STEMdiff™ Cerebral Organoid Kit (STEMCELL Technologies, Canada, Cat. no. 08570,) was employed for embryoid body (EB) formation, which included the use of EB seeding medium (containing ROCK inhibitor), EB induction medium, and EB formation medium. Upon reaching approximately 80% confluency, the hiPSCs were dissociated with Accutase and plated onto a 96-well round-bottom ultra-low attachment plate at a density of 9,000 cells per well in 100µL of EB seeding medium. After 2 days, 100µL of EB Formation medium was added to each well. On day 4, the medium was refreshed with an additional 100µL of EB Formation medium. By day 5, the EB Formation medium was removed and replaced with 150µL of Induction medium, with the plates then incubated at 37°C for 48 hours. For cerebral organoid maturation, the STEMdiff™ Cerebral Organoid Maturation Kit (STEMCELL Technologies, Canada, Cat. no. 08571) was utilised, which included both expansion and maturation media. On day 7, each organoid was embedded in 30µL of Matrigel and incubated at 37°C for 30 minutes. Subsequently, the organoids were transferred to a new six-well ultra-low adherence plate with 3 mL of expansion medium and incubated for 3 days. After this incubation, the medium was exchanged for 3 mL of maturation medium per well, and the culture was maintained at 37°C on an orbital shaker set to 75 rpm. The medium was refreshed every 3-4 days until the organoids were harvested on day 90.

© COPYRIGHT UPM

Table 5.1 : Details of the Disomic Control and Trisomic DS iPSC Lines

Cell label	Cell line	Donor origin	Reprogramming method	Provider
C1 DS1	UWWC1-DS2U UWWC1-DS1	• Mosaic DS individual • Male • Aged 1 • Skin fibroblast	Viral transfection system	WiCell Research Institute, University of Wisconsin
C2 DS2	WC-24-02-DS-A WC-24-02-DS-M	• Mosaic DS individual • Female • Aged 25 • Skin fibroblast	Non-integrating episomal vector	WiCell Research Institute, University of Wisconsin
C5 DS4	HPS4272 HPS4270	• Trisomy 21 individual • Male • Aged <10 • Skin fibroblast	Non-integrating episomal vector	RIKEN BioResource Center, Japan

5.3.9 Immunohistochemistry Staining of Cerebral Organoids

5.3.9.1 Cryopreservation Procedure

Cerebral organoids were removed from the culture medium and rinsed twice with D-PBS. The organoids were then immersed in 4% PFA (VWR, USA, Cat. no. J531) and incubated overnight at 4°C on a shaker. The following day, the cerebral organoids were washed three times with 1X PBS at room temperature, each wash lasting 10 minutes. The organoids were subsequently transferred to a cold 15% sucrose solution prepared with 1X PBS and allowed to sink at 4°C for approximately 24 hours. The solution was then replaced with 30% sucrose, and the organoids were incubated for an additional 24 hours at 4°C. Carefully, 2-3 cerebral organoids were removed from the sucrose solution and placed into plastic moulds pre-filled with 1-2 drops of OCT compound (Scigen, USA, Cat. no. 23-730-625). After fully filling the moulds with OCT, the organoids were rapidly frozen on dry ice. The frozen cerebral organoids were stored at -80°C until further use.

© COPYRIGHT UPM

5.3.9.2 Cryo-sectioning Procedure

To prepare for sectioning, the cryostat (Leica® CM1850, USA) must be set to -20°C at least two hours in advance, allowing sufficient time for the temperature to stabilise. Meanwhile, the cerebral organoid blocks, stored at -80°C, are retrieved and kept on dry ice to maintain their integrity until they are ready to be processed. When the cryostat is fully equilibrated, an OCT-embedded organoid block is carefully secured to a chuck. The chuck is then inserted into the specimen head, and its alignment is adjusted to ensure precise and uniform sectioning. With the setup complete, the organoid block is sectioned into thin slices, each measuring 20 µm in thickness. These delicate sections are carefully transferred onto pre-labeled Superfrost Plus slides (Sigma, USA, Cat. no. CLS294875), which are kept at room temperature before use. To maximise efficiency and minimise sample loss, up to three sections are placed on each slide. Once the sections are mounted, the slides are immediately placed into a cryobox on dry ice to prevent degradation. At this stage, the prepared slides can either be processed immediately for immunohistochemistry or stored at -80°C for future experiments, ensuring that the tissue remains well-preserved for downstream analyses.

5.3.9.3 Immunohistochemistry Procedure

To begin the immunostaining procedure, the prepared slides are placed on a slide warmer set to 37°C and allowed to dry for 30 minutes. Once dried, they are equilibrated at room temperature for an additional 10 minutes before being rehydrated in 1X PBS for 10 minutes to restore tissue integrity. Following rehydration, any excess washing buffer is removed, and autofluorescence is quenched by treating the sections with 125 mM glycine (Bio Rad, USA, Cat. no. 1610718) in PBS for two minutes. To

© COPYRIGHT UPM

ensure proper antibody localisation, a hydrophobic barrier is carefully drawn around each tissue section using an immEdge pen. For immunostaining procedures, refer to 4.3.10.2.

The primary antibodies used for immunodetection were as follows: anti-ki67 (Host: Rabbit; Sigma-Aldrich, USA, Cat. no. AB9260; 1:250 dilution), anti-TBR1 (Host: Rabbit; Cell Signalling Technology, USA, Cat. no. 49661; 1:350 dilution), and anti-SOX2 (Host: Goat; Abcam, USA, Cat. no. ab239218; 1:250 dilution). The secondary antibodies used for immunodetection were as follows: donkey anti-rabbit IgG conjugated with Alexa Fluor 488 (Invitrogen, USA, Cat. no. A-21206; 1:2000 dilution) for Ki67 and TBR1; donkey anti-goat IgG H&L with Alexa Fluor 594 (Abcam, USA, Cat. no. ab150132; 1:2000 dilution) for SOX2.

5.3.10 Quantitative Real-Time PCR

Refer to 4.3.11.

All RT-qPCR primers are shown in Table 5.2.

© COPYRIGHT UPM

Table 5.2 : List of Primer Sequences for RT-qPCR

Gene	Forward primers (5'→3')	GC%	Reverse primers (5'→3')	GC%	Annealing temperature (℃)	Amplicon size (bp)
CSTB	AGGTCCCAGCTTGAAGAGAAA	47.62	CGCAGGTGTACGAAGTCCTC	60.00	60	134
DCX	GAAGGGAAACCCATCAGCCA	55.00	GAGGTTCCGTTTGCGTCTTG	55.00	60	138
MCM3AP	GGTTGTCTGAAGACTCAGGAGC	54.55	TCCCTCATCATGTCACTCTGT	47.62	60	145
HMBS	GCCGTGCATACAGCTATGAAG	52.38	TTACGAGCAGTGATGCCTACC	52.38	60	179
JAK2	CCGGGTTTCAGAAGCA	56.25	TCAGAACATTTGCCGTCG	50.00	60	100
NFIA	TGAAGTGGAGCCAGGAATGC	55.00	ATGACAGGTCGGTGATGCTG	55.00	60	129
PFKL	CTACGAGGGCTATGAGGGC	63.16	GATGACGCACAGGTTGGTGA	55.00	60	196
POFUT2	GAGCAGTTCATCGCAGAATCT	47.62	AACCCCAAAACCATCCTCTGT	47.62	60	178
PRMT2	ACCTGCCTGCTGTTTGAGT	52.63	CAAATGACCCCGTCCTCCTTC	57.14	60	80
PSMB2	GAGGGCAGTGGAACTCCTTAG	57.14	GATGTTAGGAGCCCTGTTTGG	52.38	60	149
REST	GAGAACGCCCATATAAATGTG	42.86	CACATAACTGCACTGATCAC	45.00	60	172
RWDD2B	GCCACGGCTCAAGAAACTTAC	52.38	TCGCCCCTCCATTGTCTTCT	55.00	60	183
STAT3	AGAAGGACATCAGCGGTAAG	50.00	CGTTGGTGTCACACAGATAA	45.00	60	275

F, Forward Primer; R, Reverse Primer; *CSTB*, Cystatin B; *DCX*, Doublecortin; *MCM3AP*, Minichromosome maintenance complex component 3 associated protein; *HMBS*, Hydroxymethylbilane synthase; *JAK2*, Janus kinase 2; *NFIA*, Nuclear factor I A; *PFKL*, Phosphofructokinase-liver type; *POFUT2*, Protein O-fucosyltransferase 2; *PRMT2*, Protein arginine methyltransferase 2; *PSMB2*, Proteasome 20S subunit beta 2; *REST*, RE1 silencing transcription factor; *RWDD2B*, RWD domain containing 2B; *STAT3*, Signal transducer and activator of transcription 3.

© COPYRIGHT UPM

5.3.11 Statistical Analysis

The data are presented as mean ± standard deviation (SD), with all experiments conducted in triplicate. Statistical analyses were performed using GraphPad Prism 9.0 (version 9.5.0) or R software (version 2023.03.0+386). An independent samples t-test was used to compare the differences between the two independent experimental groups. A significance threshold of p-value < 0.05 was applied, and statistical significance is represented as follows: ns, not significant; *p-value < 0.05; **p-value < 0.01; ***p-value < 0.001.

5.4 Results

5.4.1 Differentially Expressed Genes and Their Ontologies and Pathways in Different Developmental Stages of DS Cerebral Organoids

DS iPSC-derived organoids from five different time points were screened for DEGs according to the adjusted p-value < 0.05 and |log2 FC| > 0.5. In the PRJNA721827 (bulk) dataset (days in vitro, DIV 30), 235 DEGs were identified (Figure 5.2A, 5.3A). In GSE124513 (DIV 35), 3,183 DEGs were identified (Figure 5.2B, 5.3B). In GSE208440 (DIV 56), 6,818 DEGs were identified (Figure 5.2C, 5.3C). In GSE222365 (including DIV 90 and 160 organoids), 923 DEGs were identified in 90-day organoids and 3,598 DEGs in 160-day organoids (Figure 5.2D-E, 5.3D-E).

© COPYRIGHT UPM

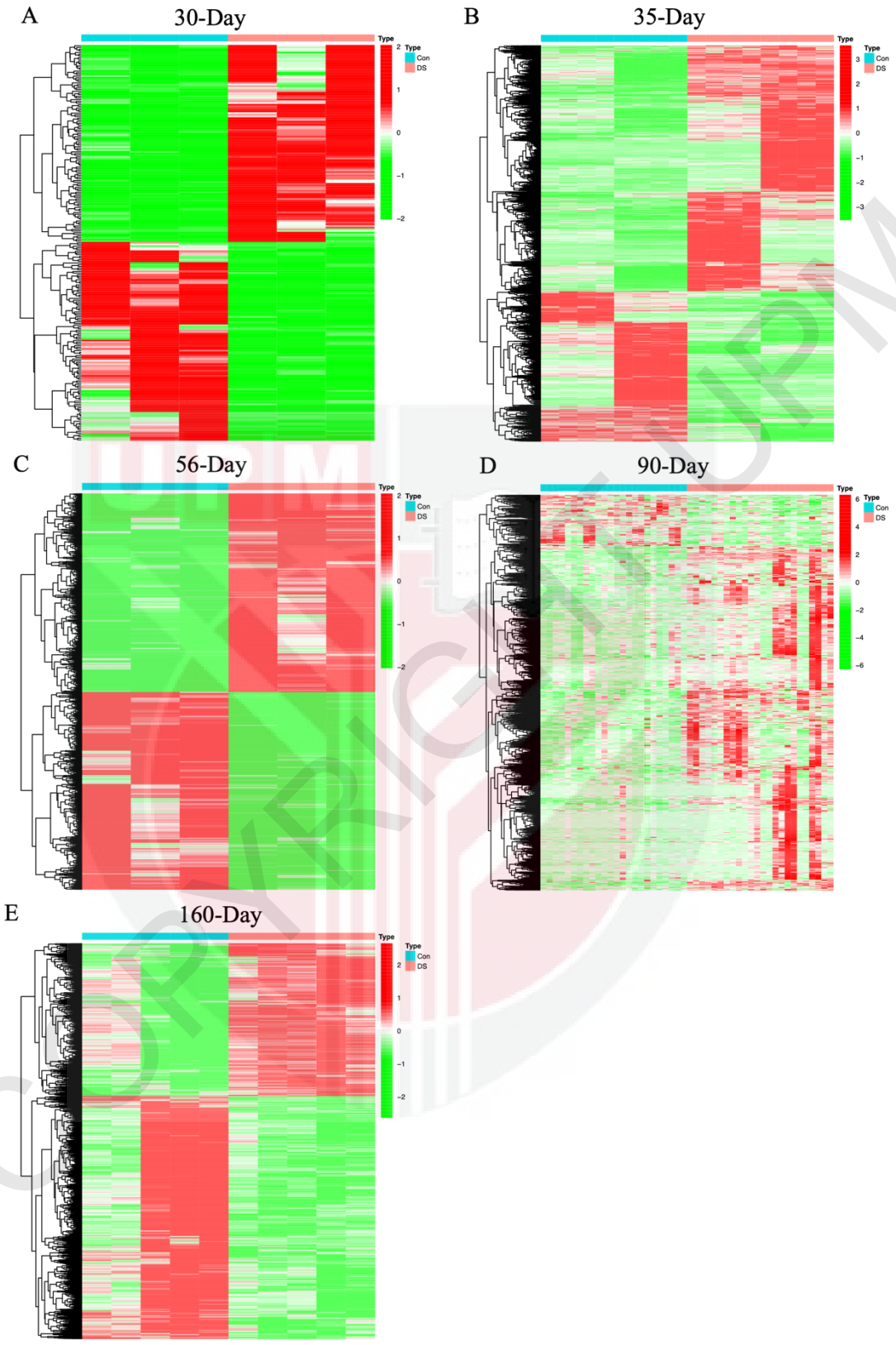


Figure 5.2 : Heat Maps Analysis of Identified DEGs between DS and Controls in Cerebral Organoids at Different Time Points. (A-E) Red represents upregulated genes, while green represents downregulated genes

© COPYRIGHT UPM

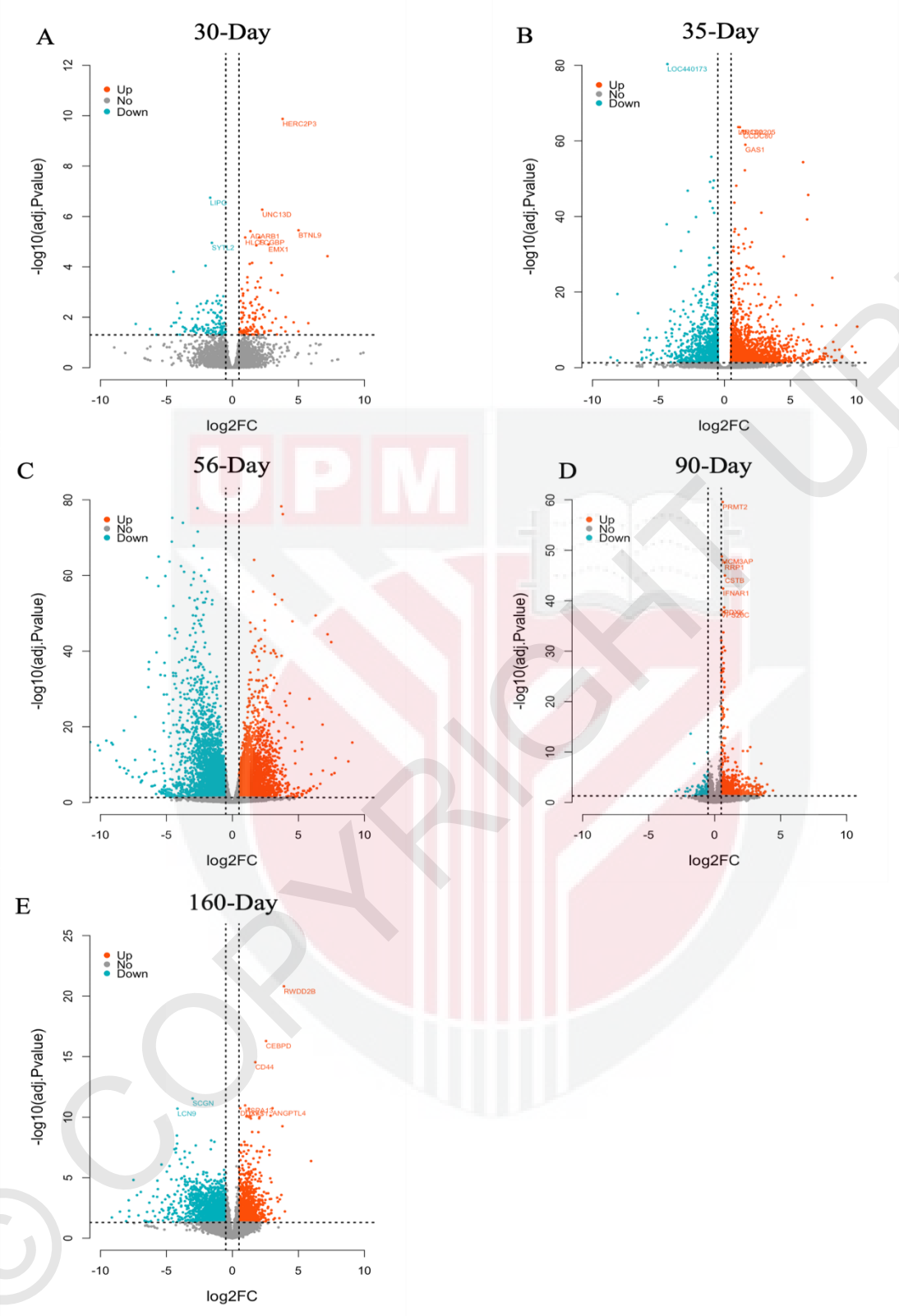


Figure 5.3 : The Volcano Plot is for DEGs in DS hiPSC-Derived in Cerebral Organoids at Different Time Points. (A-E) The top 10 DEGs with the most significant p-values are shown in Appendix C2. Red represents upregulated differentially expressed genes, green represents downregulated differentially expressed genes, and grey represents genes with no differential expression

© COPYRIGHT UPM

To investigate the functional and mechanistic characters during the DS iPSC-derived organoids development, GO and KEGG enrichment analyses were performed based on the DEGs at different time points organoids (Figure 5.4). The GO biological process results revealed that the DEGs in 30-day organoids were mainly enriched in chromosome segregation, mitotic cell cycle, and nuclear division. The KEGG pathway analysis showed that the DEGs in 30-day organoids are mainly involved in the cell cycle, oocyte meiosis, and neuroactive ligand-receptor interaction. In 35-day organoids, the GO biological processes of the DEGs mainly enriched in axon development, axonogenesis, synapse organisation, and neuron projection guidance. The KEGG pathway results predominantly highlight involvement in the Wnt signalling pathway, axon guidance, and the regulation of pluripotency of stem cells. In 56-day organoids, the GO biological process results of the DEGs were mainly involved in axon development, axonogenesis, and neuron projection development. The KEGG pathway results are mainly involved in axon guidance, MAPK signalling pathway and cell cycle. In the 90-day organoids, the DEGs were mainly enriched in extracellular matrix organisation, extracellular structure organisation and various system development. KEGG pathway analysis found that the DEGs were mainly enriched in the JAK-STAT signalling pathway, PI3K-Akt signalling pathway, and neuroactive ligand−receptor interaction. In 160-day organoids, the GO biological process reveals that the DEGs are mainly involved in chromosome segregation, nuclear division, and mitotic cell cycle. The KEGG pathway analysis showed that the DEGs were predominantly associated with the cell cycle, the HIF-1 signalling pathway, and the regulation of pluripotency of stem cells.

© COPYRIGHT UPM

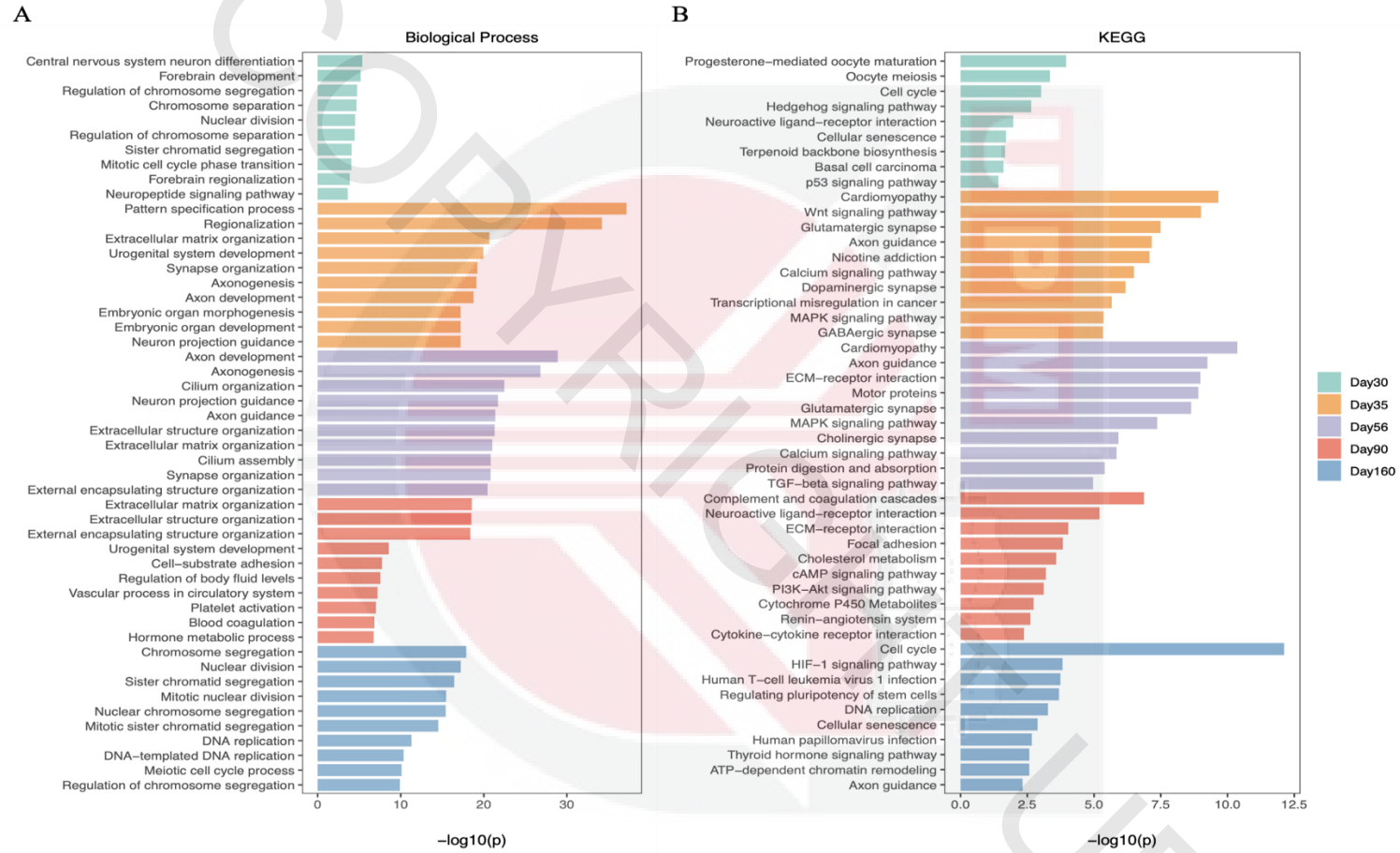


Figure 5.4 : Enrichment Analysis of DEGs in DS-Derived Cerebral Organoids at Different Time Points. Different colours indicate different time points in DS cerebral organoids. The top 10 biological processes (A) and KEGG pathways (B) for each region are shown

© COPYRIGHT UPM

5.4.2 REST-Targeted DEGs in Different Developmental Stages of DS Cerebral Organoids

This study comprehensively analysed overlapping genes between REST-target genes and DEGs in DS iPSC-derived organoids, visually presented in Venn diagrams (Figure 5.5). The findings revealed a significant overlap, with 171 (72.77%) REST-targeted DEGs identified in 30-day organoids (representation factor, RF = 1.4 and $p < 1.894 \times 10^{-11}$), 2,222 (69.81%) in 35-day organoids (RF = 1.4 and $p < 3.224 \times 10^{-109}$), 4,563 (66.93%) in 56-day organoids (RF = 1.3 and $p < 1.978 \times 10^{-188}$), 526 (84.43%) in 90-day organoids (RF = 1.3 and $p < 3.877 \times 10^{-04}$), 2,378 (66.09%) in 160-day organoids (RF = 1.3 and $p < 1.267 \times 10^{-79}$).

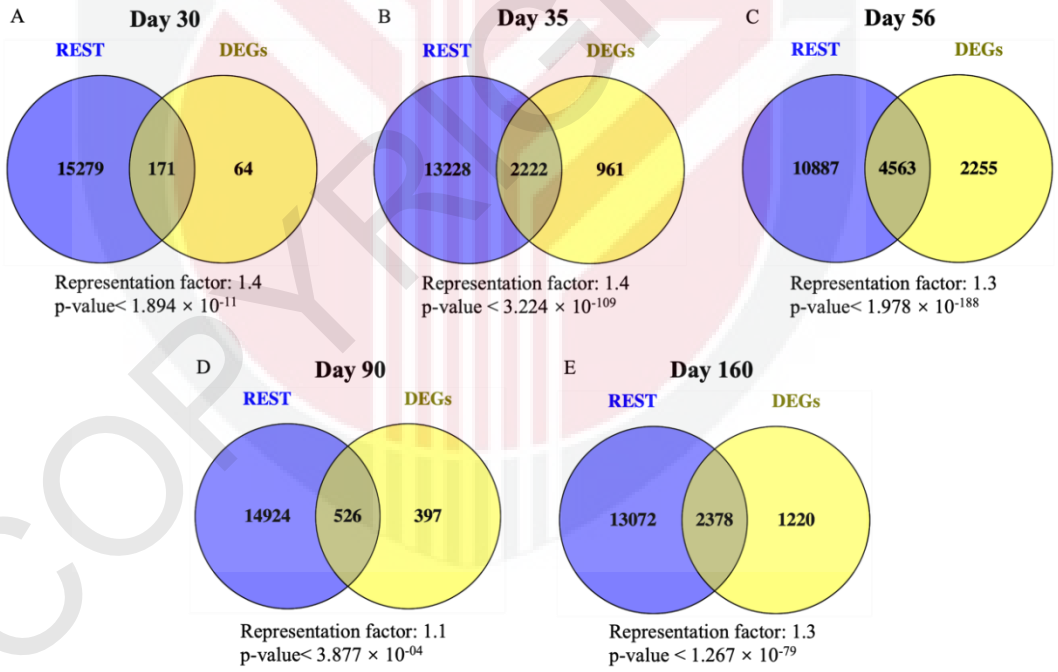


Figure 5.5 : (A-D) Depiction of the Overlap between REST Target Genes and DEGs across the Different Time Points DS iPSC-Derived Organoids. The blue circles represent REST target genes, the yellow circles represent DEGs, and the overlapping parts are REST target DEGs. Fisher's test determined the statistical significance of this gene overlap, revealing all p-values < 0.01. A representation factor > 1 indicates more overlap than expected of two independent groups, a representation factor < 1 indicates less overlap than expected, and a representation factor of 1 indicates that the two groups by the number of genes expected for independent groups of genes

© COPYRIGHT UPM

5.4.3 REST as the Pivotal Regulator during DS iPSC-Derived Cerebral Organoid Development

To further investigate the role of REST during the DS iPSC-derived organoids development, the GO and KEGG enrichment analyses were performed based on the REST-targeted DEGs at different time points organoids (Figure 5.6). Interestingly, these results showed that REST-targeted DEGs in 30-day and 160-day DS iPSC-derived organoids involved similar biological functions and pathways, mainly enriched for chromosome segregation and cell cycle. In 35- to 56-day organoids, REST-targeted DEGs were associated with axon development, axon guidance, axonogenesis, neuron projection guidance, synapse organisation, dopaminergic synapse, GABAergic synapse, glutamatergic synapse and the Wnt signalling pathway. The REST-targeted DEGs in 90-day organoids were notably enriched in the focal adhesion, cytokine receptor interaction, JAK-STAT signalling pathway, PI3K-Akt signalling pathway, and HIF-1 signalling pathway. The roles of REST-targeted DEGs in cerebral organoids at different time points were further summarised in Figure 5.7. This analysis revealed that in the 90-day DS-derived cerebral organoids, the biological functions and signalling pathways involving REST target DEGs were notably distinct compared to other time points. REST mainly targets the JAK-STAT signalling pathway and glial cell differentiation in 90-day DS-derived cerebral organoids.

© COPYRIGHT UPM

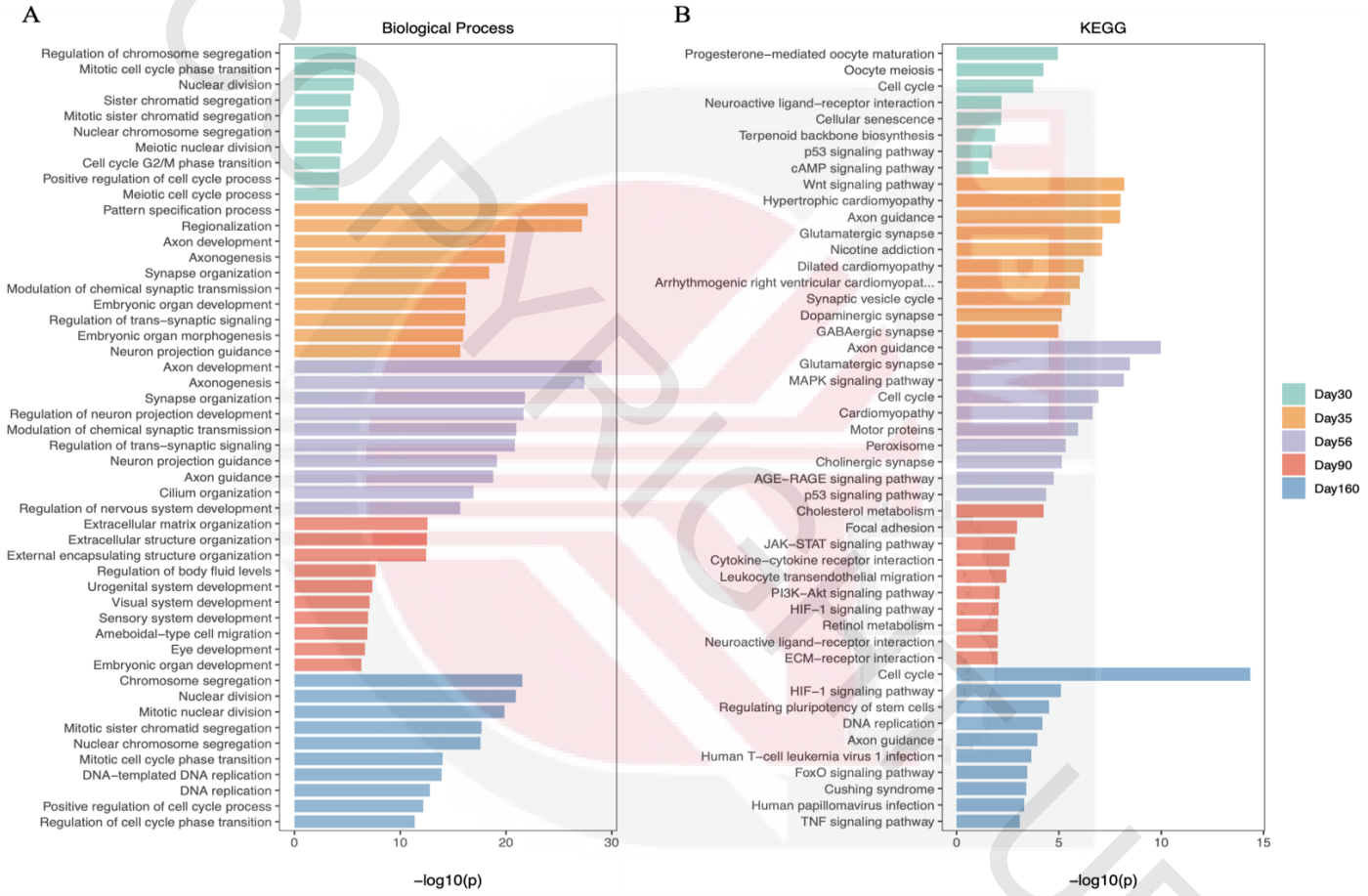


Figure 5.6 : Analysis of REST Target DEGs in DS-Derived Cerebral Organoids at Different Time Points. Different colours indicate different time points in DS cerebral organoids. The top 10 biological processes (A) and KEGG pathways (B) for each region are shown

© COPYRIGHT UPM

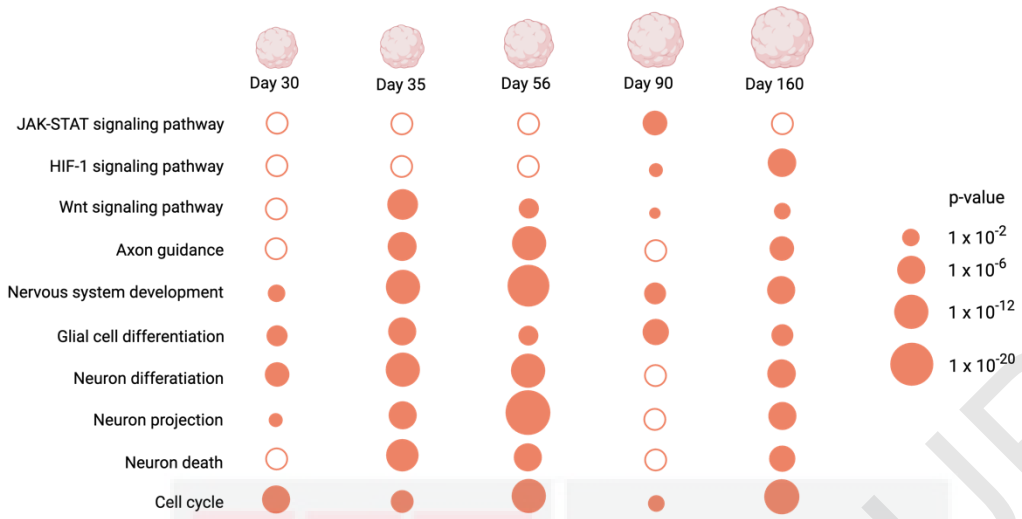


Figure 5.7 : Summary of Signalling Pathways and Biological Processes Involved in REST-Targeted DEGs in DS-Derived Cerebral Organoids at Different Time Points. Hollow circles indicate that the term was not enriched. The larger the solid circle, the smaller the p-value of the enrichment

5.4.4 GSEA Revealed Abnormal Neurodevelopment in DS-Derived 90-Day Cerebral Organoids

To further understand the biological characteristics of 90-day cerebral organoids, the GSEA analyses were performed. GSEA-GO analysis revealed defects in neuronal differentiation and increased glial cell differentiation in DS-derived 90-day organoids. Several biological processes related to neuronal differentiation were downregulated in DS-derived 90-day organoids, including midbrain dopaminergic neuron differentiation, olfactory bulb interneuron differentiation, spinal cord association neuron differentiation, and the Wnt signalling pathway involved in midbrain dopaminergic neuron differentiation (Figure 5.8A). Conversely, biological processes related to glial cell differentiation were upregulated. These GO-related gene sets were significantly enriched with NES < -1, p-value <0.05, and adjusted p-value < 0.05. Further GSEA-KEGG analysis indicated that the JAK-STAT signalling pathway was upregulated in DS-derived 90-day organoids with NES >1, p-value <0.05, and

© COPYRIGHT UPM

adjusted p-value< 0.05 (Figure 5.8B). The JAK-STAT signalling pathway is widely recognized as essential for regulating the proliferation of neural progenitor cells and the differentiation of astrocytes.

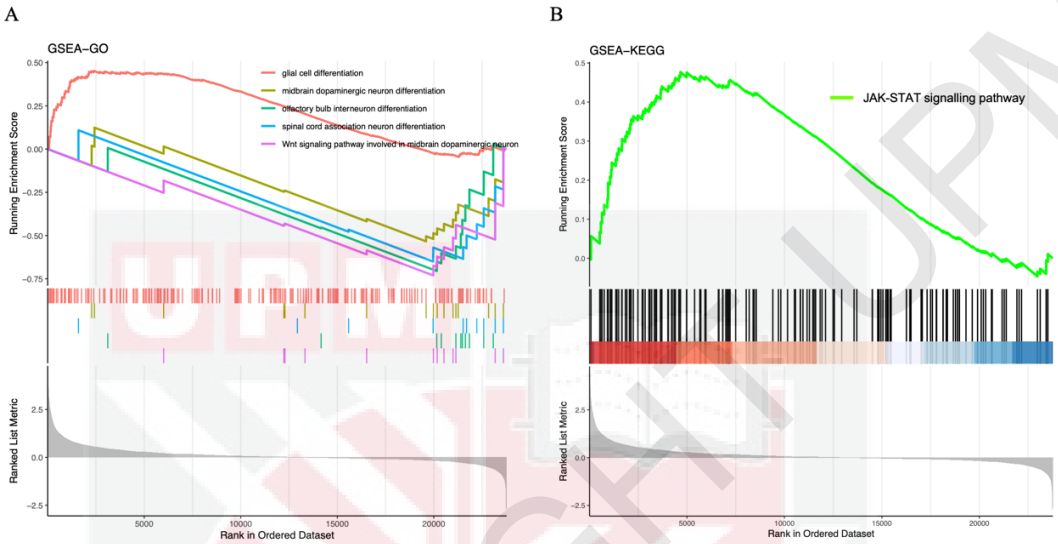


Figure 5.8 : GSEA Analysis for 90-Day DS Cerebral Organoids. (A) GSEA-GO and (B) GSEA-KEGG analysis for the DEGs in DS-derived cerebral organoids at different time points. All results shown |NES| >1 and adjusted p < 0.05. The graphical representation of the GSEA analysis results is divided into three parts. The top section displays the enrichment score (ES) curves, where different coloured curves represent the ES of gene sets associated with various biological processes and signalling pathways within the ranked gene list (expression matrix). A positive ES indicates that the gene set was enriched at the top of the list, signifying upregulated pathways, while a negative ES indicates enrichment at the bottom, signifying downregulated pathways. The middle section contains coloured bars, each line representing a gene from the corresponding gene set of biological processes and signalling pathways, indicating its position in the ranked gene list. The bottom section shown the distribution of gene expression within the ranked gene list, providing a visual representation of the gene expression levels across the dataset

5.4.5 WGCNA Identified Critical Module in DS-Derived 90-Day Cerebral Organoids

DS-related critical genes in iPSC-derived 90-day organoids were identified by constructing scale-free co-expression networks using the R package “WGCNA”. The GSE222365 dataset was selected for clustering evaluation. Hierarchical clustering of

© COPYRIGHT UPM

samples was performed based on the distribution of expression values using average chaining and Pearson's correlation to detect sample outliers. The resulting samples were then analysed by clustering and phenotypic heat map (Figure 5.9A). A power value of $\beta = 9$ was selected as a soft threshold for establishing a scale-free network to build the gene expression network (Figure 5.9B). A hierarchical clustering tree between genes was constructed based on the neighbour-joining matrix and TOM matrix between genes (Figure 5.10A). Fourteen co-expression modules were identified from the expression profiles of DS brain organoids, with different colours representing different modules. Pearson correlation analysis was conducted for the genes within each module across various groups (Figure 5.10B). Correlation analysis of module features revealed that the MElightyellow module, comprising 218 genes, exhibited the strongest association with Down syndrome, achieving a correlation coefficient of 0.98. REST-targeted DEGs were compared with MElightyellow module genes to further screen hub genes in REST-targeted DEGs, and 70 overlapping genes were obtained for subsequent analysis (Figure 5.10C).

© COPYRIGHT UPM

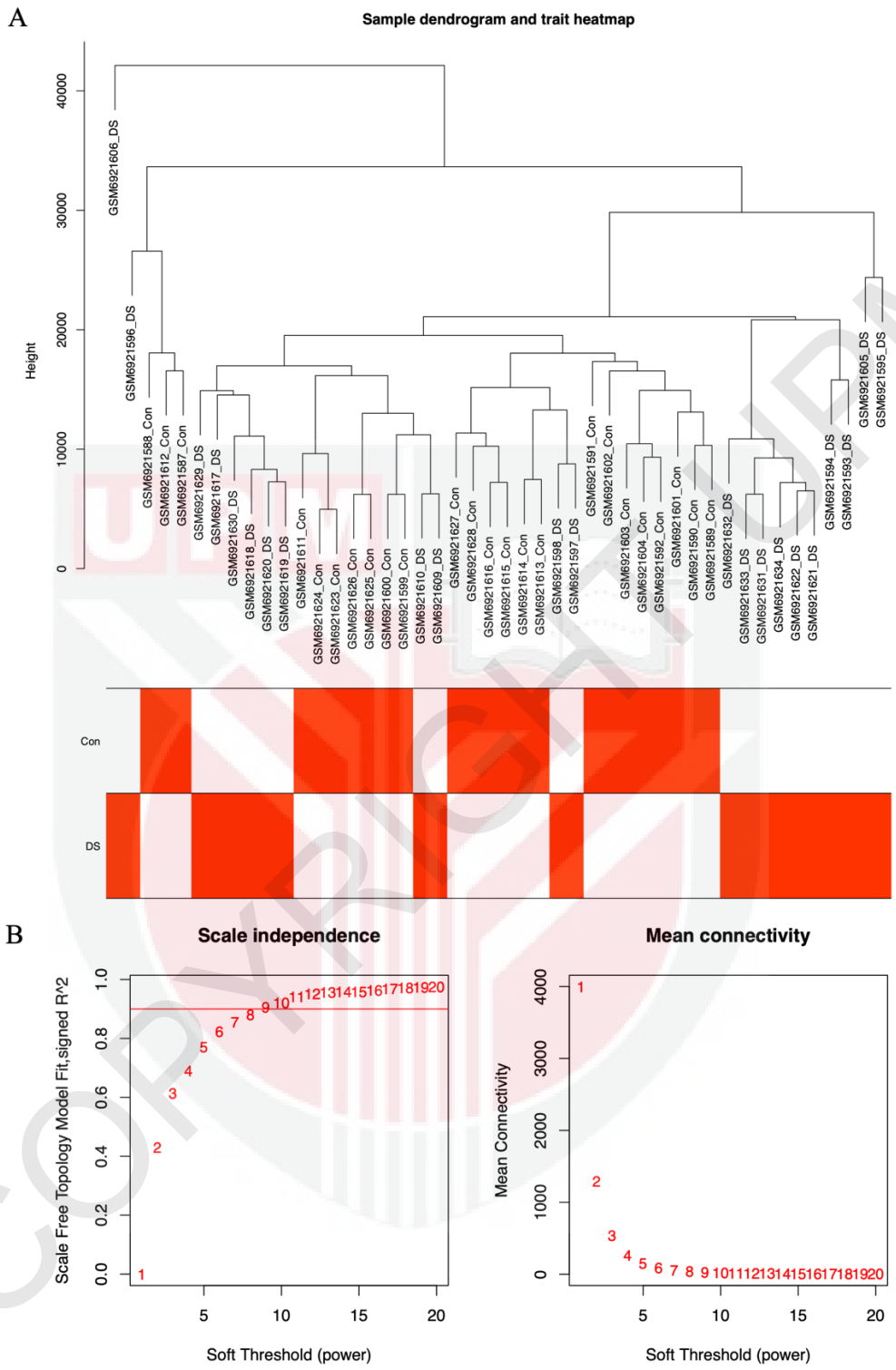


Figure 5.9 : WGCNA for Sample Clustering and Scale-Free Network Construction. (A) Sample clustering was utilised to identify outliers, and a feature heatmap was used to visualise sample characteristics. (B) The network topology was analysed at different soft threshold powers. The graph on the left displays the relationship between the scale-free fit index (y-axis) and the soft threshold powers (x-axis). The graph on the right shows the relationship between mean connectivity (degree, y-axis) and the soft threshold powers (x-axis)

© COPYRIGHT UPM

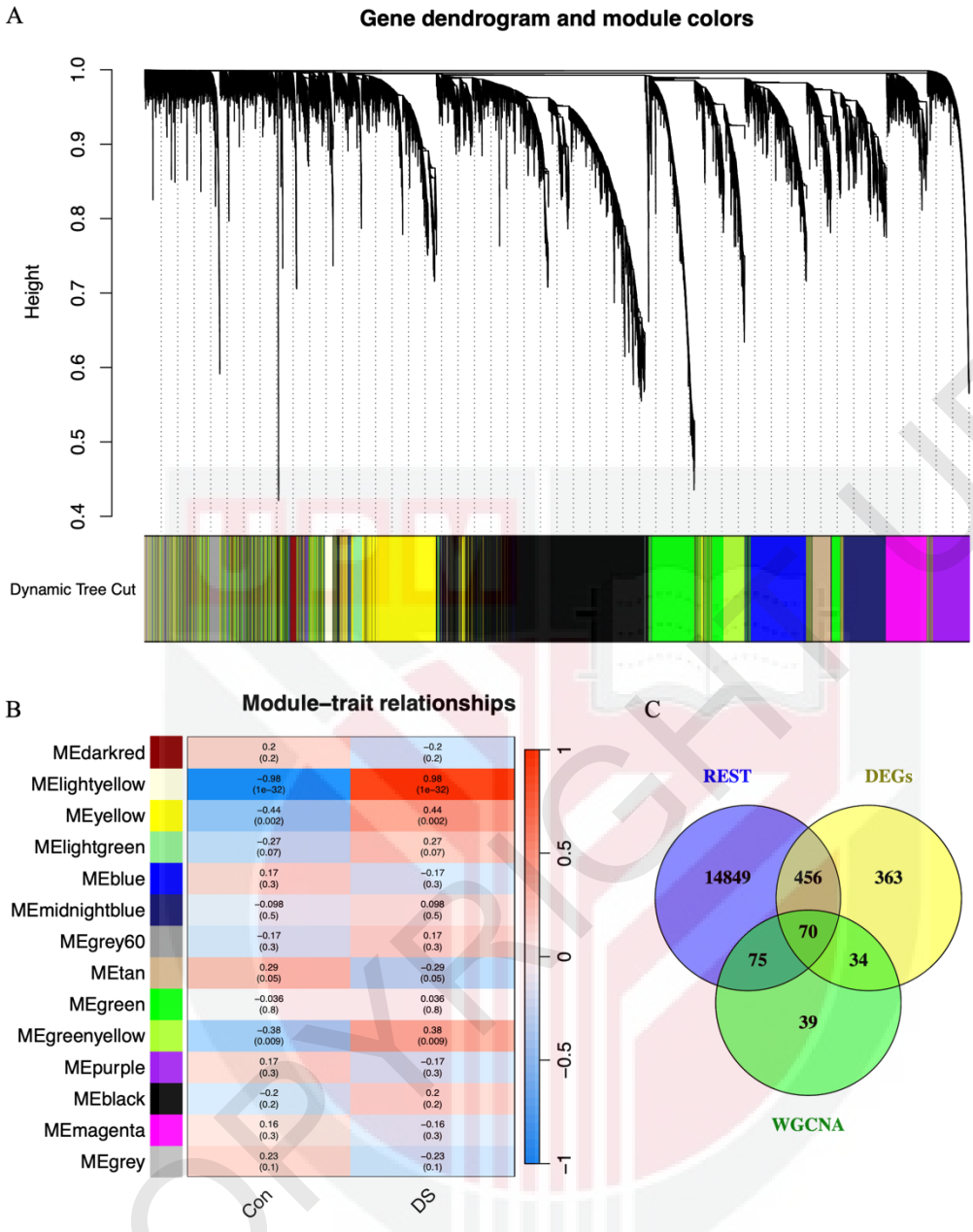


Figure 5.10 : WGCNA Unveiled Gene Co-Expression Networks and Module-Trait Relationships. (A) Clustering dendrograms of all genes based on the topological overlap and assigned module colours was constructed, resulting in 14 distinct co-expression modules represented by different colours. The image displays the relationship between the gene dendrogram at the top and the gene modules at the bottom. (B) The analysis examined the relationships between modules and traits. The table displays correlations and P-values with different traits for each module eigengene. The brown module was identified as the most significantly associated with DS. (C) A Venn diagram illustrating the overlap between REST-targeted DEGs and the genes in the light yellow module

© COPYRIGHT UPM

5.4.6 Machine Learning for Identifying Critical Genes

The 70 genes of REST target DEGs overlapping with the WGCNA core module in 90-day organoids were used to further screening hub genes. We used the LASSO logistic regression algorithm to identify 10 significant feature genes related to DS from the overlapping genes (Figure 5.11A-B). The RF algorithm identified 13 significant feature genes from the overlapping genes (Figure 5.11C). The two algorithms were finally selected, and a total of 6 overlapping genes (*CSTB*, *MCM3AP*, *PFKL*, *POFUT2*, *PRMT2* and *RWDD2B*) were obtained, as shown in the Venn diagram (Figure 5.11D).

© COPYRIGHT UPM

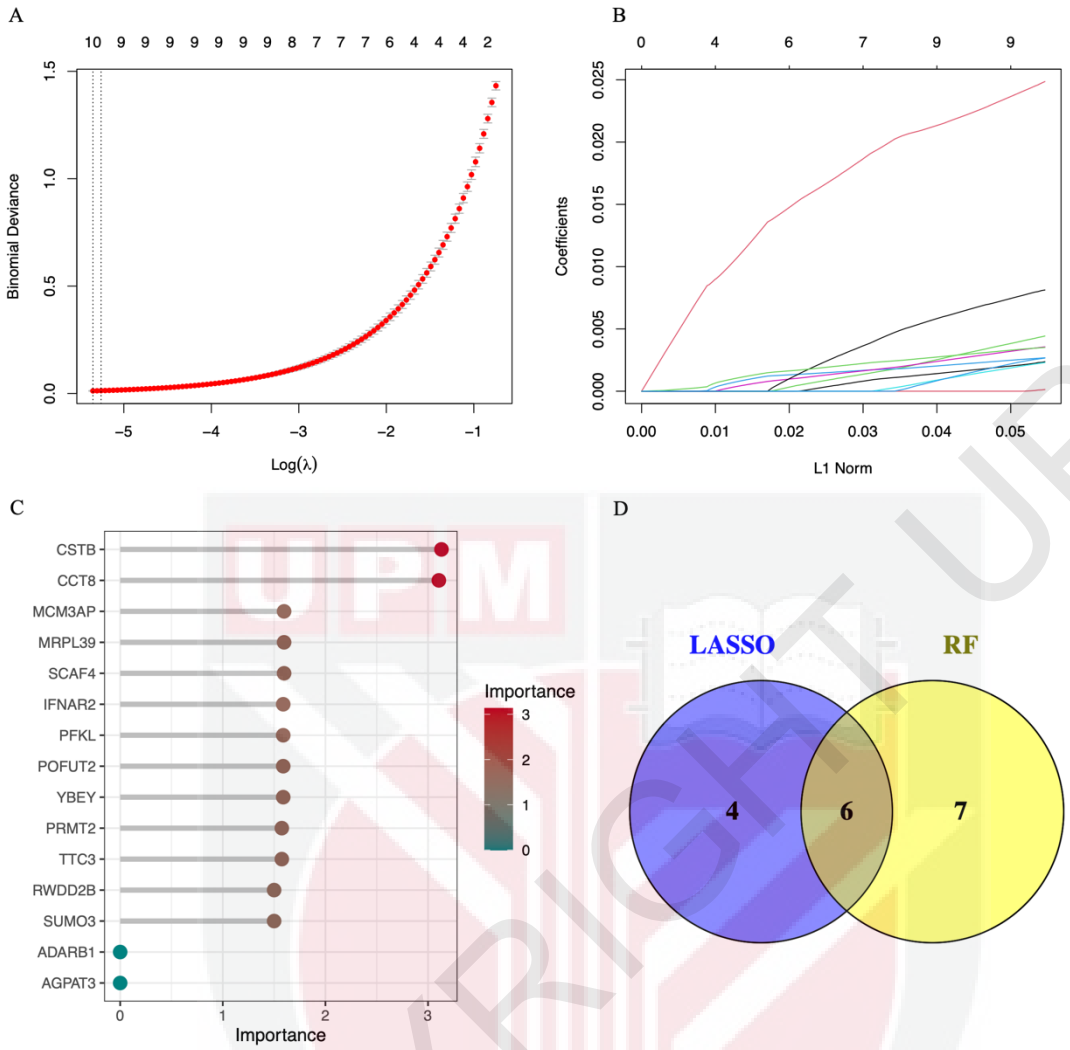


Figure 5.11 : Screening Hub Genes from REST Target DEGs in 90-Day DS iPSC-Derived Cerebral Organoids. (A-B) 10 hub genes were screened by the LASSO algorithm. (C) 13 hub genes were screened by the RF algorithm. (D) Venn diagram of 6 genes including *CSTB*, *MCM3AP*, *PFKL*, *POFUT2*, *PRMT2* and *RWDD2B* intersected by LASSO and RF algorithms

5.4.7 In Silico and Laboratory Validation of REST-Targeted Hub DEGs

To investigate variations in expression levels of the identified REST-targeted hub genes between DS hiPSC-derived cerebral organoids and controls, the expression levels of these genes from the 90-day organoids dataset were first extracted. Statistical analysis revealed significant differences in the expression levels of all hub genes between the DS-derived and control cerebral organoids (Figure 5.12). All 6 hub genes

© COPYRIGHT UPM

(*CSTB*, *MCM3AP*, *PFKL*, *POFUT2*, *PRMT2* and *RWDD2B*) were significantly upregulated (p-value < 0.0001) in the DS hiPSC-derived 90-Day cerebral organoids group compared with controls.

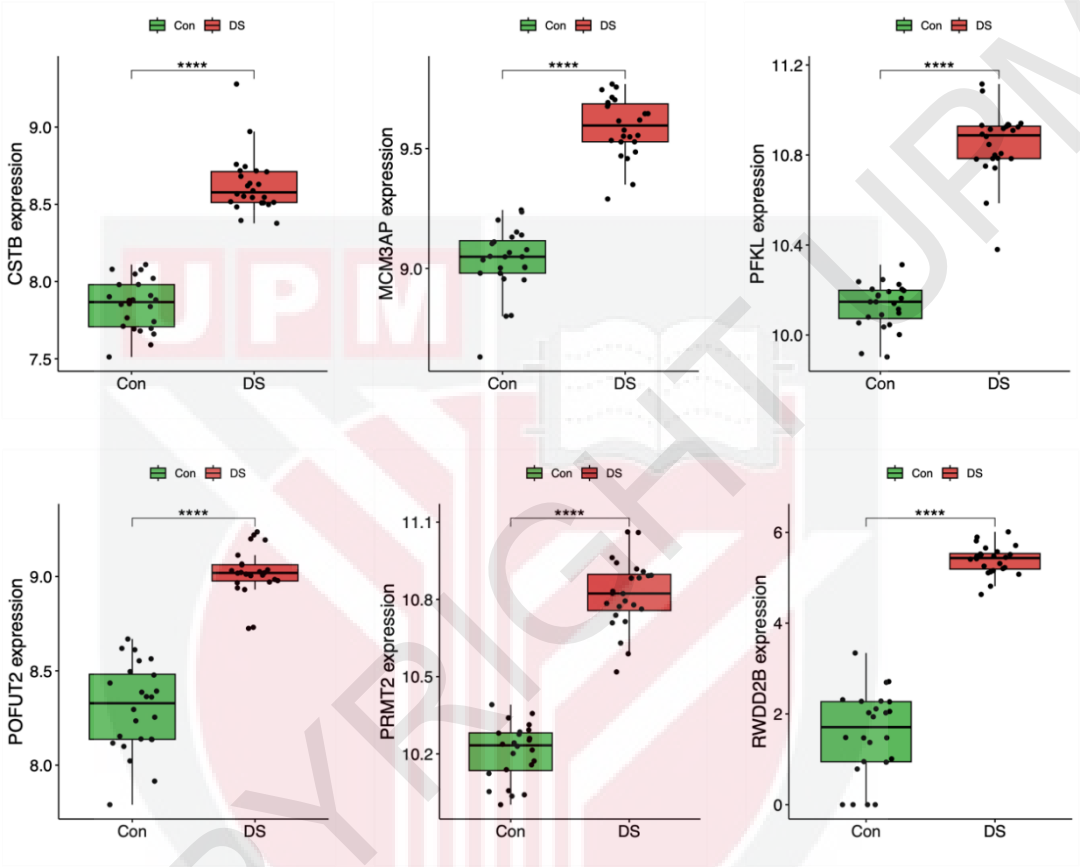


Figure 5.12 : The Silico Analysis for REST-Targeted Hub DEGs in DS hiPSC-Deirved 90-Day Cerebral Organoids. T-test analysis of the expression levels of 6 hub genes-*CSTB*, *MCM3AP*, *PFKL*, *POFUT2*, *PRMT2* and *RWDD2B*. *p-value < 0.05, **p-value < 0.01, ***p-value < 0.001, ****p-value < 0.0001

5.4.8 In Laboratory Validation of REST-Targeted Hub DEGs

To validate the predicted REST-targeted hub genes, cerebral organoids derived from three controls and DS hiPSCs were cultured for further analysis. The first 5 days of culture is the period of EB formation, and the diameter of EBs on the 5th day should be more than 300µm with rounded edges, which is conducive to the neural induction

© COPYRIGHT UPM

and growth of cerebral organoids in the later stage. The cerebral organoids grew in size as they were incubated for longer periods of time in subsequent cultures (Figure 13A). In day-45 cerebral organoids, the immunocytochemistry analysis was performed to verify the growth and development status of cerebral organoids. Positive results for cell proliferation marker Ki67, neural progenitor marker SOX2 and neuronal migration marker TBR1 indicated that the organoids were well developed (Figure 5.13B). All organoids were harvested for mRNA extraction when grown to 90 days. To verify the expression of REST-targeted hub genes, RT-qPCR analysis were performed for *CSTB*, *MCM3AP*, *PFKL*, *POFUT2*, *PRMT2* and *RWDD2B* mRNA expression levels. This study has shown that the mRNA levels of *CSTB*, *MCM3AP*, *PFKL*, *POFUT2*, *PRMT2* and *RWDD2B* were significantly upregulated (p-value < 0.05) between 1.4 and 3.2 folds in DS-derived 90-day cerebral organoids compared to the control group (Figure 5.13C).

© COPYRIGHT UPM

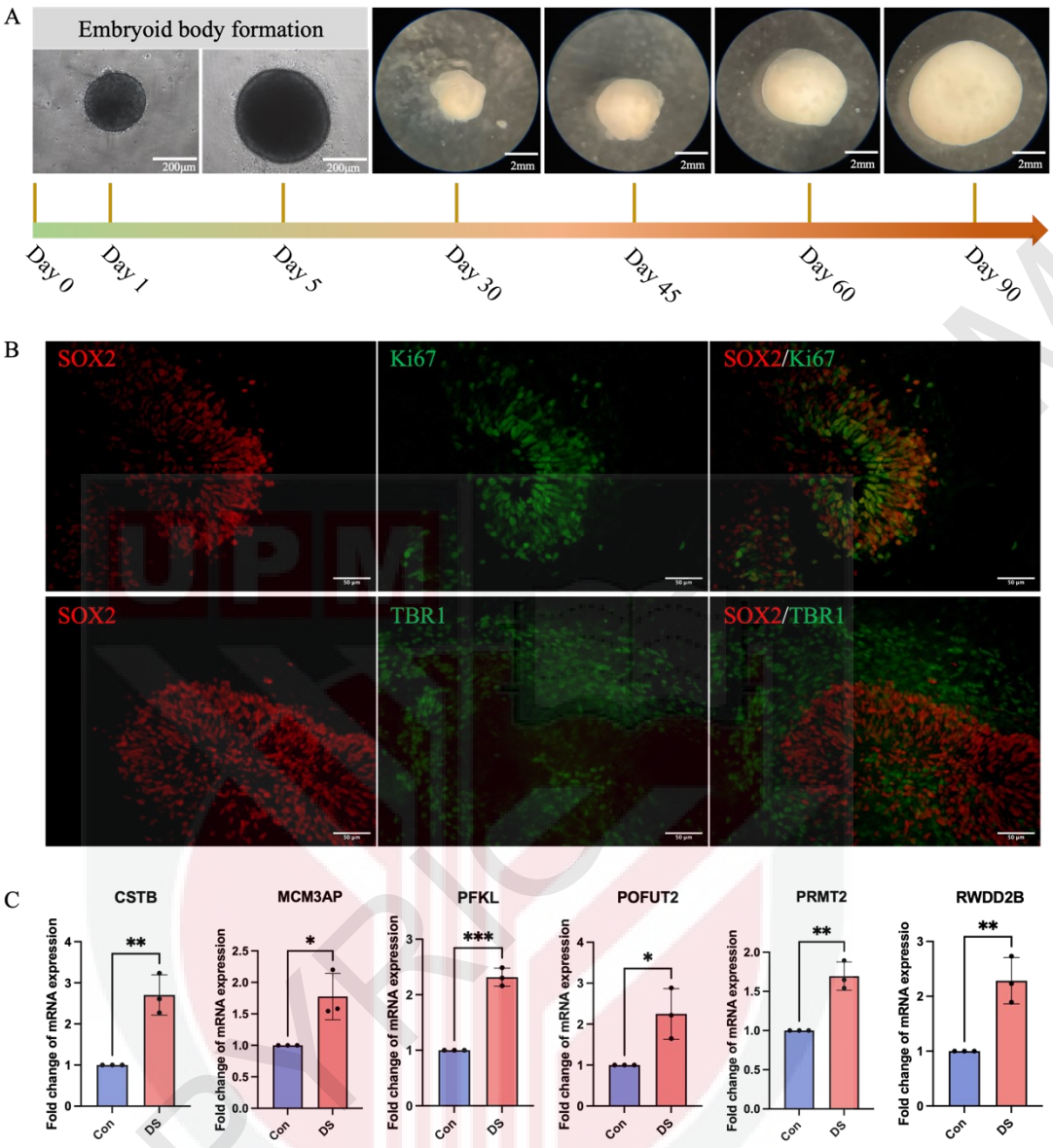


Figure 5.13 : Culture of Cerebral Organoids and Validation of REST-Targeted Hub Gene in 90-Day Cerebral Organoids. Three pairs of cell lines (C1 vs. DS1, C2 vs. DS2, and C5 vs. DS4) were used to perform qPCR analysis (n=3). (A) Culture timeline and morphology of 90-day cerebral organoids. (B) Immunochemical staining of 45-day cerebral organoids showed Ki67, SOX2, and TBR1 positivity. (C) The mRNA levels of *CSTB*, *MCM3AP*, *PFKL*, *POFUT2*, *PRMT2* and *RWDD2B* were detected by RT-qPCR. The mean ± SD is from experiments of three independent cell lines. *p-value < 0.05, **p-value < 0.01, ***p-value < 0.001. Con, Control; DS, Down syndrome

5.4.9 The Neurogenic-to-Gliogenic Shift in 90-Day DS hiPSC-Derived Organoid

To verify the role of REST in cerebral organoids, qPCR was performed to detect the expression level of *REST* mRNA. The results showed that the expression level of *REST* mRNA in 90-day DS iPSC-derived cerebral organoids was significantly downregulated (p-value < 0.0001) than that in the control group (Figure 5.14A). The mRNA expression level of *REST* in DS iPSC-derived cerebral organoids was only 16.39% of the level in the control group. To further explore the effects of REST downregulation on the neurodevelopment of DS cerebral organoids, the neuroblast marker DCX and the glioblast marker NFIA were further evaluated. The results revealed that *DCX* mRNA levels were downregulated by 3.8 fold (p-value < 0.01) in 90-day DS iPSC-derived cerebral organoids compared to control (Figure 5.14B). Whereas the expression level of *NFIA* was upregulated 1.7-fold (p-value < 0.05) in 90-day DS iPSC-derived cerebral organoids compared to control (Figure 5.14C). This suggests a neurogenic-to-gliogenic shift in 90-day DS iPSC-derived cerebral organoids. Previous analyses have revealed that REST targets the JAK-STAT signalling pathway in 90-day DS iPSC-derived cerebral organoids, and that's a key pathway affecting the differentiation of NPCs to glial cells. To explore whether this pathway is doubly activated in 90-day DS iPSC-derived cerebral organoids, mRNA expression of *JAK2* and *STAT3* was further assessed. Although this study found no statistically significant difference in the expression of *JAK2* mRNA (p-value > 0.05) between 90-day DS iPSC-derived cerebral organoids and controls (Figure 5.14D), the expression of *STAT3* mRNA was significantly upregulated by 2.14-fold (p-value < 0.0001) compared to controls (Figure 5.14E). Thus, downregulation of REST may

© COPYRIGHT UPM

lead to activation of the JAK-STAT signalling pathway, which further leads to a neurogenic-to-gliogenic shift in 90-day DS hiPSC-derived organoids.

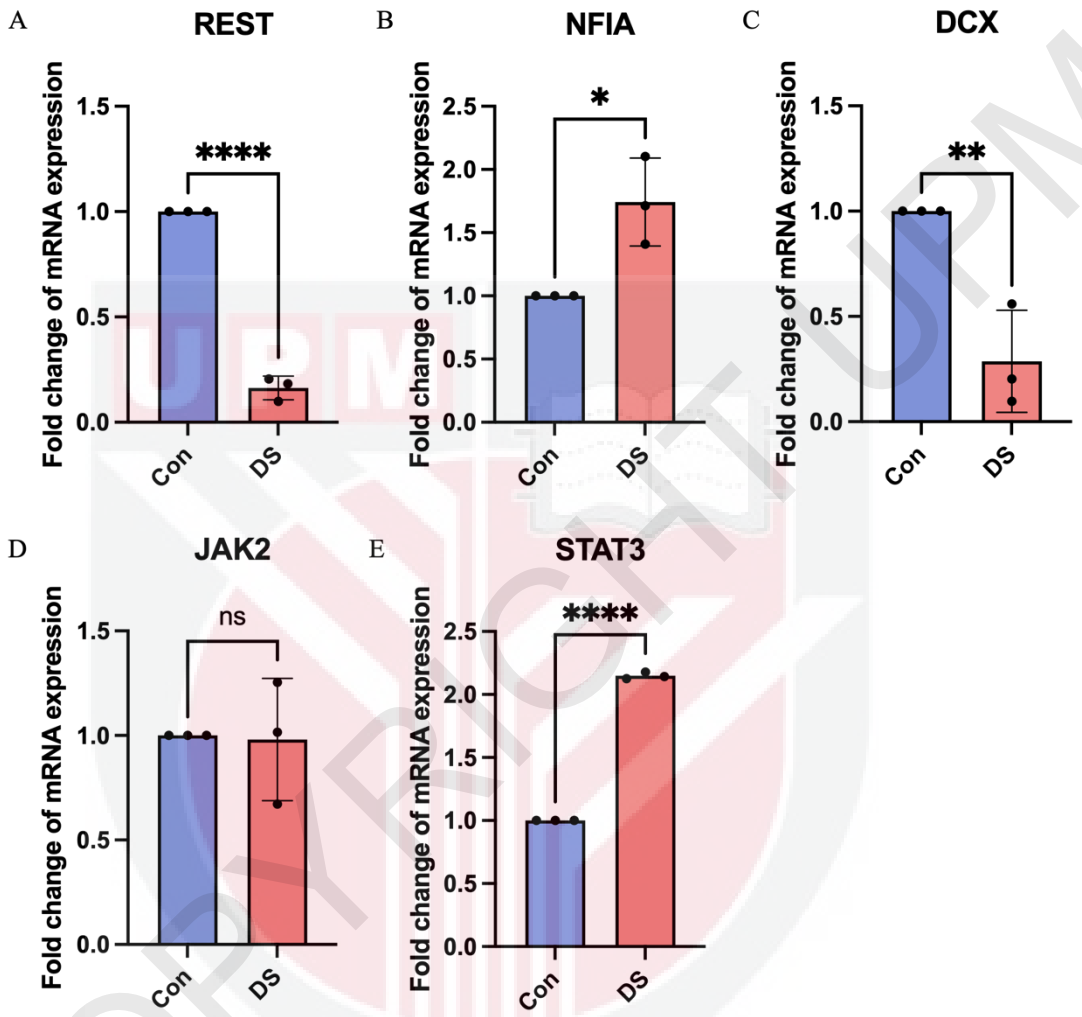


Figure 5.14 : Detection of REST and Neural Differentiation-Related Genes in 90-Day DS iPSC-Derived Cerebral Organoids. Three pairs of cell lines (C1 vs. DS1, C2 vs. DS2, and C5 vs. DS4) were used to perform qPCR analysis (n=3). All measurements were normalised by dividing DS values with the corresponding controls. (A-E) The expression levels of *REST*, *DCX*, *NFIA*, *JAK2*, and *STAT3* mRNA were detected by qPCR in DS and control groups, respectively. *p-vlue < 0.05, **p-value < 0.01, *** p-value < 0.001. Con and C, Control; DS, Down syndrome

5.5 Discussion

This study analysed bulk transcriptome data from cerebral organoids derived from hiPSCs of individuals with DS and control groups at five distinct time points: Day 30,

Day 35, Day 56, Day 90, and Day 160. These findings indicate that DEGs in DS organoids at days 30-35 are primarily enriched in pathways related to neuronal differentiation, axon development, and Wnt signalling. However, single-cell sequencing analysis revealed a delayed developmental trajectory from NPCs to neurons in 30-day cerebral organoids (Tang et al., 2021). This suggests that individuals with DS exhibit abnormal neuronal cell differentiation early in neurodevelopment. Single-cell sequencing analysis of 70-day DS cerebral organoids, revealed an increased proportion of immature deep and upper-layer neurons and a decreased proportion of mature neurons compared to controls (Tang et al., 2021). Previous studies have shown cerebral organoids older than 50-70 days express mature astrocyte markers (S100B and GFAP) (Dezonne et al., 2017; Pavlinov et al., 2023; Xu et al., 2021, 2019). In the initial report on the 56-day organoid data, S100B+ and GFAP+ cells were detected, though no statistically significant differences in astrocyte proportions were found between the DS and control groups (Xu et al., 2019). Additionally, there are no other bulk transcriptome data related to DS cerebral organoids during this period. Further studies may be needed to fill in the changes in cellular phenotypes and lineages during DS neurodevelopment in the period between 50-90 days.

Notably, bulk transcriptome analysis of 90-day cerebral organoids revealed that, compared to controls, gene sets associated with the differentiation of various types of neurons were downregulated in DS cerebral organoids. In contrast, gene sets related to glial cell differentiation were upregulated. Single-cell sequencing of 90-day organoids showed a significant increase in glial progenitor cells and astrocytes and a significant decrease in mature neurons, particularly interneurons, in DS organoids

© COPYRIGHT UPM

compared to controls (Czerminski et al., 2022). Consequently, a prominent neurogenic-to-gliogenic shift was observed in 90-day DS cerebral organoids. This may be a critical time point for future therapeutic strategies for DS brain development.

REST is a transcription factor that controls pluripotency and cell fate, and it has been widely acknowledged as a key regulator in embryonic and neural development (Greenway et al., 2007). By repressing the expression of target genes, REST regulates neurogenesis, maturation, and neuroprotection (Chen et al., 1998; Qureshi et al., 2010). However, the full extent of the role of REST has often been underestimated. The bulk transcriptome datasets analysis of cerebral organoids from DS at various time points revealed that REST target genes are involved in chromosome segregation, the cell cycle, DNA replication and transcription, cellular metabolism, neuronal differentiation and maturation, synaptic remodelling and signal transduction, glial cell differentiation and maturation, neural cell apoptosis, and neuroimmune regulation. The influence of REST spans nearly every stage of neural development in DS. Rather than regulating a single gene or a specific functional gene set, REST operates within a complex regulatory network involving numerous target genes, the REST corepressor (CoREST), and other transcription factors.

As mentioned above, transcriptome data analysis of 90-day cerebral organoids revealed a significant downregulation of neuronal differentiation and an upregulation of glial differentiation. These 90-day brain organ tissues were further analyzed to elucidate specific molecular mechanisms. We found a significant downregulation of *REST* mRNA expression and a significant upregulation of the neuroblast marker DCX in DS cerebral organoids compared to controls. A timely reduction of REST in NPCs

© COPYRIGHT UPM

is essential for their rapid differentiation into neurons (Mozzi et al., 2017). Previous studies have shown that decreased REST levels reduce repression of neuronal genes, thereby promoting neuron differentiation (Gao et al., 2011; Tang, 2009). Knockdown of *REST* causes NSCs to differentiate prematurely into neurons temporarily. This results in an increased proportion of neurons, particularly immature neurons, but ultimately reduces the total number of neurons. This reduction is due to the inability to maintain the NSC pool, leading to a loss of neurogenesis capacity (Alsaqati et al., 2022; Gao et al., 2011; Singh et al., 2008). A recent study suggested that the induction of programmed cell death may cause REST loss-induced neuronal loss and decreased expression of neuronal genes. In this study, increased Caspase-3 activation and Caspase-3 gene expression were observed in neurons (Alsaqati et al., 2022). Therefore, maintaining a neuronal level of REST is crucial during neuron differentiation and development.

Notably, in embryonic stem cells (ES), eliminating REST does not lead to the premature expression of neuron marker genes repressed by REST, as initially expected. Complete removal of REST results in embryonic lethality around E11.5 in mice (Tang, 2009). In vitro ES models show that reducing REST expression to 1% of wild-type levels causes a deficiency of nestin-positive cells in NSCs and NPCs, leading to neurogenesis defects. These defects can be partially rescued when REST expression is 8% of wild-type levels (Singh et al., 2008; Sun et al., 2008). At 50% of wild-type levels, REST loss leads to the loss of self-renewal capacity in ES cells and premature neuronal differentiation in the short term (Singh et al., 2008). Thus, severe REST deficiency hinders neural differentiation and neurogenesis.

© COPYRIGHT UPM

REST plays a role in regulating not only neuronal gene expression but also influences the epigenetic landscape of glial cells (Abrajano et al., 2009; Alsaqati et al., 2022; Liu et al., 2019). Recent research has predominantly concentrated on the link between REST expression levels and neurogenesis, often overlooking its critical role in gliogenesis. This findings indicated an upregulation in the expression of glioblast cell marker NFIA and astrocyte markers GFAP and S100B. This suggests that the REST loss may promote the differentiation and maturation of astrocytes. Physiological upregulation of REST during NPC differentiation promotes gliogenesis (Abrajano et al., 2009; Bergsland et al., 2014; Covey et al., 2012); however, pathological overexpression of REST can lead to impairments in gliogenesis (Liu et al., 2019). In an in-vitro mouse ES model, the knockdown of REST decreased the number of neurons but did not significantly affect astrocyte differentiation and number (Gao et al., 2011). This reflects the complexity of REST-level changes in astrocyte differentiation. Possible explanations include: 1) Physiological elevation of REST in NPCs and NSCs inhibits the expression of neuron-related genes, allowing the expression of glial differentiation-related genes; 2) Pathological overexpression of REST may suppress glial differentiation-related genes, while the loss of REST may release this suppression. REST and CoREST proteins are ubiquitously expressed in the cytoplasm and nuclei of glial lineage cells, including astrocytes, oligodendrocytes, and glial progenitor cells. In glial lineages derived from mouse embryonic stem cells, 3,178 REST and 4,060 CoREST target genes have been identified. Notably, 297 REST and 50 CoREST target genes are specific to astrocytes (Abrajano et al., 2009). Consequently, the loss of REST in DS cerebral organoids may lead to the upregulation of these genes, resulting in increased gliogenesis, particularly astrocytogenesis.

© COPYRIGHT UPM

In this study, 90-day DS cerebral organoids revealed that REST targets the JAK-STAT signalling pathway. Further qPCR results confirmed a significant upregulation of *JAK2* and *STAT3* mRNA in DS cerebral organoids compared to controls. The activation of the JAK-STAT signalling cascade plays a crucial role in promoting differentiation of NPCs to astrocytes during neurodevelopment. Centred around STAT3, the JAK-STAT pathway interacts with various signalling pathways, including Notch, BMP, and TGF, to promote astrocytogenesis synergistically (Chenn, 2009; Martynoga et al., 2012; Wang et al., 2016). Moreover, studies have found that the activated JAK-STAT pathway can inhibit neurogenesis and initiate astrocyte formation (Lee et al., 2016). The JAK-STAT pathway directly regulates the expression of *GFAP* and *S100B*, facilitating the differentiation of NPCs into astrocytes (Deb et al., 2023; Fukuda et al., 2007). Therefore, the loss of REST may enhance astrocyte differentiation and increase their number in DS cerebral organoids by upregulating the JAK-STAT signalling pathway.

Furthermore, REST-targeted hub DEGs (*CSTB*, *MCM3AP*, *PFKL*, *POFUT2*, *PRMT2*, and *RWDD2B*) were significantly upregulated in 90-day cerebral organoids compared to controls. These genes highlight the complex interplay between gene expression and key signalling pathways during central nervous system development. Notably, *RWDD2B* is reported in Down syndrome for the first time, and further research is needed to fully elucidate its role in the neurodevelopmental processes. To gain a deeper understanding of their roles in DS neurodevelopment, we further elaborate on the potential mechanisms involving these genes (Figure 5.14).

© COPYRIGHT UPM

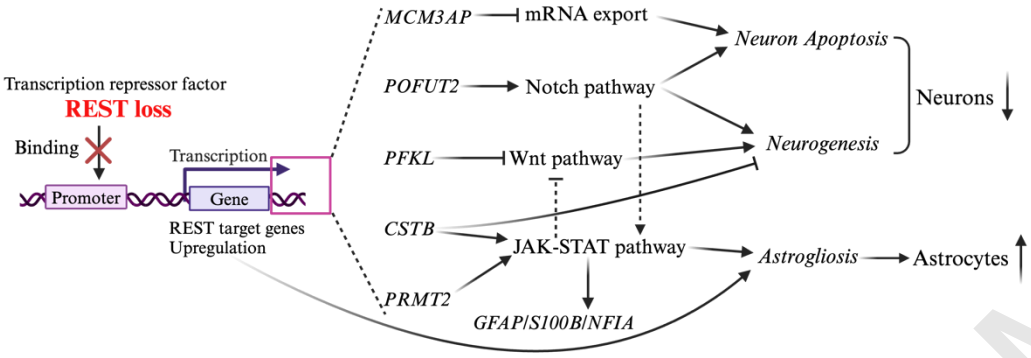


Figure 5.15 : Potential Mechanisms by Which REST-Targeted Hub DEGs Affect Neurodevelopment in DS. REST-Targeted Hub DEGs Collectively Contribute to Neuronal Reduction and Astrocyte Overproduction during Neurodevelopment in DS day-90 Organoids

The cystatin B (CSTB) is extensively present in neural cells and regulates the cell cycle, cell proliferation, differentiation, synaptic function, neuroinflammation, and oxidative stress (Brännvall et al., 2003; Čeru et al., 2010; Di Giaimo et al., 2002; Gorski et al., 2020). A key factor in differentiating neural progenitor cells (NPCs) is the transient cleavage of the N-terminal histone H3 tail, mediated by proteases B and L. In the absence of *CSTB*, the enzymatic activity of these proteases increases, causing premature cleavage in NPCs and leading to their early differentiation into neurons (Daura et al., 2021; Duncan et al., 2008). Conversely, *CSTB* overexpression increases NPC proliferation and delays their entry into the S phase, thereby preventing differentiation into neurons (Duncan et al., 2008; Sansregret et al., 2006). Notably, both *CSTB* deficiency and overexpression ultimately decrease neuronal proliferation and number (Adams-Cioaba et al., 2011; Joensuu et al., 2014; Kaasik et al., 2007; Sansregret et al., 2006). Additionally, *CSTB* upregulation activates *STAT1* and *STAT3* (Luciano-Montalvo and Meléndez, 2009; Maher et al., 2014), although the specific mechanism of *CSTB* involvement in JAK-STAT signalling remains unclear.

© COPYRIGHT UPM

The Mini Chromosome Maintenance Complex Component 3 Associated Protein (MCM3AP) gene encodes the germinal centre-associated nuclear protein (GANP) (Wickramasinghe et al., 2010). GANP is crucial for selective mRNA export and is closely related to the regulation of axon and neuron function (Wickramasinghe et al., 2014; Zappulo et al., 2017). Mutations in *MCM3AP* that result in GANP defects block mRNA export from axons, leading to mRNA accumulation in the nucleus of neurons (Woerner et al., 2016; Ylikallio et al., 2017; Zappulo et al., 2017). This accumulation is a key mechanism in various diseases, including motor neuron disease, amyotrophic lateral sclerosis, Charcot-Marie-Tooth neuropathy, and mental retardation-related disorders (Kaneb et al., 2015; Nousiainen et al., 2008; Woldegebriel et al., 2020; Ylikallio et al., 2017). However, the neural phenotype changes induced by *MCM3AP* overexpression in DS hiPSC-derived cerebral organoids require further investigation.

Hepatic phosphofructokinase (PFKL) is one of the three isoforms of phosphofructokinase (PFK), a key enzyme in glucose metabolism (Su et al., 2004). In individuals with DS, overexpression of *PFKL* has been observed throughout embryonic development. The gene dosage of *PFKL* in DS has been shown to affect *PFK* activity in the embryonic brain, but not in the adult brain, leading to impairments in embryonic brain development (Elson et al., 1994). Overexpression of *PFKL* results in increased glucose metabolism, decreased blood glucose clearance, and reduced insulin responsiveness to glucose concentrations in DS brains (Peled-Kamar et al., 1998). In *PFKL* transgenic mice, it has found an increase in brain glucose metabolism of more than 50% compared to controls, similar to young DS individuals (Peled-Kamar et al., 1998). In the brains of DS individuals, the glucose metabolic rate decreases with age, indicating that disturbances in glucose metabolism may be

© COPYRIGHT UPM

associated with the development of intellectual disability and dementia in DS (Schapiro et al., 1992, 1988; Zammit et al., 2021). Additionally, increased levels of glycolytic flux down-regulated the expression of Wnt signalling-related genes and their targets, inhibiting the activity of the Wnt signalling pathway (Miyazawa et al., 2022).

Protein O-fucosyltransferase (POFUT2) is a glycosyltransferase responsible for the post-translational O-fucosylation of proteins. POFUT2 mainly glycosylates thrombospondin type I repeats (TSRs) (Schneider et al., 2017; Vasudevan et al., 2015). Fucosylation regulates synapse formation and plasticity, axon growth and migration, and neuron morphogenesis (Kalovidouris et al., 2005; Lipscomb et al., 2003; St John et al., 2006). The *POFUT2* is a key gene in embryonic development, morphogenesis, and neuronal differentiation in DS (Menzel et al., 2004; Nordquist et al., 2018). The previous study on the *C. elegans* direct homologue of *POFUT2*, *pad-2*, showed that *pad-2* is expressed in different cell types from the embryonic stage of morphogenesis to development (Menzel et al., 2004). This study demonstrated that deletion of *pad-2* predominantly results in the loss or reduced expression of neuronal markers, whereas overexpression of *pad-2* appears to activate neuronal proliferation and/or specialisation. Notably, *pad-2* affects cell fate decisions in a dose-dependent manner during neuronal differentiation and leads to defects in neuronal morphology, size, and location (Menzel et al., 2004).

Protein arginine methyltransferase 2 (PRMT2) is a member of the PRMT family that catalyses the arginine methylation of target proteins, forming asymmetric dimethylarginine. Several studies have highlighted the complex regulatory

© COPYRIGHT UPM

relationship between *PRMT2* and the Wnt/β-catenin signalling pathway, as well as the JAK-STAT signalling pathway. In the vitro cell model, PRMT2 was found to be directly recruited by β-catenin to the promoter regions of target genes, leading to the methylation of H3R8me2a and H3K4me3. This process activates the Spindlin1-Wnt/β-catenin signalling pathway and promotes the expression of Wnt target genes (Su et al., 2014). Furthermore, the silence of *PRMT2* results in reduced hypothalamic STAT1 and STAT3 methylation and prolonged tyrosine phosphorylation (Iwasaki et al., 2010; Liu et al., 2024). Interestingly, PRMT2 interacts directly with PRMT1 to enhance its activity. Increased PRMT1 activity drives the methylation of STAT3 and activates the GFAP promoter in NSC-derived astrocytes derived from neural stem cells (Honda et al., 2017). The precise mechanism by which the JAK-STAT signalling pathway is activated through methylation rather than phosphorylation of STAT3, driving neural stem cells to differentiate into astrocytes, remains to be further explored. Nonetheless, the involvement of PRMT2 in modulating the Wnt/β-catenin and JAK-STAT signalling pathways during neurodevelopment and neural cell differentiation in DS remains poorly understood and requires further research.

5.6 Conclusions

Down syndrome exhibits specific neurodevelopmental deficits at various stages of development. However, few studies have simultaneously explored the neurodevelopmental abnormalities in the DS brain across different developmental stages. This study, analysing DS-derived cerebral organoids at various time points, reveals early neurogenesis defects and later-stage gliogenesis abnormalities, such as excessive astrocyte formation. REST and its target genes play a crucial regulatory role in these neurodevelopmental disruptions. I identified the 90-day cerebral organoids as

© COPYRIGHT UPM

critical for a neurogenic-to-gliogenic shift in DS, with REST playing a central role in this shift, providing a foundation for future research. However, the role of REST in the increased astrocyte population in DS remains unclear and requires further investigation.

© COPYRIGHT UPM

CHAPTER 6

REST RESTORATION INHIBITS DOWN SYNDROME IPSC-DERIVED ASTROCYTIC REACTIVITY

6.1 Introduction

A neurogenic-to-gliogenic shift has been observed in DS-derived NPCs and cerebral organoids. The loss of REST may be a key factor in the increase in DS gliogenesis. Although loss of REST has been shown to increase the tendency of NPCs to differentiate into astrocytes during neurodevelopment, changes in the level of REST in DS-derived astrocytes and its effect on DS astrocyte function remain unclear. Further studies to assess the role of REST in DS-derived astrocytes are essential.

Although astrocyte differentiation increases during DS neurodevelopment, their development and maturation are impaired (Ponroy and Murai, 2021). This leads to functional defects in astrocytes that disrupt their supportive effects on neurons and transform them to be neurotoxic. DS-derived astrocytes produce adverse effects in regulating synaptic development and maturation, neuronal ion channels, neuronal excitability and neuronal survival (Ponroy et al., 2020). RNA sequencing reveals that DS-derived astrocytes undergo genome-wide transcriptional disruption, leaving DS neurodevelopment, cell adhesion, mitochondrial function, and extracellular matrix-related molecules severely dysregulated (Kawatani et al., 2021; Ponroy et al., 2020). Notably, chromosome 21 genes are consistently upregulated in DS-derived astrocytes, causing S100B to preferentially and significantly accumulate in the cells, leading to astrocyte dysfunction and oxidative stress-induced neural death and impaired neurogenesis (Chen et al., 2014; Lu et al., 2011; Royston et al., 1999). Nevertheless, this change does not affect DS-derived astrocyte viability. The high proliferation rate

© COPYRIGHT UPM

of DS-derived astrocytes, which resulted in the expression of higher levels of S100B and GFAP and the generation of elevated ROS levels, indicates that DS-derived astrocytes are in a reactive state (Chen et al., 2014; Escartin et al., 2021; Liddelow and Barres, 2017). However, information on reactive astrocytes in DS is limited.

Reactive astrogliosis is a defensive response of astrocytes to pathological processes, involving complex activation programs that remodel astrocyte biochemical, morphological, metabolic, and physiological characteristics (Ding et al., 2021; Hamby and Sofroniew, 2010; Nakagawa et al., 2005). This can result in either neuroprotection or damage by upregulating or losing homeostatic cascades. Reactive astrocytes induced by neuroinflammation and/or injury can be categorised into "A1" and "A2" subtypes (Escartin et al., 2021). A1 Reactive astrocytes upregulate proinflammatory factors such as *IL-1β*, *TNF-α*, ROS, and NO, as well as release cytotoxins, which are considered neurotoxic reactive astrocytes (Li et al., 2019). A2 reactive astrocytes upregulate the neurotrophic factors *BDNF*, *VEGF*, and *bFGF*, as well as the anti-inflammatory factors *IL-10* and *TGF-β*, which are considered neuroprotective reactive astrocytes (Li et al., 2019). However, reactive astrocytes do not polarise into simple binary phenotypes, and it is difficult for a single phenotype to exist in a disease. Acquisition of neuroprotective or neurotoxic function may occur simultaneously, depending on the balance of homeostasis in the disease environment (Escartin et al., 2021; Liddelow and Barres, 2017). For example, in PD models, pathological α-syn accumulation drives the conversion of neuroprotective A2 astrocytes into neurotoxic A1 reactive astrocytes, exacerbating disease progression (Valenzuela et al., 2023; Yun et al., 2018). However, whether REST mediates the mechanism of molecular dysregulation of reactive astrocytes in DS remains unclear. This study aims to explore

© COPYRIGHT UPM

the reactivity of astrocytes derived from DS hiPSCs and investigate the impact of REST levels on astrocyte reactivity.

6.2 Experiment Design

To further investigate the role of REST in astrocytes, RNA sequencing datasets from various sources were analysed, including astrocytes derived from DS hiPSCs, DS fetal cortex, and DS fetal cerebellum. Differentially expressed gene (DEG) analysis was performed with the Galaxy web platform and R software. After identifying the overlapping genes between DEGs and REST target genes, the GO and KEGG pathway enrichment analyses on these REST-targeted DEGs were conducted. To validate REST expression and its function in DS-derived astrocytes, the astrocytes derived from trisomic and disomic hiPSCs were cultured. These cells were treated with lithium carbonate and/or X5050 to modulate REST levels and then assessed how REST levels affect astrocyte reactivity. Figure 6.1 illustrates a streamlined overview of the data processing and analytical workflow, along with the experimental procedures employed in this study.

© COPYRIGHT UPM

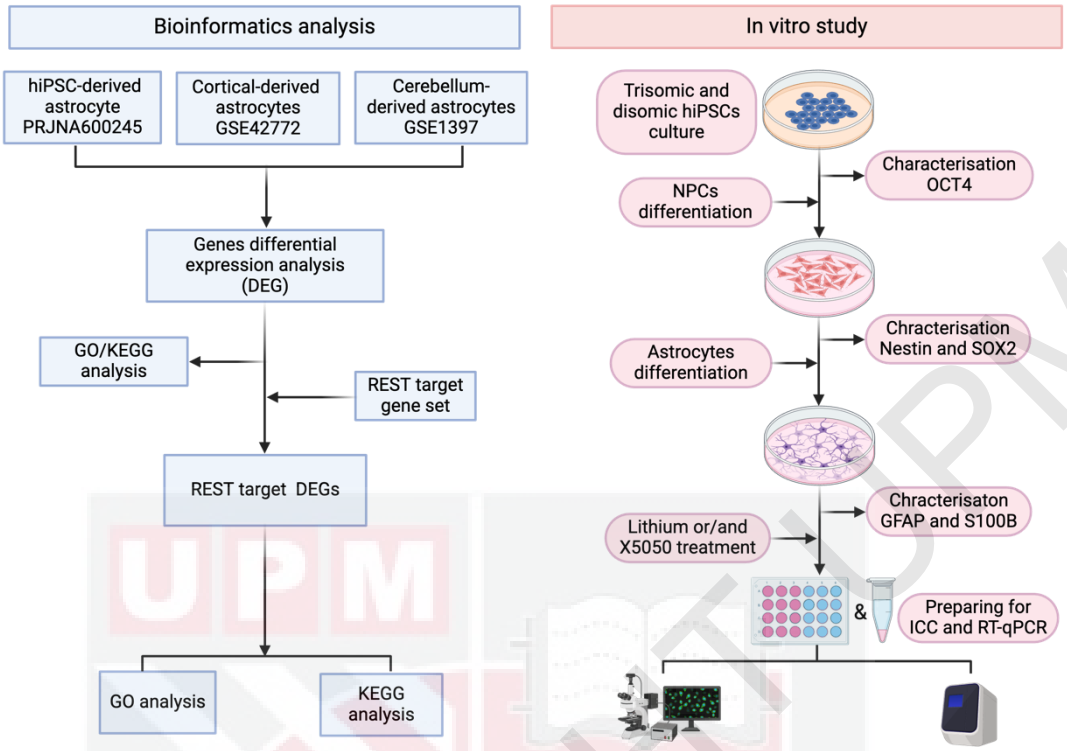


Figure 6.1 : Simplified Diagram of the Experimental Methods, Data Processing, and Analysis Workflow Used for This Study. GO, Gene Ontology; hiPSC, Human induced pluripotent stem cells; KEGG, Kyoto encyclopedia of genes and genomes; NPC, Neural progenitor cell. The figure was created in BioRender (JN27U4G15O)

6.3 Materials and Methods

6.3.1 Acquisition of DS-Derived Astrocytes Datasets

For human fetal cortical-derived astrocytes, the array of expression profiles from the Gene Expression Omnibus (GEO; http://www.ncbi.nlm.nih.gov/geo) were sourced. The GSE42772 series contained 5 DS samples and 3 controls based on the GPL6255 platform (Helguera et al., 2013). The GSE1397 series (DS fetal cerebellum-derived astrocytes) contained 2 DS samples and 2 controls based on the GPL96 platform (Mao et al., 2005). The high throughput sequencing dataset for DS hiPSC-derived astrocyte from the Sequence Read Archive database (SRA, https://www.ncbi.nlm.nih.gov/sra)

© COPYRIGHT UPM

was retrieved. The PRJNA600245 dataset included 12 DS samples, and 12 matched isogenic controls (Ponroy Bally et al., 2020).

6.3.2 Processing of the Dataset and Identification of Differentially Expressed Genes (DEGs)

Refer to 3.3.2

6.3.3 REST-Targeted DEGs in DS-Derived Astrocytes

Refer to 3.3.3

6.3.4 Gene Ontology and Pathway Enrichment Analysis

Refer to 3.3.4

6.3.5 Production of hiPSC-Derived Astrocytes

6.3.5.1 Production of Neural Progenitor Cells (NPCs) from hiPSCs

Refer to 4.3.9

Three trisomic iPSC lines [DS2 (WC-24-02-DS-M), DS3 (UWWC1-2DS3), and DS4 (HPS4270)] and three disomic iPSC lines [C2 (WC-24-02-DS-A), C4 (ATCC-DYS0100), and C5 (HPS4272)] were utilised in this study. These lines included two pairs of isogenic cell lines (DS2 and C2; DS4 and C5) and one pair of non-isogenic cell lines (DS3 and C4). DS2, C2, and DS3 were obtained from the WiCell Research Institute at the University of Wisconsin (Giffin-Rao et al., 2020; Weick et al., 2013); C5 and DS4 were sourced from the RIKEN BioResource Center in Japan (Wakita et

© COPYRIGHT UPM

al., 2022); and C4 was acquired from the American Type Culture Collection (Wren et al., 2015). Detailed information on the cell lines is provided in Table 6.1.

Table 6.1 : Details of the Disomic Control and Trisomic DS iPSC Lines

Cell label	Cell line	Donor origin	Reprogramming method	Provider
C2 DS2	WC-24-02-DS-A WC-24-02-DS-M	• Mosaic DS individual • Female • Aged 25 • Skin fibroblast	Non-integrating episomal vector	WiCell Research Institute, University of Wisconsin
C4	ATCC-DYS0100	• Healthy individual • Male • Neonate • Skin fibroblast	Sendai viral transfection system	American Type Culture Collection (ATCC)
DS3	UWWC1-2DS3	• Trisomy 21 individual • Male • Neonate • Skin fibroblast	Non-integrating episomal vector	WiCell Research Institute, University of Wisconsin
C5 DS4	HPS4272 HPS4270	• Trisomy 21 individual • Male • Aged <10 • Skin fibroblast	Non-integrating episomal vector	RIKEN BioResource Center, Japan

6.3.5.2 Production of Astrocytes from NPCs

NPCs were cultured at a density of 60,000 cells per well in a 6-well plate coated with Geltrex. The cells were cultured in 2 mL of Neural Expansion Medium (comprising Neural Induction Medium (Gibco, USA; Cat. no. A1647801) and Advanced™ DMEM/F-12 (Gibco, USA; Cat. no. 12634)) on the first day. The Neural Expansion Medium was replaced on the second day with 2 mL of complete Astrocyte Medium (Sciencell, USA; Cat. no. 1801). The Astrocyte Medium was changed every two days for 30 days. Cells were dissociated with Accutase and seeded onto a coated plate with Getrex (Gibco, USA, Cat. no. A1413301) whenever the culture reached 100% confluency. During the first 30 days, the cell density per well was kept low to facilitate differentiation. After 30 days, the differentiated astrocytes were further expanded.

© COPYRIGHT UPM

When the cells reached 80%-90% confluency, they were collected in 1.5 mL tubes or passed onto coverslips for subsequent experiments.

6.3.6 MTT Assay

After dissociating the cells with Accutase, the cells were suspended in Neural Expansion Medium and seeded in 96-well plates at a density of 25,000 cells/cm^2. The plate was incubated at 37°C with 5% CO2 for 12 hours to allow the cells to adhere. After 12 hours, an appropriate concentration of the test compound (lithium carbonate or X5050) was added, and the cells were cultured for an additional 24 hours. Following this incubation period, the supernatant was carefully removed, and 90 µL of fresh medium was added to each well. Subsequently, 10 µL of MTT solution (Solarbio, China, Cat. no. M1020) was added, and the cells were incubated for another 4 hours. Subsequently, the supernatant was discarded, and 110 µL of Formazan solubilisation solution was introduced into each well. The plate was then placed on a shaker and gently agitated for 10 minutes to ensure complete dissolution of the formazan crystals. Absorbance was subsequently assessed at 490 nm with a microplate reader. Blank wells (containing only medium, MTT, and Formazan solubilisation solution) and control wells (containing cells, the same concentration of drug solvent, medium, MTT, and Formazan solubilisation solution) were set up, with four replicates per group.

6.3.7 Quantitative Real-Time PCR

Refer to 4.3.11.

All RT-qPCR primers are shown in Table 6.2.

© COPYRIGHT UPM

Table 6.2 : List of Primer Sequences for RT-qPCR

Gene	Forward primers (5'→3')	GC%	Reverse primers (5'→3')	GC%	Annealing temperature (℃)	Amplicon size (bp)
GFAP	CAGATTCGAGGGGGCAAA	55.56	TGAGAGGCAGGCAGCTA	58.82	60	149
EAAT1	ACATGAAGGAACAGGGGCAG	55.00	CACGGGGGCATACCACATTA	55.00	60	98
EAAT2	TGCCAACAGAGGACATCAGCCT	54.55	CAGCTCAGACTTGGAGAGGTGA	54.55	60	128
HMBS	GCCGTGCATACAGCTATGAAG	52.38	TTACGAGCAGTGATGCCTACC	52.38	60	179
IL10	GGCACCCAGTCTGAGAACAG	60.00	TGGCAACCCAGGTAACCCTTA	52.38	60	176
IL1B	GCTCTGGGATTCTCTTCAGCC	57.14	CAAGTCATCCTCATTGCCACTGT	47.83	60	118
PSMB2	GAGGGCAGTGGAACTCCTTAG	57.14	GATGTTAGGAGCCCTGTTTGG	52.38	60	149
REST	GAGAACGCCCATATAAATGTG	42.86	CACATAACTGCACTGATCAC	45.00	60	172
S100A10	CGCCGCACGTACTAAGGAA	57.89	GTGTGGTCCGTTGAAGCCTTG	57.14	60	118
S100B	GTGGCCCTCATCGACGTTTT	55.00	ACCTCCTGCTCTTTGATTTCCTCT	45.83	60	134
TNF-α	GCCCATGTTGTAGCAAACC	52.63	TCTGGTAGGAGACGGCGAT	57.89	60	226
TGF-β	TTGAGGGCTTTCGCCTTAGC	55.00	CGGTAGTGAACCCGTTGATG	55.00	60	84

F, Forward Primer; R, Reverse Primer; *GFAP*, Glial fibrillary acidic protein; *EAAT1*, Excitatory amino acid transporter 1; *EAAT2*, Excitatory amino acid transporter 2; *HMBS*, Hydroxymethylbilane synthase; *IL-1B*, Interleukin-1 beta; *IL-10*, Interleukin 10; *PSMB2*, Proteasome 20S subunit beta 2; *REST*, RE1 silencing transcription factor; *S100A10*, S100 calcium-binding protein A10; *S100B*, S100 calcium-binding protein B; *TNF-α*, Tumor necrosis factor; *TGF-β*, Transforming growth factor beta.

6.3.8 Immunocytochemistry

Refer to 4.3.10.

The primary antibodies employed for immunodetection were as follows: anti-REST (Host: Rabbit; Proteintech, USA; 1:200 dilution; Cat. no. 22242-1-AP), anti-EAAT2 (Host: Rabbit; Invitrogen, USA; 1:200 dilution; Cat. no. 711020), anti-S100A10 (Host: Rabbit; Invitrogen, USA; 1:200 dilution; Cat. no. 6F4-E6-D5-C10), and anti-S100B (Host: mouse; Santa Cruz Biotechnology, USA; 1:100 dilution; Cat. no. sc-393919). The secondary antibodies employed for immunodetection were as follows: donkey anti-rabbit IgG conjugated with Alexa Fluor 488 (Invitrogen, USA; 1:1000 dilution; Cat. no. A-21206) for REST, EAAT2 and S100A10; donkey anti-mouse IgG H&L with Alexa Fluor 594 (Abcam, USA; 1:2000 dilution; Cat. no. ab150132) for S100B.

6.3.9 Statistical Analysis

The data are presented as mean ± standard deviation (SD), with all experiments conducted in triplicate. Statistical analyses were performed using GraphPad Prism 9.0 (version 9.5.0). To compare differences between two independent experimental groups, an independent samples t-test was used. For comparisons involving three or more experimental groups, one-way ANOVA (Analysis of Variance) was employed to assess the differences between groups. A significance threshold of p-value < 0.05 was applied, and statistical significance is represented as follows: ns, not significant; *p-value < 0.05; **p-value < 0.01; ***p-value < 0.001.

© COPYRIGHT UPM

6.4 Results

6.4.1 DEGs of DS Astrocytes Derived from Different Cell Sources

To comprehensively understand the differential expression genes in DS astrocytes, a thorough search of public databases was conducted, and three RNA sequencing datasets were downloaded for analysis. In the PRJNA600245 dataset (DS hiPSC-derived astrocytes), 2,373 differentially expressed genes (DEGs) were identified. In the GSE1397 dataset (DS fetal cerebellum-derived astrocytes), 492 DEGs were identified. In the GSE42772 dataset (DS fetal cortical-derived astrocytes), 136 DEGs were identified (Figure 6.2 for heat maps and volcano plots).

© COPYRIGHT UPM

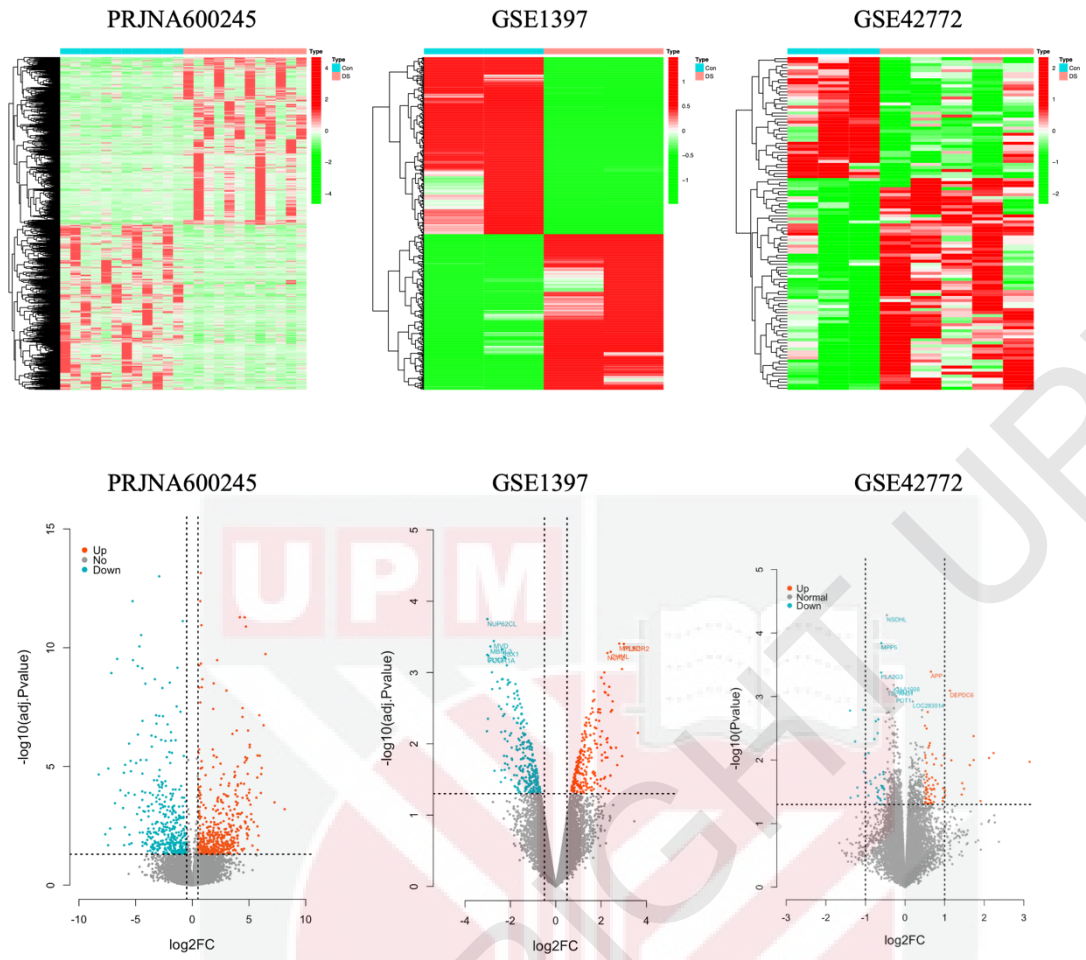


Figure 6.2 : Heat Maps and Volcano Map Visualization of Identified DEGs in DS-Derived Astrocytes. Red represents upregulated genes, while green represents downregulated genes. DS iPSC-derived astrocytes (PRJNA600245), DS fetal cerebellum-derived astrocytes (GSE1397) and DS fetal cortical-derived astrocytes (GSE42772). The top 10 DEGs with the most significant p-value are shown in Appendix D1. Red represents upregulated differentially expressed genes, green represents downregulated differentially expressed genes, and grey represents genes with no differential expression

6.4.2 REST-targeted DEGs in DS-Derived Astrocyte

The overlapping genes between REST-target genes and DEGs in DS-derived astrocytes from three datasets were comprehensively analysed and visually presented in Venn diagrams (Figure 6.3). The findings revealed a significant overlap, with 1,309 (72.77%) REST-targeted DEGs identified in DS hiPSC-derived astrocytes (representation factor, Representation factor: 1.1 and p-value < 1.069×10^{-04}), 304

© COPYRIGHT UPM

(69.81%) in DS fetal cerebellum-derived astrocytes (RF = 1.2 and p-value < 2.295×10^{-6}), 77 (70.00%) in DS fetal cortical-derived astrocytes (RF = 1.4 and p-value < 5.957×10^{-5}).

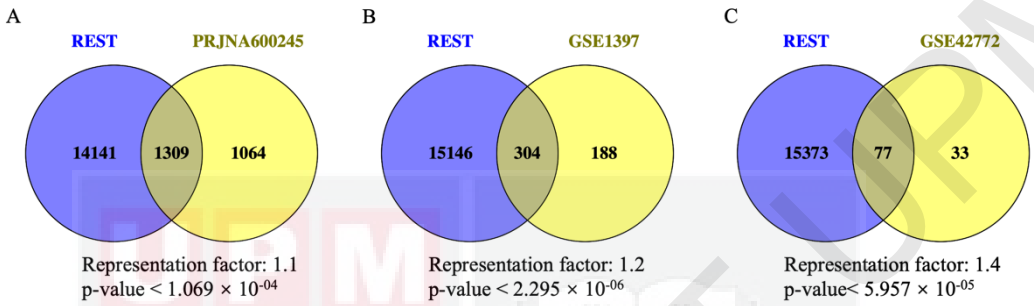


Figure 6.3 : Depiction of the Overlap between REST Target Genes and DEGs. (A) DS iPSC-derived astrocytes (PRJNA600245), (B) DS fetal cerebellum-derived astrocytes (GSE1397) and (C) DS fetal cortical-derived astrocytes (GSE42772) datasets were used. The blue circles represent REST target genes, the yellow circles represent DEGs, and the overlapping parts are REST-targeted DEGs. Fisher's test determined the statistical significance of this gene overlap, revealing all p-values < 0.01

6.4.3 REST Involved in Various Functions and Activities of Astrocytes

To further investigate the role of REST in the DS-derived astrocytes, the GO and KEGG enrichment analyses were conducted based on the REST-targeted DEGs in different tissue-derived astrocytes using the R software (Figure 6.4). The GO analysis results revealed that REST-targeted DEGs in DS hiPSC-derived astrocytes (PRJNA600245) were mainly enriched in axon development, axonogenesis, neuron projection guidance, synapse organisation and forebrain development. In addition, the KEGG pathway analysis showed enrichment for the calcium signalling pathway, neuroactive ligand-receptor interaction, cell adhesion molecules, TGF-beta signalling pathway, PI3K-Akt signalling pathway and insulin secretion. In DS fetal cerebellum-derived astrocytes (GSE1397), the GO biological processes of REST-targeted DEGs

were mainly enriched in the protection from telomere end, telomere maintenance, regulation of blood pressure, peptide hormone processing, signalling receptor ligand precursor processing, granulocyte chemotaxis and neutrophil chemotaxis. The KEGG pathway results mainly indicated the neuroactive ligand-receptor interaction, steroid hormone biosynthesis, mucin type O-glycan biosynthesis, taurine and hypotaurine metabolism, phagosome and insulin secretion. In DS fetal cortical-derived astrocytes (GSE42772), the GO biological processes of REST-targeted DEGs were mainly enriched for the sterol metabolic process, fatty acid metabolic process, cholesterol metabolic process, positive regulation of inflammatory response, extracellular matrix/structure organisation. The KEGG pathway results were mainly involved in the Cushing syndrome, aldosterone/cortisol/growth hormone synthesis and secretion, fatty acid metabolism, long-term potentiation, thyroid hormone synthesis and insulin secretion. Therefore, dysregulation of REST may lead to impaired astrocyte function.

© COPYRIGHT UPM

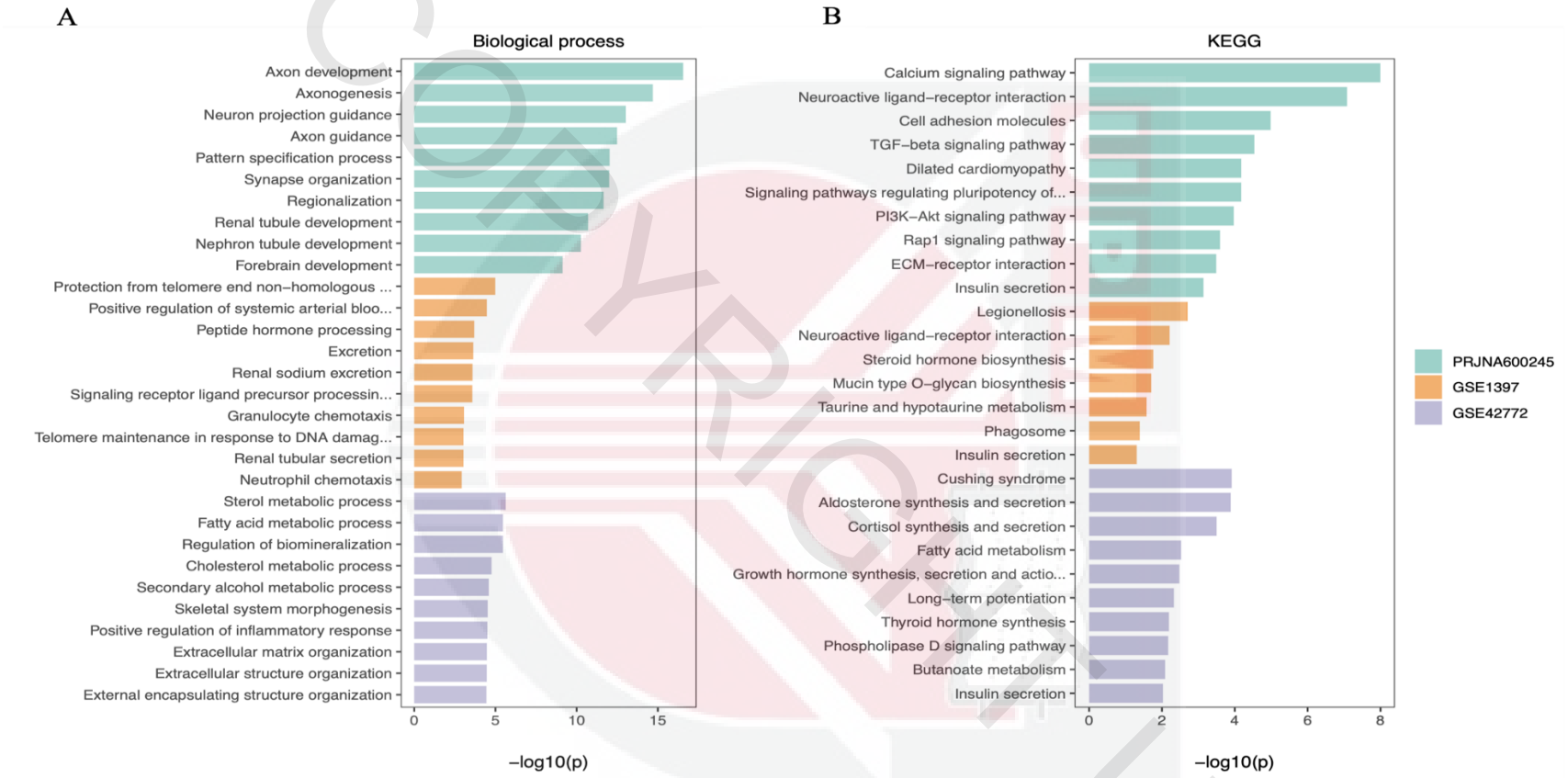


Figure 6.4 : Analysis of REST-Targeted DEGs in DS iPSC-Derived Astrocytes (PRJNA600245), DS Fetal Cerebellum-Derived Astrocytes (GSE1397) and DS Fetal Cortical-Derived Astrocytes (GSE42772). Different colours indicate DS iPSC-derived astrocytes, DS fetal cerebellum-derived astrocytes and DS fetal cortical-derived astrocytes, respectively. The top 10 biological processes (A) and KEGG pathways (B) for each region are shown

© COPYRIGHT UPM

6.4.4 REST Lost in DS-Derived Astrocytes Restored by Lithium Treatment

To investigate REST expression levels in astrocytes, the hiPSCs were differentiated into astrocytes (Figure 6.5). Subsequent immunocytochemical analysis verified the presence of the astrocyte marker S100B in these cells.

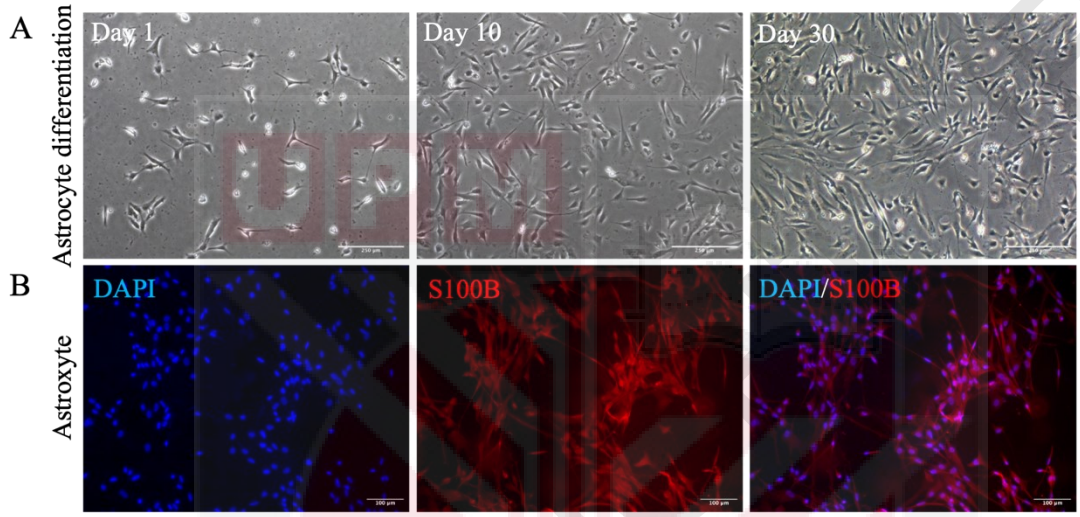


Figure 6.5 : Astrocyte Differentiation and Identification of Cellular Characteristics. (A) Bright-field microscopy images of astrocytes at day 1, day 7, and day 30 during differentiation (scale bar = 250µm). (B) After 30 days, the cultured cells were identified by immunocytochemical staining with the astrocyte marker S100B. All cells were positive for S100B expression (scale bar =100µm) (Appendix D2)

The differential REST expression levels in DS hiPSC-derived astrocytes and controls were examined (Figure 6.6 A). It was found that *REST* mRNA levels in DS hiPSC-derived astrocytes (DS group) were downregulated by 1.6-fold compared to the control group, but not statistically significant. As a nuclear transcription factor, the protein level of REST in the nucleus is crucial. Immunocytochemical analysis demonstrated a significant decrease (p-value < 0.0001) in nuclear REST protein levels in DS hiPSC-derived astrocytes relative to the control group. This finding suggests

that the diminished presence of nuclear REST protein could play a crucial role in the observed dysfunction of DS hiPSC-derived astrocytes (Figure 6.6 D, E).

To further explore the effects of REST loss and its restoration in DS hiPSC-derived astrocytes, these cells were treated with lithium carbonate to restore nuclear REST protein levels. An MTT assay was employed to assess the impact of different concentrations of lithium carbonate on the viability of DS hiPSC-derived astrocytes over 24 hours. The results indicated that treatment with 5 mM lithium carbonate yielded the best relative viability for DS hiPSC-derived astrocytes, at 122.5% (Figure 6.6 B). After 24-hour treatment with 5 mM lithium carbonate (DS+Li group) in 6-well plate with 50% cell confluence, *REST* mRNA levels in DS hiPSC-derived astrocytes were significantly upregulated (p-value < 0.05) by 3.3-fold compared to untreated DS-derived astrocytes (DS group) (Figure 6.6 A). Immunocytochemistry analysis revealed a significant increase (p-value < 0.0001) in nuclear REST protein levels in the DS+Li group compared to the DS group (Figure 6.6 D, E).

Additionally, we assessed the impact of 24-hour treatment with X5050, a compound that degrades REST protein, on the viability of astrocytes. The results showed that 100µM was the optimal concentration for X5050 treatment of DS hiPSC-derived astrocytes for 24 hours (Figure 6.6 C). Following a 24-hour exposure to 100µM X5050 in control astrocytes (Con+X5050) in 6-well plate with 50% cell confluence, *REST* mRNA expression levels remained unchanged and did not exhibit statistically significant differences relative to the control group. However, immunocytochemistry results indicated a significant reduction (p-value < 0.0001) in nuclear REST protein levels in Con+X5050 astrocytes compared to the control group astrocytes.

© COPYRIGHT UPM

Furthermore, when DS-derived astrocytes were treated with 5 mM lithium carbonate and 100μM X5050 (DS+Li+X5050 group) for 24 hours, X5050 counteracted the lithium-induced upregulation of nuclear REST protein (Figure 6.6 D, E).

© COPYRIGHT UPM

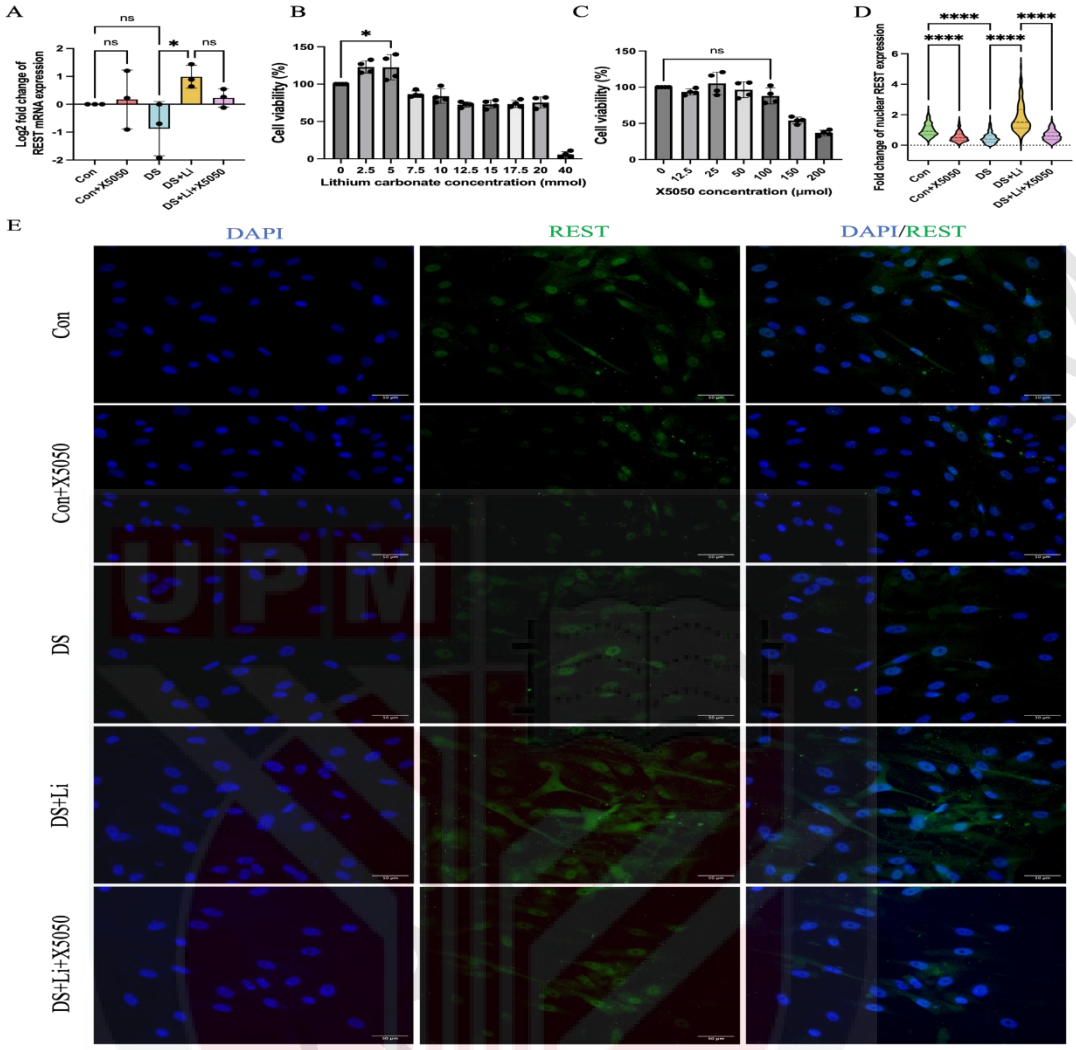


Figure 6.6 : The Detection of REST mRNA and Protein in Treated and Untreated DS hiPSC-Derived Astrocytes and Controls. Three pairs of cell lines (C1 vs. DS1, C2 vs. DS2, and C5 vs. DS4) were used to perform ICC (n=3). (A) The mRNA expression levels of REST in different groups: Con group (Control; Disomic astrocytes), Con+X5050 group (Disomic astrocytes with X5050 treatment), DS+Li group (Trisomic astrocytes with lithium carbonate treatment), DS+Li+X5050 (Trisomic astrocytes treated with both lithium carbonate and X5050). The mRNA expression levels were normalized to two reference genes (*HMBS* and *PSMB2*), and the relative mRNA expression levels for each group were calculated. The relative expression levels of each group were normalized to those of the Con group to obtain $\log_2$ fold changes for statistical analyses. (B) Optimisation of safety dosage of lithium treatment in iPSC-derived astrocytes through MTT cell viability assay. Treatment with lithium carbonate up to 5mM for 24 hours is considered safe for astrocytes in which the cell viability does not drop below 100%. (C) Optimising safe doses of lithium for iPSC-derived astrocytes via MTT cell viability assay. Cell viability treated with 100μM X5050 for 24 hours was not statistically significant compared to the control and was considered safe. (D, E) Fluorescence micrographs of REST staining and statistical analysis of nuclear REST. The one-way ANOVA was employed to assess the differences between groups. ns, not significant; *p-value < 0.05; **p-value < 0.01; ***p-value < 0.001, ****p-value< 0.0001

6.4.5 Restoration of REST Downregulated the REST-Targeted Inflammatory Genes

Neuroinflammation spans the entire lifespan of individuals with DS, presenting different patterns at various life stages. To explore the impact of REST loss on astrocyte inflammatory factor levels, the mRNA expression levels of *TGF-β*, *TNF-α*, *IL-1B*, and *IL-10* were quantified (Figure 6.7). Notably, *TGF-β* and *IL-10* expression in DS-derived astrocytes (DS group) exhibited significant upregulation (p-value < 0.05) compared to controls (Con group), with increases of 2.4-fold and 2.8-fold, respectively. While *TNFα* and *IL-1B* expression levels did not show significant differences compared to the controls (p-value > 0.05), *TNF-α* was upregulated by 4.1-fold, and *IL-1B* was downregulated by 2.0-fold.

To confirm that these changes in inflammatory factor levels were due to the loss of nuclear REST in DS-derived astrocytes, control group astrocytes treated with X5050 (Con+X5050 group) were examined. The results indicated that, compared to untreated control astrocytes, X5050-treated astrocytes showed significant differences (p-value < 0.001) in the expression levels of *TGF-β* and *IL-10*, with *TNF-α* and *IL-1B* expression levels remaining no significant (p-value > 0.05) (upregulated by 8.5-fold and 2.3-fold, respectively) (Figure 6.7). However, the expression trends of these inflammatory factors in X5050-treated astrocytes mirrored those observed in DS-derived astrocytes. These findings suggest that REST loss leads to dysregulation of inflammatory levels in DS-derived astrocytes.

Additionally, the alterations were examined in inflammatory factor expression following the restoration of REST levels in DS-derived astrocytes through lithium

© COPYRIGHT UPM

carbonate treatment lithium carbonate treatment. Compared to DS group astrocytes, the DS+Li group showed significant downregulation in the mRNA expression levels of *TGF-β* (p-value < 0.01), *TNF-α* (p-value < 0.01), and *IL-10* (p-value < 0.001), except for *IL-1B* (Figure 6.7). Interestingly, in the DS+Li+X5050 group, *TGF-β* (p-value < 0.001), *TNF-α* (p-value < 0.001), and *IL-10* (p-value < 0.05)expression levels were significantly increased compared to those in the DS+Li group (Figure 6.7). This indicates that the X5050 treatment counteracted the effects of lithium treatment on DS-derived astrocytes. The expression level of *IL-1B* is inconsistent with the changes in REST level, which may be because the different concentrations of REST in cells have different inhibitory effects on genes. The results demonstrate that restoring REST can rescue the upregulation of REST target inflammatory genes in DS-derived astrocytes.

© COPYRIGHT UPM

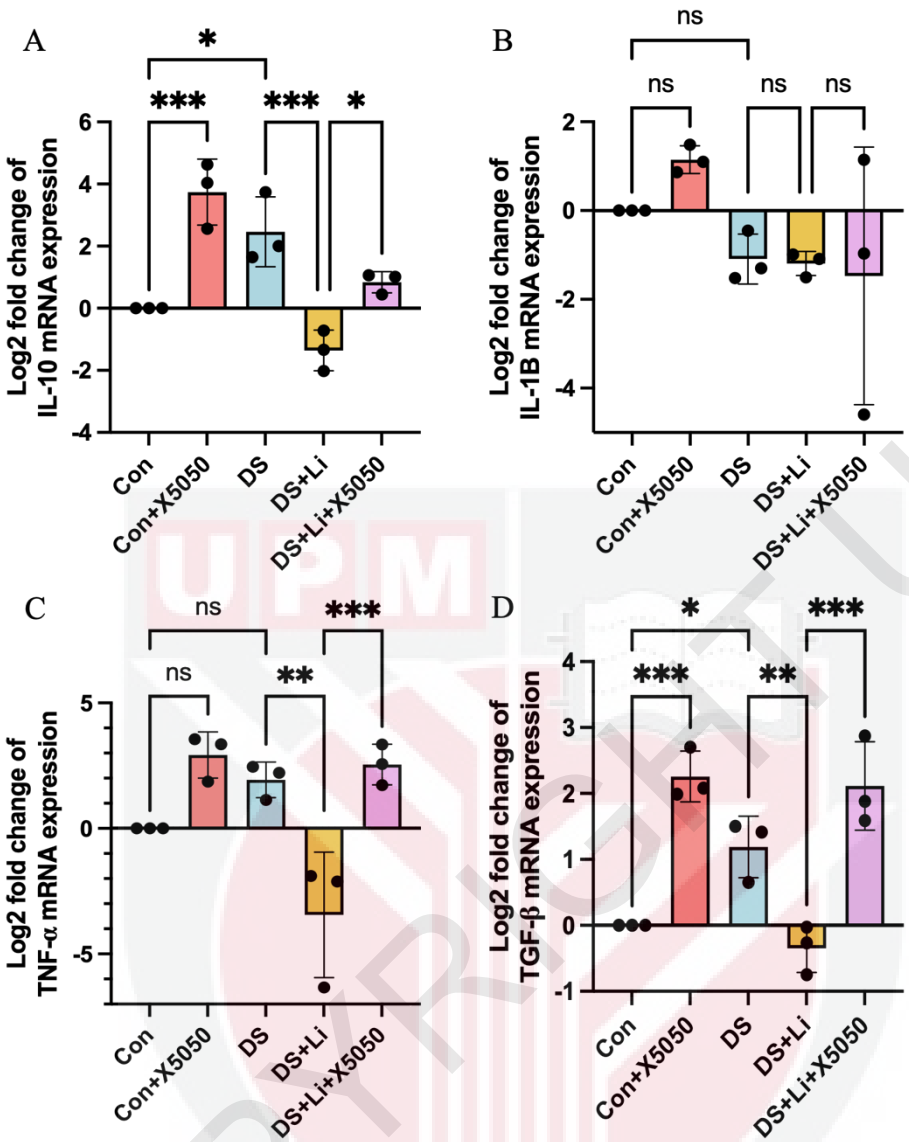


Figure 6.7 : The Detection of Inflammation Factors in Treated and Untreated DS hiPSC-Derived Astrocytes and Controls. Three pairs of cell lines (C1 vs. DS1, C2 vs. DS2, and C5 vs. DS4) were used to perform RT-qPCR (n=3). The mRNA expression levels of inflammatory cytokines *IL-10* (A), *IL-1B* (B), *TNF-α* (C), and *TGF-β* (D) were analysed across different groups: Con group (Disomic astrocytes), Con+X5050 group (Disomic astrocytes with X5050 treatment), DS+Li group (Trisomic astrocytes with lithium carbonate treatment for 24h), DS+Li+X5050 (Trisomic astrocytes with both lithium carbonate and X5050 treatment for 24h). The mRNA expression levels were normalized to two reference genes (*HMBS* and *PSMB2*), and the relative mRNA expression levels for each group were calculated. The relative expression levels of each group were normalized to those of the Con group to obtain $\log_2$ fold changes for statistical analyses. The one-way ANOVA was employed to assess the differences between groups. ns, not significant; *p-value < 0.05; **p-value < 0.01; ***p-value < 0.001

© COPYRIGHT UPM

6.4.6 Restoration of REST Suppresses the Expression of Reactive Astrocyte Cell Makers

In response to inflammatory mediators, astrocytes can be activated from a resting state, transforming into reactive astrocytes characterised by increased expression of inflammatory factors. To explore the relationship between the loss of nuclear REST in astrocytes and reactive astrocytes, we examined the mRNA expression levels of reactive astrocyte markers *EAAT1*, *EAAT2*, *GFAP*, *S100A10*, and *S100B* (Figure 6.8). Astrocytes derived from DS exhibited a significant upregulation in mRNA expression of *GFAP* (p-value < 0.05) and *S100B* (p-value < 0.001) compared to controls. While the mRNA expression levels of *EAAT1*, *EAAT2*, and *S100A10* were not statistically significant differences (p-value > 0.05), *EAAT2* and *S100A10* were increased by 6.3-fold and 1.53-fold, respectively, whereas *EAAT1* was reduced by 2.9-fold. Immunocytochemistry further validated that EAAT2, S100B, and S100A10 protein levels were significantly upregulated in DS-derived astrocytes compared with Con group (p-value < 0.0001), indicating dysregulation of reactive astrocyte markers in DS (Figure 6.9).

© COPYRIGHT UPM

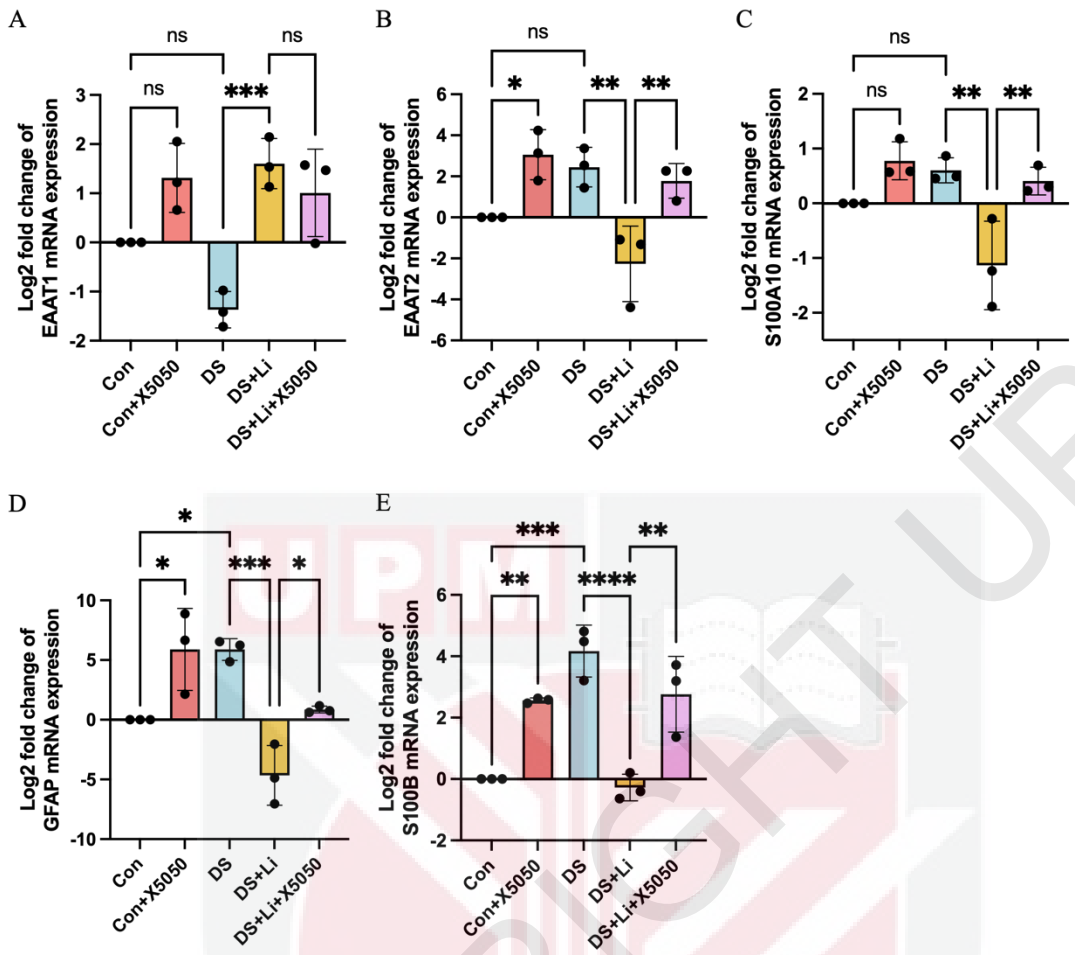


Figure 6.8 : The mRNA Expression of Reactive Astrocyte Cell Markers in Treated and Untreated DS hiPSC-Derived Astrocytes and Controls. Three pairs of cell lines (C1 vs. DS1, C2 vs. DS2, and C5 vs. DS4) were used to perform RT-qPCR (n=3). The mRNA expression levels of reactive astrocyte cell markers *EAAT1* (A), *EAAT2* (B), *GFAP* (C), *S100A10* (D) and *S100B* (E) were analysed across different groups: Con group (Control; Disomic astrocytes), Con+X5050 group (Disomic astrocytes with X5050 treatment), DS+Li group (Trisomic astrocytes with lithium carbonate treatment), DS+Li+X5050 (Trisomic astrocytes with both lithium carbonate and X5050 treatment). The mRNA expression levels were normalized to two reference genes (*HMBS* and *PSMB2*), and the relative mRNA expression levels for each group were calculated. The relative expression levels of each group were normalized to those of the Con group to obtain $\log_2$ fold changes for statistical analyses. The resulting values were then log-transformed (base 2) for standardisation, and the results were analyzed statistically. The one-way ANOVA was employed to assess the differences between groups. ns, not significant; *p-value< 0.05; **p-value< 0.01; ***p-value< 0.001, ****p-value< 0.0001

To further investigate the contribution of REST to the dysregulation of reactive astrocyte markers in DS-derived astrocytes, the control astrocytes were treated with

X5050 (Con+X5050 group) to reduce REST protein levels and subsequently analysed the expression of these markers (Figure 6.9). The results showed that, compared to the control group, the Con+X5050 group exhibited significant upregulation in the mRNA expression of *EAAT2* (p-value< 0.05), *GFAP* (p-value< 0.05), and *S100B* (p-value< 0.01). In the Con+X5050 group, the expression levels of *EAAT1* and *S100A10* were elevated by 2.7-fold and 1.7-fold, respectively, relative to the control group. Immunocytochemical analysis further demonstrated significant increases in the protein levels of EAAT2, S100B, and S100A10 in the Con+X5050 group compared with Con group (p-value < 0.0001). These results support the conclusion that REST loss contributes to the upregulation of reactive astrocyte markers in DS-derived cells (Figure 6.9).

Additionally, we examined how the expression of reactive astrocyte markers was altered following the restoration of REST expression levels in DS-derived astrocytes through lithium carbonate treatment (Figure 6.9). The results showed that, after REST upregulation, the DS+Li group astrocytes exhibited significant downregulation in the mRNA expression levels of *EAAT2* (p-value< 0.01), *GFAP* (p-value< 0.001), *S100A10* (p-value< 0.01), and *S100B* (p-value< 0.0001) compared to the DS group. To further validate that these changes were due to the upregulation of REST, we treated DS-derived astrocytes with both lithium carbonate and X5050 (DS+Li+X5050 group). The results revealed that, compared to the DS+Li group, the DS+Li+X5050 group showed significant upregulation in the mRNA expression levels of *EAAT2* (p-value< 0.01), *GFAP* (p-value< 0.05), *S100A10* (p-value< 0.01), and *S100B* (p-value< 0.01). Interestingly, it was observed that *EAAT1* expression was elevated in the DS+Li group relative to the DS group. This could be because *EAAT1* is not a REST

© COPYRIGHT UPM

target gene and is thus unaffected by changes in REST levels. Moreover, the immunocytochemical analysis validated a significant decrease in the protein expression of EAAT2 (p-value< 0.0001), S100A10 (p-value< 0.0001), and S100B (p-value< 0.0001) in astrocytes from the DS+Li group compared with those from the DS group. Conversely, the DS+Li+X5050 group demonstrated a significant increase in the protein levels of EAAT2 (p-value< 0.001), S100A10 (p-value< 0.0001), and S100B (p-value< 0.0001) compared with DS+Li group (Figure 6.9). These findings indicate that restoring REST can rescue the upregulation of REST-targeted reactive astrocyte markers in DS.

© COPYRIGHT UPM

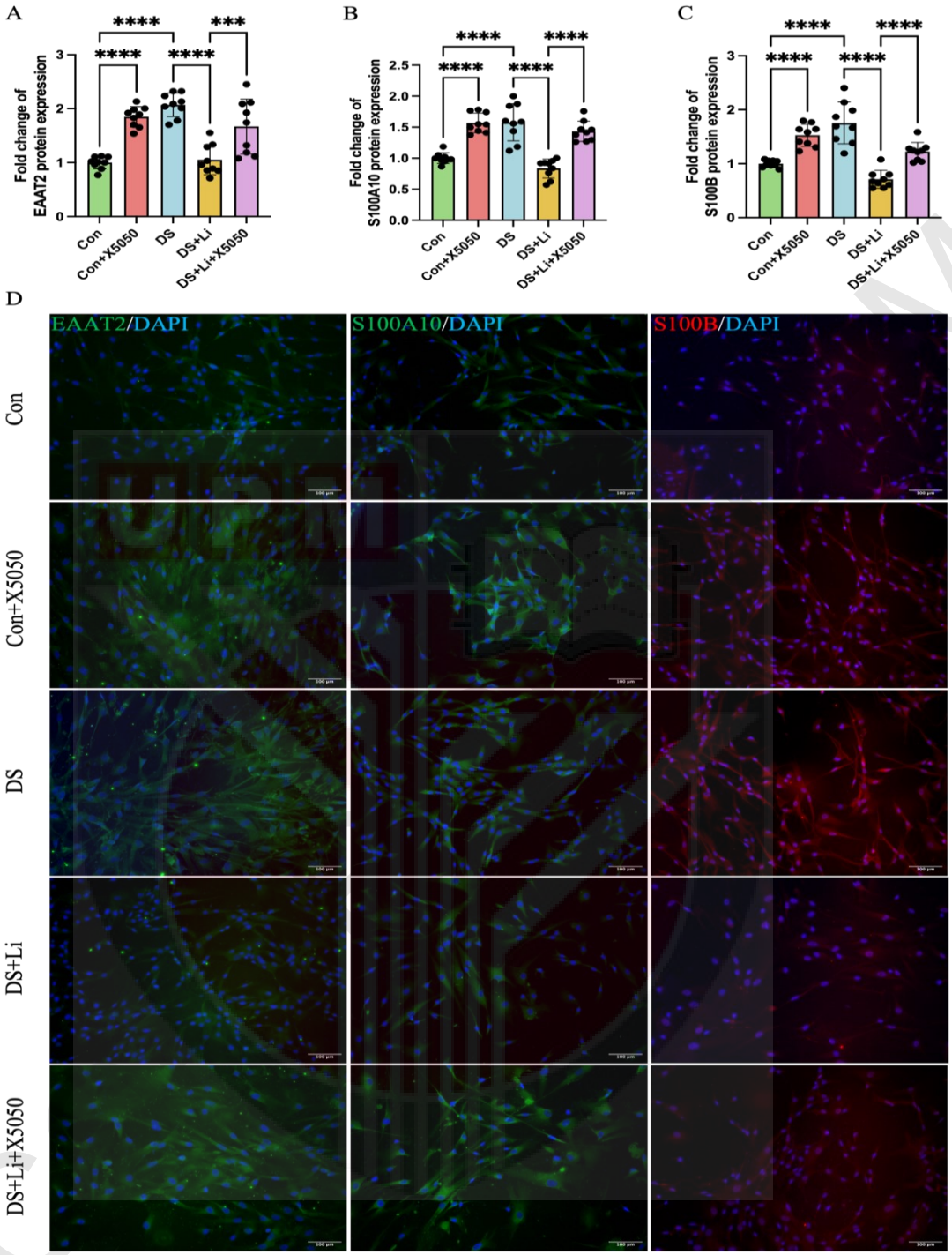


Figure 6.9 : Immunocytochemical Detection of DS hiPSC-Derived Reactive Astrocyte Markers. Three pairs of cell lines (C1 vs. DS1, C2 vs. DS2, and C5 vs. DS4) were used to perform ICC (n=3). Fluorescence micrographs of EAAT2, S100A10 and S100B staining and statistical analysis across different groups: Con group (Disomic astrocytes), Con+X5050 group (Disomic astrocytes with X5050 treatment), DS+Li group (Trisomic astrocytes with lithium carbonate treatment), DS+Li+X5050 (Trisomic astrocytes with both lithium carbonate and X5050 treatment).The one-way ANOVA was employed to assess the differences between groups. ns, not significant; *p-value< 0.05; **p-value< 0.01; ***p-value < 0.001, ****p-value< 0.0001

6.5 Discussion

Reactive astrocytes are a prominent feature of neuropathological processes. Upon activation, astrocytes exhibit altered functions, including neurotrophic support, neurotransmitter regulation, energy metabolism, maintenance of the blood-brain barrier, lipid metabolism, and phagocytosis, which can either be enhanced or impaired. An increased number of astrocytes in the DS individuals is a central issue in DS neuropathology. The maturation and morphogenesis of DS-derived astrocytes are impaired, leading to functional abnormalities. These findings confirm the presence of reactive astrocytes in DS. The loss of REST results in upregulating REST-targeted inflammatory genes and reactive astrocyte marker genes in DS-derived astrocytes. However, upon restoring REST in these astrocytes, the expression of these genes is suppressed. Thus, the loss of nuclear REST protein may be a critical factor in astrocyte astrocyte reactivity in DS.

REST, as a significant transcriptional repressor, regulates the numerous biological processes and signalling pathways associated with the functions of neural progenitor cells, neurons, and astrocytes (Huang et al., 2023). Its dysregulation is a key mechanism in many neurological disorders. Our transcriptomic analysis revealed many REST-regulated DEGs in DS astrocytes (hiPSC-derived astrocytes, cerebellar-derived astrocytes, and cortical-derived astrocytes). These REST-targeted DEGs are involved in various biological processes and pathways crucial for astrocyte function, including axon development, synapse organisation, neuron projection, extracellular matrix organisation, regulation of stem cell pluripotency, inflammatory response, fatty acid synthesis and metabolism, TGF-β signalling pathway, and PI3K-Akt signalling pathway. REST has been shown to regulate a set of genes and signalling pathways

© COPYRIGHT UPM

related to astrocyte development and function, including cell proliferation (Conti et al., 2012), differentiation (Notch, JAK-STAT, BMP) (Kohyama et al., 2010; Lee et al., 2016), inflammation [nuclear factor-κB (NF-κB), MAPK, and cyclooxygenase-2 (COX-2)] (Li et al., 2017; Repovic et al., 2003; Saijo et al., 2009), neurotrophic tyrosine kinase receptor 3 (TrkC) (Andrés et al., 1999), glutamate uptake (Pajarillo et al., 2021), synapse formation and remodelling (Hwang and Zukin, 2018), and oxidative stress response (Pajarillo et al., 2021). Interestingly, this study indicates the loss of nuclear REST in DS astrocytes. When co-cultured with rodent neurons, human DS astrocytes secrete fewer synaptogenic factors, leading to dendritic spine morphology abnormalities and reduced synapses (Christopherson et al., 2005; Garcia et al., 2010). Dysregulation of intracellular GABA and extracellular glutamate concentrations in DS astrocytes results in excitatory/inhibitory defects at the cellular and circuit levels in the developing brain (Pajarillo et al., 2021; Ponroy and Murai, 2021). Mitochondrial impairment and elevated oxidative stress in astrocytes associated with DS play a significant role in the neuronal cell death observed in the Down syndrome brain (Chen et al., 2014). Therefore, the loss of REST may be a key factor underlying these functional impairments in DS astrocytes.

Chromosome 21 houses 20 triplicated genes related to neuroinflammatory responses, including 4 genes (*IFNAR1*, *IFNAR2*, *IFNGR2*, and *IL10RB*) encoding interferon receptors, which trigger a cascade of inflammatory signals in individuals with DS (Ahmed et al., 2021; Powers et al., 2019). The expression patterns of inflammatory factors in DS individuals vary across different life stages. Many inflammation-related molecules and signalling pathways are REST targets, with their expression regulated by REST (Abrajano et al., 2009; Kong et al., 2016). In this study, the loss of REST in

© COPYRIGHT UPM

DS astrocytes was a key factor in the elevated *IL-10*, *TNFα*, and *TGF-β* expression levels. This upregulation was further confirmed in control astrocytes treated with X5050. Interestingly, we found that the expression of *IL-1B* was downregulated in DS-derived astrocytes. However, in this study, we observed that in control astrocytes treated with X5050 (which degrades REST protein), *IL-1B* was upregulated by 2.2-fold compared to the control group. Conversely, in DS-derived astrocytes treated with lithium carbonate (which upregulates REST), *IL-1B* was downregulated by 2.3-fold compared to the control group. In PD-derived astrocytes, it was observed that knockout of REST led to the upregulation of *IL-1B*, *IL-10*, and *TNF-α*, which supports our findings (Li et al., 2020). A study suggested that IL-1B can mediate rapid transcription and translation of REST, with both REST and REST4 being downstream participants in IL-1B signalling (Buffolo et al., 2021). This may explain the simultaneous downregulation of *IL-1B* and REST in DS-derived astrocytes in this study. During nuclear transfer-mediated reprogramming of porcine oocytes, the transfer of cytoplasmic REST to the donor nucleus is essential for successful reprogramming by inhibiting the TGF-β pathway. REST deficiency during this process leads to upregulation of TGF-β pathway-related genes, including *TGF-β*, *ACVR2A*, *ACVR2B*, *Smad2*, and *Smad3* (Kong et al., 2016). Notably, *IL-1B* and *TNF-α* are recognised pro-inflammatory cytokines, whereas *IL-10* and *TGF-β* serve as anti-inflammatory agents. Therefore, the loss of REST in DS-derived astrocytes results in upregulating REST-targeted inflammatory genes.

The overexpression of inflammatory cytokines indicates that astrocytes are potentially activated and in an inflammatory state. Reactive astrocytes respond to functional abnormalities and/or environmental stimuli (Ding et al., 2021). This study confirms

© COPYRIGHT UPM

that the markers for reactive astrocytes—*EAAT2*, *GFAP*, and *S100B*—are significantly upregulated when REST is downregulated (DS-derived group and Con+X5050 group) compared to controls. Additionally, S100A10 expression showed an upward trend when REST was downregulated. The upregulation of *GFAP* and *S100B* and excessive pro-inflammatory responses and oxidative stress indicate a neurotoxic reactive astrocyte phenotype (Escartin et al., 2021; Liddelow and Barres, 2017). S100B is a key marker of reactive astrocytes, signifying an inflammatory state and potentially inducing microglial activation (Villarreal et al., 2014). GFAP, a significant component of astrocyte intermediate filaments, signifies cytoskeletal reorganisation and astrocyte dysfunction (Escartin et al., 2021). Conversely, the upregulation of EAAT2 and S100A10 and the activation of anti-inflammatory responses characterise a neuroprotective reactive astrocyte phenotype (Escartin et al., 2021; Liddelow and Barres, 2017). EAAT1 and EAAT2, considered protective markers, prevent synaptic glutamate overflow and minimise overactivation of extrasynaptic receptors, protecting against excitotoxicity (Price et al., 2021). Notably, our study found no significant correlation between *EAAT1* expression in DS-derived astrocytes and REST levels, consistent with findings by Pajarillo and colleagues in PD-derived astrocytes, which showed that REST does not influence *EAAT1* transcription (Pajarillo et al., 2021). The coexistence of neurotoxic and neuroprotective reactive astrocytes aligns with our previous findings of activated pro-inflammatory and anti-inflammatory responses in DS-derived astrocytes. This dual role of reactive astrocytes in DS highlights their complex functions. Interestingly, REST levels restored in DS-derived astrocytes via lithium treatment downregulated these reactive astrocyte markers, indicating that REST loss is a key factor in astrocyte

© COPYRIGHT UPM

reactivity in DS. Therefore, targeting REST may be a promising therapeutic strategy for DS.

6.6 Conclusions

This study underscores the critical role of REST in regulating astrocyte function and reactivity in Down syndrome. The loss of REST in DS-derived astrocytes leads to significant dysregulation of inflammatory responses and the upregulation of reactive astrocyte markers, affecting the homeostasis of the central nervous system. These findings suggest that REST deficiency contributes to both neurotoxic and neuroprotective astrocyte phenotypes, reflecting the dual nature of reactive astrocytes in DS. The restoration of REST levels appears to mitigate these effects, highlighting the potential of REST as a therapeutic target for managing astrocyte-related neuropathology in DS. Meanwhile the in vivo model provides valuable insights, it may not fully capture the complexity of astrocyte behaviour in the DS brain environment. Future research should explore the mechanisms underlying REST-mediated regulation of astrocyte functions and its impact on neuronal networks in more detail.

© COPYRIGHT UPM

CHAPTER 7

GENERAL DISCUSSION AND CONCLUSION

7.1 General Discussion

The molecular mechanisms and gene regulatory networks involved in the complex neuropathological phenotype of Down syndrome (DS) have long been a focus of interest for neuroscientists. The neuropathology core of DS is the reduction in neurogenesis accompanied by increased astrogenesis, a neurodevelopmental defect known as neurogenic-to-gliogenic shift (Lee et al., 2016). REST, a crucial transcription factor, binds to specific DNA sequences to repress gene transcription. It is known that REST targets over 2,000 neuronal genes (McGann et al., 2021) and more than 4,000 glial-specific genes (Abrajano et al., 2009), all of which are involved in NPC differentiation, neurogenesis, gliogenesis, and various regulatory processes of the homeostasis of nervous system. Significantly, a reduction in REST expression has been detected in the brains of fetuses with DS (Bahn et al., 2002). Dysregulation of REST is associated with various neurological disorders, and its disruption may interfere with the transcription of its target genes, leading to neurodevelopmental deficits. However, the role of REST and its target genes in the brains and neural cells of individuals with DS has not yet been fully elucidated.

A major challenge in advancing research on the neuropathology of trisomy 21 (HSA21) has been the scarcity of brain samples from individuals with DS. Although transgenic cell and mouse models carrying the Down syndrome critical region (DSCR) genes offer significant research advantages, they have inherent limitations in replicating human neurodevelopmental diseases (Belichenko et al., 2009). The DS phenotype

© COPYRIGHT UPM

cannot be solely attributed to the DSCR; instead, the widespread transcriptional misregulation and disruptions in proteostasis arising from the extra copy of HSA2 are major contributors to the complex manifestations of DS (Krivega et al., 2022). Fortunately, the advent of human induced pluripotent stem cells (hiPSCs) derived from individuals with DS, 2D neural cell models and 3D cerebral organoids have more accurately replicated the genomic phenotype and provided a more reliable understanding of DS neuropathological mechanisms (Centeno et al., 2018; Paşca et al., 2015).

Additionally, advancements in transcriptomic technologies, including array and high-throughput sequencing, have significantly enhanced research into the genetic phenotypes associated with DS. To date, this study is the first to utilise transcriptomic sequencing data from DS-derived human brain tissue and neural cells, as well as 2D and 3D models derived from DS hiPSCs, to assess the role of REST and its target genes in DS neuropathological mechanisms. This study aimed to comprehensively elucidate the expression levels of REST and its regulatory roles in the DS neurophenotype, including gene regulatory networks, signalling pathways, and candidate REST-targeted hub differentially expressed genes (DEGs), to identify the disrupted molecular mechanisms leading to neurogenic defects and increased astrogliogenesis. Furthermore, in light of the observed increase in astrogliogenesis, the impact of changes in REST expression levels on the reactivity of DS astrocytes was assessed. These findings provided foundational insights into the role of REST in regulating the DS neurogenetic phenotype and supported future DS research and therapeutic approaches.

© COPYRIGHT UPM

This study confirms that REST is a key regulatory factor in the neurophenotype of DS through DS human brain tissue transcriptomic analysis. The role of REST and its target genes were identified by analysing RNA sequencing data from eight different brain regions and across four distinct developmental stages in individuals with DS. Across all brain regions, 51 REST-targeted DEGs were identified, with 41 showing consistent upregulation. Additionally, 56 REST-targeted DEGs were found to be consistently expressed across all developmental stages of the DS brain, with 39 genes being upregulated. Enrichment analysis indicated that these REST-targeted DEGs were implicated in pathways associated with energy metabolism, neuroinflammation, neurodevelopment, neurogenesis, gliogenesis, the JAK-STAT signalling cascade, and the HIF-1 signalling pathway. The JAK-STAT pathway plays a crucial role in the proliferation and migration of neural stem/progenitor cells, cell differentiation, fate determination, neurogenesis, gliogenesis, and neuroinflammation (Chen et al., 2021; Gutiérrez and Soto, 2020; Todd et al., 2016). Throughout brain development, the JAK-STAT signalling pathway plays a pivotal role in directing NPCs towards glial cell differentiation, thereby influencing glial fate (Nicolas et al., 2013). The phosphorylation of JAK1 and JAK2 initiates STAT3 activation, which subsequently drives the transcription of genes specific to astrocytes, including S100B and GFAP (Hong and Song, 2014; Nicolas et al., 2013). This study underscored that the involvement of REST and its target genes in modulating the JAK-STAT pathway is essential for NPC function and astrogliogenesis. REST dysregulation may contribute to the upregulation of REST-targeted DEGs, including those related to the JAK-STAT pathway, in Down syndrome brains, potentially underlying neurogenic deficits and enhanced gliogenesis seen in the condition.

© COPYRIGHT UPM

This study confirms that there is a loss of nuclear REST and downregulation of the neuroblast marker DCX, alongside an upregulation of the glioblast marker NFIA in DS-derived NPCs. A deep analysis of transcriptomic sequencing data from DS-derived NPCs revealed that biological processes and signalling pathways related to neurogenesis and neuron development, such as the Wnt signalling pathway, cell fate commitment, central nervous system neuron differentiation, neuron fate commitment, and regulation of neurogenesis, were downregulated in DS NPCs. Interestingly, processes and pathways associated with gliogenesis, including the regulation of gliogenesis and the JAK-STAT signalling pathway, were upregulated in DS. It hypothesises that the impairment in REST nuclear translocation contributes to the neurogenic-to-gliogenic shift observed in DS NPCs. The abundance of nuclear REST protein determines the differentiation outcomes of NPCs, guiding them toward either neuronal or astrocytic fates (Baldelli and Meldolesi, 2015; Pajarillo et al., 2021). The loss of REST not only results in the de-repression and increased expression of neuronal genes but also leads to the de-repression of glial-specific REST target genes (Abrajano et al., 2009; Alsaqati et al., 2022; Liu et al., 2019). This indicates the complex role of REST downregulation in regulating NPC fate determination. The upregulation of JAK2 and STAT3 mRNA in DS hiPSC-derived NPCs further confirms the bias towards glial differentiation in these cells. Additionally, the study validated the upregulation of REST-targeted hub DEGs—*CD44*, *TGFB1*, *FN1*, *ITGB1*, and *COL1A1*—in DS hiPSC-derived NPCs. These genes are closely linked to processes involved in neurogenesis and gliogenesis. For example, *CD44* promotes astrocyte formation (Liu et al., 2004), *TGF-β1* drives the switch from neurogenesis to gliogenesis (Stipursky et al., 2014), and *FN1* (Song et al., 2021), *ITGB1* (Chang et al., 2021), and *COL1A1* (Hayashi et al., 2014) are involved in cell adhesion, migration

© COPYRIGHT UPM

and signalling pathways that regulate NPC differentiation. In conclusion, this study made significant contributions to understanding the neuropathological mechanisms of DS by identifying the loss of nuclear REST and the dysregulation of its target genes in DS-derived NPCs.

This study confirmed that *REST* mRNA is downregulated in DS hiPSC-derived cerebral organoids and that REST plays a crucial role in nearly every stage of neurodevelopment in DS. By analysing extensive transcriptomic data from DS hiPSC-derived cerebral organoids at five different time points (Day 30, Day 35, Day 56, Day 90, Day 160), the results showed that REST-targeted DEGs were involved in various processes, including chromosome segregation, cell cycle regulation, DNA replication and transcription, cell metabolism, neuronal differentiation and maturation, synaptic remodelling and signalling, glial cell differentiation and maturation, neuronal apoptosis, and neuroimmune regulation in DS cerebral organoids. The results indicated that decreased REST expression may contribute to a reduced neuronal population in the early development of DS cerebral organoids, whereas the later stages are marked by an elevated presence of glial cells. REST knockdown accelerates the differentiation of NSCs into neurons, initially increasing the proportion of immature neurons but subsequently resulting in a diminished total neuronal population. This reduction is due to the failure to maintain the NSC pool, leading to diminished neurogenic potential and neuronal apoptosis triggered by REST insufficiency (Alsaqati et al., 2022; Gao et al., 2011; Singh et al., 2008). When REST expression reaches 50% (only one REST allele) of wild-type levels, NSCs/NPCs lose their self-renewal capacity, reducing the final number of neurons despite the temporary increase in premature differentiation (Sun et al., 2008). Therefore, neurogenesis critically

© COPYRIGHT UPM

depends on maintaining appropriate REST levels in NSCs/NPCs. In vivo studies using mouse embryonic stem cell models have shown that REST knockdown reduces the number of neurons without significantly affecting astrocyte differentiation or numbers (Gao et al., 2011). The loss of REST in DS cerebral organoids may result in the upregulation of glia-specific REST target genes, leading to increased gliogenesis, particularly astrogenesis. Moreover, in Day 90 DS cerebral organoids, it was observed that a significant upregulation of gliogenesis-related signalling pathways involved REST-targeted DEGs, while neurogenic processes and pathways were downregulated. Thus, Day 90 may represent a critical time point in the neurogenic-to-gliogenic shift observed in DS cerebral organoids. This study further elucidated the crucial role of REST in the neurodevelopmental defects associated with DS, particularly its involvement in the neurogenic-to-gliogenic shift in the DS brain. Additionally, this research provided a foundational contribution to the future study of the pathological mechanisms of neurodevelopment in DS through spatiotemporal transcriptomics.

In DS, the NPCs accelerated their differentiation into astrocytes. These DS-derived astrocytes exhibit impaired maturation and morphogenesis, leading to various functional abnormalities that contribute to central nervous system dysfunction. This research emphasises the critical role of the REST in regulating astrocyte function in DS. The transcriptomic analysis revealed that losing nuclear REST in DS astrocytes may lead to the upregulation of numerous REST-targeted DEGs. These DEGs were involved in key astrocyte functions, including axon development, synapse organisation, inflammatory responses, energy metabolism, and signalling pathways. The overexpression of inflammatory cytokines suggested that astrocytes in DS were in an activated or reactive state. Markers such as *EAAT2*, *GFAP*, *S100A10*, and *S100B*

© COPYRIGHT UPM

were significantly elevated with the REST reduced, reflecting the coexistence of both neurotoxic and neuroprotective reactive astrocyte phenotypes in DS. This coexistence highlights the complexity of the role of REST in the pathology of DS astrocyte reactivity. Restoring REST levels in DS-derived astrocytes using lithium carbonate effectively suppressed the expression of inflammatory genes and reactive astrocyte markers. This finding suggested that targeting REST may offer a promising therapeutic strategy to mitigate astrocyte-mediated neuropathology in DS. This study highlighted the essential role of REST in regulating normal astrocyte function and emphasises its potential as a therapeutic target for mitigating the complex neuropathological characteristics associated with Down syndrome.

Lithium has emerged as a promising therapeutic candidate for Down syndrome (DS) because its ability to restore REST expression may reverse neurodevelopmental defects caused by REST loss (Lam et al., 2025). The translational potential of lithium therapy for DS lies in its well-documented neuroprotective effects, including modulation of neurogenesis, inhibition of GSK-3β, and suppression of neuroinflammation (Lam et al., 2025; Shen et al., 2024). This study demonstrated that lithium treatment restores nuclear REST levels, downregulates reactive astrocyte markers, and rescues neuronal differentiation defects in DS-derived models. Given these mechanistic insights, lithium holds potential for clinical applications in DS by targeting key molecular pathways implicated in neurodevelopmental dysfunction.

To achieve optimal clinical outcomes, the timing of lithium administration is a critical factor. Neurodevelopmental abnormalities in DS begin in utero, with reduced neurogenesis and enhanced gliogenesis occurring as early as mid-gestation

© COPYRIGHT UPM

(Antonarakis et al., 2020; Bull, 2020). Thus, early intervention—potentially during fetal or neonatal stages—could provide maximal therapeutic benefits by rescuing NPC fate determination and preventing the irreversible neurogenic-to-gliogenic shift. However, long-term lithium treatment must be carefully optimized to minimize adverse effects, including renal and thyroid dysfunction. Future clinical trials should focus on determining the optimal dosage, treatment window, and biomarkers for monitoring efficacy, ensuring that lithium therapy provides sustained neuroprotection without compromising safety.

7.2 Study Limitations and Recommendations for Future Research

This study identified the downregulation of REST in DS hiPSC-derived NPCs, astrocytes, and cerebral organoids. Transcriptomic data from DS-derived human brain tissue, cerebral organoids, and neural cells were utilised to comprehensively analyse REST and its target genes, highlighting their pivotal role in the neurodevelopmental processes associated with DS. While the study utilised 2D and 3D models (cerebral organoids) derived from DS hiPSCs, these models may still fall short of fully replicating the complexity of human brain development and pathology. The inherent differences between in vivo models and in vivo conditions may lead to incomplete or biased interpretations of the role of REST in DS neurodevelopment. The study utilised cerebral organoids at various developmental stages to reveal the temporal dynamics of REST and its target genes in DS brain development. However, different cerebral organoid cultivation protocols may introduce variability in determining key developmental time points. The focus on transcriptomic data to assess the impact of REST does not fully account for changes at the protein level, post-translational

© COPYRIGHT UPM

modifications, or functional outcomes. Consequently, the complete effects of REST on DS brain cell processes may not be fully understood.

In this study, although potential target genes for REST were predicted by silico analysis, this approach has some limitations. First, bioinformatics tools rely on existing databases and algorithms that may not accurately capture the actual regulatory network of REST. Second, these predictions may have false-positive or false-negative results due to the lack of experimental data to validate them. In addition, the function of REST may vary in different cell types or environmental conditions, which can lead to differences in REST target genes in different cells. ChIP-seq is able to accurately detect REST binding sites on a genome-wide scale, thus providing direct experimental evidence to help validate and refine the results of silico analyses. Therefore, further experimental validation using ChIP-seq technology is still required to confirm the actual target genes of REST in DS-derived neuronal nuclei cerebral organoids.

Although the study proposed potential therapeutic strategies targeting REST and explored lithium as a possible treatment, the long-term safety and efficacy of such interventions require further research. Integrating proteomics with transcriptomics could help clarify how changes in REST expression affect protein function and cellular processes. Functional analyses could further elucidate the impact of REST dysregulation on NPCs, neurons, glial cells, synaptic activity, and neuroinflammation. This could advance research to uncover the specific molecular mechanisms of the role of REST in neurogenic to gliogenic transitions and other aspects of DS neuropathology. Longitudinal studies using cerebral organoids at different developmental stages could provide deeper insights into how REST dysregulation

© COPYRIGHT UPM

affects brain development over time. This will help pinpoint optimal intervention windows for treatment and guide further research on the safety, efficacy, and long-term effects of REST-targeted therapies in Down syndrome. These trials should consider intervention timing, as early developmental stages may present critical windows for therapeutic intervention to mitigate the progression of DS-related neuropathology.

7.3 General Conclusion

In summary, this study provided compelling evidence that REST is a crucial regulatory factor in the neuropathology of DS, playing a pivotal role in neurodevelopmental processes and contributing to the neurogenic-to-gliogenic shift observed in DS brains. Through extensive transcriptomic analysis of DS brain tissue, NPCs, and cerebral organoids, the research identified the common REST-targeted DEGs dysregulation across various brain regions and developmental stages. The downregulation of REST and the subsequent upregulation of its target genes were linked to critical pathways involved in neurogenesis, gliogenesis, and neuroinflammation, shedding light on the molecular mechanisms underlying the increased gliogenesis and altered neuronal development characteristic of DS. Moreover, the study highlighted the functional implications of REST dysregulation in astrocytes, where its loss leads to a reactive astrocyte phenotype associated with both neurotoxic and neuroprotective effects. This revealed accelerated differentiation of NPCs into astrocytes, which were also more reactive due to reduced nuclear REST. The therapeutic potential of lithium by restoring REST levels to mitigate astrocyte-mediated neuropathology in DS was also underscored, offering a promising avenue for future interventions. Overall, this research significantly advanced the

© COPYRIGHT UPM

understanding of the role of REST in DS, laying the groundwork for future studies that may explore REST-targeted therapies to address the complex neurodevelopmental and neuropathological challenges in DS.

© COPYRIGHT UPM

REFERENCES

Abbott, N.J., Rönnbäck, L., Hansson, E., 2006. Astrocyte–endothelial interactions at the blood–brain barrier. Nat Rev Neurosci 7, 41–53. https://doi.org/10.1038/nrn1824

Abjean, L., Ben Haim, L., Riquelme-Perez, M., Gipchtein, P., Derbois, C., Palomares, M.-A., Petit, F., Hérard, A.-S., Gaillard, M.-C., Guillermier, M., Gaudin-Guérif, M., Aurégan, G., Sagar, N., Héry, C., Dufour, N., Robil, N., Kabani, M., Melki, R., De la Grange, P., Bemelmans, A.P., Bonvento, G., Deleuze, J.-F., Hantraye, P., Flament, J., Bonnet, E., Brohard, S., Olaso, R., Brouillet, E., Carrillo-de Sauvage, M.-A., Escartin, C., 2023. Reactive astrocytes promote proteostasis in Huntington's disease through the JAK2-STAT3 pathway. Brain 146, 149–166. https://doi.org/10.1093/brain/awac068

Abrajano, J.J., Qureshi, I.A., Gokhan, S., Zheng, D., Bergman, A., Mehler, M.F., 2009. Differential deployment of REST and CoREST promotes glial subtype specification and oligodendrocyte lineage maturation. PLoS One 4, e7665. https://doi.org/10.1371/journal.pone.0007665

Adams-Cioaba, M.A., Krupa, J.C., Xu, C., Mort, J.S., Min, J., 2011. Structural basis for the recognition and cleavage of histone H3 by cathepsin L. Nat Commun 2, 197. https://doi.org/10.1038/ncomms1204

Aguirre, A., Rubio, M.E., Gallo, V., 2010. Notch and EGFR pathway interaction regulates neural stem cell number and self-renewal. Nature 467, 323–327. https://doi.org/10.1038/nature09347

Ahmed, Md.M., Johnson, N.R., Boyd, T.D., Coughlan, C., Chial, H.J., Potter, H., 2021. Innate Immune System Activation and Neuroinflammation in Down Syndrome and Neurodegeneration: Therapeutic Targets or Partners? Front Aging Neurosci 13, 718426. https://doi.org/10.3389/fnagi.2021.718426

Aksoy, I., Marcy, G., Chen, J., Divakar, U., Kumar, V., John-Sanchez, D., Rahmani, M., Buckley, N.J., Stanton, L.W., 2016. A Role for RE-1-Silencing Transcription Factor in Embryonic Stem Cells Cardiac Lineage Specification. Stem Cells 34, 860–872. https://doi.org/10.1002/stem.2304

Allen, A.P., McGlinchey, E., Fallon, M., McCallion, P., McCarron, M., 2023. Cognitive reserve and dementia risk management in people with an intellectual disability. International Journal of Geriatric Psychiatry 38, e5906. https://doi.org/10.1002/gps.5906

Alsaqati, M., Davis, B.A., Wood, J., Jones, M.M., Jones, L., Westwood, A., Petter, O., Isles, A.R., Linden, D., Van den Bree, M., Owen, M., Hall, J., Harwood, A.J., 2022. NRSF/REST lies at the intersection between epigenetic regulation, miRNA-mediated gene control and neurodevelopmental pathways associated with Intellectual disability (ID) and Schizophrenia. Transl Psychiatry 12, 1–10. https://doi.org/10.1038/s41398-022-02199-z

© COPYRIGHT UPM

Althammer, F., Ferreira-Neto, H.C., Rubaharan, M., Roy, R.K., Patel, A.A., Murphy, A., Cox, D.N., Stern, J.E., 2020. Three-dimensional morphometric analysis reveals time-dependent structural changes in microglia and astrocytes in the central amygdala and hypothalamic paraventricular nucleus of heart failure rats. J Neuroinflammation 17, 221. https://doi.org/10.1186/s12974-020-01892-4

Alvarez, J.I., Katayama, T., Prat, A., 2013. Glial influence on the blood brain barrier. Glia 61, 1939–1958. https://doi.org/10.1002/glia.22575

Amin, N.D., Paşca, S.P., 2018. Building Models of Brain Disorders with Three-Dimensional Organoids. Neuron 100, 389–405. https://doi.org/10.1016/j.neuron.2018.10.007

Anderson, C.M., Swanson, R.A., 2000. Astrocyte glutamate transport: review of properties, regulation, and physiological functions. Glia 32, 1–14.

Andrés, M.E., Burger, C., Peral-Rubio, M.J., Battaglioli, E., Anderson, M.E., Grimes, J., Dallman, J., Ballas, N., Mandel, G., 1999. CoREST: a functional corepressor required for regulation of neural-specific gene expression. Proc Natl Acad Sci U S A 96, 9873–9878. https://doi.org/10.1073/pnas.96.17.9873

Antonarakis, S.E., Skotko, B.G., Rafii, M.S., Strydom, A., Pape, S.E., Bianchi, D.W., Sherman, S.L., Reeves, R.H., 2020. Down syndrome. Nat Rev Dis Primers 6, 9. https://doi.org/10.1038/s41572-019-0143-7

Aoki, H., Ogino, H., Tomita, H., Hara, A., Kunisada, T., 2016. Disruption of Rest Leads to the Early Onset of Cataracts with the Aberrant Terminal Differentiation of Lens Fiber Cells. PLOS ONE 11, e0163042. https://doi.org/10.1371/journal.pone.0163042

Araujo, B.H.S., Kaid, C., De Souza, J.S., Gomes da Silva, S., Goulart, E., Caires, L.C.J., Musso, C.M., Torres, L.B., Ferrasa, A., Herai, R., Zatz, M., Okamoto, O.K., Cavalheiro, E.A., 2018. Down Syndrome iPSC-Derived Astrocytes Impair Neuronal Synaptogenesis and the mTOR Pathway In Vitro. Mol Neurobiol 55, 5962–5975. https://doi.org/10.1007/s12035-017-0818-6

Ashburner, M., Ball, C.A., Blake, J.A., Botstein, D., Butler, H., Cherry, J.M., Davis, A.P., Dolinski, K., Dwight, S.S., Eppig, J.T., Harris, M.A., Hill, D.P., Issel-Tarver, L., Kasarskis, A., Lewis, S., Matese, J.C., Richardson, J.E., Ringwald, M., Rubin, G.M., Sherlock, G., 2000. Gene Ontology: tool for the unification of biology. Nat Genet 25, 25–29. https://doi.org/10.1038/75556

Astudillo, P., 2020. Extracellular matrix stiffness and Wnt/β-catenin signaling in physiology and disease. Biochem Soc Trans 48, 1187–1198. https://doi.org/10.1042/BST20200026

Atagun, M.I., Balaban, O.D., Lordoglu, D.Y., Evren, C., 2013. Lithium and valproate may affect motor and sensory speed in patients with bipolar disorder. Klinik Psikofarmakoloji Bülteni / Bulletin of Clinical Psychopharmacology 23, 305–314. https://doi.org/10.5455/bcp.20130304010158

© COPYRIGHT UPM

Aude Marie Lepagnol-Bestel, Aude-Marie Lepagnol-Bestel, Ágnes Zvara, Gilles Maussion, Gilles Maussion, Frédérique Quignon, Bedel Ngimbous, Nicolas Ramoz, Sandrine Imbeaud, Yann Loe-Mie, Karim Benihoud, Nicolas Agier, Nicolas Agier, Nicolas Agier, Paul A. Salin, Ana Cardona, Suonavy Khung-Savatovsky, Pekka Kallunki, Jean-Maurice Delabar, László G. Puskás, Hervé Delacroix, Lawrence Aggerbeck, Lawrence Aggerbeck, Lawrence Aggerbeck, Anne Lise Delezoide, Anne Lise Delezoide, Olivier Delattre, Philip Gorwood, Jean Marie Moalic, Michel Simonneau, 2009. DYRK1A interacts with the REST/NRSF-SWI/SNF chromatin remodelling complex to deregulate gene clusters involved in the neuronal phenotypic traits of Down syndrome. Human Molecular Genetics 18, 1405–1414. https://doi.org/10.1093/hmg/ddp047

Baburamani, A.A., Vontell, R.T., Uus, A., Pietsch, M., Patkee, P.A., Wyatt-Ashmead, J., Chin-Smith, E.C., Supramaniam, V.G., Donald Tournier, J., Deprez, M., Rutherford, M.A., 2020. Assessment of radial glia in the frontal lobe of fetuses with Down syndrome. Acta Neuropathol Commun 8, 141. https://doi.org/10.1186/s40478-020-01015-3

Bahn, S., Mimmack, M., Ryan, M., Caldwell, M.A., Jauniaux, E., Starkey, M., Svendsen, C.N., Emson, P., 2002. Neuronal target genes of the neuron-restrictive silencer factor in neurospheres derived from fetuses with Down's syndrome: a gene expression study. Lancet 359, 310–315. https://doi.org/10.1016/S0140-6736(02)07497-4

Baldelli, P., Meldolesi, J., 2015. The Transcription Repressor REST in Adult Neurons: Physiology, Pathology, and Diseases. eNeuro 2, ENEURO.0010-15.2015. https://doi.org/10.1523/ENEURO.0010-15.2015

Ballas, N., Grunseich, C., Lu, D.D., Speh, J.C., Mandel, G., 2005. REST and its corepressors mediate plasticity of neuronal gene chromatin throughout neurogenesis. Cell 121, 645–657. https://doi.org/10.1016/j.cell.2005.03.013

Bandettini, W.P., Kellman, P., Mancini, C., Booker, O.J., Vasu, S., Leung, S.W., Wilson, J.R., Shanbhag, S.M., Chen, M.Y., Arai, A.E., 2012. MultiContrast Delayed Enhancement (MCODE) improves detection of subendocardial myocardial infarction by late gadolinium enhancement cardiovascular magnetic resonance: a clinical validation study. J Cardiovasc Magn Reson 14, 83. https://doi.org/10.1186/1532-429X-14-83

Barral, S., Kurian, M.A., 2016. Utility of Induced Pluripotent Stem Cells for the Study and Treatment of Genetic Diseases: Focus on Childhood Neurological Disorders. Front. Mol. Neurosci. 9. https://doi.org/10.3389/fnmol.2016.00078

Bates, G.P., Dorsey, R., Gusella, J.F., Hayden, M.R., Kay, C., Leavitt, B.R., Nance, M., Ross, C.A., Scahill, R.I., Wetzel, R., Wild, E.J., Tabrizi, S.J., 2015. Huntington disease. Nat Rev Dis Primers 1, 1–21. https://doi.org/10.1038/nrdp.2015.5

Belichenko, N.P., Belichenko, P.V., Kleschevnikov, A.M., Salehi, A., Reeves, R.H., Mobley, W.C., 2009. The "Down syndrome critical region" is sufficient in the mouse model to confer behavioral, neurophysiological, and synaptic

© COPYRIGHT UPM

phenotypes characteristic of Down syndrome. J Neurosci 29, 5938–5948. https://doi.org/10.1523/JNEUROSCI.1547-09.2009

Belvindrah, R., Graus-Porta, D., Goebbels, S., Nave, K.-A., Müller, U., 2007. β1 Integrins in Radial Glia But Not in Migrating Neurons Are Essential for the Formation of Cell Layers in the Cerebral Cortex. J. Neurosci. 27, 13854–13865. https://doi.org/10.1523/JNEUROSCI.4494-07.2007

Ben Haim, L., Ceyzériat, K., Carrillo-de Sauvage, M.A., Aubry, F., Auregan, G., Guillermier, M., Ruiz, M., Petit, F., Houitte, D., Faivre, E., Vandesquille, M., Aron-Badin, R., Dhenain, M., Déglon, N., Hantraye, P., Brouillet, E., Bonvento, G., Escartin, C., 2015. The JAK/STAT3 pathway is a common inducer of astrocyte reactivity in Alzheimer's and Huntington's diseases. J Neurosci 35, 2817–2829. https://doi.org/10.1523/JNEUROSCI.3516-14.2015

Bergsland, M., Covacu, R., Perez Estrada, C., Svensson, M., Brundin, L., 2014. Nitric Oxide-Induced Neuronal to Glial Lineage Fate-Change Depends on NRSF/REST Function in Neural Progenitor Cells. Stem Cells 32, 2539–2549. https://doi.org/10.1002/stem.1749

Beurel, E., Jope, R.S., 2009. Lipopolysaccharide-induced interleukin-6 production is controlled by glycogen synthase kinase-3 and STAT3 in the brain. Journal of Neuroinflammation 6, 9. https://doi.org/10.1186/1742-2094-6-9

Bhardwaj, A., Roy, V., Ghadlinge's, M.S., Dua, A., 2021. Lithium carbonate toxicity in an elderly patient: a case report. International Journal of Basic & Clinical Pharmacology 10, 766–768. https://doi.org/10.18203/2319-2003.ijbcp20212091

Bhattacharyya, A., McMillan, E., Chen, S.I., Wallace, K., Svendsen, C.N., 2009. A Critical Period in Cortical Interneuron Neurogenesis in Down Syndrome Revealed by Human Neural Progenitor Cells. Developmental Neuroscience 31, 497–510. https://doi.org/10.1159/000236899

Bi, F., Huang, C., Tong, J., Qiu, G., Huang, B., Wu, Q., Li, F., Xu, Z., Bowser, R., Xia, X.-G., Zhou, H., 2013. Reactive astrocytes secrete lcn2 to promote neuron death. Proc Natl Acad Sci U S A 110, 4069–4074. https://doi.org/10.1073/pnas.1218497110

Bianco, K., Gormley, M., Farrell, J., Zhou, Y., Oliverio, O., Tilden, H., McMaster, M., Fisher, S.J., 2016. Placental transcriptomes in the common aneuploidies reveal critical regions on the trisomic chromosomes and genome-wide effects. Prenat Diagn 36, 812–822. https://doi.org/10.1002/pd.4862

Brännvall, K., Hjelm, H., Korhonen, L., Lahtinen, U., Lehesjoki, A.-E., Lindholm, D., 2003. Cystatin-B is expressed by neural stem cells and by differentiated neurons and astrocytes. Biochemical and Biophysical Research Communications 308, 369–374. https://doi.org/10.1016/S0006-291X(03)01386-X

© COPYRIGHT UPM

Briggs, J.A., Sun, J., Shepherd, J., Ovchinnikov, D.A., Chung, T.-L., Nayler, S.P., Kao, L.-P., Morrow, C.A., Thakar, N.Y., Soo, S.-Y., Peura, T., Grimmond, S., Wolvetang, E.J., 2013. Integration-free induced pluripotent stem cells model genetic and neural developmental features of down syndrome etiology. Stem Cells 31, 467–478. https://doi.org/10.1002/stem.1297

Bruce, A.W., Donaldson, I.J., Wood, I.C., Yerbury, S.A., Sadowski, M.I., Chapman, M., Göttgens, B., Buckley, N.J., 2004. Genome-wide analysis of repressor element 1 silencing transcription factor/neuron-restrictive silencing factor (REST/NRSF) target genes. Proceedings of the National Academy of Sciences 101, 10458–10463. https://doi.org/10.1073/pnas.0401827101

Bruce, A.W., López-Contreras, A.J., Flicek, P., Down, T.A., Dhami, P., Dillon, S.C., Koch, C.M., Langford, C.F., Dunham, I., Andrews, R.M., Vetrie, D., 2009. Functional diversity for REST (NRSF) is defined by in vivo binding affinity hierarchies at the DNA sequence level. Genome Res 19, 994–1005. https://doi.org/10.1101/gr.089086.108

Bruckner, T.A., Singh, P., Lelong, N., Khoshnood, B., 2019. Down syndrome among primiparae at older maternal age: A test of the relaxed filter hypothesis. Birth Defects Res 111, 1611–1617. https://doi.org/10.1002/bdr2.1553

Buckley, N.A., Cheng, S., Isoardi, K., Chiew, A.L., Siu, W., Vecellio, E., Chan, B.S., 2020. Haemodialysis for lithium poisoning: Translating EXTRIP recommendations into practical guidelines. British Journal of Clinical Pharmacology 86, 999–1006. https://doi.org/10.1111/bcp.14212

Buffolo, F., Petrosino, V., Albini, M., Moschetta, M., Carlini, F., Floss, T., Kerlero de Rosbo, N., Cesca, F., Rocchi, A., Uccelli, A., Benfenati, F., 2021. Neuroinflammation induces synaptic scaling through IL-1β-mediated activation of the transcriptional repressor REST/NRSF. Cell Death Dis 12, 1–15. https://doi.org/10.1038/s41419-021-03465-6

Bull, M.J., 2020. Down Syndrome. N Engl J Med 382, 2344–2352. https://doi.org/10.1056/NEJMra1706537

Burke, E.E., Chenoweth, J.G., Shin, J.H., Collado-Torres, L., Kim, S.-K., Micali, N., Wang, Y., Colantuoni, C., Straub, R.E., Hoeppner, D.J., Chen, H.-Y., Sellers, A., Shibbani, K., Hamersky, G.R., Diaz Bustamante, M., Phan, B.N., Ulrich, W.S., Valencia, C., Jaishankar, A., Price, A.J., Rajpurohit, A., Semick, S.A., Bürli, R.W., Barrow, J.C., Hiler, D.J., Page, S.C., Martinowich, K., Hyde, T.M., Kleinman, J.E., Berman, K.F., Apud, J.A., Cross, A.J., Brandon, N.J., Weinberger, D.R., Maher, B.J., McKay, R.D.G., Jaffe, A.E., 2020. Dissecting transcriptomic signatures of neuronal differentiation and maturation using iPSCs. Nat Commun 11, 462. https://doi.org/10.1038/s41467-019-14266-z

Burkholder, N.T., Mayfield, J.E., Yu, X., Irani, S., Arce, D.K., Jiang, F., Matthews, W.L., Xue, Y., Zhang, Y.J., 2018. Phosphatase activity of small C-terminal domain phosphatase 1 (SCP1) controls the stability of the key neuronal regulator RE1-silencing transcription factor (REST). Journal of Biological Chemistry 293, 16851–16861. https://doi.org/10.1074/jbc.RA118.004722

© COPYRIGHT UPM

Busciglio, J., Pelsman, A., Wong, C., Pigino, G., Yuan, M., Mori, H., Yankner, B.A., 2002. Altered Metabolism of the Amyloid β Precursor Protein Is Associated with Mitochondrial Dysfunction in Down's Syndrome. Neuron 33, 677–688. https://doi.org/10.1016/S0896-6273(02)00604-9

Bushong, E.A., Martone, M.E., Jones, Y.Z., Ellisman, M.H., 2002. Protoplasmic Astrocytes in CA1 Stratum Radiatum Occupy Separate Anatomical Domains. J. Neurosci. 22, 183–192. https://doi.org/10.1523/JNEUROSCI.22-01-00183.2002

Butler-Ryan, R., Wood, I.C., 2021. The functions of repressor element 1-silencing transcription factor in models of epileptogenesis and post-ischemia. Metab Brain Dis 36, 1135–1150. https://doi.org/10.1007/s11011-021-00719-2

Bylicky, M.A., Mueller, G.P., Day, R.M., 2018. Mechanisms of Endogenous Neuroprotective Effects of Astrocytes in Brain Injury. Oxidative Medicine and Cellular Longevity 2018, e6501031. https://doi.org/10.1155/2018/6501031

Bystron, I., Blakemore, C., Rakic, P., 2008. Development of the human cerebral cortex: Boulder Committee revisited. Nat Rev Neurosci 9, 110–122. https://doi.org/10.1038/nrn2252

Cai, Z., Wan, C.-Q., Liu, Z., 2017. Astrocyte and Alzheimer's disease. J Neurol 264, 2068–2074. https://doi.org/10.1007/s00415-017-8593-x

Calderone, A., Jover, T., Noh, K., Tanaka, H., Yokota, H., Lin, Y., Grooms, S.Y., Regis, R., Bennett, M.V.L., Zukin, R.S., 2003. Ischemic Insults Derepress the Gene Silencer REST in Neurons Destined to Die. J. Neurosci. 23, 2112–2121. https://doi.org/10.1523/JNEUROSCI.23-06-02112.2003

Camins, A., Verdaguer, E., Junyent, F., Yeste-Velasco, M., Pelegrí, C., Vilaplana, J., Pallás, M., 2009. Potential mechanisms involved in the prevention of neurodegenerative diseases by lithium. CNS Neurosci Ther 15, 333–344. https://doi.org/10.1111/j.1755-5949.2009.00086.x

Campbell, N.B., Patel, Y., Moore, T.L., Medalla, M., Zeldich, E., 2023. Extracellular Vesicle Treatment Alleviates Neurodevelopmental and Neurodegenerative Pathology in Cortical Spheroid Model of Down Syndrome. Int J Mol Sci 24, 3477. https://doi.org/10.3390/ijms24043477

Campos, L.S., Leone, D.P., Relvas, J.B., Brakebusch, C., Fässler, R., Suter, U., ffrench-Constant, C., 2004. Beta1 integrins activate a MAPK signalling pathway in neural stem cells that contributes to their maintenance. Development 131, 3433–3444. https://doi.org/10.1242/dev.01199

Canzonetta, C., Mulligan, C., Deutsch, S., Ruf, S., O'Doherty, A., Lyle, R., Borel, C., Lin-Marq, N., Delom, F., Groet, J., Schnappauf, F., De Vita, S., Averill, S., Priestley, J.V., Martin, J.E., Shipley, J., Denyer, G., Epstein, C.J., Fillat, C., Estivill, X., Tybulewicz, V.L.J., Fisher, E.M.C., Antonarakis, S.E., Nizetic, D., 2008. DYRK1A-Dosage Imbalance Perturbs NRSF/REST Levels, Deregulating Pluripotency and Embryonic Stem Cell Fate in Down Syndrome.

The American Journal of Human Genetics 83, 388–400. https://doi.org/10.1016/j.ajhg.2008.08.012

Cao, F., Hata, R., Zhu, P., Nakashiro, K., Sakanaka, M., 2010. Conditional deletion of Stat3 promotes neurogenesis and inhibits astrogliogenesis in neural stem cells. Biochem Biophys Res Commun 394, 843–847. https://doi.org/10.1016/j.bbrc.2010.03.092

Carlsson, R., Özen, I., Barbariga, M., Gaceb, A., Roth, M., Paul, G., 2018. STAT3 precedes HIF1α transcriptional responses to oxygen and oxygen and glucose deprivation in human brain pericytes. PLOS ONE 13, e0194146. https://doi.org/10.1371/journal.pone.0194146

Cau, E., Blader, P., 2009. Notch activity in the nervous system: to switch or not switch? Neural Development 4, 36. https://doi.org/10.1186/1749-8104-4-36

Cavadas, M.A.S., Mesnieres, M., Crifo, B., Manresa, M.C., Selfridge, A.C., Keogh, C.E., Fabian, Z., Scholz, C.C., Nolan, K.A., Rocha, L.M.A., Tambuwala, M.M., Brown, S., Wdowicz, A., Corbett, D., Murphy, K.J., Godson, C., Cummins, E.P., Taylor, C.T., Cheong, A., 2016. REST is a hypoxia-responsive transcriptional repressor. Sci Rep 6, 31355. https://doi.org/10.1038/srep31355

Cavadas, M.A.S., Mesnieres, M., Crifo, B., Manresa, M.C., Selfridge, A.C., Scholz, C.C., Cummins, E.P., Cheong, A., Taylor, C.T., 2015. REST mediates resolution of HIF-dependent gene expression in prolonged hypoxia. Sci Rep 5, 17851. https://doi.org/10.1038/srep17851

Centeno, E.G.Z., Cimarosti, H., Bithell, A., 2018. 2D versus 3D human induced pluripotent stem cell-derived cultures for neurodegenerative disease modelling. Mol Neurodegener 13, 27. https://doi.org/10.1186/s13024-018-0258-4

Čeru, S., Konjar, Š., Maher, K., Repnik, U., Križaj, I., Benčina, M., Renko, M., Nepveu, A., Žerovnik, E., Turk, B., Kopitar-Jerala, N., 2010. Stefin B interacts with histones and cathepsin L in the nucleus. J Biol Chem 285, 10078–10086. https://doi.org/10.1074/jbc.M109.034793

Ceyzériat, K., Abjean, L., Carrillo-de Sauvage, M.-A., Ben Haim, L., Escartin, C., 2016. The complex STATes of astrocyte reactivity: How are they controlled by the JAK-STAT3 pathway? Neuroscience 330, 205–218. https://doi.org/10.1016/j.neuroscience.2016.05.043

Ceyzériat, K., Ben Haim, L., Denizot, A., Pommier, D., Matos, M., Guillemaud, O., Palomares, M.-A., Abjean, L., Petit, F., Gipchtein, P., Gaillard, M.-C., Guillermier, M., Bernier, S., Gaudin, M., Aurégan, G., Joséphine, C., Déchamps, N., Veran, J., Langlais, V., Cambon, K., Bemelmans, A.P., Baijer, J., Bonvento, G., Dhenain, M., Deleuze, J.-F., Oliet, S.H.R., Brouillet, E., Hantraye, P., Carrillo-de Sauvage, M.-A., Olaso, R., Panatier, A., Escartin, C., 2018. Modulation of astrocyte reactivity improves functional deficits in mouse models of Alzheimer's disease. Acta Neuropathologica Communications 6, 104. https://doi.org/10.1186/s40478-018-0606-1

© COPYRIGHT UPM

Chang, R., Xiao, X., Fu, Y., Zhang, C., Zhu, X., Gao, Y., 2021. ITGB1-DT Facilitates Lung Adenocarcinoma Progression via Forming a Positive Feedback Loop With ITGB1/Wnt/β-Catenin/MYC. Frontiers in Cell and Developmental Biology 9, 631259.

Chen, C., Jiang, P., Xue, H., Peterson, S.E., Tran, H.T., McCann, A.E., Parast, M.M., Li, S., Pleasure, D.E., Laurent, L.C., Loring, J.F., Liu, Y., Deng, W., 2014. Role of astroglia in Down's syndrome revealed by patient-derived human-induced pluripotent stem cells. Nat Commun 5, 4430. https://doi.org/10.1038/ncomms5430

Chen, H., Zhang, M., Zhang, J., Chen, Yapei, Zuo, Y., Xie, Z., Zhou, G., Chen, S., Chen, Yaoyong, 2022. Application of Induced Pluripotent Stem Cell-Derived Models for Investigating microRNA Regulation in Developmental Processes. Front. Genet. 13. https://doi.org/10.3389/fgene.2022.899831

Chen, M., Xiao, L., Dai, G., Lu, P., Zhang, Y., Li, Y., Ni, M., Rui, Y., 2021. Inhibition of JAK-STAT Signaling Pathway Alleviates Age-Related Phenotypes in Tendon Stem/Progenitor Cells. Frontiers in Cell and Developmental Biology 9.

Chen, Z.-F., Paquette, A.J., Anderson, D.J., 1998. NRSF/REST is required in vivo for repression of multiple neuronal target genes during embryogenesis. Nat Genet 20, 136–142. https://doi.org/10.1038/2431

Cheng, J., Shen, W., Jin, L., Pan, J., Zhou, Y., Pan, G., Xie, Q., Hu, Q., Wu, S., Zhang, H., Chen, X., 2020. Treadmill exercise promotes neurogenesis and myelin repair via upregulating Wnt/β-catenin signaling pathways in the juvenile brain following focal cerebral ischemia/reperfusion. International Journal of Molecular Medicine 45, 1447–1463. https://doi.org/10.3892/ijmm.2020.4515

Cheng, Y., Zhou, Y., Lv, W., Luo, Q., Song, G., 2021. Simulated Microgravity Inhibits Rodent Dermal Fibroblastic Differentiation of Mesenchymal Stem Cells by Suppressing ERK/β-Catenin Signaling Pathway. International Journal of Molecular Sciences 22, 10702. https://doi.org/10.3390/ijms221910702

Chenn, A., 2009. A Top-NOTCH Way to Make Astrocytes. Developmental Cell 16, 158–159. https://doi.org/10.1016/j.devcel.2009.01.019

Cheroni, C., Trattaro, S., Caporale, N., López-Tobón, A., Tenderini, E., Sebastiani, S., Troglio, F., Gabriele, M., Bressan, R.B., Pollard, S.M., Gibson, W.T., Testa, G., 2022. Benchmarking brain organoid recapitulation of fetal corticogenesis. Transl Psychiatry 12, 520. https://doi.org/10.1038/s41398-022-02279-0

Chin, C.-H., Chen, S.-H., Wu, H.-H., Ho, C.-W., Ko, M.-T., Lin, C.-Y., 2014. cytoHubba: identifying hub objects and sub-networks from complex interactome. BMC Syst Biol 8 Suppl 4, S11. https://doi.org/10.1186/1752-0509-8-S4-S11

Chong-Teik Lim, Lam, X.-J., Crystal, A.-A., Huang, T., Jusoh, N., Cheah, P.-S., Ling, K.-H., 2024. Reduced REST Expression in Neural Progenitor Cells, Adult

© COPYRIGHT UPM

Cortex, and Impaired REST Nuclear Translocation in the Prefrontal Cortex of Ts1Cje Mouse Model of Down Syndrome. Neurochem. J. 18, 147–161. https://doi.org/10.1134/S1819712424010148

Christopherson, K.S., Ullian, E.M., Stokes, C.C.A., Mullowney, C.E., Hell, J.W., Agah, A., Lawler, J., Mosher, D.F., Bornstein, P., Barres, B.A., 2005. Thrombospondins are astrocyte-secreted proteins that promote CNS synaptogenesis. Cell 120, 421–433. https://doi.org/10.1016/j.cell.2004.12.020

Conforti, P., Mas Monteys, A., Zuccato, C., Buckley, N.J., Davidson, B., Cattaneo, E., 2013. In vivo delivery of DN:REST improves transcriptional changes of REST-regulated genes in HD mice. Gene Ther 20, 678–685. https://doi.org/10.1038/gt.2012.84

Cong, J., Cheng, B., Liu, J., He, P., 2021. RTEF-1 Inhibits Vascular Smooth Muscle Cell Calcification through Regulating Wnt/β-Catenin Signaling Pathway. Calcif Tissue Int 109, 203–214. https://doi.org/10.1007/s00223-021-00833-4

Cong, T., Sun, Y., Zhou, Y., Wu, H., Li, L., Chu, Z., Chen, X., Li, J., Zhao, D., Wang, Y., Liu, Y., Yin, S., Xiao, Z., 2023. Blocking Two-Pore Domain Potassium Channel TREK-1 Inhibits the Activation of A1-Like Reactive Astrocyte Through the NF-κB Signaling Pathway in a Rat Model of Major Depressive Disorder. Neurochem Res 48, 1737–1754. https://doi.org/10.1007/s11064-023-03857-4

Contestabile, A., Fila, T., Ceccarelli, C., Bonasoni, P., Bonapace, L., Santini, D., Bartesaghi, R., Ciani, E., 2007. Cell cycle alteration and decreased cell proliferation in the hippocampal dentate gyrus and in the neocortical germinal matrix of fetuses with Down syndrome and in Ts65Dn mice. Hippocampus 17, 665–678. https://doi.org/10.1002/hipo.20308

Conti, L., Crisafulli, L., Caldera, V., Tortoreto, M., Brilli, E., Conforti, P., Zunino, F., Magrassi, L., Schiffer, D., Cattaneo, E., 2012. REST controls self-renewal and tumorigenic competence of human glioblastoma cells. PLoS One 7, e38486. https://doi.org/10.1371/journal.pone.0038486

Coronel, R., Bernabeu-Zornoza, A., Palmer, C., González-Sastre, R., Rosca, A., Mateos-Martínez, P., López-Alonso, V., Liste, I., 2023. Amyloid Precursor Protein (APP) Regulates Gliogenesis and Neurogenesis of Human Neural Stem Cells by Several Signaling Pathways. International Journal of Molecular Sciences 24, 12964. https://doi.org/10.3390/ijms241612964

Couillard-Despres, S., Winner, B., Schaubeck, S., Aigner, R., Vroemen, M., Weidner, N., Bogdahn, U., Winkler, J., Kuhn, H.-G., Aigner, L., 2005. Doublecortin expression levels in adult brain reflect neurogenesis. Eur J Neurosci 21, 1–14. https://doi.org/10.1111/j.1460-9568.2004.03813.x

Covey, M.V., Streb, J.W., Spektor, R., Ballas, N., 2012. REST regulates the pool size of the different neural lineages by restricting the generation of neurons and oligodendrocytes from neural stem/progenitor cells. Development 139, 2878–2890. https://doi.org/10.1242/dev.074765

© COPYRIGHT UPM

Czerminski, J.T., King, O.D., Lawrence, J.B., 2022. Large-scale organoid study suggests effects of trisomy 21 on early fetal neurodevelopment are more subtle than variability between isogenic lines and experiments. Front Neurosci 16, 972201. https://doi.org/10.3389/fnins.2022.972201

Daniels, C.M.L., Paffenroth, E., Austin, E.V., Glebov, K., Lewis, D., Walter, J., Messing, A., 2015. Lithium Decreases Glial Fibrillary Acidic Protein in a Mouse Model of Alexander Disease. PLOS ONE 10, e0138132. https://doi.org/10.1371/journal.pone.0138132

Dashinimaev, E.B., Artyuhov, A.S., Bolshakov, A.P., Vorotelyak, E.A., Vasiliev, A.V., 2017. Neurons Derived from Induced Pluripotent Stem Cells of Patients with Down Syndrome Reproduce Early Stages of Alzheimer's Disease Type Pathology in vitro. J Alzheimers Dis 56, 835–847. https://doi.org/10.3233/JAD-160945

Dauphinot, L., Lyle, R., Rivals, I., Dang, M.T., Moldrich, R.X., Golfier, G., Ettwiller, L., Toyama, K., Rossier, J., Personnaz, L., Antonarakis, S.E., Epstein, C.J., Sinet, P.-M., Potier, M.-C., 2005. The cerebellar transcriptome during postnatal development of the Ts1Cje mouse, a segmental trisomy model for Down syndrome. Human Molecular Genetics 14, 373–384. https://doi.org/10.1093/hmg/ddi033

Daura, E., Tegelberg, S., Yoshihara, M., Jackson, C., Simonetti, F., Aksentjeff, K., Ezer, S., Hakala, P., Katayama, S., Kere, J., Lehesjoki, A.-E., Joensuu, T., 2021. Cystatin B-deficiency triggers ectopic histone H3 tail cleavage during neurogenesis. Neurobiol Dis 156, 105418. https://doi.org/10.1016/j.nbd.2021.105418

de Almeida Souza, A., da Silva, G.S.S., Velez, B.S., Santoro, A.B.M., Montero-Lomelí, M., 2010. Glycogen synthesis in brain and astrocytes is inhibited by chronic lithium treatment. Neuroscience Letters 482, 128–132. https://doi.org/10.1016/j.neulet.2010.07.016

de Graaf, G., Buckley, F., Skotko, B.G., 2021. Estimation of the number of people with Down syndrome in Europe. Eur J Hum Genet 29, 402–410. https://doi.org/10.1038/s41431-020-00748-y

de Graaf, G., Buckley, F., Skotko, B.G., 2017. Estimation of the number of people with Down syndrome in the United States. Genet Med 19, 439–447. https://doi.org/10.1038/gim.2016.127

de Sampaio e Spohr, T.C.L., Martinez, R., da Silva, E.F., Neto, V.M., Gomes, F.C.A., 2002. Neuro-glia interaction effects on GFAP gene: a novel role for transforming growth factor-beta1. Eur J Neurosci 16, 2059–2069. https://doi.org/10.1046/j.1460-9568.2002.02283.x

de Vasconcellos, A.P.S., Nieto, F.B., Crema, L.M., Diehl, L.A., de Almeida, L.M., Prediger, M.E., da Rocha, E.R., Dalmaz, C., 2006. Chronic lithium treatment has antioxidant properties but does not prevent oxidative damage induced by chronic variate stress. Neurochem Res 31, 1141–1151.

https://doi.org/10.1007/s11064-006-9139-2

Deb, B.K., Li, T.L., Blair, J.D., Hockemeyer, D., Bateup, H.S., 2023. STAT3 regulates the generation of astroglia in human brain organoids with high mTORC1 activity. https://doi.org/10.1101/2023.12.21.572786

De-Paula, V.J., Kerr, D.S., Scola, G., Gattaz, W.F., Forlenza, O.V., 2016. Lithium Distinctly Modulates the Secretion of Pro- and Anti- Inflammatory Interleukins in Co-Cultures of Neurons and Glial Cells at Therapeutic and Sub-Therapeutic Concentrations. Curr Alzheimer Res 13, 848–852. https://doi.org/10.2174/1567205013666160219112612

Dezonne, R.S., Sartore, R.C., Nascimento, J.M., Saia-Cereda, V.M., Romão, L.F., Alves-Leon, S.V., de Souza, J.M., Martins-de-Souza, D., Rehen, S.K., Gomes, F.C.A., 2017. Derivation of Functional Human Astrocytes from Cerebral Organoids. Sci Rep 7, 45091. https://doi.org/10.1038/srep45091

Di Giaimo, R., Riccio, M., Santi, S., Galeotti, C., Ambrosetti, D.C., Melli, M., 2002. New insights into the molecular basis of progressive myoclonus epilepsy: a multiprotein complex with cystatin B. Hum Mol Genet 11, 2941–2950. https://doi.org/10.1093/hmg/11.23.2941

Diaz-Castro, B., Gangwani, M.R., Yu, X., Coppola, G., Khakh, B.S., 2019. Astrocyte molecular signatures in Huntington's disease. Science Translational Medicine 11, eaaw8546. https://doi.org/10.1126/scitranslmed.aaw8546

Ding, Z.-B., Song, L.-J., Wang, Q., Kumar, G., Yan, Y.-Q., Ma, C.-G., 2021. Astrocytes: a double-edged sword in neurodegenerative diseases. Neural Regen Res 16, 1702–1710. https://doi.org/10.4103/1673-5374.306064

Dräger, N.M., Sattler, S.M., Huang, C.T.-L., Teter, O.M., Leng, K., Hashemi, S.H., Hong, J., Aviles, G., Clelland, C.D., Zhan, L., Udeochu, J.C., Kodama, L., Singleton, A.B., Nalls, M.A., Ichida, J., Ward, M.E., Faghri, F., Gan, L., Kampmann, M., 2022. A CRISPRi/a platform in human iPSC-derived microglia uncovers regulators of disease states. Nat Neurosci 25, 1149–1162. https://doi.org/10.1038/s41593-022-01131-4

Du, J., Yi, M., Zhou, F., He, W., Yang, A., Qiu, M., Huang, H., 2021. S100B is selectively expressed by gray matter protoplasmic astrocytes and myelinating oligodendrocytes in the developing CNS. Molecular Brain 14, 154. https://doi.org/10.1186/s13041-021-00865-9

Duncan, E.M., Muratore-Schroeder, T.L., Cook, R.G., Garcia, B.A., Shabanowitz, J., Hunt, D.F., Allis, C.D., 2008. Cathepsin L proteolytically processes histone H3 during mouse embryonic stem cell differentiation. Cell 135, 284–294. https://doi.org/10.1016/j.cell.2008.09.055

Dvorakova, K., Skarkova, V., Vitovcova, B., Soukup, J., Vosmikova, H., Pleskacova, Z., Skarka, A., Bartos, M.C., Krupa, P., Kasparova, P., Petera, J., Rudolf, E., 2024. Expression of STAT3 and hypoxia markers in long-term surviving malignant glioma patients. BMC Cancer 24, 509.

© COPYRIGHT UPM

https://doi.org/10.1186/s12885-024-12221-w

Dzwonek, J., Wilczynski, G.M., 2015. CD44: molecular interactions, signaling and functions in the nervous system. Front Cell Neurosci 9, 175. https://doi.org/10.3389/fncel.2015.00175

Eck, N. van, Waltman, L., 2009. Software survey: VOSviewer, a computer program for bibliometric mapping. Scientometrics 84, 523–538. https://doi.org/10.1007/s11192-009-0146-3

Edward Alain B. Pajarillo, Asha Rizor, Deok Soo Son, Deok-Soo Son, Michael Aschner, Michael Aschner, Eun Sook Lee, 2020. The transcription factor REST up-regulates tyrosine hydroxylase and antiapoptotic genes and protects dopaminergic neurons against manganese toxicity. Journal of Biological Chemistry 295, 3040–3054. https://doi.org/10.1074/jbc.ra119.011446

Elson, A., Levanon, D., Weiss, Y., Groner, Y., 1994. Overexpression of liver-type phosphofructokinase (PFKL) in transgenic-PFKL mice: implication for gene dosage in trisomy 21. Biochem J 299, 409–415.

Escartin, C., Galea, E., Lakatos, A., O'Callaghan, J.P., Petzold, G.C., Serrano-Pozo, A., Steinhäuser, C., Volterra, A., Carmignoto, G., Agarwal, A., Allen, N.J., Araque, A., Barbeito, L., Barzilai, A., Bergles, D.E., Bonvento, G., Butt, A.M., Chen, W.-T., Cohen-Salmon, M., Cunningham, C., Deneen, B., De Strooper, B., Díaz-Castro, B., Farina, C., Freeman, M., Gallo, V., Goldman, J.E., Goldman, S.A., Götz, M., Gutiérrez, A., Haydon, P.G., Heiland, D.H., Hol, E.M., Holt, M.G., Iino, M., Kastanenka, K.V., Kettenmann, H., Khakh, B.S., Koizumi, S., Lee, C.J., Liddelow, S.A., MacVicar, B.A., Magistretti, P., Messing, A., Mishra, A., Molofsky, A.V., Murai, K.K., Norris, C.M., Okada, S., Oliet, S.H.R., Oliveira, J.F., Panatier, A., Parpura, V., Pekna, M., Pekny, M., Pellerin, L., Perea, G., Pérez-Nievas, B.G., Pfrieger, F.W., Poskanzer, K.E., Quintana, F.J., Ransohoff, R.M., Riquelme-Perez, M., Robel, S., Rose, C.R., Rothstein, J.D., Rouach, N., Rowitch, D.H., Semyanov, A., Sirko, S., Sontheimer, H., Swanson, R.A., Vitorica, J., Wanner, I.-B., Wood, L.B., Wu, J., Zheng, B., Zimmer, E.R., Zorec, R., Sofroniew, M.V., Verkhratsky, A., 2021. Reactive astrocyte nomenclature, definitions, and future directions. Nat Neurosci 24, 312–325. https://doi.org/10.1038/s41593-020-00783-4

Fan, G., Martinowich, K., Chin, M.H., He, F., Fouse, S.D., Hutnick, L., Hattori, D., Ge, W., Shen, Y., Wu, H., ten Hoeve, J., Shuai, K., Sun, Y.E., 2005. DNA methylation controls the timing of astrogliogenesis through regulation of JAK-STAT signaling. Development 132, 3345–3356. https://doi.org/10.1242/dev.01912

Fan, Y.-Y., Huo, J., 2021. A1/A2 astrocytes in central nervous system injuries and diseases: Angels or devils? Neurochemistry International 148, 105080. https://doi.org/10.1016/j.neuint.2021.105080

Ferrer, I., Gullotta, F., 1990. Down's syndrome and Alzheimer's disease: dendritic spine counts in the hippocampus. Acta Neuropathol 79, 680–685. https://doi.org/10.1007/BF00294247

© COPYRIGHT UPM

Flores-Aguilar, L., Florencia Iulita, M., Kovecses, O., Torres, M.D., Levi, S.M., Zhang, Y., Askenazi, M., Wisniewski, T., Busciglio, J., Cuello, A.C., 2020. Evolution of neuroinflammation across the lifespan of individuals with Down syndrome. Brain 143, 3653–3671. https://doi.org/10.1093/brain/awaa326

Foliaki, S.T., Schwarz, B., Groveman, B.R., Walters, R.O., Ferreira, N.C., Orrù, C.D., Smith, A., Wood, A., Schmit, O.M., Freitag, P., Yuan, J., Zou, W., Bosio, C.M., Carroll, J.A., Haigh, C.L., 2021. Neuronal excitatory-to-inhibitory balance is altered in cerebral organoid models of genetic neurological diseases. Mol Brain 14, 156. https://doi.org/10.1186/s13041-021-00864-w

Forlenza, O.V., De-Paula, V.J.R., Diniz, B.S.O., 2014. Neuroprotective Effects of Lithium: Implications for the Treatment of Alzheimer's Disease and Related Neurodegenerative Disorders. ACS Chem. Neurosci. 5, 443–450. https://doi.org/10.1021/cn5000309

Foulser, P., Abbasi, Y., Mathilakath, A., Nilforooshan, R., 2017. Do not treat the numbers: lithium toxicity. Case Reports 2017, bcr. https://doi.org/10.1136/bcr-2017-220079

Franco, S.J., Müller, U., 2011. Extracellular matrix functions during neuronal migration and lamination in the mammalian central nervous system. Dev Neurobiol 71, 889–900. https://doi.org/10.1002/dneu.20946

Freeman, M.R., 2010. Specification and morphogenesis of astrocytes. Science 330, 774–778. https://doi.org/10.1126/science.1190928

Frey, B.N., Valvassori, S.S., Réus, G.Z., Martins, M.R., Petronilho, F.C., Bardini, K., Dal-Pizzol, F., Kapczinski, F., Quevedo, J., 2006. Effects of lithium and valproate on amphetamine-induced oxidative stress generation in an animal model of mania. J Psychiatry Neurosci 31, 326–332.

Fukuda, S., Abematsu, M., Mori, H., Yanagisawa, M., Kagawa, T., Nakashima, K., Yoshimura, A., Taga, T., 2007. Potentiation of Astrogliogenesis by STAT3-Mediated Activation of Bone Morphogenetic Protein-Smad Signaling in Neural Stem Cells. Molecular and Cellular Biology 27, 4931–4937. https://doi.org/10.1128/MCB.02435-06

Galaxy Community, 2022. The Galaxy platform for accessible, reproducible and collaborative biomedical analyses: 2022 update. Nucleic Acids Res 50, W345–W351. https://doi.org/10.1093/nar/gkac247

Gao, M., Yan, X., Weng, H.-R., 2013. Inhibition of glycogen synthase kinase 3beta activity with lithium prevents and attenuates paclitaxel-induced neuropathic pain. Neuroscience 254, 301–311. https://doi.org/10.1016/j.neuroscience.2013.09.033

Gao, Z., Ure, K., Ding, P., Nashaat, M., Yuan, L., Ma, J., Hammer, R.E., Hsieh, J., 2011. The Master Negative Regulator REST/NRSF Controls Adult Neurogenesis by Restraining the Neurogenic Program in Quiescent Stem Cells. J Neurosci 31, 9772–9786. https://doi.org/10.1523/JNEUROSCI.1604-

© COPYRIGHT UPM

11.2011

García, O., Flores-Aguilar, L., 2022. Astroglial and microglial pathology in Down syndrome: Focus on Alzheimer's disease. Frontiers in Cellular Neuroscience 16. https://doi.org/10.3389/fncel.2022.987212

Garcia, O., Torres, M., Helguera, P., Coskun, P., Busciglio, J., 2010. A role for thrombospondin-1 deficits in astrocyte-mediated spine and synaptic pathology in Down's syndrome. PLoS One 5, e14200. https://doi.org/10.1371/journal.pone.0014200

Garcia-Manteiga, J.M., D'Alessandro, R., Meldolesi, J., 2019. News about the Role of the Transcription Factor REST in Neurons: From Physiology to Pathology. Int J Mol Sci 21, 235. https://doi.org/10.3390/ijms21010235

Gardner, R.J.Mk., Sutherland, G.R., Shaffer, L.G., 2012. Chromosome Abnormalities and Genetic Counseling. Oxford University Press, USA.

Gawlik-Kotelnicka, O., Mielicki, W., Rabe-Jabłońska, J., Strzelecki, D., 2016. Impact of lithium alone or in combination with haloperidol on selected oxidative stress parameters in human plasma in vitro. Redox Report 21, 45–49. https://doi.org/10.1179/1351000215Y.0000000030

Ghanaatfar, F., Ghanaatfar, A., Isapour, P., Farokhi, N., Bozorgniahosseini, S., Javadi, M., Gholami, M., Ulloa, L., Coleman-Fuller, N., Motaghinejad, M., 2023. Is lithium neuroprotective? An updated mechanistic illustrated review. Fundamental & Clinical Pharmacology 37, 4–30. https://doi.org/10.1111/fcp.12826

Giffin-Rao, Y., Sheng, J., Strand, B., Xu, K., Huang, L., Medo, M., Risgaard, K.A., Dantinne, S., Mohan, S., Keshan, A., Daley, R.A., Levesque, B., Amundson, L., Reese, R., Sousa, A.M.M., Tao, Y., Wang, D., Zhang, S.-C., Bhattacharyya, A., 2022. Altered patterning of trisomy 21 interneuron progenitors. Stem Cell Reports 17, 1366–1379. https://doi.org/10.1016/j.stemcr.2022.05.001

Giffin-Rao, Y., Strand, B., Medo, M., Keshan, A., Daley, R.A., Mohan, S., Dantienne, S., Levesque, B., Amundson, L., Huang, L., Reese, R., Wang, D., Zhang, S.-C., Bhattacharyya, A., 2020. Altered patterning of interneuron progenitors in Down syndrome. https://doi.org/10.1101/2020.02.18.951756

Girgrah, N., Letarte, M., Becker, L.E., Cruz, T.F., Theriault, E., Moscarello, M.A., 1991. Localization of the CD44 glycoprotein to fibrous astrocytes in normal white matter and to reactive astrocytes in active lesions in multiple sclerosis. J Neuropathol Exp Neurol 50, 779–792. https://doi.org/10.1097/00005072-199111000-00009

Glasson, E., Sullivan, S., Hussain, R., Petterson, B., Montgomery, P., Bittles, A., 2002. The changing survival profile of people with Down's syndrome: implications for genetic counselling. Clinical Genetics 62, 390–393. https://doi.org/10.1034/j.1399-0004.2002.620506.x

© COPYRIGHT UPM

Gomez-Arboledas, A., Davila, J.C., Sanchez-Mejias, E., Navarro, V., Nuñez-Diaz, C., Sanchez-Varo, R., Sanchez-Mico, M.V., Trujillo-Estrada, L., Fernandez-Valenzuela, J.J., Vizuete, M., Comella, J.X., Galea, E., Vitorica, J., Gutierrez, A., 2018. Phagocytic clearance of presynaptic dystrophies by reactive astrocytes in Alzheimer's disease. Glia 66, 637–653. https://doi.org/10.1002/glia.23270

Gómez-Sintes, R., Lucas, J.J., 2010. NFAT/Fas signaling mediates the neuronal apoptosis and motor side effects of GSK-3 inhibition in a mouse model of lithium therapy. J Clin Invest 120, 2432–2445. https://doi.org/10.1172/JCI37873

Gonzales, P.K., Roberts, C.M., Fonte, V., Jacobsen, C., Stein, G.H., Link, C.D., 2018. Transcriptome analysis of genetically matched human induced pluripotent stem cells disomic or trisomic for chromosome 21. PLoS One 13, e0194581. https://doi.org/10.1371/journal.pone.0194581

Gordon, A., Yoon, S.-J., Tran, S.S., Makinson, C.D., Park, J.Y., Andersen, J., Valencia, A.M., Horvath, S., Xiao, X., Huguenard, J.R., Pașca, S.P., Geschwind, D.H., 2021. Long-term maturation of human cortical organoids matches key early postnatal transitions. Nat Neurosci 24, 331–342. https://doi.org/10.1038/s41593-021-00802-y

Gorski, K., Spoljaric, A., Nyman, T.A., Kaila, K., Battersby, B.J., Lehesjoki, A.-E., 2020. Quantitative Changes in the Mitochondrial Proteome of Cerebellar Synaptosomes From Preclinical Cystatin B-Deficient Mice. Front Mol Neurosci 13, 570640. https://doi.org/10.3389/fnmol.2020.570640

Grandbarbe, L., Bouissac, J., Rand, M., Hrabé de Angelis, M., Artavanis-Tsakonas, S., Mohier, E., 2003. Delta-Notch signaling controls the generation of neurons/glia from neural stem cells in a stepwise process. Development 130, 1391–1402. https://doi.org/10.1242/dev.00374

Green, H.F., Nolan, Y.M., 2012. GSK-3 mediates the release of IL-1β, TNF-α and IL-10 from cortical glia. Neurochem Int 61, 666–671. https://doi.org/10.1016/j.neuint.2012.07.003

Greenway, D.J., Street, M., Jeffries, A., Buckley, N.J., 2007. RE1 Silencing Transcription Factor Maintains a Repressive Chromatin Environment in Embryonic Hippocampal Neural Stem Cells. Stem Cells 25, 354–363. https://doi.org/10.1634/stemcells.2006-0207

Gufran, K., Alqutaym, O.S., Alqahtani, A.A.M., Alqarni, A.M., Hattan, E.A.E., Alqahtani, R.O., 2019. Prevalence of Dental Caries and Periodontal Status among Down's Syndrome Population in Riyadh City. Journal of Pharmacy and Bioallied Sciences 11, S252. https://doi.org/10.4103/JPBS.JPBS_2_19

Guidi, S., Bonasoni, P., Ceccarelli, C., Santini, D., Gualtieri, F., Ciani, E., Bartesaghi, R., 2008. Neurogenesis impairment and increased cell death reduce total neuron number in the hippocampal region of fetuses with Down syndrome.

© COPYRIGHT UPM

Brain Pathol 18, 180–197. https://doi.org/10.1111/j.1750-3639.2007.00113.x

Guidi, S., Ciani, E., Bonasoni, P., Santini, D., Bartesaghi, R., 2011. Widespread proliferation impairment and hypocellularity in the cerebellum of fetuses with down syndrome. Brain Pathol 21, 361–373. https://doi.org/10.1111/j.1750-3639.2010.00459.x

Guidi, S., Giacomini, A., Stagni, F., Emili, M., Uguagliati, B., Bonasoni, M.P., Bartesaghi, R., 2018. Abnormal development of the inferior temporal region in fetuses with Down syndrome. Brain Pathol 28, 986–998. https://doi.org/10.1111/bpa.12605

Guo, H., Fan, Z., Wang, S., Ma, L., Wang, J., Yu, D., Zhang, Z., Wu, L., Peng, Z., Liu, W., Hou, W., Cai, Y., 2021. Astrocytic A1/A2 paradigm participates in glycogen mobilization mediated neuroprotection on reperfusion injury after ischemic stroke. Journal of Neuroinflammation 18, 230. https://doi.org/10.1186/s12974-021-02284-y

Guo, S., Arai, K., Stins, M.F., Chuang, D.-M., Lo, E.H., 2009. Lithium upregulates vascular endothelial growth factor in brain endothelial cells and astrocytes. Stroke 40, 652–655. https://doi.org/10.1161/STROKEAHA.108.524504

Gutiérrez-Hoya, A., Soto-Cruz, I., 2020. Role of the JAK/STAT Pathway in Cervical Cancer: Its Relationship with HPV E6/E7 Oncoproteins. Cells 9, 2297. https://doi.org/10.3390/cells9102297

Habib, N., Avraham-Davidi, I., Basu, A., Burks, T., Shekhar, K., Hofree, M., Choudhury, S.R., Aguet, F., Gelfand, E., Ardlie, K., Weitz, D.A., Rozenblatt-Rosen, O., Zhang, F., Regev, A., 2017. Massively parallel single-nucleus RNA-seq with DroNc-seq. Nat Methods 14, 955–958. https://doi.org/10.1038/nmeth.4407

Halevy, T., Biancotti, J.-C., Yanuka, O., Golan-Lev, T., Benvenisty, N., 2016. Molecular Characterization of Down Syndrome Embryonic Stem Cells Reveals a Role for RUNX1 in Neural Differentiation. Stem Cell Reports 7, 777–786. https://doi.org/10.1016/j.stemcr.2016.08.003

Hamby, M.E., Sofroniew, M.V., 2010. Reactive astrocytes as therapeutic targets for CNS disorders. Neurotherapeutics 7, 494–506. https://doi.org/10.1016/j.nurt.2010.07.003

Hastings, J.F., Skhinas, J.N., Fey, D., Croucher, D.R., Cox, T.R., 2019. The extracellular matrix as a key regulator of intracellular signalling networks. Br J Pharmacol 176, 82–92. https://doi.org/10.1111/bph.14195

Hayashi, M., Nomoto, S., Hishida, M., Inokawa, Y., Kanda, M., Okamura, Y., Nishikawa, Y., Tanaka, C., Kobayashi, D., Yamada, S., Nakayama, G., Fujii, T., Sugimoto, H., Koike, M., Fujiwara, M., Takeda, S., Kodera, Y., 2014. Identification of the collagen type 1 alpha 1 gene (COL1A1) as a candidate survival-related factor associated with hepatocellular carcinoma. BMC Cancer 14, 108. https://doi.org/10.1186/1471-2407-14-108

© COPYRIGHT UPM

He, F., Ge, W., Martinowich, K., Becker-Catania, S., Coskun, V., Zhu, W., Wu, H., Castro, D., Guillemot, F., Fan, G., de Vellis, J., Sun, Y.E., 2005. A positive autoregulatory loop of Jak-STAT signaling controls the onset of astrogliogenesis. Nat Neurosci 8, 616–625. https://doi.org/10.1038/nn1440

Hedges, E.C., Mehler, V.J., Nishimura, A.L., 2016. The Use of Stem Cells to Model Amyotrophic Lateral Sclerosis and Frontotemporal Dementia: From Basic Research to Regenerative Medicine. Stem Cells International 2016, e9279516. https://doi.org/10.1155/2016/9279516

Helguera, P., Seiglie, J., Rodriguez, J., Hanna, M., Helguera, G., Busciglio, J., 2013. Adaptive downregulation of mitochondrial function in down syndrome. Cell Metab 17, 132–140. https://doi.org/10.1016/j.cmet.2012.12.005

Herrmann, J.E., Imura, T., Song, B., Qi, J., Ao, Y., Nguyen, T.K., Korsak, R.A., Takeda, K., Akira, S., Sofroniew, M.V., 2008. STAT3 is a Critical Regulator of Astrogliosis and Scar Formation after Spinal Cord Injury. J. Neurosci. 28, 7231–7243. https://doi.org/10.1523/JNEUROSCI.1709-08.2008

Hertz, L., Song, D., Li, B., Du, T., Xu, J., Gu, L., Chen, Y., Peng, L., 2014. Signal Transduction in Astrocytes during Chronic or Acute Treatment with Drugs (SSRIs, Antibipolar Drugs, GABA-ergic Drugs, and Benzodiazepines) Ameliorating Mood Disorders. Journal of Signal Transduction 2014, e593934. https://doi.org/10.1155/2014/593934

Hibaoui, Y., Grad, I., Letourneau, A., Sailani, M.R., Dahoun, S., Santoni, F.A., Gimelli, S., Guipponi, M., Pelte, M.F., Béna, F., Antonarakis, S.E., Feki, A., 2014. Modelling and rescuing neurodevelopmental defect of Down syndrome using induced pluripotent stem cells from monozygotic twins discordant for trisomy 21. EMBO Mol Med 6, 259–277. https://doi.org/10.1002/emmm.201302848

Hirabayashi, Y., Itoh, Y., Tabata, H., Nakajima, K., Akiyama, T., Masuyama, N., Gotoh, Y., 2004. The Wnt/beta-catenin pathway directs neuronal differentiation of cortical neural precursor cells. Development 131, 2791–2801. https://doi.org/10.1242/dev.01165

Hirata, K., Nambara, T., Kawatani, K., Nawa, N., Yoshimatsu, H., Kusakabe, H., Banno, K., Nishimura, K., Ohtaka, M., Nakanishi, M., Taniguchi, H., Arahori, H., Wada, K., Ozono, K., Kitabatake, Y., 2020. 4-Phenylbutyrate ameliorates apoptotic neural cell death in Down syndrome by reducing protein aggregates. Sci Rep 10, 14047. https://doi.org/10.1038/s41598-020-70362-x

Hoe, T.S., Boo, N.Y., Clyde, M.M., 1989. Incidence of Down's syndrome in a large Malaysian maternity hospital over an 18 month period. Singapore Med J 30, 246–248.

Honda, M., Nakashima, K., Katada, S., 2017. PRMT1 regulates astrocytic differentiation of embryonic neural stem/precursor cells. J Neurochem 142, 901–907. https://doi.org/10.1111/jnc.14123

© COPYRIGHT UPM

Hong, S., Song, M.-R., 2014. STAT3 but not STAT1 is required for astrocyte differentiation. PLoS One 9, e86851. https://doi.org/10.1371/journal.pone.0086851

Hou, Q., Le, W., Kan, S., Shi, J., Lang, Y., Liu, Z., Chen, Z., 2021. Nuclear Receptor Interacting Protein-2 Mediates the Stabilization and Activation of β-Catenin During Podocyte Injury. Front. Cell Dev. Biol. 9. https://doi.org/10.3389/fcell.2021.781792

Huang, T., Fakurazi, S., Cheah, P.-S., Ling, K.-H., 2023. REST Targets JAK–STAT and HIF-1 Signaling Pathways in Human Down Syndrome Brain and Neural Cells. IJMS 24, 9980. https://doi.org/10.3390/ijms24129980

Hubler, Z., Allimuthu, D., Bederman, I., Elitt, M.S., Madhavan, M., Allan, K.C., Shick, H.E., Garrison, E., T Karl, M., Factor, D.C., Nevin, Z.S., Sax, J.L., Thompson, M.A., Fedorov, Y., Jin, J., Wilson, W.K., Giera, M., Bracher, F., Miller, R.H., Tesar, P.J., Adams, D.J., 2018. Accumulation of 8,9-unsaturated sterols drives oligodendrocyte formation and remyelination. Nature 560, 372–376. https://doi.org/10.1038/s41586-018-0360-3

Huo, H.-Q., Qu, Z.-Y., Yuan, F., Ma, L., Yao, L., Xu, M., Hu, Y., Ji, J., Bhattacharyya, A., Zhang, S.-C., Liu, Y., 2018. Modeling Down Syndrome with Patient iPSCs Reveals Cellular and Migration Deficits of GABAergic Neurons. Stem Cell Reports 10, 1251–1266. https://doi.org/10.1016/j.stemcr.2018.02.001

Hwang, I.K., Yoo, K.-Y., Yi, S.S., Kwon, Y.-G., Ahn, Y.-K., Seong, J.K., Lee, I.S., Yoon, Y.S., Won, M.-H., 2008. Age-related differentiation in newly generated DCX immunoreactive neurons in the subgranular zone of the gerbil dentate gyrus. Neurochem Res 33, 867–872. https://doi.org/10.1007/s11064-007-9528-1

Hwang, J.-Y., Zukin, R.S., 2018. REST, a master transcriptional regulator in neurodegenerative disease. Curr Opin Neurobiol 48, 193–200. https://doi.org/10.1016/j.conb.2017.12.008

Imayoshi, I., Isomura, A., Harima, Y., Kawaguchi, K., Kori, H., Miyachi, H., Fujiwara, T., Ishidate, F., Kageyama, R., 2013. Oscillatory control of factors determining multipotency and fate in mouse neural progenitors. Science 342, 1203–1208. https://doi.org/10.1126/science.1242366

Imayoshi, I., Sakamoto, M., Yamaguchi, M., Mori, K., Kageyama, R., 2010. Essential roles of Notch signaling in maintenance of neural stem cells in developing and adult brains. J Neurosci 30, 3489–3498. https://doi.org/10.1523/JNEUROSCI.4987-09.2010

Inada, M., Xu, H., Takeuchi, M., Ito, M., Chen, M., 2021. Microglia increase tight-junction permeability in coordination with Müller cells under hypoxic condition in an in vitro model of inner blood-retinal barrier. Experimental Eye Research 205, 108490. https://doi.org/10.1016/j.exer.2021.108490

© COPYRIGHT UPM

Inui, K., Zhao, Z., Yuan, J., Jayaprakash, S., Le, L.T.M., Drakulic, S., Sander, B., Golas, M.M., 2017. Stepwise assembly of functional C-terminal REST/NRSF transcriptional repressor complexes as a drug target. Protein Science 26, 997–1011. https://doi.org/10.1002/pro.3142

Ioannou, M.S., Jackson, J., Sheu, S.-H., Chang, C.-L., Weigel, A.V., Liu, H., Pasolli, H.A., Xu, C.S., Pang, S., Matthies, D., Hess, H.F., Lippincott-Schwartz, J., Liu, Z., 2019. Neuron-Astrocyte Metabolic Coupling Protects against Activity-Induced Fatty Acid Toxicity. Cell 177, 1522-1535.e14. https://doi.org/10.1016/j.cell.2019.04.001

Ito, D., Okano, H., Suzuki, N., 2012. Accelerating progress in induced pluripotent stem cell research for neurological diseases. Annals of Neurology 72, 167–174. https://doi.org/10.1002/ana.23596

Iwasaki, H., Kovacic, J.C., Olive, M., Beers, J.K., Yoshimoto, T., Crook, M.F., Tonelli, L.H., Nabel, E.G., 2010. Disruption of Protein Arginine N-Methyltransferase 2 regulates leptin signaling and produces leanness in vivo through loss of STAT3 methylation. Circ Res 107, 992–1001. https://doi.org/10.1161/CIRCRESAHA.110.225326

Izsak, J., Vizlin-Hodzic, D., Iljin, M., Strandberg, J., Jadasz, J., Olsson Bontell, T., Theiss, S., Hanse, E., Ågren, H., Funa, K., Illes, S., 2020. TGF-β1 Suppresses Proliferation and Induces Differentiation in Human iPSC Neural in vitro Models. Front Cell Dev Biol 8, 571332. https://doi.org/10.3389/fcell.2020.571332

Jin, Z., El-Deiry, W.S., 2005. Overview of cell death signaling pathways. Cancer Biol Ther 4, 139–163. https://doi.org/10.4161/cbt.4.2.1508

Joensuu, T., Tegelberg, S., Reinmaa, E., Segerstråle, M., Hakala, P., Pehkonen, H., Korpi, E.R., Tyynelä, J., Taira, T., Hovatta, I., Kopra, O., Lehesjoki, A.-E., 2014. Gene expression alterations in the cerebellum and granule neurons of Cstb(-/-) mouse are associated with early synaptic changes and inflammation. PLoS One 9, e89321. https://doi.org/10.1371/journal.pone.0089321

Johnson, R., Gamblin, R.J., Ooi, L., Bruce, A.W., Donaldson, I.J., Westhead, D.R., Wood, I.C., Jackson, R.M., Buckley, N.J., 2006. Identification of the REST regulon reveals extensive transposable element-mediated binding site duplication. Nucleic Acids Res 34, 3862–3877. https://doi.org/10.1093/nar/gkl525

Johnson, R., Teh, C.H., Kunarso, G., Wong, K.Y., Srinivasan, G., Cooper, M.L., Volta, M., Chan, S.S., Lipovich, L., Pollard, S.M., Karuturi, R.K.M., Wei, C., Buckley, N.J., Stanton, L.W., 2008. REST regulates distinct transcriptional networks in embryonic and neural stem cells. PLoS Biol 6, e256. https://doi.org/10.1371/journal.pbio.0060256

Joseph, K., Teja, G.R., Srinivas, M., 2022. Study of the clinical features of Downs's syndrome and relation between dermatoglyphics and congenital heart disease if any. International journal of health sciences 10922–10941.

© COPYRIGHT IPM

https://doi.org/10.53730/ijhs.v6nS5.10965

Kaasik, A., Kuum, M., Aonurm, A., Kalda, A., Vaarmann, A., Zharkovsky, A., 2007. Seizures, ataxia, and neuronal loss in cystatin B heterozygous mice. Epilepsia 48, 752–757. https://doi.org/10.1111/j.1528-1167.2007.00985.x

Kalovidouris, S.A., Gama, C.I., Lee, L.W., Hsieh-Wilson, L.C., 2005. A role for fucose alpha(1-2) galactose carbohydrates in neuronal growth. J Am Chem Soc 127, 1340–1341. https://doi.org/10.1021/ja044631v

Kamal, M.M., Sathyan, P., Singh, S.K., Zinn, P.O., Marisetty, A.L., Liang, S., Gumin, J., El - Mesallamy, H.O., Suki, D., Colman, H., Fuller, G.N., Lang, F.F., Majumder, S., 2012. REST Regulates Oncogenic Properties of Glioblastoma Stem Cells. Stem Cells 30, 405–414. https://doi.org/10.1002/stem.1020

Kaneb, H.M., Folkmann, A.W., Belzil, V.V., Jao, L.-E., Leblond, C.S., Girard, S.L., Daoud, H., Noreau, A., Rochefort, D., Hince, P., Szuto, A., Levert, A., Vidal, S., André-Guimont, C., Camu, W., Bouchard, J.-P., Dupré, N., Rouleau, G.A., Wente, S.R., Dion, P.A., 2015. Deleterious mutations in the essential mRNA metabolism factor, hGle1, in amyotrophic lateral sclerosis. Hum Mol Genet 24, 1363–1373. https://doi.org/10.1093/hmg/ddu545

Kanehisa, M., Goto, S., 2000. KEGG: kyoto encyclopedia of genes and genomes. Nucleic Acids Res 28, 27–30. https://doi.org/10.1093/nar/28.1.27

Kang, H.J., Kawasawa, Y.I., Cheng, F., Zhu, Y., Xu, X., Li, M., Sousa, A.M.M., Pletikos, M., Meyer, K.A., Sedmak, G., Guennel, T., Shin, Y., Johnson, M.B., Krsnik, Z., Mayer, S., Fertuzinhos, S., Umlauf, S., Lisgo, S.N., Vortmeyer, A., Weinberger, D.R., Mane, S., Hyde, T.M., Huttner, A., Reimers, M., Kleinman, J.E., Sestan, N., 2011. Spatio-temporal transcriptome of the human brain. Nature 478, 483–489. https://doi.org/10.1038/nature10523

Kang, J., Wu, J., 2021. The trends in maternal age distribution and the estimated live birth and population prevalence of Down's syndrome in China: 1985-2012. https://doi.org/10.1101/2021.04.05.21254264

Kawamura, M., Sato, S., Matsumoto, G., Fukuda, T., Shiba-Fukushima, K., Noda, S., Takanashi, M., Mori, N., Hattori, N., 2019. Loss of nuclear REST/NRSF in aged-dopaminergic neurons in Parkinson's disease patients. Neurosci Lett 699, 59–63. https://doi.org/10.1016/j.neulet.2019.01.042

Kawatani, K., Nambara, T., Nawa, N., Yoshimatsu, H., Kusakabe, H., Hirata, K., Tanave, A., Sumiyama, K., Banno, K., Taniguchi, H., Arahori, H., Ozono, K., Kitabatake, Y., 2021. A human isogenic iPSC-derived cell line panel identifies major regulators of aberrant astrocyte proliferation in Down syndrome. Commun Biol 4, 1–15. https://doi.org/10.1038/s42003-021-02242-7

Khakh, B.S., Deneen, B., 2019. The Emerging Nature of Astrocyte Diversity. Annual Review of Neuroscience 42, 187–207. https://doi.org/10.1146/annurev-neuro-070918-050443

Khayachi, A., Ase, A., Liao, C., Kamesh, A., Kuhlmann, N., Schorova, L., Chaumette, B., Dion, P., Alda, M., Séguéla, P., Rouleau, G., Milnerwood, A., 2021. Chronic lithium treatment alters the excitatory/inhibitory balance of synaptic networks and reduces mGluR5–PKC signalling in mouse cortical neurons. Journal of Psychiatry and Neuroscience 46, E402–E414. https://doi.org/10.1503/jpn.200185

Kim, I.S., Lee, M., Park, K.C., Jeon, Y., Park, J.H., Hwang, E.J., Jeon, T.I., Ko, S., Lee, H., Baek, S.H., Kim, K.I., 2012. Roles of Mis18α in epigenetic regulation of centromeric chromatin and CENP-A loading. Mol Cell 46, 260–273. https://doi.org/10.1016/j.molcel.2012.03.021

Kim, Y.-H., Rane, A., Lussier, S., Andersen, J.K., 2011. Lithium protects against oxidative stress-mediated cell death in α-synuclein-overexpressing in vitro and in vivo models of Parkinson's disease. Journal of Neuroscience Research 89, 1666–1675. https://doi.org/10.1002/jnr.22700

Kinboshi, M., Ikeda, A., Ohno, Y., 2020. Role of Astrocytic Inwardly Rectifying Potassium (Kir) 4.1 Channels in Epileptogenesis. Frontiers in Neurology 11.

King, A., Szekely, B., Calapkulu, E., Ali, H., Rios, F., Jones, S., Troakes, C., 2020. The Increased Densities, But Different Distributions, of Both C3 and S100A10 Immunopositive Astrocyte-Like Cells in Alzheimer's Disease Brains Suggest Possible Roles for Both A1 and A2 Astrocytes in the Disease Pathogenesis. Brain Sciences 10, 503. https://doi.org/10.3390/brainsci10080503

Kirby, E.D., Kuwahara, A.A., Messer, R.L., Wyss-Coray, T., 2015. Adult hippocampal neural stem and progenitor cells regulate the neurogenic niche by secreting VEGF. Proc Natl Acad Sci U S A 112, 4128–4133. https://doi.org/10.1073/pnas.1422448112

Klein, J.A., Li, Z., Rampam, S., Cardini, J., Ayoub, A., Shaw, P., Rachubinski, A.L., Espinosa, J.M., Zeldich, E., Haydar, T.F., 2022. Sonic Hedgehog Pathway Modulation Normalizes Expression of Olig2 in Rostrally Patterned NPCs With Trisomy 21. Front. Cell. Neurosci. 15. https://doi.org/10.3389/fncel.2021.794675

Knotek, T., Janeckova, L., Kriska, J., Korinek, V., Anderova, M., 2020. Glia and Neural Stem and Progenitor Cells of the Healthy and Ischemic Brain: The Workplace for the Wnt Signaling Pathway. Genes 11, 804. https://doi.org/10.3390/genes11070804

Kochlamazashvili, G., Henneberger, C., Bukalo, O., Dvoretskova, E., Senkov, O., Lievens, P.M.-J., Westenbroek, R., Engel, A.K., Catterall, W.A., Rusakov, D.A., Schachner, M., Dityatev, A., 2010. The Extracellular Matrix Molecule Hyaluronic Acid Regulates Hippocampal Synaptic Plasticity by Modulating Postsynaptic L-Type Ca2+ Channels. Neuron 67, 116–128. https://doi.org/10.1016/j.neuron.2010.05.030

Kohyama, J., Sanosaka, T., Tokunaga, A., Takatsuka, E., Tsujimura, K., Okano, H., Nakashima, K., 2010. BMP-induced REST regulates the establishment and

© COPYRIGHT UPM

maintenance of astrocytic identity. Journal of Cell Biology 189, 159–170. https://doi.org/10.1083/jcb.200908048

Koizumi, H., Higginbotham, H., Poon, T., Tanaka, T., Brinkman, B.C., Gleeson, J.G., 2006. Doublecortin maintains bipolar shape and nuclear translocation during migration in the adult forebrain. Nat Neurosci 9, 779–786. https://doi.org/10.1038/nn1704

Kolmykov, S., Yevshin, I., Kulyashov, M., Sharipov, R., Kondrakhin, Y., Makeev, V.J., Kulakovskiy, I.V., Kel, A., Kolpakov, F., 2021. GTRD: an integrated view of transcription regulation. Nucleic Acids Research 49, D104–D111. https://doi.org/10.1093/nar/gkaa1057

Kong, Q.-R., Xie, B.-T., Zhang, H., Li, J.-Y., Huang, T.-Q., Wei, R.-Y., Liu, Z.-H., 2016. RE1-silencing Transcription Factor (REST) Is Required for Nuclear Reprogramming by Inhibiting Transforming Growth Factor β Signaling Pathway *. Journal of Biological Chemistry 291, 27334–27342. https://doi.org/10.1074/jbc.M116.743849

Kong, X., Gong, Z., Zhang, L., Sun, X., Ou, Z., Xu, B., Huang, J., Long, D., He, X., Lin, X., Li, Q., Xu, L., Xuan, A., 2019. JAK2/STAT3 signaling mediates IL-6-inhibited neurogenesis of neural stem cells through DNA demethylation/methylation. Brain Behav Immun 79, 159–173. https://doi.org/10.1016/j.bbi.2019.01.027

Krivega, M., Stiefel, C.M., Karbassi, S., Andersen, L.L., Chunduri, N.K., Donnelly, N., Pichlmair, A., Storchová, Z., 2021. Genotoxic stress in constitutive trisomies induces autophagy and the innate immune response via the cGAS-STING pathway. Commun Biol 4, 1–16. https://doi.org/10.1038/s42003-021-02278-9

Krivega, M., Stiefel, C.M., Storchova, Z., 2022. Consequences of chromosome gain: A new view on trisomy syndromes. The American Journal of Human Genetics 109, 2126–2140. https://doi.org/10.1016/j.ajhg.2022.10.014

Krivega, M., Storchova, Z., 2023. Consequences of trisomy syndromes – 21 and beyond. Trends in Genetics 39, 172–174. https://doi.org/10.1016/j.tig.2022.11.004

Kurabayashi, N., Nguyen, M.D., Sanada, K., 2015. DYRK1A overexpression enhances STAT activity and astrogliogenesis in a Down syndrome mouse model. EMBO Rep 16, 1548–1562. https://doi.org/10.15252/embr.201540374

Kuwahara, A., Hirabayashi, Y., Knoepfler, P.S., Taketo, M.M., Sakai, J., Kodama, T., Gotoh, Y., 2010. Wnt signaling and its downstream target N-myc regulate basal progenitors in the developing neocortex. Development 137, 1035–1044. https://doi.org/10.1242/dev.046417

Kwak, J.H., Lee, S.W., Cha, H.R., Huh, J., Kang, I.-S., Jun, T.-G., Yang, J.-H., Han, M.Y., Song, J., 2022. Long-Term Observational Outcomes after Total Correction of Congenital Heart Disease in Korean Patients with Down

© COPYRIGHT UPM

Syndrome: A National Cohort Study. Children (Basel) 9, 1329. https://doi.org/10.3390/children9091329

Lam, X.-J., Maniam, S., Cheah, P.-S., Ling, K.-H., 2023. REST in the Road Map of Brain Development. Cell Mol Neurobiol 43, 3417–3433. https://doi.org/10.1007/s10571-023-01394-w

Lam, X.-J., Maniam, S., Ling, K.-H., Cheah, P.-S., 2025. Lithium restores nuclear REST and Mitigates oxidative stress in down syndrome iPSC-Derived neurons. Neuroscience 567, 86–95. https://doi.org/10.1016/j.neuroscience.2024.12.061

Lancaster, M.A., Renner, M., Martin, C.-A., Wenzel, D., Bicknell, L.S., Hurles, M.E., Homfray, T., Penninger, J.M., Jackson, A.P., Knoblich, J.A., 2013. Cerebral organoids model human brain development and microcephaly. Nature 501, 373–379. https://doi.org/10.1038/nature12517

Lange, C., Huttner, W.B., Calegari, F., 2009. Cdk4/CyclinD1 Overexpression in Neural Stem Cells Shortens G1, Delays Neurogenesis, and Promotes the Generation and Expansion of Basal Progenitors. Cell Stem Cell 5, 320–331. https://doi.org/10.1016/j.stem.2009.05.026

Lashgari, N.-A., Roudsari, N.M., Momtaz, S., Sathyapalan, T., Abdolghaffari, A.H., Sahebkar, A., 2021. The involvement of JAK/STAT signaling pathway in the treatment of Parkinson's disease. J Neuroimmunol 361, 577758. https://doi.org/10.1016/j.jneuroim.2021.577758

Lee, H.-C., Md Yusof, H.H., Leong, M.P.-Y., Zainal Abidin, S., Seth, E.A., Hewitt, C.A., Vidyadaran, S., Nordin, N., Scott, H.S., Cheah, P.-S., Ling, K.-H., 2019. Gene and protein expression profiles of JAK-STAT signalling pathway in the developing brain of the Ts1Cje down syndrome mouse model. Int J Neurosci 129, 871–881. https://doi.org/10.1080/00207454.2019.1580280

Lee, H.-C., Tan, K.-L., Cheah, P.-S., Ling, K.-H., 2016. Potential Role of JAK-STAT Signaling Pathway in the Neurogenic-to-Gliogenic Shift in Down Syndrome Brain. Neural Plast 2016, 7434191. https://doi.org/10.1155/2016/7434191

Lee, J.A., Hall, B., Allsop, J., Alqarni, R., Allen, S.P., 2021. Lipid metabolism in astrocytic structure and function. Seminars in Cell & Developmental Biology 112, 123–136. https://doi.org/10.1016/j.semcdb.2020.07.017

Lepagnol-Bestel, A.-M., Maussion, G., Ramoz, N., Moalic, J.-M., Gorwood, P., Simonneau, M., 2007. Nrsf silencing induces molecular and subcellular changes linked to neuronal plasticity. NeuroReport 18, 441. https://doi.org/10.1097/WNR.0b013e328011dc81

Letourneau, A., Santoni, F.A., Bonilla, X., Sailani, M.R., Gonzalez, D., Kind, J., Chevalier, C., Thurman, R., Sandstrom, R.S., Hibaoui, Y., Garieri, M., Popadin, K., Falconnet, E., Gagnebin, M., Gehrig, C., Vannier, A., Guipponi, M., Farinelli, L., Robyr, D., Migliavacca, E., Borel, C., Deutsch, S., Feki, A., Stamatoyannopoulos, J.A., Herault, Y., van Steensel, B., Guigo, R., Antonarakis, S.E., 2014. Domains of genome-wide gene expression

© COPYRIGHT UPM

dysregulation in Down's syndrome. Nature 508, 345–350. https://doi.org/10.1038/nature13200

Lewis, E.M.A., Kaushik, K., Sandoval, L.A., Antony, I., Dietmann, S., Kroll, K.L., 2021. Epigenetic regulation during human cortical development: Seq-ing answers from the brain to the organoid. Neurochem Int 147, 105039. https://doi.org/10.1016/j.neuint.2021.105039

Li, B., Jia, S., Yue, T., Yang, L., Huang, C., Verkhratsky, A., Peng, L., 2017. Biphasic Regulation of Caveolin-1 Gene Expression by Fluoxetine in Astrocytes: Opposite Effects of PI3K/AKT and MAPK/ERK Signaling Pathways on c-fos. Front Cell Neurosci 11, 335. https://doi.org/10.3389/fncel.2017.00335

Li, H., Liu, Z., Wu, Y., Chen, Y., Wang, J., Wang, Z., Huang, D., Wang, M., Yu, M., Fei, J., Huang, F., 2020. The deficiency of NRSF/REST enhances the pro-inflammatory function of astrocytes in a model of Parkinson's disease. Biochim Biophys Acta Mol Basis Dis 1866, 165590. https://doi.org/10.1016/j.bbadis.2019.165590

Li, K., Li, J., Zheng, J., Qin, S., 2019. Reactive Astrocytes in Neurodegenerative Diseases. Aging Dis 10, 664–675. https://doi.org/10.14336/AD.2018.0720

Li, X., Tao, Yezheng, Bradley, R., Du, Z., Tao, Yunlong, Kong, L., Dong, Y., Jones, J., Yan, Y., Harder, C.R.K., Friedman, L.M., Bilal, M., Hoffmann, B., Zhang, S.-C., 2018. Fast Generation of Functional Subtype Astrocytes from Human Pluripotent Stem Cells. Stem Cell Reports 11, 998–1008. https://doi.org/10.1016/j.stemcr.2018.08.019

Li, Z., Klein, J.A., Rampam, S., Kurzion, R., Campbell, N.B., Patel, Y., Haydar, T.F., Zeldich, E., 2022. Asynchronous excitatory neuron development in an isogenic cortical spheroid model of Down syndrome. Front. Neurosci. 16. https://doi.org/10.3389/fnins.2022.932384

Liddelow, S.A., Barres, B.A., 2017. Reactive Astrocytes: Production, Function, and Therapeutic Potential. Immunity 46, 957–967. https://doi.org/10.1016/j.immuni.2017.06.006

Lim, C.-T., Lam, X.-J., Crystal, A.-A., Huang, T., Jusoh, N., Cheah, P.-S., Ling, K.-H., 2024. Reduced REST Expression in Neural Progenitor Cells, Adult Cortex, and Impaired REST Nuclear Translocation in the Prefrontal Cortex of Ts1Cje Mouse Model of Down Syndrome. Neurochem. J. 18, 147–161. https://doi.org/10.1134/S1819712424010148

Lindenhofer, D., Haendeler, S., Esk, C., Littleboy, J.B., Brunet Avalos, C., Naas, J., Pflug, F.G., van de Ven, E.G.P., Reumann, D., Baffet, A.D., von Haeseler, A., Knoblich, J.A., 2024. Cerebral organoids display dynamic clonal growth and tunable tissue replenishment. Nat Cell Biol 26, 710–718. https://doi.org/10.1038/s41556-024-01412-z

Lipscomb, B.W., Treloar, H.B., Klenoff, J., Greer, C.A., 2003. Cell surface carbohydrates and glomerular targeting of olfactory sensory neuron axons in

© COPYRIGHT UPM

the mouse. J Comp Neurol 467, 22–31. https://doi.org/10.1002/cne.10910

Liu, H., Wu, X., Luo, J., Wang, X., Guo, H., Feng, D., Zhao, L., Bai, H., Song, M., Liu, X., Guo, W., Li, X., Yue, L., Wang, B., Qu, Y., 2019. Pterostilbene Attenuates Astrocytic Inflammation and Neuronal Oxidative Injury After Ischemia-Reperfusion by Inhibiting NF-κB Phosphorylation. Frontiers in Immunology 10.

Liu, T., Li, Y., Xu, M., Huang, H., Luo, Y., 2024. PRMT2 silencing regulates macrophage polarization through activation of STAT1 or inhibition of STAT6. BMC Immunol 25, 1. https://doi.org/10.1186/s12865-023-00593-w

Liu, Y., Borel, C., Li, L., Müller, T., Williams, E.G., Germain, P.-L., Buljan, M., Sajic, T., Boersema, P.J., Shao, W., Faini, M., Testa, G., Beyer, A., Antonarakis, S.E., Aebersold, R., 2017. Systematic proteome and proteostasis profiling in human Trisomy 21 fibroblast cells. Nat Commun 8, 1212. https://doi.org/10.1038/s41467-017-01422-6

Liu, Y., Deng, W., 2016. Reverse engineering human neurodegenerative disease using pluripotent stem cell technology. Brain Research, The future of stem cells in neurodegenerative disease 1638, 30–41. https://doi.org/10.1016/j.brainres.2015.09.023

Liu, Y., Han, S.S.W., Wu, Y., Tuohy, T.M.F., Xue, H., Cai, J., Back, S.A., Sherman, L.S., Fischer, I., Rao, M.S., 2004. CD44 expression identifies astrocyte-restricted precursor cells. Developmental Biology 276, 31–46. https://doi.org/10.1016/j.ydbio.2004.08.018

Liu, Z., Osipovitch, M., Benraiss, A., Huynh, N.P.T., Foti, R., Bates, J., Chandler-Militello, D., Findling, R.L., Tesar, P.J., Nedergaard, M., Windrem, M.S., Goldman, S.A., 2019. Dysregulated Glial Differentiation in Schizophrenia May Be Relieved by Suppression of SMAD4- and REST-Dependent Signaling. Cell Reports 27, 3832-3843.e6. https://doi.org/10.1016/j.celrep.2019.05.088

Long, K.R., Huttner, W.B., 2022. The Role of the Extracellular Matrix in Neural Progenitor Cell Proliferation and Cortical Folding During Human Neocortex Development. Frontiers in Cellular Neuroscience 15, 804649.

Lu, J., Esposito, G., Scuderi, C., Steardo, L., Delli-Bovi, L.C., Hecht, J.L., Dickinson, B.C., Chang, C.J., Mori, T., Sheen, V., 2011. S100B and APP Promote a Gliocentric Shift and Impaired Neurogenesis in Down Syndrome Neural Progenitors. PLOS ONE 6, e22126. https://doi.org/10.1371/journal.pone.0022126

Lu, J., Lian, G., Zhou, H., Esposito, G., Steardo, L., Delli-Bovi, L.C., Hecht, J.L., Lu, Q.R., Sheen, V., 2012. OLIG2 over-expression impairs proliferation of human Down syndrome neural progenitors. Human Molecular Genetics 21, 2330–2340. https://doi.org/10.1093/hmg/dds052

Lu, M., Zheng, L., Han, B., Wang, L., Wang, P., Liu, H., Sun, X., 2011. REST regulates DYRK1A transcription in a negative feedback loop. J Biol Chem 286, 10755–

© COPYRIGHT UPM

10763. https://doi.org/10.1074/jbc.M110.174540

Lu, T., Aron, L., Zullo, J., Pan, Y., Kim, H., Chen, Y., Yang, T.-H., Kim, H.-M., Drake, D., Liu, X.S., Bennett, D.A., Colaiácovo, M.P., Yankner, B.A., 2014. REST and stress resistance in ageing and Alzheimer's disease. Nature 507, 448–454. https://doi.org/10.1038/nature13163

Luciano-Montalvo, C., Meléndez, L.M., 2009. Cystatin B associates with signal transducer and activator of transcription 1 in monocyte-derived and placental macrophages. Placenta 30, 464–467. https://doi.org/10.1016/j.placenta.2009.03.003

Luo, C., Lancaster, M.A., Castanon, R., Nery, J.R., Knoblich, J.A., Ecker, J.R., 2016. Cerebral Organoids Recapitulate Epigenomic Signatures of the Human Fetal Brain. Cell Rep 17, 3369–3384. https://doi.org/10.1016/j.celrep.2016.12.001

Luu-The, V., Paquet, N., Calvo, E., Cumps, J., 2005. Improved real-time RT-PCR method for high-throughput measurements using second derivative calculation and double correction. Biotechniques 38, 287–293. https://doi.org/10.2144/05382RR05

Maclean, G.A., Menne, T.F., Guo, G., Sanchez, D.J., Park, I.-H., Daley, G.Q., Orkin, S.H., 2012. Altered hematopoiesis in trisomy 21 as revealed through in vitro differentiation of isogenic human pluripotent cells. Proc Natl Acad Sci U S A 109, 17567–17572. https://doi.org/10.1073/pnas.1215468109

Madhavan, M., Nevin, Z.S., Shick, H.E., Garrison, E., Clarkson-Paredes, C., Karl, M., Clayton, B.L.L., Factor, D.C., Allan, K.C., Barbar, L., Jain, T., Douvaras, P., Fossati, V., Miller, R.H., Tesar, P.J., 2018. Induction of myelinating oligodendrocytes in human cortical spheroids. Nat Methods 15, 700–706. https://doi.org/10.1038/s41592-018-0081-4

Maher, K., Završnik, J., Jerič-Kokelj, B., Vasiljeva, O., Turk, B., Kopitar-Jerala, N., 2014. Decreased IL-10 expression in stefin B-deficient macrophages is regulated by the MAP kinase and STAT-3 signaling pathways. FEBS Lett 588, 720–726. https://doi.org/10.1016/j.febslet.2014.01.015

Mahmoud, S., Gharagozloo, M., Simard, C., Gris, D., 2019. Astrocytes Maintain Glutamate Homeostasis in the CNS by Controlling the Balance between Glutamate Uptake and Release. Cells 8, 184. https://doi.org/10.3390/cells8020184

Makarava, N., Mychko, O., Chang, J.C.-Y., Molesworth, K., Baskakov, I.V., 2021. The degree of astrocyte activation is predictive of the incubation time to prion disease. Acta Neuropathologica Communications 9, 87. https://doi.org/10.1186/s40478-021-01192-9

Mandel, G., Fiondella, C.G., Covey, M.V., Lu, D.D., Loturco, J.J., Ballas, N., 2011. Repressor element 1 silencing transcription factor (REST) controls radial migration and temporal neuronal specification during neocortical development. Proc Natl Acad Sci U S A 108, 16789–16794.

© COPYRIGHT UPM

https://doi.org/10.1073/pnas.1113486108

Mao, R., Wang, X., Spitznagel, E.L., Frelin, L.P., Ting, J.C., Ding, H., Kim, J., Ruczinski, I., Downey, T.J., Pevsner, J., 2005. Primary and secondary transcriptional effects in the developing human Down syndrome brain and heart. Genome Biol 6, R107. https://doi.org/10.1186/gb-2005-6-13-r107

Margiotta, A., 2021. Role of SNAREs in Neurodegenerative Diseases. Cells 10, 991. https://doi.org/10.3390/cells10050991

Mariani, J., Coppola, G., Zhang, P., Abyzov, A., Provini, L., Tomasini, L., Amenduni, M., Szekely, A., Palejev, D., Wilson, M., Gerstein, M., Grigorenko, E.L., Chawarska, K., Pelphrey, K.A., Howe, J.R., Vaccarino, F.M., 2015. FOXG1-Dependent Dysregulation of GABA/Glutamate Neuron Differentiation in Autism Spectrum Disorders. Cell 162, 375–390. https://doi.org/10.1016/j.cell.2015.06.034

Maroof, A.M., Keros, S., Tyson, J.A., Ying, S.-W., Ganat, Y.M., Merkle, F.T., Liu, B., Goulburn, A., Stanley, E.G., Elefanty, A.G., Widmer, H.R., Eggan, K., Goldstein, P.A., Anderson, S.A., Studer, L., 2013. Directed differentiation and functional maturation of cortical interneurons from human embryonic stem cells. Cell Stem Cell 12, 559–572. https://doi.org/10.1016/j.stem.2013.04.008

Marques, S., van Bruggen, D., Vanichkina, D.P., Floriddia, E.M., Munguba, H., Väremo, L., Giacomello, S., Falcão, A.M., Meijer, M., Björklund, Å.K., Hjerling-Leffler, J., Taft, R.J., Castelo-Branco, G., 2018. Transcriptional Convergence of Oligodendrocyte Lineage Progenitors during Development. Developmental Cell 46, 504-517.e7. https://doi.org/10.1016/j.devcel.2018.07.005

Martynoga, B., Drechsel, D., Guillemot, F., 2012. Molecular Control of Neurogenesis: A View from the Mammalian Cerebral Cortex. Cold Spring Harb Perspect Biol 4, a008359. https://doi.org/10.1101/cshperspect.a008359

Marullo, M., Valenza, M., Mariotti, C., Di Donato, S., Cattaneo, E., Zuccato, C., 2010. Analysis of the Repressor Element-1 Silencing Transcription Factor/Neuron-Restrictive Silencer Factor Occupancy of Non-Neuronal Genes in Peripheral Lymphocytes from Patients with Huntington's Disease. Brain Pathology 20, 96–105. https://doi.org/10.1111/j.1750-3639.2008.00249.x

McDermott, K.W., Barry, D.S., McMahon, S.S., 2005. Role of radial glia in cytogenesis, patterning and boundary formation in the developing spinal cord. J Anat 207, 241–250. https://doi.org/10.1111/j.1469-7580.2005.00462.x

McGann, J.C., Spinner, M.A., Garg, S.K., Mullendorff, K.A., Woltjer, R.L., Mandel, G., 2021. The Genome-Wide Binding Profile for Human RE1 Silencing Transcription Factor Unveils a Unique Genetic Circuitry in Hippocampus. J. Neurosci. 41, 6582–6595. https://doi.org/10.1523/JNEUROSCI.2059-20.2021

Meharena, H.S., Marco, A., Dileep, V., Lockshin, E.R., Akatsu, G.Y., Mullahoo, J., Watson, L.A., Ko, T., Guerin, L.N., Abdurrob, F., Rengarajan, S.,

© COPYRIGHT UPM

Papanastasiou, M., Jaffe, J.D., Tsai, L.-H., 2022. Down-syndrome-induced senescence disrupts the nuclear architecture of neural progenitors. Cell Stem Cell 29, 116-130.e7. https://doi.org/10.1016/j.stem.2021.12.002

Mehrafza, S., Kermanshahi, S., Mostafidi, S., Motaghinejad, M., Motevalian, M., Fatima, S., 2019. Pharmacological evidence for lithium-induced neuroprotection against methamphetamine-induced neurodegeneration via Akt-1/GSK3 and CREB-BDNF signaling pathways. Iran J Basic Med Sci 22, 856–865. https://doi.org/10.22038/ijbms.2019.30855.7442

Meldrum, B.S., 2000. Glutamate as a neurotransmitter in the brain: review of physiology and pathology. J Nutr 130, 1007S–15S. https://doi.org/10.1093/jn/130.4.1007S

Mendioroz, M., Do, C., Jiang, X., Liu, C., Darbary, H.K., Lang, C.F., Lin, J., Thomas, A., Abu-Amero, S., Stanier, P., Temkin, A., Yale, A., Liu, M.-M., Li, Y., Salas, M., Kerkel, K., Capone, G., Silverman, W., Yu, Y.E., Moore, G., Wegiel, J., Tycko, B., 2015. Trans effects of chromosome aneuploidies on DNA methylation patterns in human Down syndrome and mouse models. Genome Biol 16, 263. https://doi.org/10.1186/s13059-015-0827-6

Menzel, O., Vellai, T., Takacs-Vellai, K., Reymond, A., Mueller, F., Antonarakis, S.E., Guipponi, M., 2004. The Caenorhabditis elegans ortholog of C21orf80, a potential new protein O-fucosyltransferase, is required for normal development. Genomics 84, 320–330. https://doi.org/10.1016/j.ygeno.2004.04.002

Meraz-Ríos, M.A., Toral-Rios, D., Franco-Bocanegra, D., Villeda-Hernández, J., Campos-Peña, V., 2013. Inflammatory process in Alzheimer's Disease. Front Integr Neurosci 7, 59. https://doi.org/10.3389/fnint.2013.00059

Meyer, K., Ling, K.-H., Yeo, P.-L., Spathopoulou, A., Drake, D., Choi, J., Aron, L., Garcia-Corral, M., Ko, T., Lee, E.A., Tam, J.M., Perlis, R.H., Church, G.M., Tsai, L.-H., Yankner, B.A., 2023. Impaired neural stress resistance and loss of REST in bipolar disorder. Mol Psychiatry. https://doi.org/10.1038/s41380-023-02313-7

Miller, F.D., Gauthier, A.S., 2007. Timing is everything: making neurons versus glia in the developing cortex. Neuron 54, 357–369. https://doi.org/10.1016/j.neuron.2007.04.019

Min, W., Zou, C., Dai, D., Zuo, Q., Chen, C., Xu, J., Li, Y., Yue, Z., 2020. Integrin Beta 1 Promotes Glioma Cell Proliferation by Negatively Regulating the Notch Pathway. J Oncol 2020, 8297017. https://doi.org/10.1155/2020/8297017

Miyajima, M., Tabata, H., Nakajima, K., 2024. Migratory mode transition of astrocyte progenitors in the cerebral cortex: an intrinsic or extrinsic cell process? Neural Regeneration Research 19, 471. https://doi.org/10.4103/1673-5374.380886

© COPYRIGHT UPM

Miyazawa, H., Snaebjornsson, M.T., Prior, N., Kafkia, E., Hammarén, H.M., Tsuchida-Straeten, N., Patil, K.R., Beck, M., Aulehla, A., 2022. Glycolytic flux-signaling controls mouse embryo mesoderm development. Elife 11, e83299. https://doi.org/10.7554/eLife.83299

Mizuno, G.O., Wang, Yinxue, Shi, G., Wang, Yizhi, Sun, J., Papadopoulos, S., Broussard, G.J., Unger, E.K., Deng, W., Weick, J., Bhattacharyya, A., Chen, C.-Y., Yu, G., Looger, L.L., Tian, L., 2018. Aberrant Calcium Signaling in Astrocytes Inhibits Neuronal Excitability in a Human Down Syndrome Stem Cell Model. Cell Rep 24, 355–365. https://doi.org/10.1016/j.celrep.2018.06.033

Mo, A., Paz-Ebstein, E., Yanovsky-Dagan, S., Lai, A., Mor-Shaked, H., Gilboa, T., Yang, E., Shao, D.D., Walsh, C.A., Harel, T., 2023. A recurrent de novo variant in NUSAP1 escapes nonsense-mediated decay and leads to microcephaly, epilepsy, and developmental delay. Clinical Genetics 104, 73–80. https://doi.org/10.1111/cge.14335

Montoliu-Gaya, L., Alcolea, D., Ashton, N.J., Pegueroles, J., Levin, J., Bosch, B., Lantero-Rodriguez, J., Carmona-Iragui, M., Wagemann, O., Balasa, M., Kac, P.R., Barroeta, I., Lladó, A., Brum, W.S., Videla, L., Gonzalez-Ortiz, F., Benejam, B., Arranz Martínez, J.J., Karikari, T.K., Nübling, G., Bejanin, A., Benedet, A.L., Blesa, R., Lleó, A., Blennow, K., Sánchez-Valle, R., Zetterberg, H., Fortea, J., 2023. Plasma and cerebrospinal fluid glial fibrillary acidic protein levels in adults with Down syndrome: a longitudinal cohort study. eBioMedicine 90, 104547. https://doi.org/10.1016/j.ebiom.2023.104547

Morante-Redolat, J.M., Porlan, E., 2019. Neural Stem Cell Regulation by Adhesion Molecules Within the Subependymal Niche. Front Cell Dev Biol 7, 102. https://doi.org/10.3389/fcell.2019.00102

Motegi, N., Morisaki, N., Suto, M., Tamai, H., Mori, R., Nakayama, T., 2021. Secular trends in longevity among people with Down syndrome in Japan, 1995–2016. Pediatrics International 63, 94–101. https://doi.org/10.1111/ped.14354

Mozzi, A., Guerini, F.R., Forni, D., Costa, A.S., Nemni, R., Baglio, F., Cabinio, M., Riva, S., Pontremoli, C., Clerici, M., Sironi, M., Cagliani, R., 2017. REST, a master regulator of neurogenesis, evolved under strong positive selection in humans and in non human primates. Sci Rep 7, 9530. https://doi.org/10.1038/s41598-017-10245-w

Murray, A., Letourneau, A., Canzonetta, C., Stathaki, E., Gimelli, S., Sloan-Bena, F., Abrehart, R., Goh, P., Lim, S., Baldo, C., Dagna-Bricarelli, F., Hannan, S., Mortensen, M., Ballard, D., Syndercombe Court, D., Fusaki, N., Hasegawa, M., Smart, T.G., Bishop, C., Antonarakis, S.E., Groet, J., Nizetic, D., 2015. Brief report: isogenic induced pluripotent stem cell lines from an adult with mosaic down syndrome model accelerated neuronal ageing and neurodegeneration. Stem Cells 33, 2077–2084. https://doi.org/10.1002/stem.1968

© COPYRIGHT UPM

Nahman, S., Belmaker, R.H., Azab, A.N., 2012. Effects of lithium on lipopolysaccharide-induced inflammation in rat primary glia cells. Innate Immun 18, 447–458. https://doi.org/10.1177/1753425911421512

Nakagawa, T., Yabe, T., Schwartz, J.P., 2005. Gene expression profiles of reactive astrocytes cultured from dopamine-depleted striatum. Neurobiol Dis 20, 275–282. https://doi.org/10.1016/j.nbd.2005.03.009

Nakashima, K., Yanagisawa, M., Arakawa, H., Kimura, N., Hisatsune, T., Kawabata, M., Miyazono, K., Taga, T., 1999. Synergistic signaling in fetal brain by STAT3-Smad1 complex bridged by p300. Science 284, 479–482. https://doi.org/10.1126/science.284.5413.479

Namihira, M., Kohyama, J., Semi, K., Sanosaka, T., Deneen, B., Taga, T., Nakashima, K., 2009. Committed neuronal precursors confer astrocytic potential on residual neural precursor cells. Dev Cell 16, 245–255. https://doi.org/10.1016/j.devcel.2008.12.014

Naruse, M., Shibasaki, K., Yokoyama, S., Kurachi, M., Ishizaki, Y., 2013. Dynamic Changes of CD44 Expression from Progenitors to Subpopulations of Astrocytes and Neurons in Developing Cerebellum. PLoS One 8, e53109. https://doi.org/10.1371/journal.pone.0053109

Nassar, A., Azab, A.N., 2014. Effects of lithium on inflammation. ACS Chem Neurosci 5, 451–458. https://doi.org/10.1021/cn500038f

Nesti, E., Corson, G.M., McCleskey, M., Oyer, J.A., Mandel, G., 2014. C-terminal domain small phosphatase 1 and MAP kinase reciprocally control REST stability and neuronal differentiation. Proceedings of the National Academy of Sciences 111, E3929–E3936. https://doi.org/10.1073/pnas.1414770111

Neuhäuser, M., Krackow, S., 2007. Adaptive-filtering of trisomy 21: risk of Down syndrome depends on family size and age of previous child. Naturwissenschaften 94, 117–121. https://doi.org/10.1007/s00114-006-0165-3

Neyrinck, K., Van Den Daele, J., Vervliet, T., De Smedt, J., Wierda, K., Nijs, M., Vanbokhoven, T., D'hondt, A., Planque, M., Fendt, S.-M., Shih, P.-Y., Seibt, F., Almenar, J.P., Kreir, M., Kumar, D., Broccoli, V., Bultynck, G., Ebneth, A., Cabrera-Socorro, A., Verfaillie, C., 2021. SOX9-induced Generation of Functional Astrocytes Supporting Neuronal Maturation in an All-human System. Stem Cell Rev Rep 17, 1855–1873. https://doi.org/10.1007/s12015-021-10179-x

Ng, N., Flygare Wallén, E., Ahlström, G., 2017. Mortality patterns and risk among older men and women with intellectual disability: a Swedish national retrospective cohort study. BMC Geriatr 17, 269. https://doi.org/10.1186/s12877-017-0665-3

Nho, K., Kim, S., Risacher, S.L., Shen, L., Corneveaux, J.J., Swaminathan, S., Lin, H., Ramanan, V.K., Liu, Y., Foroud, T.M., Inlow, M.H., Siniard, A.L., Reiman,

© COPYRIGHT UPM

R.A., Aisen, P.S., Petersen, R.C., Green, R.C., Jack Jr, C.R., Weiner, M.W., Baldwin, C.T., Lunetta, K.L., Farrer, L.A., Study, for the M. (Multi-I.R. on A.G.E., Furney, S.J., Lovestone, S., Simmons, A., Mecocci, P., Vellas, B., Tsolaki, M., Kloszewska, I., Soininen, H., Consortium, for the A., McDonald, B.C., Farlow, M.R., Ghetti, B., for the Indiana Memory and Aging Study, Huentelman, M.J., Saykin, A.J., Initiative, for the A.D.N., 2015. Protective variant for hippocampal atrophy identified by whole exome sequencing. Annals of Neurology 77, 547–552. https://doi.org/10.1002/ana.24349

Nicholas, C.R., Chen, J., Tang, Y., Southwell, D.G., Chalmers, N., Vogt, D., Arnold, C.M., Chen, Y.-J.J., Stanley, E.G., Elefanty, A.G., Sasai, Y., Alvarez-Buylla, A., Rubenstein, J.L.R., Kriegstein, A.R., 2013. Functional maturation of hPSC-derived forebrain interneurons requires an extended timeline and mimics human neural development. Cell Stem Cell 12, 573–586. https://doi.org/10.1016/j.stem.2013.04.005

Nicolas, C.S., Amici, M., Bortolotto, Z.A., Doherty, A., Csaba, Z., Fafouri, A., Dournaud, P., Gressens, P., Collingridge, G.L., Peineau, S., 2013. The role of JAK-STAT signaling within the CNS. JAK-STAT 2, e22925. https://doi.org/10.4161/jkst.22925

Nishihara, S., Tsuda, L., Ogura, T., 2003. The canonical Wnt pathway directly regulates NRSF/REST expression in chick spinal cord. Biochem Biophys Res Commun 311, 55–63. https://doi.org/10.1016/j.bbrc.2003.09.158

Nordquist, S.K., Smith, S.R., Pierce, J.T., 2018. Systematic Functional Characterization of Human 21st Chromosome Orthologs in Caenorhabditis elegans. G3 (Bethesda) 8, 967–979. https://doi.org/10.1534/g3.118.200019

Nousiainen, H.O., Kestilä, M., Pakkasjärvi, N., Honkala, H., Kuure, S., Tallila, J., Vuopala, K., Ignatius, J., Herva, R., Peltonen, L., 2008. Mutations in mRNA export mediator GLE1 result in a fetal motoneuron disease. Nat Genet 40, 155–157. https://doi.org/10.1038/ng.2007.65

Nunes, P.V., Forlenza, O.V., Gattaz, W.F., 2007. Lithium and risk for Alzheimer's disease in elderly patients with bipolar disorder. The British Journal of Psychiatry 190, 359–360. https://doi.org/10.1192/bjp.bp.106.029868

Obara, K., Imota, T., Mamiya, S., Toyoshima, I., 2020. The Effectiveness of Perampanel for Myoclonic Seizures in Down Syndrome with Isodicentric Chromosome 21. Case Reports in Neurology 12, 270–275. https://doi.org/10.1159/000508357

Oberheim, N.A., Takano, T., Han, X., He, W., Lin, J.H.C., Wang, F., Xu, Q., Wyatt, J.D., Pilcher, W., Ojemann, J.G., Ransom, B.R., Goldman, S.A., Nedergaard, M., 2009. Uniquely Hominid Features of Adult Human Astrocytes. J. Neurosci. 29, 3276–3287. https://doi.org/10.1523/JNEUROSCI.4707-08.2009

Ohata, S., Aoki, R., Kinoshita, S., Yamaguchi, M., Tsuruoka-Kinoshita, S., Tanaka, H., Wada, H., Watabe, S., Tsuboi, T., Masai, I., Okamoto, H., 2011. Dual roles of Notch in regulation of apically restricted mitosis and apicobasal polarity of

© COPYRIGHT UPM

neuroepithelial cells. Neuron 69, 215–230. https://doi.org/10.1016/j.neuron.2010.12.026

Ohno, Y., Kunisawa, N., Shimizu, S., 2021. Emerging Roles of Astrocyte Kir4.1 Channels in the Pathogenesis and Treatment of Brain Diseases. International Journal of Molecular Sciences 22, 10236. https://doi.org/10.3390/ijms221910236

Olmos-Serrano, J.L., Kang, H.J., Tyler, W.A., Silbereis, J.C., Cheng, F., Zhu, Y., Pletikos, M., Jankovic-Rapan, L., Cramer, N.P., Galdzicki, Z., Goodliffe, J., Peters, A., Sethares, C., Delalle, I., Golden, J.A., Haydar, T.F., Sestan, N., 2016. Down Syndrome Developmental Brain Transcriptome Reveals Defective Oligodendrocyte Differentiation and Myelination. Neuron 89, 1208–1222. https://doi.org/10.1016/j.neuron.2016.01.042

Oria, M., Pathak, B., Li, Z., Bakri, K., Gouwens, K., Varela, M.F., Lampe, K., Murphy, K.P., Lin, C.-Y., Peiro, J.L., 2022. Premature Neural Progenitor Cell Differentiation Into Astrocytes in Retinoic Acid-Induced Spina Bifida Rat Model. Front Mol Neurosci 15, 888351. https://doi.org/10.3389/fnmol.2022.888351

Ou, A., Ott, M., Fang, D., Heimberger, A.B., 2021. The Role and Therapeutic Targeting of JAK/STAT Signaling in Glioblastoma. Cancers 13, 437. https://doi.org/10.3390/cancers13030437

Ovando-Roche, P., Yu, J.S.L., Testori, S., Ho, C., Cui, W., 2014. TRF2-Mediated Stabilization of hREST4 Is Critical for the Differentiation and Maintenance of Neural Progenitors. Stem Cells 32, 2111–2122. https://doi.org/10.1002/stem.1725

Pajarillo, Alexis Digman, Ivan Nyarko-Danquah, Deok-Soo Son, Karam F.A. Soliman, Michael Aschner, Eun Sook Lee, 2021. Astrocytic transcription factor REST upregulates glutamate transporter EAAT2, protecting dopaminergic neurons from manganese-induced excitotoxicity. Journal of Biological Chemistry 101372. https://doi.org/10.1016/j.jbc.2021.101372

Pankov, R., Yamada, K.M., 2002. Fibronectin at a glance. J Cell Sci 115, 3861–3863. https://doi.org/10.1242/jcs.00059

Papavassiliou, P., Charalsawadi, C., Rafferty, K., Jackson-Cook, C., 2015. Mosaicism for trisomy 21: a review. Am J Med Genet A 167A, 26–39. https://doi.org/10.1002/ajmg.a.36861

Paşca, A.M., Sloan, S.A., Clarke, L.E., Tian, Y., Makinson, C.D., Huber, N., Kim, C.H., Park, J.-Y., O'Rourke, N.A., Nguyen, K.D., Smith, S.J., Huguenard, J.R., Geschwind, D.H., Barres, B.A., Paşca, S.P., 2015. Functional cortical neurons and astrocytes from human pluripotent stem cells in 3D culture. Nat Methods 12, 671–678. https://doi.org/10.1038/nmeth.3415

Pavlinov, I., Tambe, M., Abbott, J., Nguyen, H.N., Xu, M., Pradhan, M., Farkhondeh, A., Zheng, W., 2023. In depth characterization of midbrain organoids derived

from wild type iPSC lines. PLoS One 18, e0292926. https://doi.org/10.1371/journal.pone.0292926

Peled-Kamar, M., Degani, H., Bendel, P., Margalit, R., Groner, Y., 1998. Altered brain glucose metabolism in transgenic-PFKL mice with elevated l-phosphofructokinase: in vivo NMR studies. Brain Research 810, 138–145. https://doi.org/10.1016/S0006-8993(98)00899-3

Pelleri, M.C., Cicchini, E., Locatelli, C., Vitale, L., Caracausi, M., Piovesan, A., Rocca, A., Poletti, G., Seri, M., Strippoli, P., Cocchi, G., 2016. Systematic reanalysis of partial trisomy 21 cases with or without Down syndrome suggests a small region on 21q22.13 as critical to the phenotype. Hum Mol Genet 25, 2525–2538. https://doi.org/10.1093/hmg/ddw116

Petersen, M.B., Mikkelsen, M., 2000. Nondisjunction in trisomy 21: origin and mechanisms. Cytogenet Cell Genet 91, 199–203. https://doi.org/10.1159/000056844

Piper, M., Barry, G., Hawkins, J., Mason, S., Lindwall, C., Little, E., Sarkar, A., Smith, A.G., Moldrich, R.X., Boyle, G.M., Tole, S., Gronostajski, R.M., Bailey, T.L., Richards, L.J., 2010. NFIA Controls Telencephalic Progenitor Cell Differentiation through Repression of the Notch Effector Hes1. J Neurosci 30, 9127–9139. https://doi.org/10.1523/JNEUROSCI.6167-09.2010

Ponroy Bally, B., Farmer, W.T., Jones, E.V., Jessa, S., Kacerovsky, J.B., Mayran, A., Peng, H., Lefebvre, J.L., Drouin, J., Hayer, A., Ernst, C., Murai, K.K., 2020. Human iPSC-derived Down syndrome astrocytes display genome-wide perturbations in gene expression, an altered adhesion profile, and increased cellular dynamics. Hum Mol Genet 29, 785–802. https://doi.org/10.1093/hmg/ddaa003

Ponroy Bally, B., Murai, K.K., 2021. Astrocytes in Down Syndrome Across the Lifespan. Front Cell Neurosci 15, 702685. https://doi.org/10.3389/fncel.2021.702685

Powers, R.K., Culp-Hill, R., Ludwig, M.P., Smith, K.P., Waugh, K.A., Minter, R., Tuttle, K.D., Lewis, H.C., Rachubinski, A.L., Granrath, R.E., Carmona-Iragui, M., Wilkerson, R.B., Kahn, D.E., Joshi, M., Lleó, A., Blesa, R., Fortea, J., D'Alessandro, A., Costello, J.C., Sullivan, K.D., Espinosa, J.M., 2019. Trisomy 21 activates the kynurenine pathway via increased dosage of interferon receptors. Nat Commun 10, 4766. https://doi.org/10.1038/s41467-019-12739-9

Prandini, P., Deutsch, S., Lyle, R., Gagnebin, M., Vivier, C.D., Delorenzi, M., Gehrig, C., Descombes, P., Sherman, S., Bricarelli, F.D., Baldo, C., Novelli, A., Dallapiccola, B., Antonarakis, S.E., 2007. Natural Gene-Expression Variation in Down Syndrome Modulates the Outcome of Gene-Dosage Imbalance. The American Journal of Human Genetics 81, 252–263. https://doi.org/10.1086/519248

© COPYRIGHT UPM

Preman, P., Alfonso-Triguero, M., Alberdi, E., Verkhratsky, A., Arranz, A.M., 2021. Astrocytes in Alzheimer's Disease: Pathological Significance and Molecular Pathways. Cells 10, 540. https://doi.org/10.3390/cells10030540

Price, B.R., Johnson, L.A., Norris, C.M., 2021. Reactive astrocytes: The nexus of pathological and clinical hallmarks of Alzheimer's disease. Ageing Research Reviews 68, 101335. https://doi.org/10.1016/j.arr.2021.101335

Prutton, K.M., Marentette, J.O., Maclean, K.N., Roede, J.R., 2023. Characterization of mitochondrial and metabolic alterations induced by trisomy 21 during neural differentiation. Free Radic Biol Med 196, 11–21. https://doi.org/10.1016/j.freeradbiomed.2023.01.009

Qi, G., Mi, Y., Shi, X., Gu, H., Brinton, R.D., Yin, F., 2021. ApoE4 Impairs Neuron-Astrocyte Coupling of Fatty Acid Metabolism. Cell Reports 34. https://doi.org/10.1016/j.celrep.2020.108572

Qian, X., Nguyen, H.N., Song, M.M., Hadiono, C., Ogden, S.C., Hammack, C., Yao, B., Hamersky, G.R., Jacob, F., Zhong, C., Yoon, K.-J., Jeang, W., Lin, L., Li, Y., Thakor, J., Berg, D.A., Zhang, C., Kang, E., Chickering, M., Nauen, D., Ho, C.-Y., Wen, Z., Christian, K.M., Shi, P.-Y., Maher, B.J., Wu, H., Jin, P., Tang, H., Song, H., Ming, G.-L., 2016. Brain-Region-Specific Organoids Using Mini-bioreactors for Modeling ZIKV Exposure. Cell 165, 1238–1254. https://doi.org/10.1016/j.cell.2016.04.032

Qiu, J.-J., Liu, Y.-N., Wei, H., Zeng, F., Yan, J.-B., 2023. Single-cell RNA sequencing of neural stem cells derived from human trisomic iPSCs reveals the abnormalities during neural differentiation of Down syndrome. Front Mol Neurosci 16, 1137123. https://doi.org/10.3389/fnmol.2023.1137123

Qureshi, I.A., Gokhan, S., Mehler, M.F., 2010. REST and CoREST are transcriptional and epigenetic regulators of seminal neural fate decisions. Cell Cycle 9, 4477–4486. https://doi.org/10.4161/cc.9.22.13973

Radakovits, R., Barros, C.S., Belvindrah, R., Patton, B., Müller, U., 2009. Regulation of Radial Glial Survival by Signals from the Meninges. J. Neurosci. 29, 7694–7705. https://doi.org/10.1523/JNEUROSCI.5537-08.2009

Ramasamy, S.K., Lenka, N., 2010. Notch Exhibits Ligand Bias and Maneuvers Stage-Specific Steering of Neural Differentiation in Embryonic Stem Cells. Molecular and Cellular Biology 30, 1946–1957. https://doi.org/10.1128/MCB.01419-09

Ravache, M., Weber, C., Mérienne, K., Trottier, Y., 2010. Transcriptional Activation of REST by Sp1 in Huntington's Disease Models. PLOS ONE 5, e14311. https://doi.org/10.1371/journal.pone.0014311

Repovic, P., Mi, K., Benveniste, E.N., 2003. Oncostatin M enhances the expression of prostaglandin E2 and cyclooxygenase-2 in astrocytes: synergy with interleukin-1beta, tumor necrosis factor-alpha, and bacterial lipopolysaccharide. Glia 42, 433–446. https://doi.org/10.1002/glia.10182

© COPYRIGHT UPM

Rispoli, P., Scandiuzzi Piovesan, T., Decorti, G., Stocco, G., Lucafò, M., 2024. iPSCs as a groundbreaking tool for the study of adverse drug reactions: A new avenue for personalized therapy. WIREs Mechanisms of Disease 16, e1630. https://doi.org/10.1002/wsbm.1630

Rivera, A.D., Butt, A.M., 2019. Astrocytes are direct cellular targets of lithium treatment: novel roles for lysyl oxidase and peroxisome-proliferator activated receptor-γ as astroglial targets of lithium. Transl Psychiatry 9, 211. https://doi.org/10.1038/s41398-019-0542-2

Rizor, A., Pajarillo, E., Johnson, J., Aschner, M., Lee, E., 2019. Astrocytic Oxidative/Nitrosative Stress Contributes to Parkinson's Disease Pathogenesis: The Dual Role of Reactive Astrocytes. Antioxidants 8, 265. https://doi.org/10.3390/antiox8080265

Rocchi, A., Carminati, E., De Fusco, A., Kowalska, J.A., Floss, T., Benfenati, F., 2021. REST/NRSF deficiency impairs autophagy and leads to cellular senescence in neurons. Aging Cell 20, e13471. https://doi.org/10.1111/acel.13471

Rockenstein, E., Torrance, M., Adame, A., Mante, M., Bar-on, P., Rose, J.B., Crews, L., Masliah, E., 2007. Neuroprotective Effects of Regulators of the Glycogen Synthase Kinase-3β Signaling Pathway in a Transgenic Model of Alzheimer's Disease Are Associated with Reduced Amyloid Precursor Protein Phosphorylation. J. Neurosci. 27, 1981–1991. https://doi.org/10.1523/JNEUROSCI.4321-06.2007

Rockowitz, S., Zheng, D., 2015. Significant expansion of the REST/NRSF cistrome in human versus mouse embryonic stem cells: potential implications for neural development. Nucleic Acids Res 43, 5730–5743. https://doi.org/10.1093/nar/gkv514

Royston, McKenzie, Gentleman, Sheng, Mann, Griffin, Mrak, 1999. Overexpression of S100β in Down's syndrome: correlation with patient age and with β-amyloid deposition. Neuropathology and Applied Neurobiology 25, 387–393. https://doi.org/10.1046/j.1365-2990.1999.00196.x

Rubenstein, E., Tewolde, S., Michals, A., Weuve, J., Fortea, J., Fox, M.P., Pescador Jimenez, M., Scott, A., Tripodis, Y., Skotko, B.G., 2024. Alzheimer Dementia Among Individuals With Down Syndrome. JAMA Network Open 7, e2435018. https://doi.org/10.1001/jamanetworkopen.2024.35018

Rybakowski, J.K., Suwalska, A., Hajek, T., 2018. Clinical Perspectives of Lithium's Neuroprotective Effect. Pharmacopsychiatry 51, 194–199. https://doi.org/10.1055/s-0043-124436

Ryu, H.U., Chung, J.Y., Shin, B.-S., Kang, H.G., 2020. Lithium induced reversible Splenial lesion in neuroleptic malignant syndrome like symptoms: two case reports. BMC Neurology 20, 164. https://doi.org/10.1186/s12883-020-01742-z

© COPYRIGHT UPM

Saijo, K., Winner, B., Carson, C.T., Collier, J.G., Boyer, L., Rosenfeld, M.G., Gage, F.H., Glass, C.K., 2009. A Nurr1/CoREST pathway in microglia and astrocytes protects dopaminergic neurons from inflammation-induced death. Cell 137, 47–59. https://doi.org/10.1016/j.cell.2009.01.038

Salehi, A., Delcroix, J.-D., Belichenko, P.V., Zhan, K., Wu, C., Valletta, J.S., Takimoto-Kimura, R., Kleschevnikov, A.M., Sambamurti, K., Chung, P.P., Xia, W., Villar, A., Campbell, W.A., Kulnane, L.S., Nixon, R.A., Lamb, B.T., Epstein, C.J., Stokin, G.B., Goldstein, L.S.B., Mobley, W.C., 2006. Increased App expression in a mouse model of Down's syndrome disrupts NGF transport and causes cholinergic neuron degeneration. Neuron 51, 29–42. https://doi.org/10.1016/j.neuron.2006.05.022

Sanalkumar, R., Indulekha, C.L., Divya, T.S., Divya, M.S., Anto, R.J., Vinod, B., Vidyanand, S., Jagatha, B., Venugopal, S., James, J., 2010. ATF2 maintains a subset of neural progenitors through CBF1/Notch independent Hes-1 expression and synergistically activates the expression of Hes-1 in Notch-dependent neural progenitors. Journal of Neurochemistry 113, 807–818. https://doi.org/10.1111/j.1471-4159.2010.06574.x

Sansregret, L., Goulet, B., Harada, R., Wilson, B., Leduy, L., Bertoglio, J., Nepveu, A., 2006. The p110 isoform of the CDP/Cux transcription factor accelerates entry into S phase. Mol Cell Biol 26, 2441–2455. https://doi.org/10.1128/MCB.26.6.2441-2455.2006

Satoh, J.-I., Kawana, N., Yamamoto, Y., 2013. ChIP-Seq Data Mining: Remarkable Differences in NRSF/REST Target Genes between Human ESC and ESC-Derived Neurons. Bioinform Biol Insights 7, BBI.S13279. https://doi.org/10.4137/BBI.S13279

Sauter, C., Morin, T., Guidez, F., Simonet, J., Fournier, C., Row, C., Masnikov, D., Pernon, B., Largeot, A., Aznague, A., Hérault, Y., Sauvageau, G., Maynadié, M., Callanan, M., Bastie, J.-N., Aucagne, R., Delva, L., 2024. Protein arginine methyltransferase 2 controls inflammatory signaling in acute myeloid leukemia. Commun Biol 7, 1–12. https://doi.org/10.1038/s42003-024-06453-6

Sawa, M., Overk, C., Becker, A., Derse, D., Albay, R., Weldy, K., Salehi, A., Beach, T.G., Doran, E., Head, E., Yu, Y.E., Mobley, W.C., 2022. Impact of increased APP gene dose in Down syndrome and the Dp16 mouse model. Alzheimers Dement 18, 1203–1234. https://doi.org/10.1002/alz.12463

Schapiro, M.B., Ball, M.J., Grady, C.L., Haxby, J.V., Kaye, J.A., Rapoport, S.I., 1988. Dementia in Down's syndrome: cerebral glucose utilization, neuropsychological assessment, and neuropathology. Neurology 38, 938–942. https://doi.org/10.1212/wnl.38.6.938

Schapiro, M.B., Haxby, J.V., Grady, C.L., 1992. Nature of mental retardation and dementia in Down syndrome: study with PET, CT, and neuropsychology. Neurobiol Aging 13, 723–734. https://doi.org/10.1016/0197-4580(92)90096-g

© COPYRIGHT UPM

Schneider, M., Al-Shareffi, E., Haltiwanger, R.S., 2017. Biological functions of fucose in mammals. Glycobiology 27, 601–618. https://doi.org/10.1093/glycob/cwx034

Scott, H.S., Antonarakis, S.E., Lalioti, M.D., Rossier, C., Silver, P.A., Henry, M.F., 1998. Identification and characterization of two putative human arginine methyltransferases (HRMT1L1 and HRMT1L2). Genomics 48, 330–340. https://doi.org/10.1006/geno.1997.5190

Shaker, M.R., Slonchak, A., Al-Mhanawi, B., Morrison, S.D., Sng, J.D.J., Cooper-White, J., Khromykh, A.A., Wolvetang, E.J., 2024. Choroid plexus defects in Down syndrome brain organoids enhance neurotropism of SARS-CoV-2. Sci Adv 10, eadj4735. https://doi.org/10.1126/sciadv.adj4735

Shannon, P., Markiel, A., Ozier, O., Baliga, N.S., Wang, J.T., Ramage, D., Amin, N., Schwikowski, B., Ideker, T., 2003. Cytoscape: a software environment for integrated models of biomolecular interaction networks. Genome Res 13, 2498–2504. https://doi.org/10.1101/gr.1239303

Shapiro, B.L., Hermann, J., Opitz, J.M., 1983. Down syndrome—a disruption of homeostasis. American Journal of Medical Genetics 14, 241–269. https://doi.org/10.1002/ajmg.1320140206

Shen, C., Xian, W., Zhou, H., Chen, L., Pei, Z., 2016. Potential protective effects of autophagy activated in MPP+ treated astrocytes. Experimental and Therapeutic Medicine 12, 2803–2810. https://doi.org/10.3892/etm.2016.3736

Shen, Y., Zhao, M., Zhao, P., Meng, L., Zhang, Y., Zhang, G., Taishi, Y., Sun, L., 2024. Molecular mechanisms and therapeutic potential of lithium in Alzheimer's disease: repurposing an old class of drugs. Front. Pharmacol. 15. https://doi.org/10.3389/fphar.2024.1408462

Sherman, S.L., Allen, E.G., Bean, L.H., Freeman, S.B., 2007. Epidemiology of Down syndrome. Mental Retardation and Developmental Disabilities Research Reviews 13, 221–227. https://doi.org/10.1002/mrdd.20157

Shi, X., Wang, B., Liu, Y., Zhang, J., Huang, Y., Cao, P., Shen, Y., Lyu, J., 2017. Carnosine modulates glutamine synthetase expression in senescent astrocytes exposed to oxygen-glucose deprivation/recovery. Brain Res Bull 130, 138–145. https://doi.org/10.1016/j.brainresbull.2017.01.014

Shu, T., Tseng, H.-C., Sapir, T., Stern, P., Zhou, Y., Sanada, K., Fischer, A., Coquelle, F.M., Reiner, O., Tsai, L.-H., 2006. Doublecortin-like Kinase Controls Neurogenesis by Regulating Mitotic Spindles and M Phase Progression. Neuron 49, 25–39. https://doi.org/10.1016/j.neuron.2005.10.039

Shue, Y.T., Drainas, A.P., Li, N.Y., Pearsall, S.M., Morgan, D., Sinnott-Armstrong, N., Hipkins, S.Q., Coles, G.L., Lim, J.S., Oro, A.E., Simpson, K.L., Dive, C., Sage, J., 2022. A conserved YAP/Notch/REST network controls the neuroendocrine cell fate in the lungs. Nat Commun 13, 2690. https://doi.org/10.1038/s41467-022-30416-2

© COPYRIGHT UPM

Singh, A., Rokes, C., Gireud, M., Fletcher, S., Baumgartner, J., Fuller, G., Stewart, J., Zage, P., Gopalakrishnan, V., 2011. Retinoic acid induces REST degradation and neuronal differentiation by modulating the expression of SCFβ-TRCP in neuroblastoma cells. Cancer 117, 5189–5202. https://doi.org/10.1002/cncr.26145

Singh, S.K., Kagalwala, M.N., Parker-Thornburg, J., Adams, H., Majumder, S., 2008. REST maintains self-renewal and pluripotency of embryonic stem cells. Nature 453, 223–227. https://doi.org/10.1038/nature06863

Siracusa, R., Fusco, R., Cuzzocrea, S., 2019. Astrocytes: Role and Functions in Brain Pathologies. Frontiers in Pharmacology 10. https://doi.org/10.3389/fphar.2019.01114

Sobol, M., Klar, J., Laan, L., Shahsavani, M., Schuster, J., Annerén, G., Konzer, A., Mi, J., Bergquist, J., Nordlund, J., Hoeber, J., Huss, M., Falk, A., Dahl, N., 2019. Transcriptome and Proteome Profiling of Neural Induced Pluripotent Stem Cells from Individuals with Down Syndrome Disclose Dynamic Dysregulations of Key Pathways and Cellular Functions. Mol Neurobiol 56, 7113–7127. https://doi.org/10.1007/s12035-019-1585-3

Soldati, C., Bithell, A., Johnston, C., Wong, K., Teng, S., Beglopoulos, V., Stanton, L.W., Buckley, N.J., 2012. Repressor Element 1 Silencing Transcription Factor Couples Loss of Pluripotency with Neural Induction and Neural Differentiation. Stem Cells 30, 425–434. https://doi.org/10.1002/stem.1004

Song, J., Zhao, D., Sun, G., Yang, J., Lv, Z., Jiao, B., 2021. PTPRM methylation induced by FN1 promotes the development of glioblastoma by activating STAT3 signalling. Pharm Biol 59, 902–909. https://doi.org/10.1080/13880209.2021.1944220

Song, Z., Shah, S.Z.A., Yang, W., Dong, H., Yang, L., Zhou, X., Zhao, D., 2017a. Downregulation of the Repressor Element 1-Silencing Transcription Factor (REST) Is Associated with Akt-mTOR and Wnt-β-Catenin Signaling in Prion Diseases Models. Front. Mol. Neurosci. 10. https://doi.org/10.3389/fnmol.2017.00128

Song, Z., Yang, W., Zhou, X., Yang, L., Zhao, D., 2017b. Lithium alleviates neurotoxic prion peptide-induced synaptic damage and neuronal death partially by the upregulation of nuclear target REST and the restoration of Wnt signaling. Neuropharmacology 123, 332–348. https://doi.org/10.1016/j.neuropharm.2017.05.021

Soppa, U., Schumacher, J., Florencio Ortiz, V., Pasqualon, T., Tejedor, F., Becker, W., 2014. The Down syndrome-related protein kinase DYRK1A phosphorylates p27Kip1 and Cyclin D1 and induces cell cycle exit and neuronal differentiation. Cell Cycle 13, 2084–2100. https://doi.org/10.4161/cc.29104

© COPYRIGHT UPM

St John, J.A., Claxton, C., Robinson, M.W., Yamamoto, F., Domino, S.E., Key, B., 2006. Genetic manipulation of blood group carbohydrates alters development and pathfinding of primary sensory axons of the olfactory systems. Dev Biol 298, 470–484. https://doi.org/10.1016/j.ydbio.2006.06.052

Stagni, F., Bartesaghi, R., 2022. The Challenging Pathway of Treatment for Neurogenesis Impairment in Down Syndrome: Achievements and Perspectives. Front Cell Neurosci 16, 903729. https://doi.org/10.3389/fncel.2022.903729

Stagni, F., Giacomini, A., Emili, M., Guidi, S., Bartesaghi, R., 2018a. Neurogenesis impairment: An early developmental defect in Down syndrome. Free Radic Biol Med 114, 15–32. https://doi.org/10.1016/j.freeradbiomed.2017.07.026

Stagni, F., Giacomini, A., Emili, M., Guidi, S., Bartesaghi, R., 2018b. Neurogenesis impairment: An early developmental defect in Down syndrome. Free Radic Biol Med 114, 15–32. https://doi.org/10.1016/j.freeradbiomed.2017.07.026

Stagni, F., Giacomini, A., Emili, M., Guidi, S., Bartesaghi, R., 2018c. Neurogenesis impairment: An early developmental defect in Down syndrome. Free Radic Biol Med 114, 15–32. https://doi.org/10.1016/j.freeradbiomed.2017.07.026

Stagni, F., Giacomini, A., Emili, M., Uguagliati, B., Bonasoni, M.P., Bartesaghi, R., Guidi, S., 2020. Neuroanatomical alterations in higher-order thalamic nuclei of fetuses with Down syndrome. Clin Neurol Neurosurg 194, 105870. https://doi.org/10.1016/j.clineuro.2020.105870

Stipursky, J., Francis, D., Dezonne, R.S., Bérgamo de Araújo, A.P., Souza, L., Moraes, C.A., Alcantara Gomes, F.C., 2014. TGF-β1 promotes cerebral cortex radial glia-astrocyte differentiation in vivo. Front Cell Neurosci 8, 393. https://doi.org/10.3389/fncel.2014.00393

Stipursky, J., Francis, D., Gomes, F.C.A., 2012. Activation of MAPK/PI3K/SMAD Pathways by TGF-β1 Controls Differentiation of Radial Glia into Astrocytes in vitro. Developmental Neuroscience 34, 68–81. https://doi.org/10.1159/000338108

Su, A.I., Wiltshire, T., Batalov, S., Lapp, H., Ching, K.A., Block, D., Zhang, J., Soden, R., Hayakawa, M., Kreiman, G., Cooke, M.P., Walker, J.R., Hogenesch, J.B., 2004. A gene atlas of the mouse and human protein-encoding transcriptomes. Proceedings of the National Academy of Sciences 101, 6062–6067. https://doi.org/10.1073/pnas.0400782101

Su, W., Foster, S.C., Xing, R., Feistel, K., Olsen, R.H.J., Acevedo, S.F., Raber, J., Sherman, L.S., 2017. CD44 Transmembrane Receptor and Hyaluronan Regulate Adult Hippocampal Neural Stem Cell Quiescence and Differentiation. J Biol Chem 292, 4434–4445. https://doi.org/10.1074/jbc.M116.774109

Su, X., Zhu, G., Ding, X., Lee, S.Y., Dou, Y., Zhu, B., Wu, W., Li, H., 2014. Molecular basis underlying histone H3 lysine–arginine methylation pattern readout by Spin/Ssty repeats of Spindlin1. Genes Dev 28, 622–636.

© COPYRIGHT UPM

https://doi.org/10.1101/gad.233239.113

Su, X.-J., Shen, B.-D., Wang, K., Song, Q.-X., Yang, X., Wu, D.-S., Shen, H.-X., Zhu, C., 2022. Roles of the Neuron-Restrictive Silencer Factor in the Pathophysiological Process of the Central Nervous System. Front Cell Dev Biol 10, 834620. https://doi.org/10.3389/fcell.2022.834620

Subramanian, A., Tamayo, P., Mootha, V.K., Mukherjee, S., Ebert, B.L., Gillette, M.A., Paulovich, A., Pomeroy, S.L., Golub, T.R., Lander, E.S., Mesirov, J.P., 2005. Gene set enrichment analysis: a knowledge-based approach for interpreting genome-wide expression profiles. Proc Natl Acad Sci U S A 102, 15545–15550. https://doi.org/10.1073/pnas.0506580102

Suetsugu, M., Mehraein, P., 1980. Spine distribution along the apical dendrites of the pyramidal neurons in Down's syndrome. A quantitative Golgi study. Acta Neuropathol 50, 207–210. https://doi.org/10.1007/BF00688755

Sun, Y.-M., Cooper, M., Finch, S., Lin, H.-H., Chen, Z.-F., Williams, B.P., Buckley, N.J., 2008. Rest-mediated regulation of extracellular matrix is crucial for neural development. PLoS One 3, e3656. https://doi.org/10.1371/journal.pone.0003656

Synnestvedt, M.B., Chen, C., Holmes, J.H., 2005. CiteSpace II: Visualization and Knowledge Discovery in Bibliographic Databases. AMIA Annu Symp Proc 2005, 724–728.

Szklarczyk, D., Gable, A.L., Lyon, D., Junge, A., Wyder, S., Huerta-Cepas, J., Simonovic, M., Doncheva, N.T., Morris, J.H., Bork, P., Jensen, L.J., Mering, C. von, 2019. STRING v11: protein-protein association networks with increased coverage, supporting functional discovery in genome-wide experimental datasets. Nucleic Acids Res 47, D607–D613. https://doi.org/10.1093/nar/gky1131

Takahashi, K., Tanabe, K., Ohnuki, M., Narita, M., Ichisaka, T., Tomoda, K., Yamanaka, S., 2007. Induction of Pluripotent Stem Cells from Adult Human Fibroblasts by Defined Factors. Cell 131, 861–872. https://doi.org/10.1016/j.cell.2007.11.019

Takashima, S., Becker, L.E., Armstrong, D.L., Chan, F., 1981. Abnormal neuronal development in the visual cortex of the human fetus and infant with down's syndrome. A quantitative and qualitative Golgi study. Brain Res 225, 1–21. https://doi.org/10.1016/0006-8993(81)90314-0

Tang, B.L., 2009. REST regulation of neural development. Cell Adh Migr 3, 141–142.

Tang, X.-Y., Xu, L., Wang, J., Hong, Y., Wang, Y., Zhu, Q., Wang, D., Zhang, X.-Y., Liu, C.-Y., Fang, K.-H., Han, X., Wang, S., Wang, X., Xu, M., Bhattacharyya, A., Guo, X., Lin, M., Liu, Y., 2021. DSCAM/PAK1 pathway suppression reverses neurogenesis deficits in iPSC-derived cerebral organoids from patients with Down syndrome. J Clin Invest 131, 135763. https://doi.org/10.1172/JCI135763

© COPYRIGHT UPM

Tchieu, J., Calder, E.L., Guttikonda, S.R., Gutzwiller, E.M., Aromolaran, K.A., Steinbeck, J.A., Goldstein, P.A., Studer, L., 2019. NFIA is a gliogenic switch enabling rapid derivation of functional human astrocytes from pluripotent stem cells. Nat Biotechnol 37, 267–275. https://doi.org/10.1038/s41587-019-0035-0

Tecalco-Cruz, A.C., Ramírez-Jarquín, J.O., Alvarez-Sánchez, M.E., Zepeda-Cervantes, J., 2020. Epigenetic basis of Alzheimer disease. World Journal of Biological Chemistry 11, 62–75. https://doi.org/10.4331/wjbc.v11.i2.62

Teles e Silva, A.L., Yokota, B.Y., Sertié, A.L., Zampieri, B.L., 2023. Generation of Urine-Derived Induced Pluripotent Stem Cells and Cerebral Organoids for Modeling Down Syndrome. Stem Cell Rev and Rep 19, 1116–1123. https://doi.org/10.1007/s12015-022-10497-8

Thiel, G., Ekici, M., Rössler, O.G., 2015. RE-1 silencing transcription factor (REST): a regulator of neuronal development and neuronal/endocrine function. Cell Tissue Res 359, 99–109. https://doi.org/10.1007/s00441-014-1963-0

Thompson, R., Chan, C., 2018. NRSF and Its Epigenetic Effectors: New Treatments for Neurological Disease. Brain Sciences 8, 226. https://doi.org/10.3390/brainsci8120226

Todd, L., Squires, N., Suarez, L., Fischer, A.J., 2016. Jak/Stat signaling regulates the proliferation and neurogenic potential of Müller glia-derived progenitor cells in the avian retina. Sci Rep 6, 35703. https://doi.org/10.1038/srep35703

Toshikawa, H., Ikenaka, A., Li, L., Nishinaka-Arai, Y., Niwa, A., Ashida, A., Kazuki, Y., Nakahata, T., Tamai, H., Russell, D.W., Saito, M.K., 2021. N-Acetylcysteine prevents amyloid-β secretion in neurons derived from human pluripotent stem cells with trisomy 21. Sci Rep 11, 17377. https://doi.org/10.1038/s41598-021-96697-7

Trevino, A.E., Sinnott-Armstrong, N., Andersen, J., Yoon, S.-J., Huber, N., Pritchard, J.K., Chang, H.Y., Greenleaf, W.J., Pașca, S.P., 2020. Chromatin accessibility dynamics in a model of human forebrain development. Science 367, eaay1645. https://doi.org/10.1126/science.aay1645

Uzquiano, A., Kedaigle, A.J., Pigoni, M., Paulsen, B., Adiconis, X., Kim, K., Faits, T., Nagaraja, S., Antón-Bolaños, N., Gerhardinger, C., Tucewicz, A., Murray, E., Jin, X., Buenrostro, J., Chen, F., Velasco, S., Regev, A., Levin, J.Z., Arlotta, P., 2022. Proper acquisition of cell class identity in organoids allows definition of fate specification programs of the human cerebral cortex. Cell 185, 3770-3788.e27. https://doi.org/10.1016/j.cell.2022.09.010

Valenzuela-Arzeta, I.E., Soto-Rojas, L.O., Flores-Martinez, Y.M., Delgado-Minjares, K.M., Gatica-Garcia, B., Mascotte-Cruz, J.U., Nava, P., Aparicio-Trejo, O.E., Reyes-Corona, D., Martínez-Dávila, I.A., Gutierrez-Castillo, M.E., Espadas-Alvarez, A.J., Orozco-Barrios, C.E., Martinez-Fong, D., 2023. LPS Triggers Acute Neuroinflammation and Parkinsonism Involving NLRP3 Inflammasome Pathway and Mitochondrial CI Dysfunction in the Rat. Int J

© COPYRIGHT UPM

Mol Sci 24, 4628. https://doi.org/10.3390/ijms24054628

Vallée, A., Vallée, J.-N., Lecarpentier, Y., 2021. Lithium and Atypical Antipsychotics: The Possible WNT/β Pathway Target in Glaucoma. Biomedicines 9, 473. https://doi.org/10.3390/biomedicines9050473

Vasudevan, D., Takeuchi, H., Johar, S.S., Majerus, E., Haltiwanger, R.S., 2015. Peters plus syndrome mutations disrupt a noncanonical ER quality-control mechanism. Curr Biol 25, 286–295. https://doi.org/10.1016/j.cub.2014.11.049

Velasco, S., Kedaigle, A.J., Simmons, S.K., Nash, A., Rocha, M., Quadrato, G., Paulsen, B., Nguyen, L., Adiconis, X., Regev, A., Levin, J.Z., Arlotta, P., 2019. Individual brain organoids reproducibly form cell diversity of the human cerebral cortex. Nature 570, 523–527. https://doi.org/10.1038/s41586-019-1289-x

Velosa, J., Delgado, A., Finger, E., Berk, M., Kapczinski, F., de Azevedo Cardoso, T., 2020. Risk of dementia in bipolar disorder and the interplay of lithium: a systematic review and meta-analyses. Acta Psychiatrica Scandinavica 141, 510–521. https://doi.org/10.1111/acps.13153

Villarreal, A., Seoane, R., González Torres, A., Rosciszewski, G., Angelo, M.F., Rossi, A., Barker, P.A., Ramos, A.J., 2014. S100B protein activates a RAGE-dependent autocrine loop in astrocytes: implications for its role in the propagation of reactive gliosis. J Neurochem 131, 190–205. https://doi.org/10.1111/jnc.12790

Volterra, A., Meldolesi, J., 2005. Astrocytes, from brain glue to communication elements: the revolution continues. Nat Rev Neurosci 6, 626–640. https://doi.org/10.1038/nrn1722

von Mering, C., Huynen, M., Jaeggi, D., Schmidt, S., Bork, P., Snel, B., 2003. STRING: a database of predicted functional associations between proteins. Nucleic Acids Res 31, 258–261. https://doi.org/10.1093/nar/gkg034

Voulgaris, D., Nikolakopoulou, P., Herland, A., 2022. Generation of Human iPSC-Derived Astrocytes with a mature star-shaped phenotype for CNS modeling. Stem Cell Rev Rep 18, 2494–2512. https://doi.org/10.1007/s12015-022-10376-2

Wada, A., 2009. Lithium and Neuropsychiatric Therapeutics: Neuroplasticity via Glycogen Synthase Kinase-3β, β-Catenin, and Neurotrophin Cascades. Journal of Pharmacological Sciences 110, 14–28. https://doi.org/10.1254/jphs.09R02CR

Wakita, S., Hara, M., Kitabatake, Y., Kawatani, K., Kurahashi, H., Hashizume, R., 2022. Experimental method for haplotype phasing across the entire length of chromosome 21 in trisomy 21 cells using a chromosome elimination technique. J Hum Genet 67, 565–572. https://doi.org/10.1038/s10038-022-01049-6

© COPYRIGHT UPM

Wang, C., Li, L., 2023. The critical role of KLF4 in regulating the activation of A1/A2 reactive astrocytes following ischemic stroke. Journal of Neuroinflammation 20, 44. https://doi.org/10.1186/s12974-023-02742-9

Wang, G., Yu, Y., Sun, C., Liu, T., Liang, T., Zhan, L., Lin, X., Feng, X.-H., 2016. STAT3 selectively interacts with Smad3 to antagonize TGF-β signalling. Oncogene 35, 4388–4398. https://doi.org/10.1038/onc.2015.446

Wang, H.-M., Zhang, T., Li, Q., Huang, J.-K., Chen, R.-F., Sun, X.-J., 2013. Inhibition of glycogen synthase kinase-3β by lithium chloride suppresses 6-hydroxydopamine-induced inflammatory response in primary cultured astrocytes. Neurochem Int 63, 345–353. https://doi.org/10.1016/j.neuint.2013.07.003

Wang, W., Lu, D., Shi, Y., Wang, Y., 2024. Exploring the Neuroprotective Effects of Lithium in Ischemic Stroke: A literature review. Int. J. Med. Sci. 21, 284–298. https://doi.org/10.7150/ijms.88195

Wang, X., Ren, J., Wang, Z., Yao, J., Fei, J., 2012. NRSF/REST is required for gastrulation and neurogenesis during zebrafish development. ABBS 44, 385–393. https://doi.org/10.1093/abbs/gms016

Wang, Xin, Du, Z., Xu, T., Wang, Xiao-jun, Li, W., Gao, J., Li, J., Zhu, H., 2021. HIF-1α Is a Rational Target for Future Ovarian Cancer Therapies. Frontiers in Oncology 11. https://doi.org/10.3389/fonc.2021.785111

Wei, M., Ni, J., Shi, J., Li, T., Xu, X., Li, C., Qin, B., Fan, D., Xie, H., Wang, Z., Wang, Y., Lu, T., Tian, J., 2022. Plasma repressor element 1-silencing transcription factor levels are decreased in patients with Alzheimer's disease. BMC Geriatrics 22, 471. https://doi.org/10.1186/s12877-022-03163-8

Weick, Held, D.L., Bonadurer, G.F., Doers, M.E., Liu, Y., Maguire, C., Clark, A., Knackert, J.A., Molinarolo, K., Musser, M., Yao, L., Yin, Y., Lu, J., Zhang, X., Zhang, S.-C., Bhattacharyya, A., 2013. Deficits in human trisomy 21 iPSCs and neurons. Proceedings of the National Academy of Sciences 110, 9962–9967. https://doi.org/10.1073/pnas.1216575110

Weick, J.P., Held, D.L., Bonadurer, G.F., Doers, M.E., Liu, Y., Maguire, C., Clark, A., Knackert, J.A., Molinarolo, K., Musser, M., Yao, L., Yin, Y., Lu, J., Zhang, X., Zhang, S.-C., Bhattacharyya, A., 2013. Deficits in human trisomy 21 iPSCs and neurons. Proc Natl Acad Sci U S A 110, 9962–9967. https://doi.org/10.1073/pnas.1216575110

Wickramasinghe, V.O., Andrews, R., Ellis, P., Langford, C., Gurdon, J.B., Stewart, M., Venkitaraman, A.R., Laskey, R.A., 2014. Selective nuclear export of specific classes of mRNA from mammalian nuclei is promoted by GANP. Nucleic Acids Res 42, 5059–5071. https://doi.org/10.1093/nar/gku095

Wickramasinghe, V.O., McMurtrie, P.I.A., Mills, A.D., Takei, Y., Penrhyn-Lowe, S., Amagase, Y., Main, S., Marr, J., Stewart, M., Laskey, R.A., 2010. mRNA export from mammalian cell nuclei is dependent on GANP. Curr Biol 20, 25–

© COPYRIGHT UPM

31. https://doi.org/10.1016/j.cub.2009.10.078

Woerner, A.C., Frottin, F., Hornburg, D., Feng, L.R., Meissner, F., Patra, M., Tatzelt, J., Mann, M., Winklhofer, K.F., Hartl, F.U., Hipp, M.S., 2016. Cytoplasmic protein aggregates interfere with nucleocytoplasmic transport of protein and RNA. Science 351, 173–176. https://doi.org/10.1126/science.aad2033

Woldegebriel, R., Kvist, J., Andersson, N., Õunap, K., Reinson, K., Wojcik, M.H., Bijlsma, E.K., Hoffer, M.J.V., Ryan, M.M., Stark, Z., Walsh, M., Cuppen, I., van den Boogaard, M.-J.H., Bharucha-Goebel, D., Donkervoort, S., Winchester, S., Zori, R., Bönnemann, C.G., Maroofian, R., O'Connor, E., Houlden, H., Zhao, F., Carpén, O., White, M., Sreedharan, J., Stewart, M., Ylikallio, E., Tyynismaa, H., 2020. Distinct effects on mRNA export factor GANP underlie neurological disease phenotypes and alter gene expression depending on intron content. Hum Mol Genet 29, 1426–1439. https://doi.org/10.1093/hmg/ddaa051

Wren, M.C., Zhao, J., Liu, C.-C., Murray, M.E., Atagi, Y., Davis, M.D., Fu, Y., Okano, H.J., Ogaki, K., Strongosky, A.J., Tacik, P., Rademakers, R., Ross, O.A., Dickson, D.W., Wszolek, Z.K., Kanekiyo, T., Bu, G., 2015. Frontotemporal dementia-associated N279K tau mutant disrupts subcellular vesicle trafficking and induces cellular stress in iPSC-derived neural stem cells. Mol Neurodegener 10, 46. https://doi.org/10.1186/s13024-015-0042-7

Wu, F., Gao, J., Kang, J., Wang, X., Niu, Q., Liu, J., Zhang, L., 2022. Knowledge Mapping of Exosomes in Autoimmune Diseases: A Bibliometric Analysis (2002-2021). Front Immunol 13, 939433. https://doi.org/10.3389/fimmu.2022.939433

Wu, T., Hu, E., Xu, S., Chen, M., Guo, P., Dai, Z., Feng, T., Zhou, L., Tang, W., Zhan, L., Fu, X., Liu, S., Bo, X., Yu, G., 2021. clusterProfiler 4.0: A universal enrichment tool for interpreting omics data. Innovation (Camb) 2, 100141. https://doi.org/10.1016/j.xinn.2021.100141

Xiao, C.-L., Zhu, S., He, M., Chen, D., Zhang, Q., Chen, Y., Yu, G., Liu, J., Xie, S.-Q., Luo, F., Liang, Z., Wang, D.-P., Bo, X.-C., Gu, X.-F., Wang, K., Yan, G.-R., 2018. N6-Methyladenine DNA Modification in the Human Genome. Mol Cell 71, 306-318.e7. https://doi.org/10.1016/j.molcel.2018.06.015

Xu, J., Dawson, V.L., Dawson, T.M., 2013. Usp16: key controller of stem cells in Down syndrome. EMBO J 32, 2788–2789. https://doi.org/10.1038/emboj.2013.220

Xu, R., Boreland, A.J., Li, X., Erickson, C., Jin, M., Atkins, C., Pang, Z.P., Daniels, B.P., Jiang, P., 2021. Developing human pluripotent stem cell-based cerebral organoids with a controllable microglia ratio for modeling brain development and pathology. Stem Cell Reports 16, 1923–1937. https://doi.org/10.1016/j.stemcr.2021.06.011

Xu, R., Brawner, A.T., Li, S., Liu, J.-J., Kim, H., Xue, H., Pang, Z.P., Kim, W.-Y., Hart, R.P., Liu, Y., Jiang, P., 2019. OLIG2 Drives Abnormal Neurodevelopmental

© COPYRIGHT UPM

Phenotypes in Human iPSC-Based Organoid and Chimeric Mouse Models of Down Syndrome. Cell Stem Cell 24, 908-926.e8. https://doi.org/10.1016/j.stem.2019.04.014

Yang, J., Liao, X., Agarwal, M.K., Barnes, L., Auron, P.E., Stark, G.R., 2007. Unphosphorylated STAT3 accumulates in response to IL-6 and activates transcription by binding to NFkappaB. Genes Dev 21, 1396–1408. https://doi.org/10.1101/gad.1553707

Yang, X., Klein, R., Tian, X., Cheng, H.-T., Kopan, R., Shen, J., 2004. Notch activation induces apoptosis in neural progenitor cells through a p53-dependent pathway. Developmental Biology 269, 81–94. https://doi.org/10.1016/j.ydbio.2004.01.014

Yi, J.J., Barnes, A.P., Hand, R., Polleux, F., Ehlers, M.D., 2010. TGF-β Signaling Specifies Axons during Brain Development. Cell 142, 144–157. https://doi.org/10.1016/j.cell.2010.06.010

Ylikallio, E., Woldegebriel, R., Tumiati, M., Isohanni, P., Ryan, M.M., Stark, Z., Walsh, M., Sawyer, S.L., Bell, K.M., Oshlack, A., Lockhart, P.J., Shcherbii, M., Estrada-Cuzcano, A., Atkinson, D., Hartley, T., Tetreault, M., Cuppen, I., van der Pol, W.L., Candayan, A., Battaloglu, E., Parman, Y., van Gassen, K.L.I., van den Boogaard, M.-J.H., Boycott, K.M., Kauppi, L., Jordanova, A., Lönnqvist, T., Tyynismaa, H., 2017. MCM3AP in recessive Charcot-Marie-Tooth neuropathy and mild intellectual disability. Brain 140, 2093–2103. https://doi.org/10.1093/brain/awx138

Yoon, P.W., Freeman, S.B., Sherman, S.L., Taft, L.F., Gu, Y., Pettay, D., Flanders, W.D., Khoury, M.J., Hassold, T.J., 1996. Advanced maternal age and the risk of Down syndrome characterized by the meiotic stage of chromosomal error: a population-based study. Am J Hum Genet 58, 628–633.

Yu, Z., Lin, D., Zhong, Y., Luo, B., Liu, S., Fei, E., Lai, X., Zou, S., Wang, S., 2019. Transmembrane protein 108 involves in adult neurogenesis in the hippocampal dentate gyrus. Cell & Bioscience 9, 9. https://doi.org/10.1186/s13578-019-0272-4

Yuan, J.-B., Yang, L.-Y., Tang, Z.-Y., Zu, X.-B., Qi, L., 2012. Down-regulation of EZH2 by RNA Interference Inhibits Proliferation and Invasion of ACHN Cells via the Wnt/β-catenin Pathway. Asian Pacific Journal of Cancer Prevention 13, 6197–6201. https://doi.org/10.7314/APJCP.2012.13.12.6197

Yun, S.P., Kam, T.-I., Panicker, N., Kim, SangMin, Oh, Y., Park, J.-S., Kwon, S.-H., Park, Y.J., Karuppagounder, S.S., Park, H., Kim, Sangjune, Oh, N., Kim, N.A., Lee, Saebom, Brahmachari, S., Mao, X., Lee, J.H., Kumar, M., An, D., Kang, S.-U., Lee, Y., Lee, K.C., Na, D.H., Kim, D., Lee, S.H., Roschke, V.V., Liddelow, S.A., Mari, Z., Barres, B.A., Dawson, V.L., Lee, Seulki, Dawson, T.M., Ko, H.S., 2018. Block of A1 astrocyte conversion by microglia is neuroprotective in models of Parkinson's disease. Nat Med 24, 931–938. https://doi.org/10.1038/s41591-018-0051-5

© COPYRIGHT UPM

Yuskaitis, C.J., Jope, R.S., 2009. Glycogen synthase kinase-3 regulates microglial migration, inflammation, and inflammation-induced neurotoxicity. Cell Signal 21, 264–273. https://doi.org/10.1016/j.cellsig.2008.10.014

Zamanian Azodi, M., Rezaei Tavirani, Mostafa, Rezaei Tavirani, Majid, Rostami Nejad, M., 2021. Bioinformatics Investigation and Contribution of Other Chromosomes Besides Chromosome 21 in the Risk of Down Syndrome Development. Basic Clin Neurosci 12, 79–88. https://doi.org/10.32598/bcn.12.1.941.6

Zammit, M.D., Laymon, C.M., Tudorascu, D.L., Hartley, S.L., Piro-Gambetti, B., Johnson, S.C., Stone, C.K., Mathis, C.A., Zaman, S.H., Klunk, W.E., Handen, B.L., Cohen, A.D., Christian, B.T., 2021. Patterns of glucose hypometabolism in Down syndrome resemble sporadic Alzheimer's disease except for the putamen. Alzheimers Dement (Amst) 12, e12138. https://doi.org/10.1002/dad2.12138

Zappulo, A., van den Bruck, D., Ciolli Mattioli, C., Franke, V., Imami, K., McShane, E., Moreno-Estelles, M., Calviello, L., Filipchyk, A., Peguero-Sanchez, E., Müller, T., Woehler, A., Birchmeier, C., Merino, E., Rajewsky, N., Ohler, U., Mazzoni, E.O., Selbach, M., Akalin, A., Chekulaeva, M., 2017. RNA localization is a key determinant of neurite-enriched proteome. Nat Commun 8, 583. https://doi.org/10.1038/s41467-017-00690-6

Zdaniuk, G., Wierzba-Bobrowicz, T., Szpak, G.M., Stępień, T., 2011. Astroglia disturbances during development of the central nervous system in fetuses with Down's syndrome. Folia Neuropathol 49, 109–114.

Zhang, B., Horvath, S., 2005. A general framework for weighted gene co-expression network analysis. Stat Appl Genet Mol Biol 4, Article17. https://doi.org/10.2202/1544-6115.1128

Zhang, H.-Y., Wang, Y., He, Y., Wang, T., Huang, X.-H., Zhao, C.-M., Zhang, L., Li, S.-W., Wang, C., Qu, Y.-N., Jiang, X.-X., 2020. A1 astrocytes contribute to murine depression-like behavior and cognitive dysfunction, which can be alleviated by IL-10 or fluorocitrate treatment. Journal of Neuroinflammation 17, 200. https://doi.org/10.1186/s12974-020-01871-9

Zhang, L., He, C.H., Coffey, S., Yin, D., Hsu, I.-U., Su, C., Ye, Y., Zhang, C., Spurrier, J., Nicholson, L., Rothlin, C.V., Ghosh, S., Gopal, P.P., Hafler, D.A., Zhao, H., Strittmatter, S.M., 2023. Single-cell transcriptomic atlas of Alzheimer's disease middle temporal gyrus reveals region, cell type and sex specificity of gene expression with novel genetic risk for MERTK in female. medRxiv 2023.02.18.23286037. https://doi.org/10.1101/2023.02.18.23286037

Zhang, P., Tian, Q., Gao, H., Zhao, A., Shao, Y., Yang, J., 2022. Inhibition of MAC30 exerts antitumor effects in nasopharyngeal carcinoma via affecting the Akt/GSK-3β/β-catenin pathway. Journal of Biochemical and Molecular Toxicology 36, e23061. https://doi.org/10.1002/jbt.23061

© COPYRIGHT UPM

Zhang, Y., Sloan, S.A., Clarke, L.E., Caneda, C., Plaza, C.A., Blumenthal, P.D., Vogel, H., Steinberg, G.K., Edwards, M.S.B., Li, G., Duncan, J.A., Cheshier, S.H., Shuer, L.M., Chang, E.F., Grant, G.A., Gephart, M.G.H., Barres, B.A., 2016. Purification and Characterization of Progenitor and Mature Human Astrocytes Reveals Transcriptional and Functional Differences with Mouse. Neuron 89, 37–53. https://doi.org/10.1016/j.neuron.2015.11.013

Zhao, H.H., Haddad, G.G., 2022. Alzheimer's disease like neuropathology in Down syndrome cortical organoids. Front. Cell. Neurosci. 16. https://doi.org/10.3389/fncel.2022.1050432

Zhao, J., Huai, J., 2023. Role of primary aging hallmarks in Alzheimer´s disease. Theranostics 13, 197–230. https://doi.org/10.7150/thno.79535

Zhao, Y., Min Zhu, Yanlan Yu, Linli Qiu, Yuanyuan Zhang, Li He, Jiqiang Zhang, 2017. Brain REST/NRSF Is Not Only a Silent Repressor but Also an Active Protector. Molecular Neurobiology 54, 541–550. https://doi.org/10.1007/s12035-015-9658-4

Zou, L.-H., Shi, Y.-J., He, H., Jiang, S.-M., Huo, F.-F., Wang, X.-M., Wu, F., Ma, L., 2019. Effects of FGF2/FGFR1 Pathway on Expression of A1 Astrocytes After Infrasound Exposure. Frontiers in Neuroscience 13.

© COPYRIGHT UPM

APPENDICES

Appendix A

A 1 : Command lines/scripts used for differential gene expression analysis. ***The limma package was used to perform the differential gene expression analysis. The commands used in Rstudio are as follows:***

```
# Load required packages
> library(ggplot2)
> library(limma)
> library(pheatmap)
# Set working directory and read input files
> setwd("/huangtan/UPM/Thesis/DEG_analysis")
> expFile="SampleGeneExp.txt"
> conFile="sample1_con.txt"
> dsFile="sample2_ds.txt"
> rt=read.table(expFile,sep="\t",header=T,check.names=F)
> rt=as.matrix(rt)
> rownames(rt)=rt[,1]
> exp=rt[,2:ncol(rt)]
> dimnames=list(rownames(exp),colnames(exp))
> rt=matrix(as.numeric(as.matrix(exp)),nrow=nrow(exp),dimnames=dimnames)
> data=avereps(rt)
> data=normalizeBetweenArrays(data)
# Read control and experimental group files and merge
> datasample1=read.table(conFile,sep="\t",header=F,check.names=F)
> sample2=read.table(dsFile,sep="\t",header=F,check.names=F)
> conData=rt[,as.vector(sample1[,1])]
> dsData=rt[,as.vector(sample2[,1])]
> rt=cbind(conData,dsData)
> conNum=ncol(conData)
> dsNum=ncol(dsData)
# Perform differential expression
> analysismodType=c(rep("con",conNum),rep("ds",dsNum))
> design <- model.matrix(~0+factor(modType))
> colnames(design) <- c("con","ds")
> fit <- lmFit(rt,design)
> cont.matrix<-makeContrasts(ds-con,levels=design)
> fit2 <- contrasts.fit(fit, cont.matrix)
> fit2 <- eBayes(fit2)
# Output results of differential expression
```


© COPYRIGHT UPM

```
> analysisallDiffAna=topTable(fit2,adjust='fdr',number=2000000)
> write.table(allDiffAna,file="all.xls",sep="\t",quote=F, row.names = F)
```

A2 : Command lines/scripts used for the visualisation of heatmap and volcano plot. The commands used in Rstudio are as follows:

```
# Load packages
> library(pheatmap)
# Set working directory and read input files
> setwd("/huangtan/UPM/Thesis/ Heatmap_Volcano")
> inputFile = "DEGs_Exp.txt"
> rt = read.table(inputFile, header = T, sep = "\t", check.names = F, row.names = 1)
> Con = grepl("_Con", colnames(rt), ignore.case = T)
> DS = grepl("_DS", colnames(rt), ignore.case = T)
> ConData = rt[, Con]
> DSData = rt[, DS]
> ConNum = ncol(ConData)
> DSNum = ncol(DSData)
> data = cbind(ConData, DSData)
# Define data vector
> Type = c(rep("Con", ConNum), rep("DS", DSNum))
> names(Type) = colnames(data)
> Type = as.data.frame(Type)
# Hotmap
> pheatmap(data, annotation = Type,
        color = colorRampPalette(c(rep("green", 3), "white", rep("red", 3)))(50),
        border = NA,
        cluster_cols = F,
        show_colnames = F,
        show_rownames = F,
        scale = "row",
        fontsize = 6, fontsize_row = 6, fontsize_col = 6)
> pdf(file = "heatmap.pdf", width = 5, height = 5)

###Volcano plot
# Define colours for different gene expression categories
# Default colour for non-significant genes
> color <- rep("#999999", nrow(data))
# Upregulated genes
> color[data$adj.pvalue < 0.05 & data$log2FoldChange > 0.5] <- "#FC4E07"
# Downregulated genes
> color[data$adj.pvalue < 0.05 & data$log2FoldChange < -0.5] <- "#00AFBB"
```

```
> par(oma = c(0,2,0,0))    # Adjust outer margins
# Plot volcano
> plot(data$log2FoldChange,
       -log10(data$adj.pvalue),
       pch = 16, cex = 0.5,
       xlim = c(-10,10),
       ylim = c(0,15),
       col = color,
       frame.plot = F,
       xlab = "log2FC",
       ylab = "-log10(adj.Pvalue)",
       cex.axis = 1, cex.lab = 1.3)
# Add reference lines
> abline(h = -log10(0.05), lwd = 2, lty = 3)
> abline(v = c(-0.5, 0.5), lwd = 2, lty = 3)
# Add legend
> legend(x = -12, y = 15, legend = c("Up", "No", "Down"),
       bty = "n",
       pch = 19, cex = 1,
       x.intersp = 0.3,
       y.intersp = 0.3,
       col = c("#FC4E07", "#999999", "#00AFBB"))
# Add labels for the top 10 genes
> color = c()
> color[which(data[1:10,]$regulate == "Up")] = "#FC4E07"
> color[which(data[1:10,]$regulate == "Down")] = "#00AFBB"
> text(data$log2FoldChange[1:10], -log10(data$adj.pvalue)[1:10],
       labels = data$GeneID[1:10],
       adj = c(0,1.5),
       cex = 0.6,
       col = color)
> pdf(file = "volcano.pdf", width = 5, height = 5)
> dev.off()
```

© COPYRIGHT UPM

A3 : Command lines/scripts used for the visualisation of the results of the biological process and KEGG enrichment analysis. The commands used in Rstudio are as follows:

```
### GO analysis
# Load required packages
> library("clusterProfiler")
> library("org.Hs.eg.db")
> library("enrichplot")
> library("ggplot2")
# Set working directory and read input files
> setwd("/huangtan/UPM/Thesis/GO_KEGG")
> rt = read.table("Gene_ID.txt", sep="\t", header=T, check.names=F)
> rt = rt[is.na(rt[,"entrezID"]) == F,] column
> gene = rt$entrezID
# Define color selection criteria
> colorSel = "qvalue"
> if(qvalueFilter > 0.05){
        colorSel = "pvalue"}
# GO enrichment analysis
> kk = enrichGO(gene = gene, OrgDb = org.Hs.eg.db, pvalueCutoff = 1, qvalueCutoff
= 1, ont = "BP", readable = T)
> GO = as.data.frame(kk)
> GO = GO[(GO$pvalue < pvalueFilter & GO$qvalue < qvalueFilter),]
# Save enrichment results
> write.table(GO, file="BiologicalProcess.txt", sep="\t", quote=F, row.names=F)
# Define the number of terms to display
> showNum = 10
> if(nrow(GO) < 30){
        showNum = nrow(GO)}
# Generate bar plot
> bar = barplot(kk, drop = TRUE, showCategory = showNum, color = colorSel) +
facet_grid(scale='free')
> pdf(file = " BiologicalProcess.pdf", width = 5, height = 5)
> dev.off()

### KEGG analysis
# Load required packages
> library(clusterProfiler)
> library(org.Hs.eg.db)
> library(enrichplot)
> library(ggplot2)
> library(circlize)
> library(RColorBrewer)
```


© COPYRIGHT UPM

```
> library(dplyr)
> library(ComplexHeatmap)
# KEGG enrichment analysis
> kk <- enrichKEGG(gene = gene, organism = "hsa", pvalueCutoff = 1, qvalueCutoff
= 1)
> KEGG = as.data.frame(kk)
> KEGG$geneID = as.character(sapply(KEGG$geneID,
function(x)
> paste(rt$genes[match(strsplit(x, "/")[[1]], as.character(rt$entrezID))], collapse =
"/")))
KEGG = KEGG[(KEGG$pvalue < pvalueFilter & KEGG$qvalue < qvalueFilter),]
# Save significantly enriched results
> write.table(KEGG, file = "KEGG_R.txt", sep = "\t", quote = F, row.names = F)
# Define color selection criteria
> colorSel = "qvalue"
> if(qvalueFilter > 0.05){
   colorSel = "pvalue"}
# Define the number of terms to display
> showNum = 10
> if(nrow(KEGG) < 30){
   showNum = nrow(KEGG)}
# Generate bar plot
> bar = barplot(kk, drop = TRUE, showCategory = showNum, color = colorSel) +
facet_grid(scale = 'free')
> pdf(file = "KEGG.pdf", width = 5, height = 5)
> dev.off()
```

© COPYRIGHT UPM

A4 : The top 10 DEGs were shown in the volcano plots in DS brain different regions in GSE59630 in Figure 3.3.

Brain region	Gene symbol	p-value	LogFoldChange	Up- / Down-regulation
CBC (Cerebellar cortex)	HIF3A	4.89E-09	1.847549388	Up
	NCAM2	3.29E-08	1.245273625	Up
	IFNAR1	3.75E-08	1.0406649	Up
	WRB	1.16E-07	0.7737492	Up
	SLC30A5	2.50E-07	-0.825114029	Down
	CRYZL1	2.51E-07	1.95978495	Up
	ITGB8	3.51E-07	1.946247508	Up
	GJB6	3.57E-07	2.667094375	Up
	STOM	5.90E-07	1.997998875	Up
	METTL7A	7.64E-07	1.79055365	Up

Brain region	Gene symbol	p-value	LogFoldChange	Up- / Down-regulation
DFC (Dorsolateral prefrontal cortex)	EMP1	5.91E-09	2.48556175	Up
	IFNAR1	7.29E-08	0.977854312	Up
	PROS1	5.84E-07	1.041733073	Up
	BACH1	7.35E-07	1.290996813	Up
	SLC25A13	9.15E-07	-0.97173175	Down
	SLC44A3	1.78E-06	1.301605385	Up
	PECAM1	1.98E-06	1.966333125	Up
	PTTG1IP	2.06E-06	1.440860229	Up
	CTNNA1	2.35E-06	0.963826969	Up
	SULT1B1	2.60E-06	1.331005094	Up

Brain region	Gene symbol	p-value	LogFoldChange	Up- / Down-regulation
HIP (Hippocampus)	PROS1	1.42E-05	2.296112222	Up
	SLC14A1	2.62E-05	3.037288889	Up
	EMP2	6.37E-05	2.561586111	Up
	TIMP1	6.42E-05	1.829828333	Up
	EMP1	7.40E-05	2.725173333	Up
	SERPINF1	1.27E-04	3.110391667	Up
	PLP2	1.53E-04	1.848856667	Up
	BACH1	1.83E-04	1.493394722	Up
	WFIKKN2	1.94E-04	1.891635	Up
	PDXK	2.54E-04	1.422516667	Up

© COPYRIGHT UPM

Brain region	Gene symbol	p-value	LogFoldChange	Up- / Down-regulation
ITC (Inferior temporal cortex)	TMEM155	2.27E-07	-2.2387924	Down
	HIF3A	1.41E-06	1.7883261	Up
	RAB6C	3.92E-06	-1.859425	Down
	RDX	4.43E-06	1.7910434	Up
	NPTX2	6.72E-06	-1.7869633	Down
	IFNAR1	7.91E-06	1.2531443	Up
	CTNNA1	1.15E-05	1.56143575	Up
	METTL7A	1.25E-05	2.0290887	Up
	TBC1D22B	1.30E-05	-1.2981025	Down
	SPPL2A	1.57E-05	1.4664144	Up

Brain region	Gene symbol	p-value	LogFoldChange	Up- / Down-regulation
OFC (Prefrontal cortex)	SAMHD1	1.55E-06	1.461398125	Up
	IFNAR2	2.57E-06	1.174797431	Up
	KDM3A	5.28E-06	1.269769444	Up
	IFNAR1	8.10E-06	1.026538056	Up
	LPL	9.02E-06	1.450820972	Up
	IL13RA1	1.17E-05	1.394528958	Up
	SNRNP25	1.82E-05	-1.317471944	Down
	SSNA1	2.05E-05	-1.781879861	Down
	ROGDI	2.32E-05	-1.058368021	Down
	PMF1	2.39E-05	-1.343804722	Down

Brain region	Gene symbol	p-value	LogFoldChange	Up- / Down-regulation
S1C (Primary somatosensory cortex)	FAM223B	1.88E-07	-3.67965125	Down
	DNAJB1	2.53E-07	-4.3802575	Down
	MIR7-3HG	3.29E-07	-3.419395	Down
	PI15	6.57E-07	5.01016375	Up
	FCGR1A	6.65E-07	3.133165	Up
	HSPA1B	7.01E-07	-5.7264025	Down
	EGR2	7.21E-07	-3.71193625	Down
	ZFAND2A	8.98E-07	-2.962659375	Down
	STK17B	8.98E-07	3.054185	Up
	HILPDA	9.37E-07	3.1855325	Up

© COPYRIGHT UPM

Brain region	Gene symbol	p-value	LogFoldChange	Up- / Down-regulation
V1C (Primary visual cortex)	PI15	3.65E-11	5.006968471	Up
	IRAK3	4.87E-11	3.066464824	Up
	TMEM100	1.58E-10	3.555136539	Up
	SULT1B1	2.63E-09	2.267071033	Up
	FCGR1A	6.80E-09	2.929175248	Up
	SLC16A3	1.18E-07	1.625500579	Up
	IGFBP3	1.34E-07	2.582668254	Up
	EDN1	1.43E-07	2.835091271	Up
	FPR1	3.09E-07	2.246773884	Up
	FKBP5	4.30E-07	3.291272154	Up

Brain region	Gene symbol	p-value	LogFoldChange	Up- / Down-regulation
VFC (Ventrolateral prefrontal cortex)	WRB	1.99E-06	0.99854398	Up
	RASAL1	3.67E-06	-1.239843929	Down
	MPP2	7.44E-06	-0.922975816	Down
	BACH1	2.49E-05	1.532386735	Up
	C1orf64	2.85E-05	1.54347699	Up
	PTTG1IP	2.89E-05	1.330522296	Up
	SOD1	2.98E-05	1.415377449	Up
	FANCD2OS	3.02E-05	1.026547551	Up
	NEK6	3.06E-05	1.108900612	Up
	PRKCG	3.35E-05	-1.210114107	Down

© COPYRIGHT UPM

A5 : The top 10 DEGs were shown in the volcano plots in Down syndrome brain different age stages in GSE59630 in Figure 3.4.

Age stage	Gene symbol	p-value	LogFoldChange	Up- / Down-regulation
Fetal (16 to 22 gestational weeks)	GSTM1	2.03E-08	-3.594042813	Down
	SSNA1	1.57E-07	-2.612182813	Down
	PEBP1	4.67E-07	2.279447656	Up
	RELA	6.82E-07	-1.716030703	Down
	GRK6	7.71E-07	-1.837357813	Down
	SNAP91	9.04E-07	1.947585625	Up
	CDK5	4.54E-06	-1.590271875	Down
	GPAA1	6.47E-06	-1.181274531	Down
	SLC5A3	8.92E-06	1.309916875	Up
	DOK3	9.43E-06	-2.281158906	Down

Age stage	Gene symbol	p-value	LogFoldChange	Up- / Down-regulation
Infant (0 to 12 months)	IFNAR1	6.19E-16	1.039207991	Up
	EDN1	8.79E-15	1.902811844	Up
	NR4A1	2.17E-14	-1.741561167	Down
	HIF3A	6.58E-14	1.480284246	Up
	EMP2	7.73E-14	1.718706795	Up
	SAMD8	1.24E-13	0.934885938	Up
	ALDH1L1	2.59E-13	1.279603663	Up
	YAP1	9.35E-13	1.293222301	Up
	GINM1	1.55E-12	1.321219923	Up
	SULT1B1	3.99E-12	1.333478538	Up

Age stage	Gene symbol	p-value	LogFoldChange	Up- / Down-regulation
Child (2 to 16 years)	SOD1	5.85E-14	1.7916647	Up
	PEBP1	3.14E-13	1.476347633	Up
	RPS29	1.90E-10	1.128188856	Up
	CRYZL1	2.15E-10	1.274676044	Up
	IFNAR1	6.13E-10	1.005689867	Up
	C21orf33	1.25E-09	0.71343505	Up
	SLC43A3	2.43E-08	-1.098664822	Down
	NAT14	2.98E-08	1.169772643	Up
	SNAP91	5.10E-08	1.663368544	Up
	SLC4A2	8.15E-08	-0.794282572	Down

© COPYRIGHT UPM

Age stage	Gene symbol	p-value	LogFoldChange	Up- / Down-regulation
Adult (18 to 42 years)	WRB	6.20E-18	1.067802439	Up
	GSTM1	2.09E-16	3.820205065	Up
	PTTG1IP	3.24E-16	1.7733866	Up
	ARL4D	3.80E-16	-1.59208667	Down
	IL17RB	2.34E-14	2.128468123	Up
	STOM	6.20E-14	2.355946595	Up
	LIMK2	1.01E-13	1.334826185	Up
	NFE2L2	2.81E-13	1.571447232	Up
	PEBP1	3.71E-13	1.148001644	Up
	SRGN	4.00E-13	2.249234416	Up

© COPYRIGHT UPM

A6 : The top 10 DEGs were shown in the volcano plots in DS-derived organoids and neural cells in Figure 3.5.

Organoid	Gene symbol	p-value	LogFoldChange	Up- / Down-regulation
30-Day (PRJNA72827)	TTYH1	1.55E-14	4.232205747	Up
	HERC2P3	3.13E-11	3.804730218	Up
	LIPG	3.13E-11	-1.684058233	Down
	UNC13D	1.24E-10	2.259021039	Up
	BTNL9	4.70E-10	5.00928207	Up
	ADARB1	4.72E-10	1.364310773	Up
	FCGBP	1.03E-09	2.030934621	Up
	HLCS	2.93E-09	0.970441289	Up
	SYTL2	9.01E-09	-1.554505587	Down
	EMX1	1.87E-08	2.738025507	Up

Neural cell	Gene symbol	p-value	LogFoldChange	Up- / Down-regulation
NPC (GSE84887)	TMEM47	3.21E-06	-1.024302067	Down
	GART	6.22E-05	0.893552933	Up
	RMDN1	1.20E-04	-0.5063372	Down
	RASGRP1	1.56E-04	-0.7742266	Down
	LRCH2	1.60E-04	-1.3220636	Down
	USP25	2.24E-04	0.585342933	Up
	PABPC5	2.64E-04	-2.065073933	Down
	DSCR3	3.13E-04	0.541988333	Up
	C21orf33	3.46E-04	0.579775	Up
	RP11-382B	3.71E-04	-0.763660533	Down

Neural cell	Gene symbol	p-value	LogFoldChange	Up- / Down-regulation
Neuron (GSE48611)	NNAT	8.91E-09	5.22637	Up
	FAM218A	1.01E-08	2.077995833	Up
	ZNF248	1.11E-07	-1.77616	Down
	THEM6	1.20E-06	-1.47475	Down
	ZNF578	1.29E-06	1.0229475	Up
	TRMT12	5.09E-06	0.848035	Up
	ZNF717	5.33E-06	1.1586475	Up
	USP51	6.72E-06	-2.0788175	Down
	SPATC1L	8.72E-06	0.775521667	Up
	MAGEH1	9.77E-06	-2.427416667	Down

© COPYRIGHT UPM

Neural cell	Gene symbol	p-value	LogFoldChange	Up- / Down-regulation
Astrocyte (GSE42772**)**	NSDHL	5.26E-05	-0.459333333	Down
	MPP5	1.44E-04	-0.596666667	Down
	APP	4.06E-04	0.654	Up
	PLA2G3	4.19E-04	-0.605333333	Down
	KIAA1008	6.59E-04	-0.287333333	Down
	MLH3	7.29E-04	-0.188666667	Down
	TSPAN31	7.62E-04	-0.444	Down
	DEPDC6	8.10E-04	1.135333333	Up
	POT1	9.89E-04	-0.224666667	Down
	LOC283514	1.20E-03	0.198	Up

© COPYRIGHT UPM

A7 : The LogFoldChange value of total 51common REST-targeted DEGs across all brain regions in DS in GSE59630. Cerebellar cortex: CBC; Dorsolateral prefrontal cortex: DFC; Hippocampus: HIP; Inferior temporal cortex: ITC; Prefrontal cortex: OFC; Primary somatosensory cortex: S1C; Primary visual cortex: V1C; Ventrolateral prefrontal cortex: VFC

Gene Symbol	Log Fold Change								Up-/Down-Regulation
	CBC	DFC	HIP	ITC	OFC	S1C	V1C	VFC	
ABHD16A	-0.5989177	-0.6229893	-0.6833111	-0.8559834	-0.6340687	-1.0186088	-1.525493	-0.8575482	Down
ADAMTS9	0.8383276	1.0293349	1.9826047	1.4903403	1.4922185	1.57671	2.8424902	1.4287706	Up
ANXA3	0.53897918	1.47147899	1.11759472	1.4927367	1.1472922	2.4033919	2.7810669	1.3274609	Up
ARL4D	-0.8704065	-1.9679965	-1.0834617	-1.4087376	-1.3864972	-2.978325	-1.5984289	-1.3067516	Down
BACH1	0.8503143	1.2909968	1.4933947	1.2340701	1.2282605	1.4695962	1.7654021	1.5323867	Up
BNIP2	0.5494534	0.6208477	1.3944356	1.1204494	0.763355	1.1625925	1.4668466	0.6685655	Up
BRWD1	0.8329778	0.7842038	1.0923519	1.2110834	0.9826256	0.6710137	0.9853755	0.9425492	Up
CP	1.7980486	2.5841772	3.1004133	2.936766	2.2530696	0.8504425	0.9001301	2.3089801	Up
CRYZL1	1.9597849	1.1277159	1.3369867	1.4641438	1.0619219	1.0407388	1.5517561	1.1604039	Up
CYBRD1	1.4236605	1.6695545	1.3969394	1.0481996	0.9422422	0.9129512	2.0647476	0.8399017	Up
DONSON	0.6446805	0.5033542	0.7573639	0.5210585	0.669372	1.0540988	1.2588448	0.5098577	Up
DPH2	-0.6355503	1.1609169	-0.9227142	-0.6874134	-0.6985101	-0.8645025	-0.8341595	-0.7911445	Down
DPY19L3	1.0598725	1.16091686	1.1762611	1.4480929	1.1710199	2.1357788	2.3977634	1.1831511	Up
EPHB6	-0.570123	-0.7838854	-1.0052983	-1.4286032	-1.0169169	-1.4181587	-1.7027467	-0.8574961	Down
FERMT2	0.8986888	1.2765323	1.447665	1.4220177	1.2972729	1.8564962	2.4211005	1.1807791	Up
FKBP5	1.2518489	1.9110851	1.6341167	2.0401359	1.695051	2.7868031	3.2912722	1.7790968	Up
HILPDA	1.5381513	2.1956841	1.1774994	1.6368486	1.8620583	3.1855325	2.5911443	2.2023542	Up
HSD17B12	0.7094797	0.7182869	0.92702	0.8539457	0.5859255	0.6324069	1.2762168	0.5728101	Up
KDM3A	0.9714884	0.8072613	1.2406883	1.1293859	1.2697694	1.9601513	1.3807611	1.0511032	Up
METTL7A	1.7905537	2.3100052	1.62654	2.0290887	1.5919492	0.9683312	1.6835121	1.5636129	Up

MKLN1	0.6008579	0.9545021	0.8609056	0.800999	0.907481	0.895105	1.4086461	0.8175508	Up
MLF2	-0.5832926	-0.7448053	-0.7557597	-1.0149868	-0.8765438	-1.1461375	-0.8660951	-0.8565168	Down
PDK4	1.7710752	2.2166656	1.3878575	2.2272489	1.5975062	2.965805	3.4101889	1.8677511	Up
PDXK	0.8602447	1.2477203	1.4225167	0.9808097	0.8698015	0.7332488	1.3427952	0.7931054	Up
PLBD2	-0.5299415	-0.8519615	-1.0527889	-1.1817842	-0.8878883	-1.7621663	-1.3664451	-1.2455454	Down
PRMT2	0.9246197	0.711943	1.0551122	1.0562014	0.8304044	0.9042869	1.0399999	0.9298459	Up
PTTG1IP	1.2172908	1.4408602	1.3554528	1.8221004	1.5164093	1.492805	1.8392149	1.3305223	Up
RBM39	0.9377208	0.6463236	0.8553061	1.2295194	0.7143324	0.7688012	0.9754163	0.7268121	Up
RDX	1.0814577	0.7949003	1.0299183	1.7910434	0.9955767	1.2017125	0.8888457	0.9815658	Up
RFX4	0.9963612	1.8876481	0.9212811	1.5501825	1.4368231	1.4808594	2.3442303	1.2169228	Up
SLC25A44	-0.7479572	-0.5044606	-0.725875	-0.7543157	-0.5900275	-0.6791425	-0.5989276	-0.6171505	Down
SLCO4A1	0.6051647	0.77732	1.0200514	0.8966113	0.6834944	0.97375	0.8544871	0.8101669	Up
SSNA1	-1.8693863	-1.4705659	-1.54595	-1.6861323	-1.7818799	-1.0516025	-1.1625868	-1.5923771	Down
STOM	1.9979989	2.5582156	2.2963628	2.1728677	1.5436013	2.1758038	2.2198992	1.6199244	Up
SULT1B1	0.7727148	1.3310051	1.0926183	0.7823978	0.8371486	1.7759631	2.267071	0.7970122	Up
TP53BP2	1.0496287	1.3932955	1.1852392	1.355981	1.1967658	1.3740562	1.5560418	1.3368265	Up
USP16	0.6992183	0.7432013	0.7640153	0.9249207	0.6630526	1.1776263	1.242745	0.6086827	Up
WBSCR22	-1.139508	-0.5005314	-1.0737039	-1.0293033	-0.8708918	-0.9240237	-1.1907259	-0.8163024	Down
YAP1	1.1335487	1.6106496	1.2142997	1.4696483	1.369686	1.4931687	1.3355218	1.350882	Up
ZFYVE27	-0.6229853	-0.6121626	-0.9666139	-0.7016908	-0.7572355	-0.99968	-1.0466074	-1.0433447	Down
MAOA	1.7635562	1.6354728	1.6184603	1.1357617	1.1138719	0.7672075	2.2232505	1.2013976	Up
SLC2A1	0.7195146	1.2923173	1.1497461	1.2769823	1.0867292	1.7074137	2.0878047	1.1502092	Up
EMP2	1.2548267	1.7956525	2.5615861	1.7704578	1.1981039	1.3434594	1.4036893	1.1754139	Up
EMP1	1.5550846	2.4855618	2.7251733	2.2560317	2.1560562	1.5064506	2.6650368	1.7554082	Up
FLT1	1.257673	1.8742767	1.8697575	2.0667917	1.611031	1.3161163	2.1871795	1.2896586	Up
DDIT4	1.2332364	1.9499337	2.4220783	1.6746559	1.5539594	1.6407463	3.0642748	1.4578834	Up

ITGB8	1.9462475	1.0594522	1.0759511	1.2518082	1.1115369	2.0070181	1.9973584	1.0204891	Up
NOTCH2	0.6817572	1.3251186	1.3194542	1.3544012	1.2749825	1.0879125	1.5831642	1.1827522	Up
OSMR	0.7764431	1.6464434	1.5407417	1.2157316	1.6039842	1.7146675	1.8461877	1.52177	Up
IFNAR2	0.796892	1.0802727	1.1851126	1.1947319	1.1747974	1.2078613	1.1136803	1.0195534	Up
IFNAR1	1.0406649	0.9778543	1.1475417	1.2531443	1.0265381	1.292625	1.2845968	0.7583419	Up

© COPYRIGHT UPM

A8 : The LogFoldChange value of total 51common REST-targeted DEGs across all age groups in DS in GSE59630. Fetal (16 to 22 gestational weeks), Infant child (2 to 16 years), Child (2 to 16 years) and Adult (18 to 42 years).

Gene Symbol	Log Fold Change				Up-/Down-Regulation
	Fetal	Infant	Child	Adult	
ANGPT2	1.7462881	0.9349179	1.1267224	2.0156406	Up
ARL4D	-0.8820044	-1.4461182	-0.8548818	-1.5920867	Down
ARPC1B	0.5782325	0.6571869	0.6766181	1.3771292	Up
BACH1	1.1833397	1.0881213	1.304073	1.5651152	Up
BRWD1	1.1153069	0.709542	0.5628276	1.3074567	Up
C1QTNF4	-0.6667458	-0.9747532	-0.6001248	-0.7716609	Down
C2CD2L	-0.9110989	-0.8572735	-0.7023553	-0.8653748	Down
CDK2AP2	-1.0929588	-1.1650199	-0.8516517	-1.0312538	Down
CIART	1.19979297	0.821296	0.6293051	0.512668	Up
COX5B	-1.0160547	-0.7731818	-0.7353822	-1.0141149	Down
CRYZL1	0.9990164	1.3797354	1.274676	1.4159663	Up
CTNNA1	0.8613395	0.8468477	0.7918539	1.2014856	Up
DARS	0.6078856	0.8967701	0.5496935	1.2037927	Up
DPP3	-0.7791134	-0.7597937	-0.6853788	-0.6470082	Down
EIF4H	-1.1704884	-0.6805605	-1.1456847	-1.203546	Down
ETV3	-0.7479909	-0.6430344	-0.8434639	-1.1866218	Down
GART	0.9683453	0.5475728	0.8143666	1.1590938	Up
GPAA1	-1.1812745	-1.0127977	-1.0184993	-1.6207284	Down
HMGA1	-1.1556553	-0.6471534	-0.8653237	-0.8659095	Down
HMGN1	0.8546573	0.5704636	0.7978979	0.9131586	Up
HMGN3	0.6172844	0.5297007	0.6232014	1.4432945	Up
IFNAR1	0.971017	1.039208	1.0056899	0.9566062	Up
ITSN1	0.8027563	0.9035695	0.6439171	0.9434869	Up
KDM3A	1.1885798	0.9804632	0.7747056	0.9740911	Up
KRT86	0.6123713	0.566213	0.648773	0.5581972	Up
LIMK1	-0.6840919	-0.5708791	-0.5644881	-1.0260984	Down
MANEAL	-0.8681084	-0.5857702	-0.572684	-0.8921997	Down
MORC3	0.9839766	0.5002969	1.0030794	1.3338975	Up
MRPL39	1.0965075	0.8054741	0.6421446	0.6185795	Up
MTHFD2	0.9464394	0.6181719	0.749369	1.2152483	Up
NEK6	1.277125	0.7225016	0.8516456	1.322691	Up
NRIP1	0.6293969	0.8377055	0.560355	0.7422531	Up
PDE9A	0.7745661	0.9486508	0.6358394	0.713951	Up
PDXK	1.2091478	0.8645554	0.9300603	0.7354005	Up
PFDN5	0.6843947	0.7106195	0.5170816	0.6577858	Up
PFKL	0.6826588	0.7164471	0.7871859	0.8005926	Up
PLD3	-0.8013428	-0.8699987	-0.6610196	-1.3207087	Down
PRMT2	1.0986012	0.7874448	1.011008	1.0299845	Up
PYROXD1	-0.5847031	-0.5151932	-0.8690533	-0.6963145	Down
RBM47	0.88577	0.6260222	0.7874687	0.9528061	Up

RDX	0.58071	1.1092402	0.6592446	1.2810184	Up
RIT1	0.8870612	0.7406449	0.5463212	0.8659202	Up
RPS15A	1.1392759	1.1134234	1.8792699	2.0989449	Up
SDC4	0.6609894	1.3584686	1.1439558	1.3981032	Up
SLC2A1	1.0219622	1.1337636	0.5246817	1.1838625	Up
SOD1	1.4393522	1.096631	1.7916647	1.4487652	Up
SON	0.8404731	1.2429014	1.0670942	0.9846171	Up
SPPL2A	1.0116319	1.0036204	0.500943	1.0741104	Up
SSNA1	-2.6121828	-1.7096067	-1.0185258	-1.8619203	Down
TMEM204	0.9668697	1.2508842	1.2524376	0.9507395	Up
TP53BP2	0.5554055	1.2179039	0.7321594	1.5666985	Up
TXNL4A	-0.5007066	-0.6428045	-0.5102241	-0.9136554	Down
UBE2G2	0.6694412	0.5575733	0.7785442	0.7886841	Up
WRB	0.7571569	0.74248	0.704024	1.0678024	Up
YAP1	1.262518	1.2932223	0.6317965	1.5086155	Up
ZFYVE27	-0.8912278	-0.7170002	-0.6338157	-0.8709974	Down

© COPYRIGHT UPM

Appendix B

B1 : Command lines/scripts used for the visualisation of the results of the GSEA enrichment analysis. The commands used in Rstudio are as follows:

```
# Load required packages
> library(org.Hs.eg.db)
> library(clusterProfiler)
> library(enrichplot)
# Set working directory and read input files
> setwd("/huangtan/UPM/Thesis/GSEA")
> inputFile="GSEA.txt"
> deg=read.table(inputFile, header=T, sep="\t", check.names=F)
> colnames(deg)
> head(deg)
> nrDEG=deg[,c(1,3,6)]
> colnames(nrDEG)=c('GeneID','log2FoldChange','pvalue')
> rownames(nrDEG) = nrDEG$GeneID
> nrDEG$GeneID = NULL
#convert SYMBOL to ENTREZID
> gene <- bitr(rownames(nrDEG),
        fromType = "SYMBOL",
        toType =    "ENTREZID",
        OrgDb = org.Hs.eg.db)
# Map gene names, ENTREZID, and logFC
>                                   gene$logFC                                  <-
nrDEG$log2FoldChange[match(gene$SYMBOL,rownames(nrDEG))]
> head(gene)
> geneList=gene$logFC
> names(geneList)=gene$ENTREZID
# Sort geneList by logFC values with a small perturbation
> geneList = sort(geneList + runif(length(geneList), -1e-10, 1e-10),
decreasing = TRUE)
> head(geneList)
## GSEA-KEGG analysis
> kk_gse <- gseKEGG(geneList         = geneList,
        organism         = 'hsa',
        minGSSize        = 10,
        pvalueCutoff = 0.9,
        verbose          = FALSE)
> gseaplot2(kk_gse,
        paths, #row.names(sortkk)[1:5], # Selected pathways
        title = "GSEA-KEGG",
```


© COPYRIGHT UPM

```
        base_size = 8,
        color = “green”,
        pvalue_table = TRUE,
        ES_geom=“line”)
> ggsave(“GSEA_KEGG.pdf”, height = 6, width = 6)

## GSEA-GO analysis
> ego <- gseGO(geneList      = geneList,
        OrgDb          = org.Hs.eg.db,
        ont            = “ALL”,
        minGSSize      = 10,
        maxGSSize      = 500,
        pvalueCutoff = 0.9,
        verbose        = FALSE)
> gseaplot2(ego,
        paths, # row.names(sortgo)[1:5],    # Selected pathways
        title = “GSEA”,
        base_size = 12,
        color = “green”,
        # pvalue_table = TRUE,
        ES_geom=“line”)
> ggsave(“GSEA_GO5.pdf”, height = 9, width = 9)
```

© COPYRIGHT UPM

B2 : Command lines/scripts used for the visualisation of the results of the biological process clustering enrichment analysis. The commands used in Rstudio are as follows:

```
# Load required packages
library(rrvgo)
library(clusterProfiler)
library(org.Hs.eg.db)
library(enrichplot)
library(ggplot2)
library(writexl)
# Set working directory and read input files
> setwd("/huangtan/UPM/Thesis/GO_cluster")
rt=read.table("Input_file.txt",sep="\t",header=T,check.names=F)
deg_genes <- rt$genesymbol
# GO ORA analysis
ora_res <- enrichGO(gene = deg_genes,
        OrgDb = "org.Hs.eg.db",
        keyType = "SYMBOL",
        ont = "BP", # "ALL", "BP", "MF", "CC"
        pvalueCutoff = 0.05,
        pAdjustMethod = "BH", qvalueCutoff = 0.05,
        minGSSize = 2, maxGSSize = 500, readable = T )
#the calculateSimMatrix function to compute semantic similarity
ora_res <- ora_res[ora_res$pvalue < 0.05 & ora_res$qvalue < 0.05, ]
go_analysis <- ora_res[1:40, ]
simMatrix <- calculateSimMatrix(go_analysis$ID,
              orgdb="org.Hs.eg.db", ont="BP", method="Rel")
# Choose an appropriate threshold based on analysis goals
scores <- setNames(-log10(go_analysis$qvalue), go_analysis$ID)
reducedTerms <- reduceSimMatrix(simMatrix, scores, threshold=0.8,
orgdb="org.Hs.eg.db")
# Visualization results
heatmapPlot(simMatrix, reducedTerms,
        annotateParent=TRUE,
        annotationLabel="parentTerm",
        fontsize=7)
> pdf(file = "GO_Cluster.pdf", width = 6, height = 6)
> dev.off()
```

© COPYRIGHT UPM

B3 : Command lines/scripts used for the results visualisation of the similarity matrix heatmap of the enrichment analysis. The commands used in Rstudio are as follows:

```
# Load required packages
> library(clusterProfiler)
> library(org.Hs.eg.db)
> library(simplifyEnrichment)
> library(magick)
> library(enrichplot)
> library(ggplot2)
> library(ComplexHeatmap)
> library(writexl)
# Set working directory and read input files
> setwd("/huangtan/UPM/Thesis/heatmap_cluster")
rt = read.table("Input_file.txt", sep="\t", header=T, check.names=F)
deg_genes <- rt$genesymbol
# Perform GO ORA (Over-Representation Analysis)
> ora_res <- enrichGO(gene = deg_genes,
      OrgDb = "org.Hs.eg.db",
      keyType = "SYMBOL",    # Specify gene ID type
      ont = "ALL",    # Options: "BP", "MF", "CC"
      pvalueCutoff = 0.05,
      pAdjustMethod = "BH",
      qvalueCutoff = 0.05,
      minGSSize = 2,    # Minimum number of genes
      maxGSSize = 500,    # Maximum number of genes
      readable = T    # Convert ENTREZID to SYMBOL)
> class(ora_res) ## [1] "enrichResult" ## attr(,"package") ## [1] "DOSE"
# Extract GO IDs for different ontologies
> go_id_bp <- ora_res[ora_res$ONTOLOGY == "BP", "ID"]
# Check the number of extracted GO IDs
> length(go_id_bp); length(go_id_cc); length(go_id_mf)
> head(go_id_bp)
# Compute similarity matrix
> mat <- GO_similarity(go_id_bp, ont = "BP", db="org.Hs.eg.db")
> pdf("GO_similarity _heatmap.pdf", width = 6, height = 8)
> df <- simplifyGO(mat, plot = T)
> dev.off()
```

© COPYRIGHT UPM

B4 : Command lines/scripts used for the visualisation of the results of the WGCNA analysis. The commands used in Rstudio are as follows:

```
# Load required packages
> library(limma)
> library(WGCNA)
# Set working directory and read input files
> setwd("/huangtan/UPM/Thesis/GO_cluster")
> expFile="Input_file.txt"
> rt=read.table(expFile, header=T, sep="\t", check.names=F)
> rt=as.matrix(rt)
> rownames(rt)=rt[,1]
> exp=rt[,2:ncol(rt)]
> dimnames=list(rownames(exp),colnames(exp))
> data=matrix(as.numeric(as.matrix(exp)),nrow=nrow(exp),dimnames=dimnames)
> data=avereps(data)
> data=normalizeBetweenArrays(data)
> data=data[apply(data,1,sd)>0.7,]
# Extract control and experimental group sample information
> Type=gsub("(.*)\\_(.*)", "\\2", colnames(data))
> conCount=length(Type[Type=="Con"])
> dsCount=length(Type[Type=="DS"])
> datExpr0=t(data)
### Check for missing values
> gsg = goodSamplesGenes(datExpr0, verbose = 3)
> if (!gsg$allOK)
{if (sum(!gsg$goodGenes)>0)
      printFlush(paste("Removing genes:", paste(names(datExpr0)[!gsg$goodGenes],
collapse = ", ")))
   if (sum(!gsg$goodSamples)>0)
      printFlush(paste("Removing                                    samples:",
paste(rownames(datExpr0)[!gsg$goodSamples], collapse = ", ")))
   datExpr0 = datExpr0[gsg$goodSamples, gsg$goodGenes]}
### Sample clustering
> sampleTree = hclust(dist(datExpr0), method = "average")
> pdf(file = "1_sample_cluster.pdf", width = 12, height = 9)
> par(cex = 0.6)
> par(mar = c(0,4,2,0))
> plot(sampleTree, main = "Sample clustering to detect outliers", sub="", xlab="", >
cex.lab = 1.5, cex.axis = 1.5, cex.main = 2)
### Add cut-off line
> abline(h = 20000, col = "red")
> dev.off()
```


© COPYRIGHT UPM

```
### Remove samples below the cut-off
> clust = cutreeStatic(sampleTree, cutHeight = 20000, minSize = 10)
> table(clust)
> keepSamples = (clust==1)
> datExpr0 = datExpr0[keepSamples, ]
### Prepare desease data
> traitData=data.frame(Con=c(rep(1,conCount),rep(0,dsCount)),
        DS=c(rep(0,conCount),rep(1,dsCount)))
> row.names(traitData)=colnames(data)
> fpkmSamples = rownames(datExpr0)
> traitSamples =rownames(traitData)
> sameSample=intersect(fpkmSamples,traitSamples)
> datExpr0=datExpr0[sameSample,]
> datTraits=traitData[sameSample,]
### Sample clustering heatmap
> sampleTree2 = hclust(dist(datExpr0), method = "average")
> traitColors = numbers2colors(datTraits, signed = FALSE)
> pdf(file="2_sample_heatmap.pdf",width=12,height=12)
> plotDendroAndColors(sampleTree2, traitColors,
        groupLabels = names(datTraits),
        main = "Sample dendrogram and trait heatmap")
> dev.off()
### Power value selection plot
> allowWGCNAThreads()    # Enable multi-threading
> powers = c(1:20)         # Range of power values
> sft = pickSoftThreshold(datExpr0, powerVector = powers, verbose = 5)
> pdf(file="3_scale_independence.pdf",width=9,height=5)
> par(mfrow = c(1,2))
> cex1 = 0.9
### Scale-free topology fit plot
> plot(sft$fitIndices[,1], -sign(sft$fitIndices[,3])*sft$fitIndices[,2],
        xlab="Soft Threshold (power)",ylab="Scale Free Topology Model Fit, signed
R^2",type="n",
        main = paste("Scale independence"));
text(sft$fitIndices[,1], -sign(sft$fitIndices[,3])*sft$fitIndices[,2],
        labels=powers,cex=cex1,col="red");
abline(h=0.85,col="red")    # Can be adjusted
### Mean connectivity plot
> plot(sft$fitIndices[,1], sft$fitIndices[,5],
        xlab="Soft Threshold (power)",ylab="Mean Connectivity", type="n",
        main = paste("Mean connectivity"))
text(sft$fitIndices[,1], sft$fitIndices[,5], labels=powers, cex=cex1,col="red")
> dev.off()
```


© COPYRIGHT UPM

```
### Convert adjacency matrix
# View the best power value
> softPower = sft$powerEstimate    # Best power value
> adjacency = adjacency(datExpr0, power = softPower)
> softPower
## Scale-free topology analysis
> pdf(file="3_softConnectivity.pdf", width=9, height=5)
> k <- softConnectivity(datE=datExpr0,power=softPower)
> par(mfrow=c(1,2))
> hist(k)
> scaleFreePlot(k,main="Check Scale free topology\n")
> dev.off()
### Compute TOM matrix
> TOM = TOMsimilarity(adjacency)
> dissTOM = 1-TOM
### Gene clustering
> geneTree = hclust(as.dist(dissTOM), method = "average")
> pdf(file="4_gene_clustering.pdf",width=12,height=9)
> plot(geneTree, xlab="", sub="", main = "Gene clustering on TOM-based
dissimilarity",
        labels = FALSE, hang = 0.04)
> dev.off()
### Identify dynamic modules
> minModuleSize = 180    # Minimum module size
> dynamicMods = cutreeDynamic(dendro = geneTree, distM = dissTOM,
        deepSplit = 3, pamRespectsDendro = FALSE,
        minClusterSize = minModuleSize)
> table(dynamicMods)
> dynamicColors = labels2colors(dynamicMods)
> table(dynamicColors)
> pdf(file="5_Dynamic_Tree.pdf",width=8,height=6)
> plotDendroAndColors(geneTree, dynamicColors, "Dynamic Tree Cut",
        dendroLabels = FALSE, hang = 0.03,
        addGuide = TRUE, guideHang = 0.05,
        main = "Gene dendrogram and module colors")
> dev.off()
### Merge similar modules
> MEList = moduleEigengenes(datExpr0, colors = dynamicColors)
> MEs = MEList$eigengenes
# Handle missing values in MEs
> if (any(is.na(MEs))) {
   filled_MEs = apply(MEs, 2, function(x) ifelse(is.na(x), mean(x, na.rm = TRUE), x))
   MEDiss = 1 - cor(filled_MEs, use = 'pairwise.complete.obs')
```


© COPYRIGHT UPM

```
} else { MEDiss = 1 - cor(MEs, use = 'pairwise.complete.obs')}
# Handle NaN values
> MEDiss[is.nan(MEDiss)] = 0
> MEDiss[is.na(MEDiss)] = 0
# Convert to distance matrix and perform clustering
> METree = hclust(as.dist(MEDiss), method = “average”)
> pdf(file=“6_Clustering_module.pdf”,width=7,height=6)
> plot(METree, main = “Clustering of module eigengenes”,
        xlab = ““, sub = ““)
> MEDissThres = 0.25    # Can be adjusted
> abline(h=MEDissThres, col = “red”)
> dev.off()
### Merge similar modules
> merge = mergeCloseModules(datExpr0, dynamicColors, cutHeight = MEDissThres,
verbose = 3)
> mergedColors = merge$colors
> mergedMEs = merge$newMEs
> pdf(file=“7_merged_dynamic.pdf”, width = 9, height = 6)
> plotDendroAndColors(geneTree, mergedColors, “Dynamic Tree Cut”,
        dendroLabels = FALSE, hang = 0.03,
        addGuide = TRUE, guideHang = 0.05,
        main = “Gene dendrogram and module colors”)
> dev.off()
```

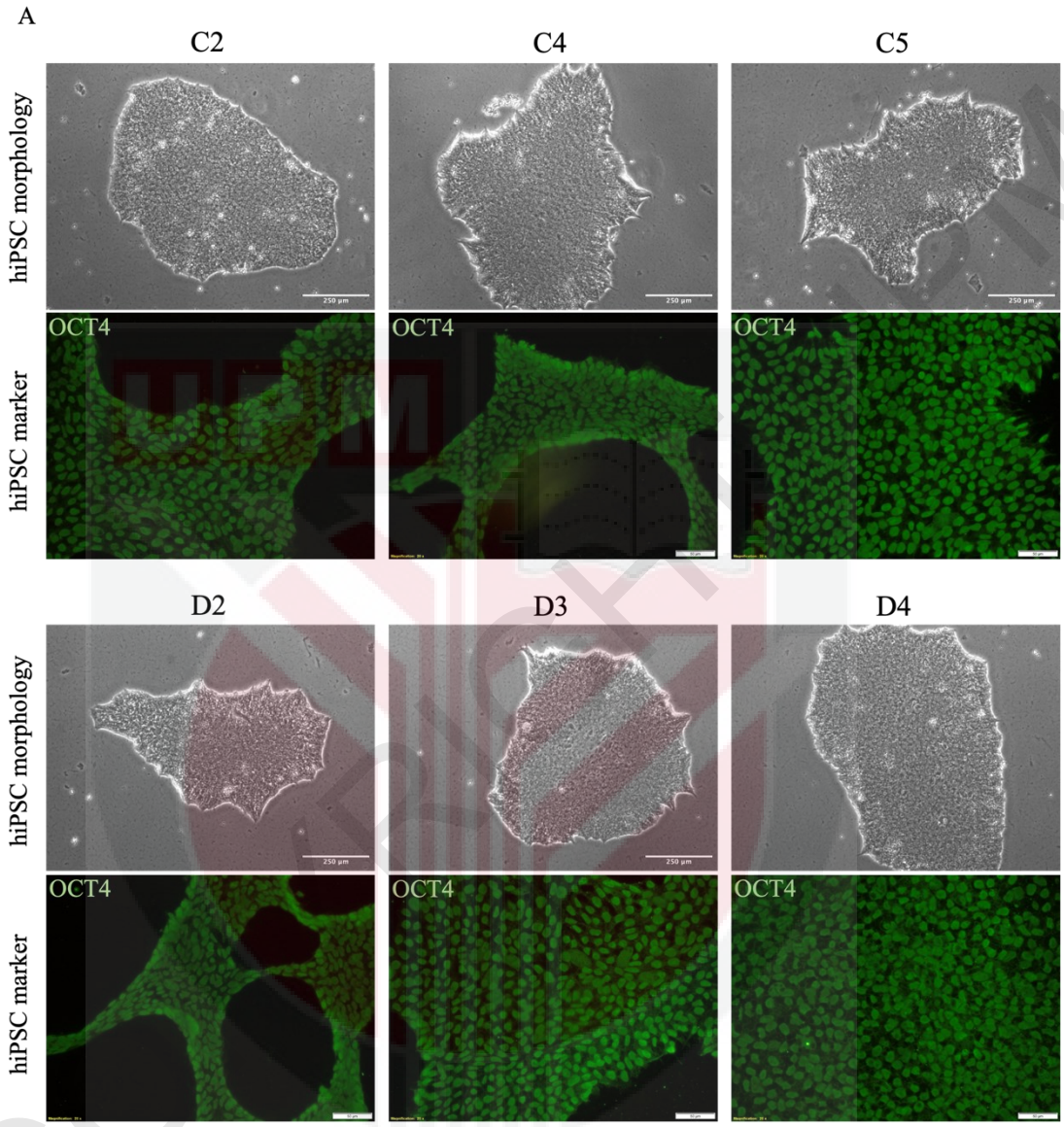
© COPYRIGHT UPM

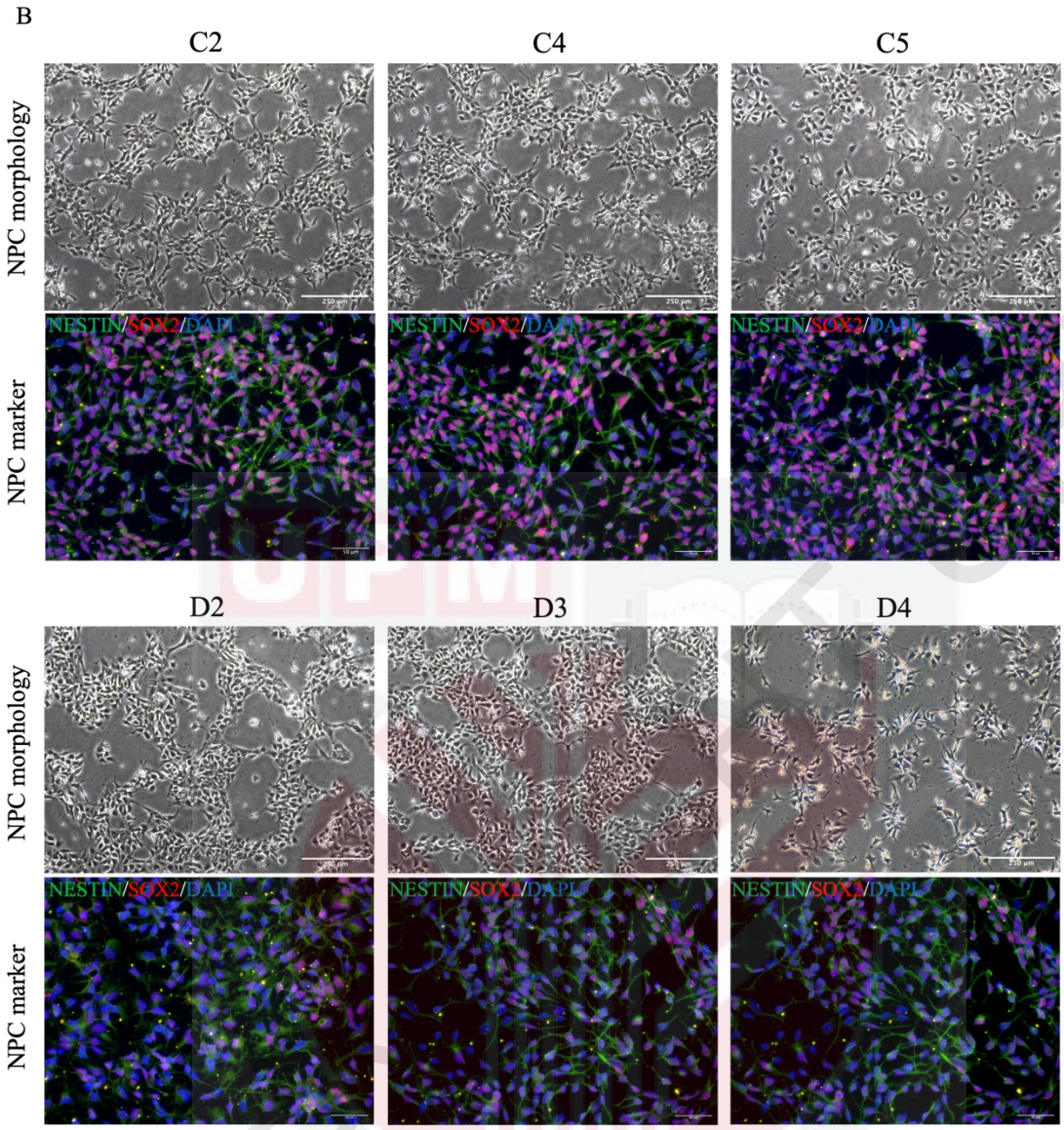
B5 : The top 10 DEGs were shown in the volcano plot in DS hiPSC-derived NPC in Figure 4.2.

Neural cell	Gene symbol	p-value	LogFoldChange	Up- / Down-regulation
NPC (GSE1851192)	RTN4R	4.29E-42	-1.1769373	Down
	CARMIL1	1.17E-35	1.22295422	Up
	KCNH1	1.67E-30	3.96653149	Up
	ATP6V0E2	1.31E-28	-1.2984662	Down
	FAM241B	1.80E-28	-1.5156781	Down
	ARMCX2	3.25E-28	1.13395785	Up
	SYT9	7.12E-27	-2.6326544	Down
	PAPPA	1.32E-26	5.64000891	Up
	ZNF664	4.60E-26	1.82024812	Up
	NUP54	1.28E-25	-1.4625012	Down

© COPYRIGHT UPM

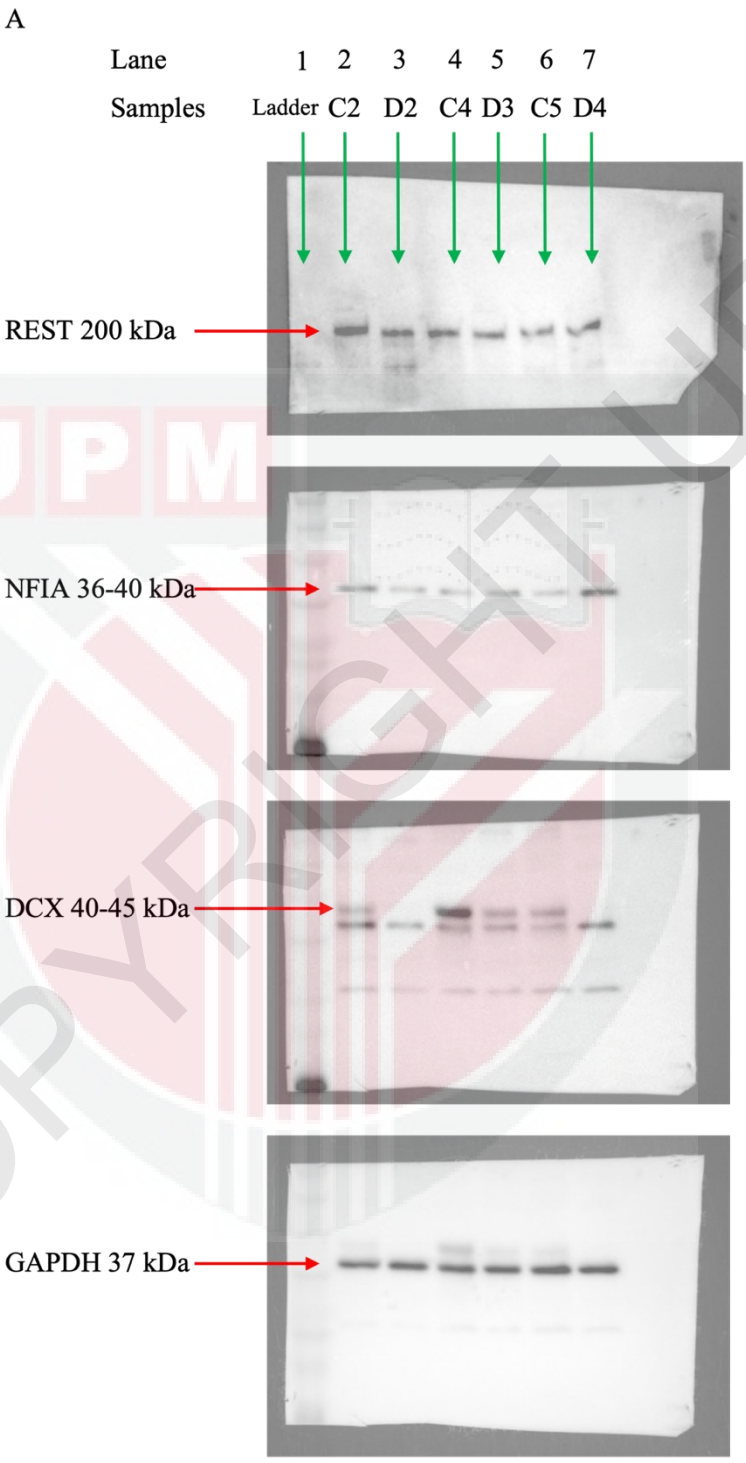
B6 : Three pairs of hiPSC and NPC cell lines (C2 vs DS2, C4 vs DS3, and C5 vs DS4) were cultured. (A) All hiPSCs expressed positive cell markers OCT4. (B) All NPCs expressed positive cell markers Nestin and SOX2.





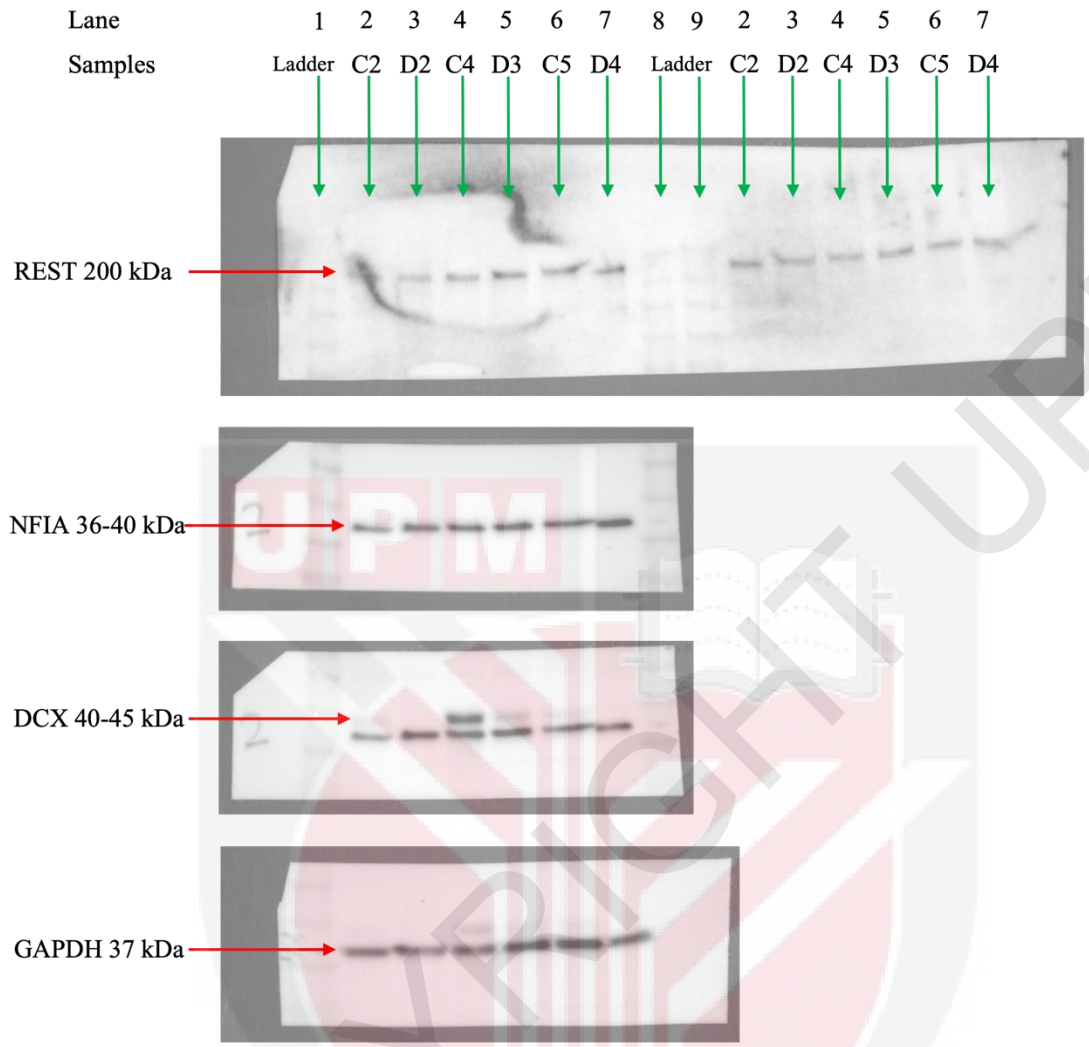
© COPYRIGHT UPM

B7 : Western blot original image (C2 vs DS2, C4 vs DS3, and C5 vs DS4). (A) Batch 1 and (B) Batch 2.



© COPYRIGHT UPM

B



© COPYRIGHT UPM

Appendix C

C1 : Command lines/scripts used for machine learning analysis to screen hub genes. The commands, including Lasso regression analysis and Random Forest analysis, used in Rstudio are as follows:

```
# Load required package
> set.seed(123)
> library(glmnet)
> library(randomForest)
> library(ggplot2)
# Set working directory and read input files
> setwd("/huangtan/UPM/Thesis/Machine_learing")
##Lasso analysis
> expFile = "Input_file1.txt"    # Expression data file
> geneFile = "Input_file2.txt"    # Gene list file
> rt = read.table(expFile, header = TRUE, sep = "\t", check.names = FALSE,
                  row.names = 1)
> geneRT = read.table(geneFile, header = FALSE, sep = "\t", check.names = FALSE)
> rt = rt[as.vector(geneRT[,1]),]
> rt = t(rt)
# Construct the Lasso regression model
> x = as.matrix(rt)
> y = gsub("(.*)\\_(.*)", "\\2", row.names(rt))
> fit = glmnet(x, y, family = "binomial", alpha = 1)
# Plot Lasso regression results
> pdf(file = "lasso.pdf", width = 6, height = 5.5)
> plot(fit)
> dev.off()
# Perform cross-validation and plot the results
> cvfit = cv.glmnet(x, y, family = "binomial", alpha = 1, type.measure = 'deviance',
                    nfolds = 10)
> pdf(file = "cvfit.pdf", width = 6, height = 5.5)
> plot(cvfit)
> dev.off()
# Extract and save feature genes identified by Lasso regression
> coef = coef(fit, s = cvfit$lambda.min)
> index = which(coef != 0)
> lassoGene = row.names(coef)[index]
> lassoGene = lassoGene[-1]    # Remove intercept term
> write.table(lassoGene, file = "LASSO.gene.txt", sep = "\t", quote = FALSE,
              row.names = FALSE, col.names = FALSE)
## Random Forest analysis
```


© COPYRIGHT UPM

```
# Read input files
> inputFile = “Input_file3.txt”    # Gene expression file
> data = read.table(inputFile, header = TRUE, sep = “\t”, check.names = FALSE,
                          row.names = 1)
> data = t(data)
> group = gsub(“(.*)\\_(.*)”, “\\2”, row.names(data))
# Build Random Forest model
> rf = randomForest(as.factor(group) ~ ., data = data, ntree = 400)
> pdf (file = “forest.pdf”, width = 6, height = 6)
> plot (rf, main = “Random Forest”, lwd = 2)
> dev.off()
# Identify the optimal number of trees with the lowest error rate
> optionTrees = which.min(rf$err.rate[, 1])
> optionTrees
> rf2 = randomForest(as.factor(group) ~ ., data = data, ntree = optionTrees)
# Obtain gene importance scores
> importance = importance(x = rf2)
# Select feature genes for disease classification
> rfGenes = importance[order(importance[, “MeanDecreaseGini”],
            decreasing = TRUE),]
> rfGenes = names(rfGenes[rfGenes > 1])
> write.table (rfGenes, file = “RF.gene.txt”, sep = “\t”, quote = FALSE,
              col.names = FALSE, row.names = FALSE)
## Generate a bubble plot for gene importance
> importance = importance[order(importance [, “MeanDecreaseGini”],
                 decreasing = TRUE), , drop = FALSE]
> rt = cbind(row.names(importance), as.data.frame(importance))
> colnames(rt) = c(“ID”, “Importance”)
> rt = rt[1:15, ]    # Select the top 15 genes
> rt$ID = factor(rt$ID, levels = rev(rt$ID))
> rt$Importance = as.numeric(rt$Importance)
> p = ggplot(rt, aes(Importance, ID)) +
      geom_segment(aes(x = 0, xend = Importance, y = ID, yend = ID),
            color = “grey”, cex = 1.5) + geom_point(aes(color = Importance),
            cex = 3.5) + scale_colour_gradient(low = “#008280FF”,
            high = “#BB0021FF”) + labs(x = “Importance”, y = ““) +
      theme(axis.text.x = element_text(color = “black”, size = 10),
            axis.text.y = element_text(color = “black”, size = 10)) + theme_bw()
> pdf(file = “geneImportance.pdf”, width = 5, height = 4.5)
> print(p)
> dev.off()
```

© COPYRIGHT UPM

C2 : The top 10 DEGs were shown in the volcano plots in DS hiPSC-derived different developmental stages cerebral organoids in Figure 5.3.

Organoid	Gene symbol	p-value	LogFoldChange	Up- / Down-regulation
30-Day (PRJNA72827)	TTYH1	1.55E-14	4.232205747	Up
	HERC2P3	3.13E-11	3.804730218	Up
	LIPG	3.13E-11	-1.684058233	Down
	UNC13D	1.24E-10	2.259021039	Up
	BTNL9	4.70E-10	5.00928207	Up
	ADARB1	4.72E-10	1.364310773	Up
	FCGBP	1.03E-09	2.030934621	Up
	HLCS	2.93E-09	0.970441289	Up
	SYTL2	9.01E-09	-1.554505587	Down
	EMX1	1.87E-08	2.738025507	Up

Organoid	Gene symbol	p-value	LogFoldChange	Up- / Down-regulation
35-Day (GSE124513)	CKB	5.41E-140	-1.164948219	Down
	XIST	1.40E-137	-10.89763301	Down
	AMOT	1.69E-128	1.365454212	Up
	POU3F3	1.87E-123	-0.869499635	Down
	TSPAN18	8.55E-92	-0.750320118	Down
	LOC440173	1.69E-84	-4.319784424	Down
	LINC00205	9.40E-68	1.048658927	Up
	AP1S2	1.15E-67	1.166708126	Up
	CCDC80	1.15E-66	1.422336229	Up
	GAS1	6.20E-63	1.584578906	Up

Organoid	Gene symbol	p-value	LogFoldChange	Up- / Down-regulation
56-Day (GSE208440)	ARMCX1	3.27E-221	-6.076021591	Down
	FN1	6.36E-155	-3.065036119	Down
	ZNF248	5.24E-151	6.351400893	Up
	TSSC2	1.21E-130	3.459870373	Up
	POSTN	8.00E-115	-3.057895368	Down
	DIO3	6.60E-110	3.511686981	Up
	COL12A1	2.77E-106	-5.360386098	Down
	POFUT1	4.43E-105	1.785089914	Up
	PDGFD	1.31E-102	2.358915521	Up
	ZNF300	3.00E-100	-6.260891085	Down

© COPYRIGHT UPM

Organoid	Gene symbol	p-value	LogFoldChange	Up- / Down-regulation
90-Day (GSE208440)	RWDD2B	8.45E-91	3.9494552	Up
	PFKL	1.86E-83	0.724706211	Up
	SON	9.83E-82	0.513915892	Up
	PRMT2	5.66E-64	0.613087953	Up
	MCM3AP	4.43E-53	0.542369907	Up
	RRP1	8.36E-52	0.76125366	Up
	CSTB	3.78E-49	0.777869098	Up
	IFNAR1	1.61E-46	0.644353853	Up
	PDXK	1.03E-42	0.717899901	Up
	VPS26C	3.80E-42	0.505174962	Up

Organoid	Gene symbol	p-value	LogFoldChange	Up- / Down-regulation
120-Day (GSE222365)	PPP1R12C	2.79E-43	3.504352358	Up
	RWDD2B	1.56E-25	3.902960494	Up
	CEBPD	7.77E-21	2.549073518	Up
	CD44	5.79E-19	1.737647666	Up
	SCGN	7.19E-16	-3.014651417	Down
	HSPA13	3.25E-15	0.964691207	Up
	ANGPTL4	7.13E-15	3.038755139	Up
	DDX41	7.36E-15	0.592523901	Up
	LCN9	8.88E-15	-4.162994406	Down
	GYS1	1.01E-14	1.245709012	Up

© COPYRIGHT UPM

Appendix D

D1 : The top 10 DEGs were shown in the volcano plots in DS-derived astrocytes in Figure 6.3.

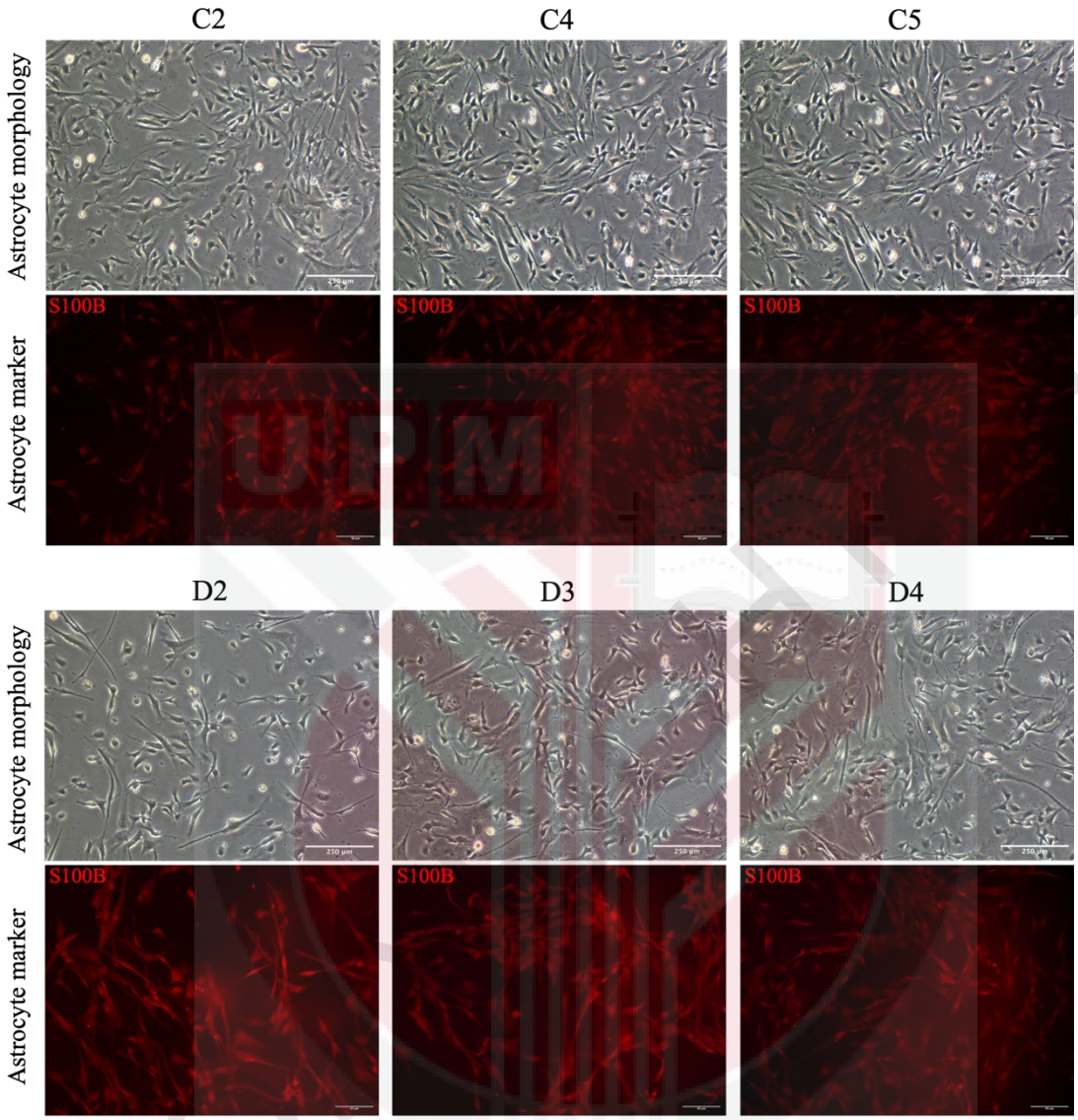
Astrocyte	Gene symbol	p-value	LogFoldChange	Up- / Down-regulation
HiPSC-derived astrocyte (PRJNA600245)	HCG18	2.92E-36	3.61536303	Up
	UBE2G2	4.42E-34	0.71730395	Up
	RGS1	2.57E-20	5.32741166	Up
	NKX2-1	9.78E-20	-24.412387	Down
	C5orf17	1.67E-18	23.1201785	Up
	ATP5PF	2.20E-17	0.7449906	Up
	A4GALT	3.55E-17	-2.9245017	Down
	IFNAR2	5.02E-16	0.6988512	Up
	LINC00654	5.09E-16	-5.265711	Down
	CNTFR	2.94E-15	4.61985306	Up

Astrocyte	Gene symbol	p-value	LogFoldChange	Up- / Down-regulation
Fetal cerebellum-derived astrocytes (GSE1397)	NUP62CL	1.78E-04	-3.0154888	Down
	MVD	3.62E-04	-2.7322673	Down
	MYLK3	3.93E-04	2.80029804	Up
	PLSCR2	3.96E-04	3.00134389	Up
	MBNL3	4.31E-04	-2.8818069	Down
	SSX1	4.71E-04	-2.3599887	Down
	CHML	5.12E-04	2.42416657	Up
	NCF2	5.32E-04	2.28127987	Up
	DLK1	5.64E-04	-3.0227609	Down
	FCGR1A	5.81E-04	-2.9678489	Down

Astrocyte	Gene symbol	p-value	LogFoldChange	Up- / Down-regulation
Fetal cortical-derived astrocytes (GSE42772)	MPP5	1.44E-04	-0.5966667	Down
	APP	4.06E-04	0.654	Up
	PLA2G3	4.19E-04	-0.6053333	Down
	DEPDC6	8.10E-04	1.13533333	Up
	FADS1	1.62E-03	-1.0593333	Down
	INHBB	1.66E-03	-1.39	Down
	USP14	1.75E-03	0.57333333	Up
	LRRC34	2.29E-03	-0.674	Down
	IDI1	2.46E-03	-0.736	Down
	KIAA0372	2.88E-03	0.504	Up

© COPYRIGHT UPM

D2 : Three pairs of astrocyte cell lines (C2 vs DS2, C4 vs DS3, and C5 vs DS4) were cultured. All astrocytes expressed positive cell markers S100B.



BIODATA OF STUDENT

Huang Tan obtained his Bachelor of Medical Science and Doctor of Medicine (BMedSci/MD) from the Institute of Medicine and Nursing, Hubei University of Medicine in 2013. From 2013 to 2016, he pursued a Master's degree in Surgery (Neurosurgery) at Wuhan University, during which the National Graduate Scholarship supported him. After graduation, he continued his studies at Tongji Hospital, Tongji Medical College, Huazhong University of Science and Technology, and completed his training in neurosurgery as a neurosurgeon specialist in 2019.

Dr. Huang has always had a strong interest in neuroscience research, which led him to pursue a PhD at Universiti Putra Malaysia. In 2021, he joined the Neurobiology and Genetics Group (NBGG) laboratory under the supervision of Professor Dr. Ling King Hwa to begin his PhD in Neuroscience. In 2022, Dr. Huang was awarded the Putra Grant IPS from Universiti Putra Malaysia for his ongoing research. He has published five papers, has two manuscripts under review, and is preparing to submit two additional manuscripts.

© COPYRIGHT UPM

LIST OF PUBLICATIONS

Publications:

Huang, T., Fakurazi, S., Cheah, P. S., & Ling, K. H. (2023). REST Targets JAK-STAT and HIF-1 Signaling Pathways in Human Down Syndrome Brain and Neural Cells. International Journal of Molecular Sciences, 24(12), 9980. https://doi.org/10.3390/ijms24129980

Huang, T., Fakurazi, S., Cheah, P. S., & Ling, K. H. (2024). Chromosomal and cellular therapeutic approaches for Down syndrome: A research update. Biochemical and biophysical research communications, 735, 150664. Advance online publication. https://doi.org/10.1016/j.bbrc.2024.150664

Huang, T., Lam, X. J., Lim, C. T., Jusoh, N., Fakurazi, S., Cheah, P. S., & Ling, K. H. (2024). Understanding perspectives and research trends in Down syndrome neuropathogenesis: A bibliometric analysis. Journal of intellectual disabilities : JOID, 17446295241299160. Advance online publication.

https://doi.org/10.1177/17446295241299160

Huang, T., Fakurazi, S., Cheah, P. S., & Ling, K. H. (2025). Dysregulation of REST and its target genes impacts the fate of neural progenitor cells in down syndrome. Scientific reports, 15(1), 2818. https://doi.org/10.1038/s41598-025-87314-y

Lim, C.-T., Lam, X.-J., Crystal, A.-A., **Huang, T.**, Jusoh, N., Cheah, P.-S., & Ling, K.-H. (2024). Reduced REST Expression in Neural Progenitor Cells, Adult Cortex, and Impaired REST Nuclear Translocation in the Prefrontal Cortex of Ts1Cje Mouse Model of Down Syndrome. Neurochemical Journal, 18(1), 147–161. https://doi.org/10.1134/S1819712424010148

Manuscript Under Review:

Huang, T., Fakurazi, S., Cheah, P. S., & Ling, K. H. REST Recover Inhibits Down Syndrome iPSC-derived Astrocyte Reactivity

Yu Y.X.; Xu Y.P.; JChen J.F; Yao Y.; Liu Y.T; **Huang T.**; Yang S.L.; Ling, K. H.; Guyette J.P.; Shaharuddin B.; Guo Z.K.; Tan J.J.. Empagliflozin and Pirfenidone Enhance Cardiac Function and Reverse Hypertrophy in HFpEF Rats

© COPYRIGHT UPM

Manuscript in Preparation:

Huang, T., Fakurazi, S., Cheah, P. S., & Ling, K. H. REST-mediated dysregulation in Down syndrome iPSC-derived Cerebral Organoids at Different development stage

Lim, C.-T., Lim, C.-W., **Huang, T.**, Elysha, N.I., Cheah, P. S., & Ling, K. H. REST in synaptic-dysfunctional neurological diseases and its regulatory roles in the synaptic system

© COPYRIGHT UPM

LIST OF CONFERENCES AND SCHOOL ATTENDED

Conferences:

30th Annual Scientific Meeting of the Malaysian Society of Neurosciences (as poster presenter): 30 September 2022 – 2 October 2022, at Kuala Lumpur, Malaysia.

3rd International Anatomical and Biomedical Scientific Conference (as poster presenter): 22 – 24 November 2022, virtual.

Neuroscience: Breach the Research Barrier (as delegate): 15 June 2023, at Universiti Putra Malaysia

31st Annual Scientific Meeting of the Malaysian Society of Neurosciences (as poster presenter): 29 September – 1 October 2023, at Sarawak, Malaysia.

Mouse Embryonic Stem Cell Culture and Applications: Comprehensive Symposium (as delegate): 5 March 2024, at Universiti Putra Malaysia.

Awards:

IBRO-APRC Travel Award (INTERNATIONAL) – Huang Tan. An award by the International Brain Research Organisation- APRC for attending the IBRO-APRC Advanced School 2022 – "Bioimaging and Proteogenomics for Cell-Based and Animal Research", from 10 to 23 October 2022, at Jeffrey Cheah School of Medicine and Health Sciences, MONASH University Malaysia.

BNC-MSN Education Grant Awards (NATIONAL) – Huang Tan. A BNC-MSN education award to attend 30th Malaysian Society of Neuroscience (MSN) Annual Scientific Meeting (ASM) from 30th September to 3rd October 2022.

BNC-MSN Education Grant Awards (NATIONAL) – Huang Tan. A BNC-MSN education grant to attend the 31st Malaysian Society of Neuroscience (MSN) Annual Scientific Meeting (ASM) from 29th September to 30th September 2023.

Schools:

IBRO-APRC Advance School of Neuroscience 2022. 10-23rd October 2022, at Monash University Malaysia.

IBRO-APRC Associate School of Neuroscience 2024: "Symposium & Workshop: Cerebral Organoids Model For Ageing Neurobiology Research". 12 – 14th August 2024, at Universiti Putra Malaysia.

© COPYRIGHT UPM